University of Alberta

Characteristic Behaviour of Slow Moving Slides

by

Mohamed Farouk Mohamed Ibrahim Mansour

A thesis submitted to the Faculty of Graduate Studies and Research
in partial fulfillment of the requirements for the degree of

Doctor of Philosophy

in

Geotechnical Engineering

Civil and Environmental Engineering Department

Fall 2009

Edmonton, Alberta

Examining Committee

Dr. C. Derek Martin, Civil and Environmental Engineering Department. Supervisor

Dr. Norbert R. Morgenstern, Civil and Environmental Engineering Department. Co-supervisor

Dr. David M. Cruden, Civil and Environmental Engineering Department. Chair

Dr. Peter Steffler, Civil and Environmental Engineering Department. Committee member

Dr. Doug Schmitt, Department of Physics. Committee member

Dr. James A. Blatz, Department of Civil Engineering, University of Manitoba. External examiner

To my mother … who sacrifices herself infinitely for the sake of my success, I dedicate this work … with my deep love and gratitude

Abstract

The vulnerability and movement behaviour of slow moving slides are investigated. The study focuses on slides moving at rates ranging from a few millimetres a year like extremely slow slides, to 13 meters per month, the upper velocity range of slow slides. An extensive review of the effect of pore pressure changes on movement reactivation of shallow and moderately thick slides is presented. The time dependent behaviour of fine geotechnical materials is also reviewed.

Although the literature has reported many cases where the accumulation of slow movements led to a complete collapse of buildings, failure of embankment slopes carrying highways or railways and serviceability problems for dams and bridges, little attention has been paid to the vulnerability to slow moving slides. Hence, this thesis aims to provide more insight into the actual damage to facilities founded on slow moving slides. More than fifty cases of extremely slow, very slow and slow slides adversely affecting urban communities, highways, railways, bridges, dams and linear infrastructure are reviewed. The survey enables the development of new damage-extent scales that use the slide velocity to help assess the degree of damage to a facility founded on a landslide-prone area.

Vulnerability is an important component of the specific risk. The other component is the hazard or the probability of occurrence of a certain damaging

phenomenon like landslides. Defining the causal factors of the landslide movements and their contributions to the total movement is an important step towards the evaluation of the hazard. Hence, the geomechanical behaviour of two typical deep-seated and moderately thick slides, the Little Chief Slide and the Little Smoky Slide, respectively, are investigated. The objective is to determine all the triggers and causal factors of movement and to quantify their contribution to the total movement. The study involves groundwater flow modeling of one of the two slides, an extensive field monitoring of pore pressures and displacements and an investigation of the creep behaviour both in the field and in the laboratory. The outcome of the study shows that the total movement of each of the two slides can be separated into creep and seasonal movements. The contribution of each component is quantitatively defined. The quantification of the different causal factors aids in choosing the proper mitigation option in addition to predicting the future movement rates after the chosen remedial measures have been installed.

Acknowledgments

All thanks and praises are due to my GOD who guided me throughout all the stages of this work.

I would like to thank deeply and gratefully my supervisors: Dr. Derek Martin and Dr. Norbert Morgenstern for the unlimited support and the invaluable help they provided during all the stages of this research. Their kindness, continuous follow-up, useful advices and constructive criticism have been so inspiring to me especially during the final stages.

I would like to thank as well Dr. David Cruden for his great help regarding the geological aspects of this research. I have learned a lot from his expertise during the field trips we had together. I also appreciate the help and efforts of Dr. John Shaw from outside the geotechnical group at the University of Alberta who helped me during the visual inspection of the drilled cores.

Any words will never suffice my deepest gratitude to Stephen Gamble, the Engineering Technologist at the University of Alberta. This professional, talented and punctual man was more than helpful to me during the experimental and the field monitoring stages of the project. Many thanks are also due to Christine Hyreygers, the geotechnical technician at the University of Alberta, Taihoon Kim, my officemate, Mahmoud Safar and Hossam Gharib, my friends for their sincere help with some of the field work. I would like to extend my thanks to Tarek Abdel-aziz and Hassan Elramly for their valuable advices and help.

The financial support provided by the National Science and Engineering Research Council of Canada and Alberta Infrastructure and Transportation is highly acknowledged. I would like to thank as well all those who provided us with the required data during the different stages of the project: Roger Skirrow and Fred Cheng from Alberta Infrastructure and Transportation, Don Proudfoot and Gurpreet Bala from Thurber Engineering Ltd., Dennis Moore and Andrew Watson from BC Hydro, Karl Li and Shawn McArthur from Karl Engineering Ltd. and Corey Froese from Alberta Geological Survey. The help provided by Environment Canada by sending the required data free of charge is highly appreciated. I extend my thanks to the Air Photo Distribution Office in Edmonton.

I am deeply indebted and grateful to the unlimited support provided by my family who encouraged me a lot in order to approach my goal. Any words will never express my gratitude to my mum to whom I have dedicated the whole work. Five million thanks to my beloved wife Sara who was very supporting and tolerant, my ever loving and supporting sisters Rehab and Lamiaa and my lovely daughters Nour and Nada.

My thanks are to be extended to all the professors of the Geotechnical Group of the Civil and Environmental Engineering Department at the University of Alberta for the valuable knowledge I learned from them during the course work: Dr. Dave Sego, Dr. Rick Chalaturnyk, Dr. Dave Chan and Dr. Kevin Biggar. Thanks are also due to all my professors and the technical team at Ain-Shams University in Egypt that I do appreciate their efforts and help to me.

Finally, I appreciate the help of the administrative team of the Civil and Environmental Engineering Department at the University of Alberta: Sally Petaske, Hope Walls, Anne Jones, Anita Mueller and Lorraine Grahn.

Thanks to all who are mentioned above and my apologies if I forgot anyone.

Thank you all … for being there.

Table of Contents

List of Tables

List of Figures

List of Symbols

A: The axial strain rate at initial time at zero deviatoric stress level; may express the hydraulic cylinder effective area

A_s : The shear strain rate at zero shear stress level and initial time

$\bar{\alpha}$: The slope of the logarithm of axial strain rate versus deviatoric stress level

$\bar{\alpha}_s$: The slope of the logarithm of shear strain rate versus shear stress level

$\alpha(t)$: Slope of the logarithm of volumetric strain rate versus mean effective stress

β : A constant determined by knowing the volumetric strain rate value at a certain time and a certain mean effective stress,

C_α: Coefficient of secondary consolidation

C_c: Compression index

C_r: Re-compression index

C_s: Swelling index,

$\bar{D}$: The deviatoric stress level; may express the shear stress level

$\bar{D}_1, \bar{D}_2$: The shear stress levels at two chosen depths

$\dot{\delta}$: Displacement rate

E: Young's modulus

E_i: Initial tangent modulus

e: Void ratio

e_0 : Initial void ratio.

$\dot{\varepsilon}$: Axial strain rate in a triaxial testing; may express shear strain rate

$\dot{\varepsilon}_{\left(t_i,\bar{D}\right)}$: Axial strain rate at unit time; a function of the deviatoric stress level

$\dot{\varepsilon}_{(t,D_0)}$: The axial strain rate at zero deviatoric stress level; a function of time

$f(\sigma')$: A stress function

φ' : Effective angle of shearing resistance

G: Shear modulus

$g(\sigma')$: A stress function

$\dot{\gamma}_{xy}$: Shear strain rate as a function of time and shear stress level,

$\dot{\gamma}_1, \dot{\gamma}_2$: The field shear strain rates at two chosen depths at the beginning of the monitoring

$h(\sigma')$: A stress function

K: Bulk modulus

m: The slope of the axial strain rate versus time log-log plots; constant for different deviatoric stress levels.

p' : Mean effective stress $\left\{\frac{\sigma'_1+2\sigma'_3}{3}\right\}$

log *p*': logarithm of effective stresses

q: Flow rate

$\bar{q}$: The deviatoric stress level at any time t from the beginning of stress relaxation

$\bar{q}_0$: The deviatoric stress level at the beginning of stress relaxation

r_u: pore pressure ratio

s: Slope of the deviatoric stress-logarithm of time relationship

σ'_v : Effective vertical stress

t_i: The initial time in creep triaxial testing in laboratory; may express the time from the initiation of creep to the start of inclinometer readings in the field

t: The time from the beginning of the primary creep

t_0: The delay time or the time since the application of a constant strain to the beginning of the deviatoric stress relaxation

τ_h : Horizontal shear stress,

u: Pore pressure

$\dot{v}$: Volumetric strain rate

1 Introduction

1.1 Statement of the Problem

Landslides have been the subject of considerable research due to casualties and economic losses caused by slope failures. The annual cost of landslides in Canada is estimated to be $50 million and more than several billion dollars in the United States, and is increasing annually (Schuster, 1996). On an episodic scale, the increased population and associated development have led to an increase in the number of landslides and to the establishment of new urban communities in landslide-prone areas. Different facilities like highways, railways, bridges, dams and pipelines exist in places where the risk of landslides is not low.

Risk assessment processes associated with landslide movements should be firmly rooted in realistic prediction of soil behaviour under a realistic description of the anticipated spectrum of causal factors. Defining the casual factors is a major step towards understanding the mechanics of movements.

While some of the previous studies used limit equilibrium analyses to evaluate the in-situ material parameters at the time of failure and to verify the shape of the rupture surface, dealing with landslides from the perspective of movement and its adverse effect on nearby facilities offers an opportunity to define the causal factors that lead to movement. The determination of the causes of landslide movements is essential in understanding the mechanisms of movement and, hence, devising adequate mitigation strategies.

Although the slow movement of natural slopes is a well known phenomenon, its process and mechanisms are not well understood, mainly because of the difficulty in capturing extremely slow movements through instrumentation. Moreover, a small number of readings are usually taken, so the trend of the movement variation with time is not clear. Hence, a quantitative effect of the causal factors on movement cannot be established. In addition, the constitutive modeling of soil behaviour should consider the effect of viscous soil properties on deformation. Hence, time effects should be included. This requirement leads to many complications in the analysis. Normal laboratory tests are not feasible for representing long term behaviour, and long term laboratory tests are generally hard to control and pose many difficulties (Vulliet and Hutter, 1988; and Bishop and Lovenbury, 1969). The literature suggests that the slow movements of shallow slides are affected mainly by hydrological boundary conditions changes, while the viscous soil properties contribute to a large percentage of the movement of deep-seated slides (Picarelli and Russo, 2004).

Slow moving slides interact with residential settlements and man-made works. Hence, a continuous maintenance of the nearby facilities is required, together

with expensive stabilization measures in order to avoid having to evacuate people or to stop the functionality of the nearby facilities. Little attention has been paid to the vulnerability of different facilities to the ongoing movements because these movements are classified as "slow" movements. The accumulation of slow movements has, however, sometimes led to a complete collapse of buildings, failure of embankment slopes carrying highways and railways and severe serviceability problems for dams and bridges. According to Cruden and Varnes (1996), the three classes of slow slides are extremely slow moving slides, which include slides moving at rates ranging from zero to 16mm/yr; very slow moving slides, which include slides moving at rates ranging from 16mm/yr to 1.6m/yr; and slow moving slides, which include slides moving at rates ranging from 1.6m/yr to 160m/yr (~13.3 m/month).

The challenge posed by slow moving slides is that the most economic solution is often to live with them, especially for large landslides (Picarelli and Russo, 2004; and Brooker and Peck, 1993). This solution requires an accurate and reliable prediction of the future movements. Prediction of the future slope behaviour is a key requirement for carrying out a proper cost-benefit analysis for different remedial options (Picarelli and Russo, 2004).

1.2 Research Objectives

This research is concerned with slow moving slides, focusing on both their movement behaviour and the vulnerability of different facilities to them. The problem of slow moving slides has been the subject of many advanced studies due to the unique nature of each particular problem with respect to the mechanisms controlling the movement initiation or reactivation. As an example, the recent comprehensive study by Eshraghian (2007), Eshraghian et al. (2007), and Eshraghian et al. (2005) of the movement mechanisms of the slow earth slides along the Thompson River valley in the Ashcroft area highlighted the interplaying effects of river level drawdown, weak preglacial lake clays and the presence of permeable strata beneath the preglacial lake clays on movement reactivation. Another study by Soe Moe et al. (2005) investigated another slow moving slide along the North Saskatchewan River in Edmonton with the rupture surface in bedrock. Soe Moe et al. (2005) highlighted the series of events that led to the strength reduction and failure initiation in the bedrock, and also studied the role of pore pressure changes in movement reactivation. More cases of slow moving slides are reviewed in Chapter 2 of this thesis in order to provide more insight into the nature of the slow moving slides problem.

A proper approach to a slow moving slide problem must define a trigger, a movement mechanism and movement behaviour. Doing so allows for an accurate evaluation of the hazard associated with the continuing slow movements. Hazard evaluation involves the determination of all the possible triggers or causal factors of movement and quantifying their effects on movement, i.e., the contribution of

each trigger to the total movement. Defining the contribution of different triggers to the total movement is the first main objective of this study.

Hazard evaluation is one of two main components of landslide risk. The other component is the vulnerability or the consequences of movement. As mentioned above, the consequences of slow, very slow and extremely slow moving slides have been sometimes underestimated. Hence, the vulnerability to slow moving slides should be defined by evaluating the expected degree of damage in response to a certain slide velocity. This evaluation can be achieved by reviewing the literature for cases that reported the different degrees of damage to different facilities, resulting from the slow movements of nearby slopes. The second objective of this research is to develop new scales for determining the vulnerability of different facilities to slow moving slides.

An important aspect of slow moving earth slides is the stratigraphic control on stability. The series of studies performed on the historical slides in the Peace River and tributaries' valley slopes (Hardy et al., 1962; Cruden et al., 1993; Cruden at al., 1997; Evans et al., 1996; Lu et al., 1998; Miller, 2000; and Miller and Cruden, 2002) have highlighted the marked impact of the material type on the location of the rupture surface and, hence, the stability. The 1939 Montagneuse River landslide (Cruden et al., 1997), the 1959 Dunvegan Creek landslide (Hardy et al., 1962), the 1973 Attachie landslide (Evans et al., 1996), the 1990 Saddle River landslide (Cruden et al., 1993) and the 1990 Eureka River landslide (Miller and Cruden, 2002) had their rupture surfaces in weak preglacial lake clays. The 1990 Hines Creek landslide (Lu et al., 1998) and the 1995 Spirit River landslide (Miller, 2000), however, had their rupture surfaces in glacial till. One of the objectives of this research is to address the stratigraphic control on the stability of slow moving slides, especially in the interior plains of Canada. Scott (1989) identified three geological settings for instability in the prairies, north-western Alberta:

1. Cretaceous clay shales, especially when disturbed by glacial tectonics.
2. Stratigraphic contacts within glacial deposits (glacial drag forces).
3. The stratified sediments overlying till.

Cruden et al. (1993) added a fourth setting: the stratified sediments of preglacial lake clay that may underlie the till.

The objectives of this research are achieved through both reviewing the literature for all the available cases that reported the vulnerability to slow moving slides, and studying the instability problems of two slides: the Little Chief Slide located about three kilometres north of Mica Dam in British Columbia, and the Little Smoky Slide in north-western Alberta. The recorded rates of movement in the Little Chief and the Little Smoky slides range from 10 to 14mm/yr and 15 to 100mm/yr, respectively. Both slides are thus characterized as extremely slow to very slow slides according to the classification by Cruden and Varnes (1996). In addition, the first time slide appears to have occurred thousands of years ago, and

the current movements are post-failure movements in both slides. However, the two slides differ in many aspects. The Little Smoky Slide is mostly retrogressive while the Little Chief Slide is presumably moving as one entity. The Little Chief Slide can be characterized as a deep-seated slide as the movement zones support columns of rock mass ranging from 100 to 300 meters (Rapp, 2006; and Moore et al., 2006). On the other hand, the rupture surface of the Little Smoky Slide lies at depths ranging from 30 to 60 meters, and hence the slide is considered a moderately thick slide (Hayley, 1968; Thomson and Hayley, 1975; Proudfoot and Tweedie, 2002; and Skirrow et al., 2005).

Chapters four and five of this thesis present both the history of instability, together with the results of the current investigations, of the two slides. The movement behaviour and the possible triggers of movements are investigated. In addition, the contribution of each of the triggering factors, as well as the contribution of creep, to the total movement is evaluated quantitatively. The creep behaviour of the slide materials under high stresses like those encountered in the Little Chief slide is investigated in the laboratory. The values of the field creep rates as resulting from the field monitoring are then compared to the results of the laboratory triaxial creep experiments.

A peculiar property of shallow slow moving earth slides is that the slow motion is essentially a reactivation of previous first-time movements that are thought to have been rapid. Since the rupture surface is shallow, slight changes in boundary conditions, either hydrological like precipitation and/or river level changes, or due to construction work, are expected to significantly affect the reactivated movement rate. Therefore, the determination of the impact of seasonal hydrological changes on the movement is a key requirement for addressing the mechanisms of the movement of shallow slow moving earth slides.

On the other hand, the effects of hydrological boundary conditions changes on deep-seated slides movements are likely to be minimal due to the great depth of the rupture surface. Viscous and time dependent soil properties appear to significantly contribute to the slow ongoing movements. Hence, the characterization of a proper time dependent or creep model is important for understanding the mechanisms of movement.

Based on the above, the research objectives can be summarized as follows:

1. Defining the vulnerability of infrastructure and facilities to slow moving slides.
2. Defining the triggering factors and the movement behaviours of two typical deep-seated and moderately thick slow moving slides.
3. Quantifying the contribution of different causal factors to the total movement.
4. Addressing the stratigraphic control on stability, especially in complex geological settings like those in the Peace River region and the interior plains.

5. Determining the possibility of evolution of catastrophic fast moving slides from slow moving ones.

1.3 Thesis Outline

The thesis is designed to provide a systematic understanding of the objectives and the outcome of this research. Chapter 2 reviews the mechanisms controlling the reactivation of slow moving slides. The review includes the role of pore pressure changes in movement reactivation. Since creep is considered a main contributor to movement in slow deep-seated slides, a review of the time dependent behaviour of cohesive soils is also presented.

Chapter 3 presents a comprehensive review of over fifty cases documenting the different degrees of damage resulting from typical rates of slow, very slow and extremely slow moving slides. The degree of damage posed by slow slides to various types of facilities is established versus the corresponding movement rate. The outcome of the literature survey is the development of four new scales describing the expected degree of damage from a certain movement rate to urban communities, highways and railways, bridges and dams. The proposed scales have practical significance that is highlighted.

Chapter 4 presents the results of the detailed investigation of the movement behaviour of the Little Chief Slide, BC. The results of the previous investigations are first reviewed. The groundwater flow regime is simulated by using a two-dimensional continuum seepage model. The outcome and the drawbacks of the model are highlighted. Based on recent movement and pore pressure records, and experimental creep testing, the movement behaviour of the Little Chief Slide is analyzed. The analysis enables the identification of the different causal factors of movement on a quantitative basis.

Chapter 5 presents the results of the detailed investigation of the Little Smoky Slides in Alberta. The outcome of all the previous investigations is first reviewed, followed by a description of the most recent field monitoring program. The movement, pore pressure and hydrological records are investigated. The results of the investigation enable the determination of all the triggers of movement and the quantification of their effects.

Chapter 6 consists of a summary of the results of this study, conclusions and recommendations for future research.

2 Mechanics of Slow Moving Slides

2.1 Introduction

This chapter reviews the mechanics of the movement of slow slides. The review includes two main divisions. The first one highlights the role of pore pressure changes in movement reactivation of slow slides. The second division reviews the time dependent behaviour of fine geotechnical materials, with a special focus on creep as a main contributor to deep-seated slides' movement.

Our review is restricted to reactivated slide movements and does not include first time failures. The velocity of first time failures depends to some extent on the stiffness of the landslide body; i.e., in brittle soils, the strength drops drastically from peak to residual, and, hence, the first-time slide velocity is quite high. After failure, the landslide progressively slows down as long as the strength approaches the residual value (Picarelli et al., 2004). Since the peak and residual strengths' values in ductile soils are not significantly different, the velocity at first-time failure is not much higher than the post-failure velocity in these kinds of soils. Therefore, both brittle and ductile soils finally approach the same velocity in the post-failure stage where the landslide behaviour is governed by the residual strength value.

The likely trigger of movement in slow moving earth slides of moderate thickness is the seasonal changes in the boundary conditions that are almost affected by the hydrological variations over the year. The variation of the rainfall, reservoir impoundment level and/or the river level affects the pore pressure regime within the slide mass. As pore pressures rise, the effective normal stresses drop, and, hence, the strength decreases along the slide plane. While pore pressures changes are considered the main trigger of movement in that kind of slides, creep also contributes to the total movement. This contribution is evidenced by the persistence of movement during periods when the hydrological boundary conditions changes tend to zero. On the other hand, for deep-seated slides, the pore pressure fluctuations represent a small fraction of the static or steady state value; hence, the role of the viscous properties of the slide materials becomes more pronounced in controlling the slide velocity.

The next section describes the mechanisms of movement of slow shallow slides. This description includes the roles of pore pressure changes and the presence of weak materials on movement reactivation. The time dependent behaviour of cohesive soils is then reviewed.

2.2 Movement Re-activation of Slow Slides

Slow active shallow slides usually move on completely developed shear zones that represent a discontinuity in the vertical profile. However, a clearly defined rupture surface is sometimes not a prerequisite, for deformations become diffuse within thick shear zones (Picarelli and Russo, 2004). Seasonal pore pressure changes have usually been strongly correlated with the movement rates of slow slides whether shallow or deep, yet the contribution of these changes varies according to the depth of the rupture surface. In this section, a review of some of the previous studies that investigated the effects of pore pressure changes on movement rates is presented.

Ribacchi et al. (2004) discussed the Porta Cassia Slide as an example of a moderately thick slide in stiff clay where the velocity is dependant on pore pressure fluctuations. The movement accelerated when the cumulative rainfall over a period of two months exceeded the average value measured over the previous 50 years. The claimed dependence was, however, qualitative. Bertini et al. (1986) found that the movement of the Fosso San Martino slide stopped when the pore pressure dropped below a certain threshold value. The movement accelerated again following the pore pressure rise during wetter periods. Bertini et al. (1986) also observed that the pore pressure threshold above which the movement was re-activated was lower than the threshold of movement arrest. Figure 2-1 shows such an effect. This figure reveals that the threshold piezometric level that triggers movement corresponds to a stress level of 95%. This finding indicates a coupled effect of the creep along the slide plane and pore pressure variations (from Picarelli and Russo, 2004).

Picarelli and Russo (2004) offered an explanation for the presence of two thresholds for the piezometric level rise and drop. During the pore pressure rise, the stress level increased, and hence the primary creep strains rate also increased. This increase was contrasted by the decrease in the creep strains rate with the passage of time. During pore pressure drop, however, the two effects worked together to decrease the strain rate. Therefore, the displacement rate during a pore pressure rise was higher than the rate during a pore pressure drop. Similar results have been reported by Moore and Brundsen (1996). However, they attributed this difference in thresholds to changes in the pore water chemistry during the periods of rest. They further concluded that each reactivation required a larger pore pressure than the previous one. While Bertini et al. (1986) postulated that the threshold piezometric level that triggered the movement corresponded to a 95% stress level, Mandolini and Urciuoli (1999) found that this threshold corresponded to a stress level of only 70% (from Picarelli and Russo, 2004).

Angeli et al. (1996) found opposite results. They observed that the threshold for slide reactivation was higher than that for arrest. They attributed this difference to a gain in the residual strength that occurs during the periods of rest. However, Gibo et al. (2002) observed that the recovery of the shear strength occurs only for

soils containing large amounts of sand and silt at effective normal stresses less than 100kPa. For clayey soils, however, the recovery of the strength is negligible as the chances of strength gain due to aging become very weak with the particles completely aligned in the direction of shearing. Picarelli and Russo (2004) stated that the complexity of the conceptual model characterizing the slide movement in addition to the difficulty in measuring the pore pressures along the slide plane might have accounted for these discrepancies.

Musso and Provenzano (2004) found a direct relation between the reservoir impoundment and the movement rate. However, the velocity during the first filling was the highest when compared to successive fillings. The viscous properties of clay were considered the main cause of this behaviour. Creep properties could be investigated by examining the displacements during the periods of zero pore pressure change (from Picarelli and Russo, 2004).

Comegna et al. (2004) set up a simple numerical model to simulate the development of pore pressures as a result of an applied rainfall function. The case under investigation was a mudslide in highly fissured sheared clay shales. Although this study focused on mudslides, it is reviewed here to highlight the effect of the built-up pore pressures on the slide velocity. Comegna et al. (2004) found that in the first stage of mudslide movement, the pore pressures were characterized by high peaks sometimes exceeding the ground surface. However, just prior to stopping, fluctuations became more governed by the seasonal climatic conditions. Picarelli et al. (1995) stated that the different movement rates of different parts of the mudslide can create a kind of "undrained thrusting". Although the researchers observed a dependence of the first-time movement acceleration on the pore pressure rise, no quantitative correlation was derived. Long term pore pressures were found to follow the hydrologic conditions changes occurring at the ground surface. Comegna et al. (2004) modeled the problem numerically and found good agreement between the pore pressures predicted by the model and the actual values in the less active zones. For active areas or for areas subjected to high internal deformation, however, peaks of pore pressure were observed, and the model was unable to capture such peaks because of the continuous stress changes caused by the soil deformation that resulted in undrained thrusting. The researchers found also that if the permeability values were changed by one order of magnitude, the agreement would have been the worst. The results of this study imply that in earth slides, where the internal deformation is not relatively significant, pore pressure fluctuations due to boundary conditions changes can be successfully modeled provided reliable values of hydraulic conductivity are chosen. Figure 2-2 shows the comparison between the measured and the calculated pore pressures from the numerical model developed by Comegna et al. (2004) in both highly active and less active zones.

Russo et al. (2004) performed numerical analyses of the effect of the pore pressure rise in an infinite slope on the movement rate and the threshold pore

pressure required for movement reactivation. The landslide body was modeled once as elastic perfectly plastic, and then viscous effects were introduced. The slip surface was, however, modeled as elastic perfectly plastic since a significant portion of the movement was due to slippage rather than viscous behaviour. The rise in the ground water level caused a decrease in the normal stresses along the slide plane. This decrease continued until the shear strength fell below the shear stress. The resulting unbalanced force was transmitted as a compressive force through the landslide body. Since the lower part of the slope experienced a smaller increase in pore pressure as mentioned by Russo et al. (2004), the lower part of the slope acted as a constraint for the upper part, and global stability conditions were assured. The model responded similarly to the water level rise when a viscous soil model was introduced. When the viscous effects were absent and the water level was lowered, no change occurred to the total stress either on the slide plane or within the landslide body. Provided the soil shear strength along the slide plane increased as a result of lowering the ground water level, no re-mobilization was expected unless the previous value of the ground water level rise was surpassed. The elastic plastic model ended up with an unrealistic stress state far from the initial conditions after a cycle of water rise and lowering. However, introducing viscous effects in the landslide body caused a stress relaxation within the landslide body during ground water lowering with a progressive cancellation of the effect of the previous rising of the ground water table. Hence, the final stress state was quite close to the initial one, and the difference depended on the used viscous soil parameters and the elapsed time. The threshold pore pressure required for movement re-activation will be almost constant after cycles of ground water rising and lowering.

Eshraghian et al. (2005) identified the mechanics of six slow moving earth slides along the Thompson River valley in British Columbia. The bedrock at the site is overlain by three glacial sequences of lacustrine or glaciolacustrine silt and clay deposits separated by highly permeable sands and gravels with minor lenses of diamicton. Eshraghian et al. (2005) found that Thompson River levels were higher than average not only in active years but also during years that experienced no movement. They concluded that the period of time the river level stays high, rather than the high river level, has the dominating effect on triggering the movement. Therefore, they calculated the cumulative river level difference (CRLD) from the average river level. The active years showed higher CRLD. Eshraghian et al. (2005) plotted the maximum CRLD in every year together with the number of active slides against time, and they found a close correlation. More than one rupture surface was detected, and rupture surfaces were all located in the lacustrine silt and clay layers. The separating high conductivity layers acted as aquifers. The piezometers installed at various depths showed that artesian pressures were built up in these layers. On the other hand, the piezometers installed in the lacustrine clay layers showed the lowest response. The researchers noticed the absence of any artesian pressures near the slides' scarps. Hence, the scarp area was considered a recharge zone while the toe was a discharge area when the river level was the lowest. Eshraghian et al. (2005) postulated that when

the river level increases, water starts seeping towards the slide mass. The lower part of the lacustrine clay layer does not respond quickly to the river level increase and needs a relatively longer time to reach equilibrium than the upper part, which responds relatively briefly as it is overlain by another high permeability layer. However, if the river level stayed high for a long time, the pore pressure in the lower part of the lacustrine clay layer would reach an equilibrium state and might offset the artesian pressures that were already developed in the underlying high permeability layer. As long as the river level stays at its highest value, no movement reactivation occurs since the pressure exerted by the river on the slope toe will have a stabilizing effect and will resist any driving seepage forces initiated in the slide mass. When the river level drops, the destabilizing seepage forces that are formed inside the slide mass by the high pore pressures will not be resisted at the toe anymore, and the movement will be reactivated. The above understanding was confirmed by the strong correlation between the average pore pressure ratio (r_u) during drawdown and the movement rate.

Eshraghian et al. (2005) also highlighted the relative impact of slide retrogression and reactivation on movement rates. Retrogression that occurs on a larger time scale causes rapid to very rapid movements, while reactivation occurs as a response to seasonal hydrologic boundary condition changes. Movements caused by reactivation are usually slow to very slow. The slides under study moved very rapidly during the late 1800s and the early 1900s due to retrogression, but are currently moving slowly to very slowly due to pore pressure changes that cause reactivation. Cruden et al. (1993) suggested that a higher possibility of slide retrogression will occur if the average slope surface angle is higher than the residual friction angle of the rupture surface.

Eshraghian et al. (2007) reviewed 17 cases of reactivated translational slides where pore pressure changes along the rupture surface were considered responsible for movement reactivation. In the 17 studied cases, the pore pressure ratio (r_u) changes on the rupture surface were strongly correlated with the movement rate through a second degree polynomial function. If the curve is re-plotted between the square root of the movement rate and the pore pressure ratio, as shown in Figure 2-3, the correlation becomes a straight line. The ordinate intercept will be the pore pressure ratio corresponding to the onset of movement reactivation (r_{uo}). The slope of the straight line (δ) will indicate the movement acceleration behaviour; the higher the value, the lower the movement rate for the same change in the pore pressure ratio (r_u). As expected, the review showed that the onset of movement in the 17 cases corresponded to a safety factor of unity. However, no correlation could be found between the movement rate and the factor of safety. According to Eshraghian (2007), rainfall, river erosion and river level drawdown are responsible for the reactivation of about 70% of the reviewed slides.

Soe Moe et al. (2007) illustrated the mechanisms of movement of the forest heights park landslide. The rupture surface is seated in the Horse Canyon formation, Upper Cretaceous age. This formation consists of deltaic and fluvial deposits of sandstone, siltstone and clay shale, containing many coal and bentonite seams. The coal mining operations took place in the early 1900's. In the tertiary periods, preglacial sands and gravels were deposited on the preglacial valley walls. During the ice advance over the area afterwards, glacial till was deposited directly above the preglacial sands and gravels overlying the bedrock. Highly plastic lacustrine clay sediments were deposited in the glacial lake Edmonton during ice retreat on top of the glacial till. Long term piezometric readings had shown that the pore pressures in the bedrock were considerably lower and not related to the pore pressures in the overlying glacial deposits, which were changing in response to snow melt and rainfall. The low bedrock pore pressures were explained by the delayed vertical swelling of some of the North American rivers. In addition, the pore pressure in the bedrock was found to drop after a significant movement takes place in the spring. This drop was attributed to the dilation of the bedrock material in response to the slope movement.

The pore pressure changes in the glacial deposits caused the reactivation of the movement on the rupture surface of the forest heights park landslide. The first time failure, however, was thought to be partly due to the coal mining operations that caused weakening of the surficial bedrock and, hence, accelerated the propagation of cracks deeper into the bedrock. The formation of cracks allowed water to flow through and soften the bedrock. Moreover, the water in the cracks exerted lateral pressures during heavy rainfalls and helped to promote failure conditions. Bedrock softening and swelling in addition to the toe erosion caused by the river flow all worked together to trigger the movement.

The above review highlights the significant effect of pore pressure changes on movement reactivation. However, this profound effect is noticed predominantly in shallow or moderately thick slides. In deep-seated slides however, the contribution of pore pressure fluctuations effects to the total movement is less pronounced because the initial value of either the pore pressure or the total stress is quite high compared to the anticipated changes. An appreciable component of movement in deep-seated slides results from creep effects. These effects are also present in shallow slides, yet they are usually masked by the effects of the seasonal pore pressure fluctuations. A comprehensive review of the time dependent behaviour of fine geotechnical materials is presented in the next section.

2.3 Time Dependent Behaviour of Soils

2.3.1 Introduction

Terzaghi's theory of consolidation had related the void ratio to the logarithm of the effective stresses through an approximately bilinear relationship. However, the observed decrease in the void ratio under the application of constant effective stresses has highlighted the importance of considering the time effects in the constitutive modeling of soil behaviour, especially for problems of continued deformations with time under constant application of load as in landslides, the stand-up time of tunnels excavated in squeezing ground, the time dependent settlement of foundations after the dissipation of all excess pore pressures and the time dependent deformation of soft embankment foundations that may fail in creep rupture before the dissipation of excess pore pressures. Time dependent behaviour is complicated by the effects of different factors like soil type, soil structure, stress history, drainage conditions and type of loading (Singh and Mitchell, 1968; Kavazanjian and Mitchell, 1980; and Watts, 1981). Time effects include many phenomena like creep, stress relaxation, strain rate effects on the shearing strength and the long term strength of soils. All these phenomena except creep are briefly reviewed in the following subsections. In section 2.3.2, creep is reviewed in more detail as it accounts for most of the time dependent deformation encountered in the field.

Time was first introduced as an explicit, rather than implicit, parameter in the constitutive modeling of soil behaviour. However, due to the problem of defining an initial time for the time dependent response, models have been developed to express time implicitly in rate effects. In other words, the behaviour of the soil becomes dependent on the current stress and strain rate, and is independent of the past history (Suklje, 1957; and Leroueil et al., 1985). The time dependent deformation phenomenon is more pronounced in clayey soils, and, hence, this review is restricted to this type of geotechnical materials. Sand exhibits relatively large deformations only at high confining stresses because of grain crushing (Augustesen et al., 2004).

2.3.2 Creep

Creep is the time dependent deformation under a constant application of stress, exclusive of hydrodynamic effects (Watts, 1981). In the literature, creep has been generally investigated in the laboratory by using both the odometer and triaxial apparatuses. Creep deformations occur if the stress level is kept constant, and hence the strains continue to increase. The strain-time curve in a creep test in a triaxial apparatus is usually characterized by three stages: the primary, secondary and tertiary stages where the strain rate is observed to be decreasing, constant and

increasing until failure, respectively. The different creep stages are illustrated in Figure 2-4.

On the other hand, the time dependent deformation under a constant effective stress in an odometer test is characterized by three stages known as primary, secondary and tertiary compression. The primary stage is characterized by the dissipation of all the excess pore pressures and is known as the primary consolidation. Due to the continuous change in effective stresses during this stage, primary consolidation is not considered a creep process. The secondary compression is the secondary consolidation that occurs due to deformations in the soil skeleton, and, hence, it may be considered a true creep. Tertiary compression is also a creep process (Augustesen et al., 2004).

In Figure 2-4 and Figure 2-5, the logarithm of the strain rate-logarithm of time plots clearly show that strain acceleration cannot happen in creep tests in an odometer, and that the three stages of compression in an odometer test correspond to the primary stage in a triaxial test where the strain rate decreases with time according to a power law (Augustesen et al., 2004).

Three main approaches have been developed to account for creep deformations: the fundamental approach, the rheological approach and the phenomenological approach. The following subsections will briefly describe the three approaches.

2.3.2.1 The Fundamental Approach

The fundamental approach deals with the creep behaviour at the particle interaction level. The approach is sometimes called the micro-mechanistic approach. The approach can be categorized into three methods. The first one considers the secondary compression to be the result of the viscous nature of the adsorbed water. The viscosity of the adsorbed water is much higher than that of the pore water. Terzaghi (1931) postulated that after the end of the primary consolidation, the load is distributed between the grain-to-grain contacts and the adsorbed water. Secondary consolidation is considered to be the time dependent transfer of the load from the adsorbed water to the grain-to-grain contacts. As particles move together, the viscosity of the adsorbed water increases, and hence the load transfer occurs at a decreasing rate. Walker (1969) extended the previous work and concluded that the increase in the viscosity of the adsorbed water is counteracted by the increase in stress; hence, the creep rate is independent of the stress level.

The rate process theory is another fundamental approach to the explanation of the creep deformations. This theory is based on the assumption that every soil particle or molecule is kept in an equilibrium position due to the presence of energy barriers. A particle needs to acquire more energy than that of the energy barrier in order to move to a new position. When a shear stress is applied, the energy barriers are distorted, and the particles move in the direction of the distortion. The

equations that describe the soil deformation according to the theory contain too many parameters that are not easily determined from routine laboratory testing. Hence, the use of the rate process theory in practice to determine creep deformation is very limited (Watts, 1981).

De Josselin De Jong (1968) developed a new fundamental approach that models the soil pores as cavities with different compressibility interconnected with channels of different conductivity. The model was called the cavity channel network and was used to account for primary and secondary consolidation. The channels of high conductivity allow the dissipation of the excess pore pressure from the cavities during primary consolidation. Hence, the excess pore pressure in such pores goes to zero. However, the excess pore pressure in some cavities remains greater than zero because of the low conductivity of the connecting channels. The slow dissipation of this excess pore pressure gives rise to secondary consolidation.

The dependence of the fundamental models on micromechanical properties rendered them impractical, as the model parameters are not interpreted in terms of macromechanical properties such as stress, strain and time. The majority of the recent reviews on the time dependent behaviour of soils has excluded the fundamental models and focused on macromechanical approaches (Liingaard et al., 2004).

2.3.2.2 The Rheological Approach

Rheological models describe uniaxial conditions and account for the stress-strain-time behaviour of soil by modeling it as a group of springs, linear and non-linear dashpots and sliders. Springs account for the elastic soil behaviour, assumed to be mainly linear, by using either Young's modulus (E) or the Bulk modulus (K) as the stress strain operator. The dashpot characteristics are chosen in accordance with the rate process theory. The differences among the various rheological models are basically in the arrangement of their different components. The rheological models developed by Murayama and Shibata (1961), Christensen and Wu (1964), De Josselin De Jong (1968), and Abdel-Hady and Herrin (1966) are some of the well known rheological representations of the time dependent behaviour of soil.

Singh and Mitchell (1968) mentioned the following limitations of rheological models:

1. Too many parameters are required to characterize the strain rate behaviour.
2. Approximations in the governing equations are needed in order to model the true time dependent behaviour as depicted by other verified models.

2.3.2.3 The Phenomenological Approach

The phenomenological approach utilizes the results of laboratory testing to develop an empirical equation that describes the creep of the soil. Although the approach does not utilize theoretical procedures, its simplicity and wide application in many actual data records renders it the most practically applicable.

Singh and Mitchell (1968) developed a three-parameter phenomenological equation based on a wide range of experimental testing on many clay types having different stress histories. These researchers found that the primary creep stage could be described by a power law where the axial strain rate decreases linearly with time on a log-log plot. Moreover, the axial strain rate was found to increase exponentially with the deviatoric stress level. Hence, Singh and Mitchell (1968) proposed the following three-parameter phenomenological equation (Equation 2-1) describing the primary creep behaviour of a wide range of clays:

$$\dot{\varepsilon} = A * e^{\bar{\alpha}\bar{D}} * \left\{ \frac{t_i}{t} \right\}^m , \qquad 2\text{-}1$$

where

$\dot{\varepsilon}$ is the axial strain rate in triaxial testing; usually expressed in %/min,
A is the axial strain rate at initial time at zero deviatoric stress level (%/min or any relevant units of strain rate),
$\bar{\alpha}$ is the slope of the logarithm of the axial strain rate versus the deviatoric stress level relationship (unitless),
$\bar{D}$ is the deviatoric stress level (unitless),
t_i is the initial time (usually set to unity),
t is the time from the beginning of the primary creep (min), and
m is the slope of the axial strain rate versus time log-log plots and is constant for different deviatoric stress levels.

Equation 2-1 is a simple three-parameter equation that describes the primary creep behaviour of clay. The equation is valid irrespective of whether the clay is normally- or over-consolidated, disturbed or remolded, wet or dry, or drained or undrained. The equation is applicable for a range of stress levels from 30% to 90%. However, creep rupture may occur at stress levels as low as 60%. The parameter "A" is sought to be the initial and the maximum strain rate at zero stress level and unit time. It is a soil property that reflects composition, structure and stress history. The parameter "$\bar{\alpha}$" represents the stress level effect on the strain rate. The parameter "m" is representative of the deceleration of strains with time and is more or less constant within the same test. However, this parameter differs from one test to another depending on the soil type, stress history, drainage

conditions and composition. The value generally lies between 0.70 and 1.30 for geotechnical materials.

The inapplicability of the equation to stress levels less than 30% is probably due to the absence of any significant creep strains below that threshold. Terzaghi (1931) presented a qualitative description for this stress level limitation without defining certain limits. At the points of contacts between the grains where the spacing is less than 10^{-10} metres, that part of the film is called the solid film. It acquires a much higher viscosity than the adjacent inter-particle liquid, which has a relatively higher viscosity than that of the pore water as well. As shear stresses are applied, flow starts when the stress exceeds the bond resistance of that solid film. A further increase in the stress produces a slow viscous flow in the adjoining liquid parts of the film. Due to the high viscosity of this part of the film, the flow is very slow. As the intensity of the stress increases, the velocity also increases until the stress becomes higher than the adhesion between the films and the solid. This marks the onset of losing the shearing resistance, and the flow continues then at a constant rate (Terzaghi, 1931).

Despite the many advantages of the proposed equation, the model has the following limitations:

1. The equation describes only primary creep. It does not account for secondary or tertiary creep.
2. It is derived from laboratory triaxial creep testing. The main challenge when applying the equation to field conditions is the definition of an initial time, i.e., the time at which creep has started. This time is always set to unity in laboratory testing. However, Watts (1981) was able to obtain the Singh-Mitchell equation parameters for the field case, as will be detailed in Section 2.3.2.6.
3. The equation has been verified for the case of first time loading, i.e., samples are considered homogeneous when each is subjected to a different deviatoric stress level. A limited number of available homogeneous samples may force the tests to be carried out on the same sample at different stress levels. According to Singh and Mitchell (1968), attention should be paid to the effects of superposition. However, Wu et al. (1978) proved that the total strain under a particular stress increment appears to be insensitive to the stress history as long as zero time denotes the time of application of the last increment.
4. Most of the studies reported by Singh and Mitchell (1968) were for samples tested under relatively low confining stresses, which are normally encountered at small depths. The only exception was the two creep tests performed by Campanella (1965) on samples of dry Illite, which were subjected to a deviatoric stress of approximately 11MPa. However, these tests were carried out to investigate the effects of temperature and stress on the parameters of an equation developed according to the rate process theory. Therefore, it is prudent to investigate the validity of the Singh-Mitchell phenomenological equation at high confining stresses.

5. The model falls into the category of Empirical Models that are derived based on specific boundary and loading conditions. Hence, it may not be applicable to more complicated conditions (Liingaard et al., 2004).

2.3.2.4 General Constitutive Models of Soil Behaviour

Singh and Mitchell's (1968) equation calculates the axial strain rate as a function of the time and deviatoric stress level. The equation requires evaluating three parameters to determine the strain rate in addition to the value of the strain at a certain time to completely define the strain function. Since other components of creep deformation are present, a more general model that would overcome the main disadvantages of the previous approaches had to be developed. These disadvantages have been summarized by Tavenas et al. (1978):

1. Previous investigations separated the problems of stability, represented by strength tests, from the problems of settlement, represented by consolidation tests. Hence, creep tests, which are related to strength problems, have been separated from secondary consolidation tests, which are related to settlement problems.
2. Previous studies focused on either developing a theoretical rheological model or an empirical equation based on experimental testing. The results were seldom applied to field problems.

Kavazanjian and Mitchell (1980) developed a general constitutive model that could predict the time dependent behaviour of cohesive soil under an arbitrary three-dimensional state of stress. The model was enclosed in a framework of pseudo-linear elasticity where strains were related to stresses by tensor operators or secant moduli rather than an elastic modulus in linear elasticity.

The model considered the general case that both volumetric and deviatoric deformations occur. In undrained creep loading, for example, no volume change is allowed; hence, volumetric strains go to zero, and the total deformation is purely deviatoric. On the other side, during isotropic consolidation, the deviatoric stress level is zero; hence, the deviatoric strains will be zero, and all the deformations will be volumetric. Both volumetric and deviatoric strains are considered to be composed of an immediate in addition to a delayed component. This concept was first proposed by Bjerrum (1967) for the one-dimensional compression of clayey soils. He introduced the time dependent aspect of the one-dimensional compression of cohesive soils as a series of parallel lines or isochrones in the void ratio (e) versus the logarithm of effective stresses (log p') space. The slope of these isochrones is constant and equals the compression index (C_c). Each isochrone represents a constant duration of loading. Under the application of a constant effective stress, a point in the e-log p' space moves vertically downwards until it joins another isochrone corresponding to the duration of loading. Figure 2-6 shows the isochrones concept proposed by Bjerrum (1967). If the effective vertical stress increases at a certain loading duration, the point will move horizontally until it reaches the equilibrium load or

the instant compression line and then will move down the new isochrone. The value of the stress after which the void ratio starts to decrease after reloading is called the quasi-preconsolidation stress. This finding suggests that even normally consolidated aged clays acquire some preconsolidation when subjected to their overburden stresses for long periods of time. In addition to the effect of load duration or aging, structuration may lead to higher values of quasi-preconsolidation pressures. Berre and Bjerrum (1973) confirmed the concept of the quasi-preconsolidation pressure by carrying out laboratory experiments on two normally consolidated clays. They found a critical value of shear stress below which the soil deformation was relatively small. The corresponding vertical pressure was equal to the quasi-preconsolidation pressure.

The spacing between the isochrones in Bjerrum (1967) model is constant and represents the rate of decrease of the void ratio with time at a certain effective stress after the dissipation of all excess pore pressures, i.e., the coefficient of secondary consolidation C_α. After generalizing the one-dimensional case to the three-dimensional state of stress and introducing the effect of the deviatoric stresses, Kavazanjian and Mitchell (1980) replaced the vertical axis of Figure 2-6 by volumetric strains and the horizontal one by the mean (octahedral) stress. In order to overcome the problems of defining an initial time of loading, Suklje (1957) implicitly included time in the rate effects. The time dependent deformation behaviour was defined in terms of a family of curves in the void ratio-logarithm of the effective vertical stress space; each represents a constant value of the volumetric strain rate. These curves are named isotaches and are equivalent to the equal duration-of-loading curves proposed by Bjerrum (1967).

The isochrones shown in Figure 2-6 describe the delayed component of the volumetric deformation. The immediate component was introduced by Kavazanjian and Mitchell (1980) in a similar way. The isochrones of the constant deviatoric stress levels are parallel lines in the void ratio versus the logarithm of the effective stresses space, having the same slope, C_c, and are equidistant.

The general volumetric model proposed by Kavazanjian and Mitchell (1980) consisted of a series of parallel planes in the volumetric strain-logarithm of the effective octahedral stresses-logarithm of time space. Each plane corresponded to a certain value of the deviatoric stress level. In the volumetric strain-logarithm of the effective octahedral stress plane, an immediate increase in octahedral stresses will cause the point representing the stress state to move along a line with slope equal to the re-compression index, C_r, until the stress state reaches the quasi-preconsolidation pressure then moves down along the virgin line with slope C_c. Upon unloading, the point will move back up along a line of slope equal to the swelling index, C_s. In the volumetric strain-logarithm of time space, the parallel isochrones have a slope equal to the coefficient of secondary consolidation, C_α.

The deviatoric component of the strain was also viewed as the sum of the immediate and delayed components. The immediate deviatoric strain can be

represented by any relevant stress strain model. Kavazanjian and Mitchell (1980) chose the hyperbolic model to represent the immediate component. The delayed deviatoric deformations were represented in the Kavazanjian and Mitchell (1980) model by the Singh-Mitchell equation (Singh and Mitchell, 1968). The general deviatoric model proposed by Kavazanjian and Mitchell (1980) evaluates both the immediate and delayed deviatoric deformations as a function of the deviatoric stress level. The behaviour is illustrated in Figure 2-7. The immediate stress strain curve follows the hyperbolic trend. If a deviatoric increment is sustained for an extended time period, the axial strains will increase according to the delayed deviatoric deformation model. The increase in the axial strains is indicated by the horizontal line shown in Figure 2-7. If an unloading reloading cycle is applied, the modulus increases considerably. The unloading reloading modulus is considered to be equal to the initial tangent modulus. This behaviour indicates that cohesive soils develop an increased resistance to subsequent immediate deformations until the original hyperbolic stress strain curve is resumed (Kavazanjian and Mitchell, 1980).

The four described phenomenological models were put together into a numerical framework in order to predict the immediate and delayed deformations. The model was verified by comparison with the results of triaxial compression tests. The results showed an excellent agreement except in predicting the rate at which the pore pressures were generated during undrained creep. Kavazanjian and Mitchell (1980) suggested that either an inadequacy of the model itself or possible pore pressures diffusion through the rubber membrane during testing could have accounted for that discrepancy. The exact source of this discrepancy was not, however, clear.

Tavenas et al. (1978) studied the undrained and drained creep behaviours of undisturbed lightly overconsolidated sensitive clay in both triaxial and odometer apparatuses. The purpose of the study was to develop a general model that would account for the time or rate effects on the strength. An important consequence of the model proposed by Bjerrum (1967) is the increase in the value of the preconsolidation pressure with increased loading duration or loading rate. Bjerrum (1967) named this increase as the acquiring of the clay of a “reserve resistance” over time. The study by Tavenas et al. (1978) was preceded by an investigation by Tavenas and Leroueil (1977) to determine the characteristics of St-Alban clay at yielding. The results showed that the position of the elliptical yield locus in the stress space depended on the magnitude of the preconsolidation stress, and that its axis was the K_0 line. In contrast, in the Cam Clay model, the critical state surface axis is the isotropic consolidation line. This contrast was attributed by Tavenas and Leroueil (1977) to the mode of the clay deposition, which led to an anisotropic stress condition. Hence, the limit state surface of St-Alban clay was proved to be age and rate-dependent. Tavenas et al. (1978) aimed at extending the principle of “isotaches” defined by Suklje (1957) to the void ratio-deviatoric stress-mean effective stress space. Each isotach represents a constant value of strain rate and has the same shape as that of the limit state

surface of the clay. The stress conditions for the drained and undrained creep tests carried out by Tavenas et al. (1978) are illustrated in Figure 2-8. The stress condition indicated by point "0" refers to in-situ conditions. The logarithm of the volumetric strain rate in the triaxial drained tests was found to drop linearly with the logarithm of time. The slope of the curves, which should be equal to the creep parameter m, was around unity for low stress levels. This finding suggests that the strains were purely secondary, which is in accordance with the classical equation of secondary consolidation derived from odometer tests:

$$\dot{v} = \frac{C_\alpha}{1 + e_0} \cdot \frac{1}{t},$$

2-2

where

$\dot{v}$ is the volumetric strain rate,
C_α is the coefficient of secondary consolidation, and
e_0 is the initial void ratio.

However, for relatively high stress levels, the parameter m had values as low as 0.52 to 0.78. These results suggest the occurrence of primary consolidation. Figure 2-9 shows the results of the test. At deviatoric stresses of 41 up to 52.8kPa, the volumetric strain rate dropped to a minimum value after which the strains accelerated, marking the onset of failure. The subsequent decrease in the volumetric strain rate at a deviatoric stress of 47.3kPa was associated with a decrease in the applied stress as failure approached. However, the applied stress was kept constant in the σ_1'=41.0kPa case, and the instability was attributed to a change in the internal soil structure. This explanation is similar to that offered by Bishop and Lovenbury (1969).

Augustesen et al. (2004) explained that change in more detail. In the studies performed by Leroueil et al. (1985), the strain time response of overconsolidated clays tested in one-dimensional compression had shown a continuous decrease in the strain rate with the logarithm of time after the end of the primary consolidation. Normally consolidated clays show, however, a different response as shown in Figure 2-10. For samples subjected to a vertical stress slightly lower than the preconsolidation pressure, the strain rate decreases at a rate similar to that of the overconsolidated clay, and then the strain rate remains constant. Finally, it decreases in the same manner as that of the normally consolidated clays. The conclusion drawn in the one-dimensional case could be extended to the triaxial state of stress by considering the "limit state surface" to correspond to the preconsolidation pressure in the one-dimensional case. Therefore, the instability that appeared in the results of Tavenas et al. (1978) and Bishop and Lovenbury (1969) can be attributed to the transition from an overconsolidated to a normally consolidated creep state.

The general form of the volumetric strain rate function developed by Tavenas et al. (1978) took a similar form to that of the Singh-Mitchell equation (Singh and Mitchell, 1968). The equation takes the form

$$\dot{v} = \beta . e^{\alpha(t).p'} . \left\{ \frac{t_i}{t} \right\}^m ,$$

2-3

where

β is a constant determined by knowing the volumetric strain rate value at a certain time and a certain mean effective stress,
$\alpha(t)$ is the slope of the logarithm of volumetric strain rate versus the mean effective stress, and
p' is the mean effective stress $\left\{ \frac{\sigma'_1 + 2\sigma'_3}{3} \right\}$.

Tavenas et al. (1978) plotted the volumetric strain rates against time on a log-log plot for different stress conditions representing undrained and drained triaxial tests with constant and variable confining stresses, in addition to odometer tests. Figure 2-11 shows the plot. The volumetric strain rates at a time of 100 minutes have been plotted against the components of the stress field. Hence, the stress conditions producing equal volumetric strain rates have been connected together in the stress space to give isotaches of an equal volumetric strain rate. Figure 2-12 shows the isotaches together with the limit state surface of the clay.

Based on the above findings, Equation 2-3 can be generalized as:

$$\dot{v} = B . f(\sigma') . \left\{ \frac{t_i}{t} \right\}^m ,$$

2-4

where $f(\sigma')$ is a stress function represented by the equation of the set of the equal volumetric strain rate curves shown in Figure 2-12. The fact that these isotaches are homothetic to each other and to the limit state surface makes it possible to derive $f(\sigma')$ from the equation of the limit state surface. Moreover, these results imply that the limit state surface is itself a surface of an equal volumetric strain rate. The main difference between the isotaches developed by Bjerrum (1967) and Suklje (1957), and those by Tavenas et al. (1978) is that the former are applicable to only normally consolidated clays under one-dimensional stresses and should not be applied in the overconsolidated range.

Tavenas et al. (1978) extended the above work to the deviatoric component of strain. Although this component could be directly evaluated from undrained test results, where volumetric strains equal zero, the hard-to-prevent small leaks together with the high modulus of overconsolidated clays make it impossible to obtain reliable results from undrained tests after 4000 minutes testing time. Hence, the results of the drained tests were analyzed in terms of the axial strains and the axial strain rate. Tavenas et al. (1978) followed the same procedure as had been followed in the volumetric strains stage and ended up with constructing loci of equal axial strain rates in the stress space. Figure 2-13 shows the equal axial strain rate lines in the stress space for some drained tests. Tavenas et al. (1978) verified the Singh-Mitchell equation (Singh and Mitchell, 1968) except in the definition of the stress function in order to include the equal axial strain rate curves. The new equation takes the form

$$\dot{\varepsilon}_1 = A.h(\sigma').\left\{\frac{t_i}{t}\right\}^m ,$$

2-5

where

$\dot{\varepsilon}_1$ is the axial strain rate,
A is the axial strain rate at zero deviatoric stress at unit time, and
$h(\sigma')$ is the stress function represented by the family of curves in Figure 2-13.

In order to validate the concept of separating the volumetric and shear deformations, Tavenas et al. (1978) performed undrained creep tests for the same previous conditions, so that the resulting strains were purely shear. The shear strains values and trend from the undrained tests were compared with the shear strains calculated by subtracting one third of the volumetric strains from the axial strains of the drained tests. The excellent agreement verifies the concept of superposition proposed later by Kavazanjian and Mitchell (1980). This agreement supported expressing the deviatoric component in terms of the shear strain rate directly rather than by using the axial strain rate. The shear strain rate function takes the form

$$\dot{\varepsilon} = A.g(\sigma').\left\{\frac{t_i}{t}\right\}^m ,$$

2-6

where

$\dot{\varepsilon}$ is the shear strain rate determined either directly from the undrained creep tests or by knowing both the axial and volumetric strain rates from the drained tests, and
$g(\sigma')$ is the appropriate stress function represented by the family of curves in Figure 2-14.

Figure 2-12 and Figure 2-14 reveal that the limit state surface is a surface of an equal volumetric strain rate below the Mohr-Coulomb envelope and is a surface of equal shear strain rate above it.

2.3.2.5 Creep Rupture and Creep Rupture Life

Creep rupture is the failure of a sample tested under a constant applied stress at a strength lower than its normal strength determined from routine laboratory testing. The majority of the previous studies on creep rupture focused on undrained loading as the pore pressure rise-up during loading was thought to cause a progressive decrease in the effective stress, and, hence, the strength is reduced. However, some investigations (Bishop and Lovenbury, 1969; Finn and Snead, 1973; and Tavenas et al., 1978) proved the occurrence of strain acceleration in drained creep tests as well. The determination of the creep rupture life, or the remaining time to failure, is an important outcome of studying the creep rupture phenomenon. This subsection will present some of the previous work on creep rupture and creep rupture life both in undrained and drained conditions.

Campanella and Vaid (1974) studied the undrained creep rupture characteristics for undisturbed normally consolidated sensitive clay. Isotropic, K_0 consolidated triaxial tests and plane strain tests were carried out in order to assess the reliability of isotropic triaxial testing to simulate actual plane strain conditions. It was found that the isotropic consolidation testing had significantly overestimated the value of the creep rupture strain. The secondary creep stage was very short and, hence, was absent from the strain rate versus the logarithm of time plots. Figure 2-15 shows the axial creep rate versus time plots for different deviatoric stress levels. It is clear that creep rupture was initiated at stress levels as low as 51%.

The accumulated axial strains up to the minimum strain rate threshold were found to be independent of the creep stresses. However, the isotropic triaxial test greatly overestimated their values. Campanella and Vaid (1974) found also that the minimum axial strain rate was inversely proportional to the total creep rupture life on a log-log plot, as shown in Figure 2-16. The creep rupture life is the time period from the initiation of creep to creep rupture. Isotropic triaxial testing also predicted rupture lives four times higher than those of the other two stress states. However, due to differences in stress history, drainage control, type of tests and temperature, higher error percentages would result if such a correlation were generalized.

Since determining the total creep rupture time involves knowing the initial time of creep, which is not always available, Campanella and Vaid (1974) plotted the axial strain and the corresponding remaining time to failure after the minimum strain rate threshold was surpassed. Figure 2-17 shows the resulting relationship for the isotropic consolidation stress state.

The pore pressures developed near rupture were found to be dependent only on the magnitude of the axial strain and were not affected by the strain rate. Hence, the effective stresses at creep rupture fitted well with the Mohr failure envelope. Similar findings were reported by Vaid et al. (1979). The main conclusion to be drawn from the study of Campanella and Vaid (1974) is that the conventional isotropic triaxial testing leads to unconservative estimates of the creep rupture life and the accumulated strains corresponding to the minimum strain rates.

Mitchell (1976) attributed the noticeably low undrained "creep" strengths to the deterioration of the cemented bonds by creep strains. As well, Nelson and Thompson (1977) attributed the drop of the strength of overconsolidated clays from peak to residual partly to the long term equalization of the induced pore pressures and also partly to the role of the creep strains under sustained stresses in deteriorating the soil bonds. Finn and Snead (1973) proposed a method to calculate the maximum deviatoric stress below which no creep rupture will occur, which is called the upper yield strength. Their study presented an explanation of the discrepancy between the normal undrained strengths and the creep strengths. Characterization of a failure envelope at the rupture point was not possible because pore pressure equalization at high strain rates could not take place. Hence, Finn and Snead (1973) evaluated the creep rupture criteria based on the samples' behaviour at the minimum strain rate point. When connecting the minimum strain rate points, a clear correlation was developed between the logarithm of the minimum strain rate and the logarithm of time for the type of clay under investigation. The correlation was the same for the undrained creep tests carried out on normally and overconsolidated clay as well as for the drained tests. Finn and Snead (1973) calculated the total rupture life from their tests and other tests and found a strong correlation with the minimum strain rate. The upper yield strength could then be determined either by performing at least two undrained creep tests at two different deviatoric stress levels and plotting the cubic root of the minimum strain rate against the deviatoric stress, or by performing two constant rate of strain tests at strain rates sufficiently low to allow for pore pressure equalization and plotting the strength against the cubic root of the strain rate. Figure 2-18 shows the results of the undrained triaxial creep tests and the constant rate of strain tests performed to determine the upper yield strength.

Campanella and Vaid (1974) and Vaid et al. (1979) obtained similar relationships. It follows, then, that the high undrained strengths obtained in normal triaxial tests were due to the application of high strain rates, which did not allow for the complete equalization of the developed pore pressure. Another explanation offered by Nelson and Thompson (1977) is the accumulation of plastic strains due to creep over a longer time at slower rates; hence, more bonds are destroyed, and the strength drops.

The problem of undrained creep rupture is usually associated with relatively high deviatoric stress levels where the creep strains are expected to accelerate after reaching a minimum value. At low stress levels, however, the creep strains may stop or continue at an imperceptible rate (Campanella and Vaid, 1974). Vaid et al. (1979) found that the pore pressure decreased rapidly at the onset of the creep strain acceleration, and, hence, the effective stress increased. This finding seems contradictory to the well known explanation of undrained creep rupture. According to that explanation, rupture occurs due to a decrease in the effective stress and, hence, strength. Moreover, Finn and Snead (1973) found that the period of time when the majority of the pore pressure increase occurred corresponded to a decreasing strain rate. The pore pressure during the transient strain rate period experienced neither a change in curvature nor a noticeable discontinuity. This finding confirms the conclusion of Vaid et al. (1979) that undrained creep rupture due to an increase in the pore pressure at the failure point cannot be a reasonable explanation for the creep rupture phenomenon.

Saito (1965) performed full scale experiments in the field in order to forecast the time to failure by sprinkling water on the slopes under study. The records of the strain, inclination, earth pressure and moisture contents were plotted against time. The monitoring with time of each of these variables showed that the strain and inclination could be considered as forecasting factors, yet the strain was superior to the inclination. Saito (1965) compared the actual records with a creep rupture formula derived from laboratory experiments and concluded that this formula was independent of the soil type or the testing method. In addition to performing full scale experiments, Saito utilized the results of many actual case histories of slope failures. His methodology involved recording the displacement with time curves, then calculating the constant strain rate that best represented the slope of the displacement time curve before movement acceleration occurred. The constant strain rate together with the creep rupture life was then plotted along with the equation derived from the laboratory. A good match was achieved in most cases.

Not enough attention had been paid to the issue of strain acceleration accompanied by high deviatoric stress levels and extended testing times under drained conditions. This problem might have been due to the understanding that drained loading acquires the soil more strength over time. Campanella and Vaid (1974) stated that if creep rupture is a possibility, then it is most likely to happen before drainage can strengthen the soil. Campanella and Vaid did not eliminate the possibility of having drained creep strain acceleration, but their statement implies that undrained creep rupture will happen faster. Bishop and Lovenbury (1969) showed that drained creep strain rates may deviate from the linear relation with the logarithm of time at extended testing times (more than 100 days). In addition, the results by Nelson and Thompson (1977) stated that bonds start to deteriorate with continued creep strains resulting from sustained loading. Therefore, in problems involving purely drained creep movements, evaluating the creep rupture life by using undrained tests will yield much lower values than the actual ones.

Bishop and Lovenbury (1969) performed drained triaxial creep tests on undisturbed overconsolidated London Clay and normally consolidated Pancone Clay, with tests durations of up to three and half years. Both clays have similar physical properties and clay content, yet the liquidity index of London clay approached zero and was a bit less than half for Pancone clay. Bishop and Lovenbury (1969) concluded that there appears to be no limiting value of the stress level below which no creep can occur; i.e., creep deformation occurs at all stress levels. Secondary creep was absent from the axial strain rate versus time curves. The researchers noticed the development of some instability in the axial strain rate versus time curves after about 90 to 100 days of testing for the undisturbed London Clay with the vertical stress increasing and the horizontal one constant. It was found that such instabilities were always accompanied by a reduction in the volume although those samples generally showed a dilatational behaviour. Another group of London Clay samples was tested by keeping the vertical stress constant and decreasing the confining stress. The development of the instabilities associated with volume reduction was noticed as well, but these instabilities were less regular than the previous ones. For the normally consolidated Pancone Clay samples (Figure 2-19), the instabilities appeared at testing times that ranged between 20 and 100 days. Obviously, normally consolidated clay exhibited a contractile behaviour whether at the time of the instability or not. Such instabilities were localized at a certain time. Afterwards, the expected trend of a decreasing strain rate with time resumed. Such instabilities were attributed to a modification in the soil structure.

Bishop and Lovenbury (1969) presented a simple way of calculating the expected life of samples under drained loading before strain acceleration occurs. Initially, a conventional drained test was performed, and the time to failure was recorded. For example, for a London Clay sample, the time to failure in the conventional drained test with vertical stress increasing was 5 days. This time corresponded to a 100% stress level. While performing the creep tests, the researchers found that for London Clay under a stress level of 89%, no failure occurred until after 1000 days. They assumed then that a drop of 11% occurred in the peak strength for a logarithmic increase in the testing time from 5 to 1000 days. Hence, a drop of 4.8% in the peak strength would occur for a tenfold increase in the testing time. The Pancone samples reached their peak strength in the conventional drained tests in 8 days. Therefore, the life of the 85% stress level would have been approximately $8X10^3$ days (~22 years).

The possibility of the creep rupture occurrence during drained tests was shown to be valid by Tavenas et al. (1978) in the same study mentioned above. Figure 2-20 shows accelerated strain rates up to failure under triaxial conditions in drained tests.

2.3.2.6 Creep Behaviour in the Field

The majority of the studies mentioned above, except for Saito's (1965), although performed on undisturbed natural samples, dealt with the creep behaviour in the laboratory. In fact, relatively few studies have dealt with the creep behaviour in the field based on actual readings of field instruments. The comprehensive review by Augustesen et al. (2004) on the time dependent deformation of clays and sands did not consider as well the in-situ behaviour. This subsection presents some of the comprehensive studies of the field creep behaviour.

Foss (1969) analyzed the settlement variation with time for a group of three buildings resting on clay. The clay was considered to be aged, and the apparent preconsolidation pressure was due to secondary consolidation as there were no signs of overconsolidation due to any geological process. In addition, the settlement resulting from stresses lower than the preconsolidation pressure was higher than what would have resulted from overconsolidated clay. It was concluded that under the effect of the overburden pressure for a period of 3000 years, time dependent secondary compression had taken place, and, hence, the state point in the void ratio-logarithm of the vertical stress space would lie on the 3000 years isochrone.

Watts (1981) analyzed the time dependent deformations of the clay foundation of the Syncrude tailings dyke near Fort McMurray in Alberta. The general stratigraphic sequence in the area consists of recent deposits overlying Pleistocene glacial deposits that rest on Cretaceous Clearwater and McMurray formations. The underlying layer is Devonian limestone. However, the meandering Athabasca River at the site eroded all the Pleistocene and Cretaceous sediments, and, hence, the Devonian limestone is overlain by sand underlying a recent deposit of silt and clay (termed Tar Island Clay hereafter). The very top layer is a tailings sand layer. The layer under creep study is the Tar Island Clay layer.

This layer consisted of 20% sand, 63% silt and 17% clay. The liquid limit of the deposit varied from 24 to 65%, and the plasticity index from 4 to 37%. The undrained strength ratio to the effective stress was 0.45. Several inclinometers and piezometers were installed and monitored over a period of four years. The piezometric results indicated the dissipation of all the excess pore pressures during the time of monitoring. The lateral compression was calculated and was found to be of negligible value. Hence, the movements were believed to result from a drained creep mechanism.

The study involved two main sections: laboratory and in-situ creep behaviours. Drained creep tests were performed in the odometer and the triaxial apparatuses. The isotropic behaviour of the samples was investigated by testing vertical samples as well as samples taken at 45^0. The results showed that the drained creep behaviour in the laboratory was isotropic and conformed well to the Singh-Mitchell equation (Singh and Mitchell, 1968). The average values of the creep parameters were A = 0.18 %/min, $\bar{\alpha}$=3.00 and m = 1.13. The shear strength tests

revealed an effective angle of shearing resistance of 24^0 and a zero cohesion intercept.

The study of the field creep behaviour by Watts (1981) did not deal with the whole study area as a complex boundary value problem as doing so would have required using a complex finite element code. Watts considered the boundary conditions in the immediate vicinity of the inclinometer as uniform and quasi-static. The creep tensor in general can be decomposed into volumetric and deviatoric components, as mentioned above. Since the lateral consolidation in that problem was of negligible value, the volumetric deformation could be considered equal to the vertical settlement. Since no instrumentation was available to calculate the vertical settlement, only the deviatoric component of the creep was analyzed. Based on the outcome of the laboratory testing program, the in-situ creep deformations were assumed to obey the Singh-Mitchell equation but in a modified form due to the difference in the stress state between the field and the laboratory. The stress state in the field of the Tar Island Clay was simple shear evidenced by the rotation of the principal stresses by approximately 45^0. Hence, the horizontal and maximum shear stresses were equal. As the shear stresses are carried by the soil skeleton and do not depend on pore pressures, a simple total stress analysis was carried out to properly evaluate the in-situ shear stresses. Odqvist (1966) derived a general multi-axial equation relating the strain rate tensor to the deviatoric stress tensor. For the stress state of pure shear, Watts (1981) cast the general equation into a modified form represented by the following equation:

$$\dot{\gamma}_{xy} = A_s . e^{\bar{\alpha}_s \bar{D}} . \left\{ \frac{t_i}{t} \right\}^m ,$$

$$\bar{D} = \frac{\tau_h}{\sigma'_v . \tan\varphi'} ,$$

2-7

where

$\dot{\gamma}_{xy}$ is the shear strain rate as a function of time and shear stress level,

A_s is the shear strain rate at zero shear stress level and initial time,

$\bar{\alpha}_s$ is the slope of the logarithm of shear strain rate versus the shear stress level,

$\bar{D}$ is the shear stress level,

τ_h is the horizontal shear stress,

σ'_v is the effective vertical stress,

φ' is the effective angle of shearing resistance,

t_i is the time from the initiation of creep to the start of inclinometer readings (does NOT equal unity in field analysis), and

m is the slope of the shear strain rate versus time plot on a log-log scale.

The evaluation of the different parameters of the field creep equation (Equation 2-7) was done by first transforming the movement versus the depth plots resulting from the inclinometer readings into plots of shear strain versus depth by differentiating the movement with respect to depth. The resulting curves were then transformed into shear strain versus time curves at different depths. A sample of such plots by Watts (1981) is shown in Figure 2-21.

The shear strain-time plots were then converted to plots of shear strain rate versus time. At every depth, the horizontal shear stress τ_h was determined from the total stress analysis. By knowing the depth and the effective angle of shearing resistance, the shear stress level $\bar{D}$ could be evaluated at every depth. The time t_i was not taken to be equal to unity as in the laboratory creep testing because the time since the start of the creep was not known. Hence, the quantity t_i was considered the time from the start of the creep deformations until the time the field movements recording started. Therefore, at the beginning of the movement monitoring using inclinometers, Equation 2-7 could be expressed as $\dot{\gamma}_{xy} = A_s.e^{\bar{\alpha}_s \bar{D}}$ because $t=t_i$.

The shear strain rates at any two depths at the beginning of the inclinometer monitoring were calculated from the field results. The parameter $\bar{\alpha}_s$ was calculated from the following equation by knowing the shear stress level:

$$\bar{\alpha}_s = \frac{\ln \dot{\gamma}_1 - \ln \dot{\gamma}_2}{\bar{D}_1 - \bar{D}_2},$$

2-8

where

$\dot{\gamma}_1, \dot{\gamma}_2$ are the field shear strain rates at two chosen depths at the beginning of the monitoring, and

$\bar{D}_1, \bar{D}_2$ are the corresponding shear stress levels.

The value of the parameter $\bar{\alpha}_s$ was found to be 5.1. Since the field creep equation at $t=t_i$ takes the form $\dot{\gamma}_{xy} = A_s.e^{\bar{\alpha}_s \bar{D}}$, and by knowing the value of the parameter $\bar{\alpha}_s$, the value of the parameter A_s can be determined by inserting the value of the shear strain rate at any depth together with the corresponding shear stress level. Watts (1981) assumed the value of the parameter m to be equal to 1 on average in

order to have simple calculations for the initial time t_i. The first estimate values of t_i were found to range between 100,000 and 300,000 minutes (70 to 210 days) by assuming that m was equal to one. In order to calculate reasonable values of t_i, the shear strain rate equation was integrated to obtain two expressions for the shear strain function for values of m equal to unity and otherwise. Values of the parameter m in the range between 0.7 and 1.3 were tried as this should be the range of this parameter for most soils, as reported by Singh and Mitchell (1968). The value of t_i was found to be approximately 3.5 years for the Tar Island Clay by applying the resulting strain functions at various depths and bearing in mind that the initial time t_i should be the same for all depths, and that the calculated strains should match the actual values. Watts (1981) commented that this value seemed reasonable based on the construction history of the tailings dyke. The procedure was further verified by comparing the predicted shear strain values from the equation based on this value of t_i. The comparison showed a good match and is shown in Figure 2-22.

The values of the in-situ shear strains were also compared to the laboratory equation for predicting creep strain rates (Singh and Mitchell, 1968). The strains calculated from the Singh-Mitchell equation were much lower than the field values. This difference was primarily due to the change in the stress state in the laboratory and the field.

Morsy (1994) extended the study by Watts (1981) of the time dependent creep movements of the Tar Island Clay foundation of the tailings dyke to account for complex boundary conditions. The constitutive behaviour of the Tar Island Clay layer was described by using a stress-strain-time model. The finite element code PISA developed at the University of Alberta (Chan and Morgenstern, 1992) was used in the analysis.

The model developed by Morsy (1994) can be categorized as a general stress-strain-time model. Such models are given in an incremental form and hence are suitable for finite element coding. These models suit any boundary conditions; hence, any stress path can be simulated. The same concept of separating the deformations into volumetric and deviatoric components was adopted, and each component was further split into immediate and deviatoric. The volumetric component was calculated according to the model proposed by Bjerrum (1967) as detailed above. The immediate deviatoric component was represented by a hyperbolic model. The delayed deviatoric component was represented by the Singh-Mitchell equation (Singh and Mitchell, 1968).

Wu et al. (1978) analyzed the displacements-time history of an excavation of a cut near Cleveland. Triaxial, plane strain and simple shear, isotropic and anisotropic, drained creep tests were carried out in the laboratory. The researchers developed a stress-strain-time law based on the results of the laboratory tests. The equations were used to calculate the field displacements, and the computed displacements were compared with the actual performance. The laboratory results

fitted to an equation similar to the Singh-Mitchell (1968) equation and indicated the insensitivity of the creep strains to previous loading. The results also highlighted the relatively insignificant effect of anisotropy and the stress state on the creep strains if compared to the natural variations between different samples. The constitutive equation used in the computations was based on the Mohr Coulomb criterion. The field instrumentation included slope indicators and piezometers. Piezometric readings showed very little change over time, which suggested that the loading conditions were drained. Although the actual final displacements agreed with the computed values, the computed creep rate was considerably smaller. Wu et al. (1978) attributed this result to the irregular construction schedule, which precluded the determination of the creep at short times, in addition to the difficulty of representing the excavation geometry by a two-dimensional model.

2.3.3 Rate Effects

Vaid et al. (1979) studied the strain rate behaviour of heavily overconsolidated naturally cemented clay. Usually, the design preconsolidation pressure and the strength derived from laboratory testing under high loading rates are higher than the actual values under the natural slow loading rates in the field. One-dimensional consolidation tests were carried out at various constant rates of strain in addition to undrained triaxial constant rate of strain and creep tests. The tested clays are known to have very high sensitivity (~100) due to the existing cementing bonds and due to leaching by fresh water. The natural moisture content is higher than the liquid limit. The consolidation tests carried out at different rates of strain showed a marked dependence of the preconsolidation stress on the rate of loading. A 50% increase occurred in the value of the preconsolidation stress for two orders of magnitude of rise in the strain rate. The results of the undrained constant rate of strain tests showed a 25-28% increase in the peak deviatoric stress for a 100 times increase in the strain rate. The peak strengths of the samples were derived mainly from cementation and proved to be strain-rate-dependent. The different resulting peak and ultimate strengths (ultimate strengths correspond to axial strains > 3%) fitted to the same linear well known Mohr-Coulomb failure envelope, irrespective of the applied strain rates.

Leroueil et al. (1985) aimed at developing a rheological model that would introduce the time effects in an elaborate way. Constant rate of strain tests, constant gradient tests, multiple stage loading tests and creep tests were carried out in the odometer apparatus. Hence, the results were applicable to the volumetric strains or settlement calculations. The increments of constant stress in the creep tests lasted for more than 70 days. The tested clays were normally consolidated and had a sensitivity of more than 15, as is usual in eastern Canadian clays due to the effect of leaching. The moisture contents were higher than the liquid limits, and the plasticity index values ranged between 19 and 43%. The constant rate of strain tests showed that the effective stresses increased with

increasing the strain rate except for very slow rates ($1.7X10^{-8}$ s^{-1}). The effective stress was plotted against the corresponding strain rate at strains of 5, 10, 15 and 20% for both the constant rate of strain and the creep tests. The results showed a well defined correlation that was independent of the type of the test. Since the effective stress rate has a positive value in the constant rate of strain tests while it equals zero in creep tests, it was concluded that the effective stress rate had no influence on the rheological behaviour of clays. An important consequence of this conclusion is that the rheological behaviour of clays can be represented by a stress-strain-strain rate relationship without encountering the effective stress rate effects. The preconsolidation pressure was found to have a similar unique relationship with the strain rate irrespective of the type of the test. Special constant rate of strain tests were carried out by varying the strain rate within the same test. By acquiring data from many types of clay in eastern Canada, the researchers confirmed that there exists a unique stress-strain-strain rate relationship that is independent of the rate of the effective stress change. This unique relation is called "isotach behaviour" (Augustesen et al., 2004). The relation was described by two curves, one representing the change of the preconsolidation pressure with the strain rate and the other being a normalized effective stress strain relationship where the stress was normalized to the value of the preconsolidation pressure associated with the corresponding strain rate value. While the first relationship proved to be the same for all the clay types tested, the second one varied from a clay type to another within a narrow range. Figure 2-23 illustrates the isotach behaviour.

This unique relationship was valid for up to 23% strains. Beyond this strain value, minor differences in the specimen characteristics and composition had a profound effect on its rheological behaviour. The unique relationship did not hold as well at very high strain rates where pore pressures were as high as 90% of the applied vertical stress. No clear justification was presented by Leroueil et al. (1985) for this result. According to Finn and Snead (1973), Campanella and Vaid (1974) and Vaid et al. (1979), the application of very high strain rates does not allow for pore pressure equalization, and, hence, the results do not follow the expected trend. On the other hand, when applying a very low strain rate (slower than $1X10^{-7}$ s^{-1}), aging and structuration effects appear to account for any additional increase in stiffness. In such a case, the stress-strain-strain rate relationship cannot be described by isotach behaviour (Augustesen et al., 2004).

Another limitation of the model proposed by Leroueil et al. (1985) is that it was based on tests on normally consolidated clays. Since elastic strains are significant in the heavily overconsolidated range, the model is expected to give poor predictions of the time dependent behaviour of overconsolidated clays (Liingaard et al., 2004).

The dependency of the preconsolidation pressure on the strain rate in the one-dimensional tests depicted by Leroueil et al. (1985) can be extended to account for the strain rate dependency of the strength in the triaxial stress conditions. As

pointed out above, the limit state surface is the transition between the overconsolidated and the normally consolidated spaces and corresponds to the preconsolidation stress in one-dimensional compression. Tavenas and Leroueil (1977) plotted the yield points for many undrained and drained triaxial tests in the stress space (Figure 2-24). The plot shows that the upper part of the yield locus (the peak strength envelope) coincides with the limit state surface in the overconsolidated range. The strength envelope in the normally consolidated range coincides with the critical state line.

Therefore, the limit state surface in the overconsolidated range will expand or contract according to the applied strain rate in a way similar to the variation of the preconsolidation pressure with the strain rate for the one-dimensional conditions. In the normally consolidated range, however, the position of the critical state line is independent of the applied strain rate.

Wedage (1995) studied the rate effects on the residual shear strength of presheared clays in the foundation of the Syncrude tailings dyke in Fort McMurray, with the aim of developing a complete constitutive deformation-rate-dependent model. A number of researchers had proposed relationships between the residual strength and the velocity or strain rate, and a linear relationship appears to exist between the logarithm of the shear strain rate and the residual strength. However, none of the previous studies developed a constitutive strain rate dependent model.

Wedage (1995) carried out a laboratory testing program on samples from the Clearwater clay shale beneath the Syncrude Tailings dyke. Both direct and ring shear tests were carried out although the researcher pointed out the relative merits of using the ring shear apparatus over the direct shear one. The main advantage of the ring shear apparatus is that the sample is sheared continuously in one direction, which allows for a complete orientation of the clay particles. The residual shear strength resulting from the direct shear test is generally higher than that from the ring shear apparatus. The constant cross-sectional area of the specimen during shearing is another added advantage of the ring shear apparatus. Moreover, the ring shear apparatus, in fact, tests a thin annular specimen. This allows for the dissipation of any developed pore pressures even under the application of high strain rates.

Wedage (1995) mentioned that the minimum and maximum field displacement rates range from 0.027 mm/day to 1000 mm/day, respectively. However, the variation of the residual strength for displacement rates less than 0.002 – 0.01mm/min in the laboratory was found to be negligible according to Skempton (1985). Moreover, very slow rate tests are time consuming. Consequently, 0.2mm/day was chosen as the minimum laboratory deformation rate. The variation of the coefficient of friction with the shear strain rate as resulting from both the direct shear and the ring shear apparatuses is illustrated in Figure 2-25. Direct shear tests gave higher residual strength values, perhaps due to the

disturbance that occurred during the reversal cycles. The results indicate that there was a 3.4 – 3.5% increase in the residual strength for a tenfold increase in the shear strain rate. Wedage (1995) considered that the static friction angle would correspond to a minimum strain rate of 0.001 day^{-1} and, hence, would be equal to 6.6^0 based on the ring shear apparatus results and 7.5^0 based on the direct shear apparatus results. Therefore, the outcome of the laboratory testing program was a simple equation relating the coefficient of friction to the shear strain rate through constants representing the minimum strain rate and the static friction coefficient. Wedage (1995) also reported a rough correlation between each of the liquid limit and plasticity index and the percentage of increase in the residual strength for an order of magnitude increase in the shear strain rate. The reported correlation was based on the researcher's experimental results as well as some previous studies. The number of data points was, however, limited, and a firm conclusion could not be drawn.

The classical plasticity theory was extended by Wedage (1995) to describe the behaviour of a clay material with a strain rate dependent residual strength by using the concept of the dynamic yield surface. The developed empirical equation was incorporated into the existing finite element program PISA (Chan and Morgenstern, 1992). The numerical model was used to simulate the continued movements with time of the Clearwater formation beneath the Syncrude tailings dyke, the movements of the Mam Tor landslide in UK and the movements of the clay foundation of a test embankment in an unstable slope in Salledes, France. The comparison of the numerical analyses results with actual measurements showed that the developed model could predict the magnitude of the field velocities and their trends over time to a reasonable accuracy.

Gibson and Henkel (1954) conducted triaxial and direct shear tests to calculate the required tests duration in the so-called "drained" tests, so the amount of the undissipated pore pressures could be neglected. The rationale for doing so was that a true drained strength would result from testing rates that are infinitely slow. The undissipated pore pressures in the slowest possible "drained" tests were measured and compared to the value of the undissipated pore pressures in an undrained test. The results of the triaxial testing showed that the undissipated pore pressure rose up to a maximum value slightly before the maximum deviatoric stress was attained and then dropped afterwards. A conservative estimate of the undissipated pore pressure at failure would be equal to that maximum value. The results were finally presented in the form of an equation that gives the required testing time to failure in order to achieve a certain degree of consolidation. Obviously, a degree of consolidation of 100% would correspond to an infinite time to failure. However, the actual experimental results showed that for extremely slow rates of loading, the opposing effects of the structural viscosity worked to decrease the strength by a value more than what was gained by the dissipation of the remaining excess pore pressure.

2.3.4 Stress Relaxation

Stress relaxation is the continuous decrease in the stress when the strains are kept constant. Stress relaxation occurs, for example, when a sample in a direct shear apparatus is left for some time after the maximum reach is achieved. Therefore, the shear deformation, and, hence, the shear strain is constant. It is observed that the stress continues to decrease.

Very few stress relaxation studies are available either for clays and sands, or one-dimensional and triaxial compression tests. One-dimensional relaxation tests on frozen sand were carried out by Ladanyi and Benyamina (1995). As the time dependent behaviour of sands is beyond the scope of this thesis, no summary of this study is provided.

Lacerda and Houston (1973) carried out some relaxation tests by keeping the strain constant after loading under a certain strain rate. It was found that the deviatoric stress started dropping with the logarithm of time after a period of time called the delay time. Hence, the stress relaxation phenomenon could be mathematically represented by a simple equation. As a strong evidence that each of the stress relaxation, creep and rate effects are basically the same phenomenon, the mathematical equation describing the stress relaxation could be easily derived from the simple three-parameter Singh-Mitchell equation (see Equations 2-9 and 2-10). A schematic representation of the variation of the deviatoric stress with time in a stress relaxation test is illustrated in Figure 2-26, which reveals that as the value of the strain rate before starting the relaxation test increases, the value of the delay time decreases. Lacerda and Houston (1973) derived the following equation from their study:

$$\frac{\bar{q}}{\bar{q}_0} = 1 - s \log\left\{\frac{t}{t_0}\right\},$$

2-9

where

$\bar{q}$ is the deviatoric stress level at any time t,

$\bar{q}_0$ is the deviatoric stress level at the beginning of the stress relaxation,

t_0 is the delay time or the time since the application of a constant strain to the beginning of the deviatoric stress relaxation, and

s is the slope of the deviatoric stress-logarithm of time relationship and is related to the Singh Mitchell equation parameters as follows:

$$s = \frac{2.3\,(1 - m)}{\bar{q}_0 \,.\, \bar{\alpha}} \quad .$$

2-10

Although Lacerda and Houston (1973) carried out their tests in undrained conditions, the variation of the excess pore pressures during the relaxation phase was practically zero. The model is limited to one-dimensional conditions since Equation 2-9 and Equation 2-10 are derived from the uniaxial Singh-Mitchell equation. The main drawback in Lacerda and Houston's (1973) model, however, is its inability to define a final relaxed value for the deviatoric stress. The equation implies non-fading stress relaxation behaviour. Prevost (1976) overcame this drawback by developing a phenomenological approach that describes the stress relaxation behaviour of saturated clays under undrained conditions. According to his equation, the deviatoric stress drops non-linearly with the logarithm of time. Moreover, the deviatoric stress drops to a minimum value or a final relaxed state when time goes to infinity.

2.4 Summary

The extensive review provided in this chapter is summarized in the following main points:

1. Pore pressure changes have a marked effect on the movement reactivation of slow earth slides. The reviewed cases show that small changes in piezometric elevations may cause significant increases in movement rates. Groundwater pressures generally respond to hydrological boundary conditions changes.
2. The component of movement triggered by pore pressure changes is usually called the seasonal component. Since the movement persists during periods of zero pore pressure changes, creep deformations also contribute to the total movement. The creep contribution is relatively lower in shallow and moderately thick slides than in deep-seated slides.
3. Phenomenological approaches to the evaluation of the creep deformations are widely used although they are derived from empirical equations due to their simplicity and applicability to a wide range of soil types and loading conditions. The phenomenological three-parameter equation developed by Singh and Mitchell (1968) is an example.
4. Undrained creep testing cause the soil to fail at strengths lower than the normal undrained strengths. The high normal undrained shear strengths are attributed to the high strain rates applied in the routine laboratory tests. On the other hand, the low undrained creep strengths may be attributed to the accumulation of plastic strains due to creep over a longer time at slower rates; hence, more bonds are destroyed, and the strength drops.

5. Undrained creep rupture due to an increase in the pore pressure at the failure point cannot be a reasonable explanation for the creep rupture phenomenon.
6. Strain acceleration takes place also in drained creep tests. However, the instability is transient and is followed by a strain rate decrease stage.
7. The majority of the creep studies in the literature were carried out in the laboratory, and, hence, the governing equations were based on the stress states applied in the laboratory. Few studies investigated the field creep behaviour.
8. The rheological behaviour of clays can be represented by a unique stress-strain-strain rate relationship, which is independent of the effective stress rate. The unique relationship is denoted "isotach behaviour".
9. The residual shear strengths of clays increase at higher applied strain or displacement rates.

The study of the mechanics of the landslides movement enables a reliable evaluation of the hazard associated with the movement. Hazards evaluation is one of two components of landslide risk. The other component is the vulnerability or the consequences of the landslide movement. The vulnerability to slow moving slides is investigated in detail in the next chapter.

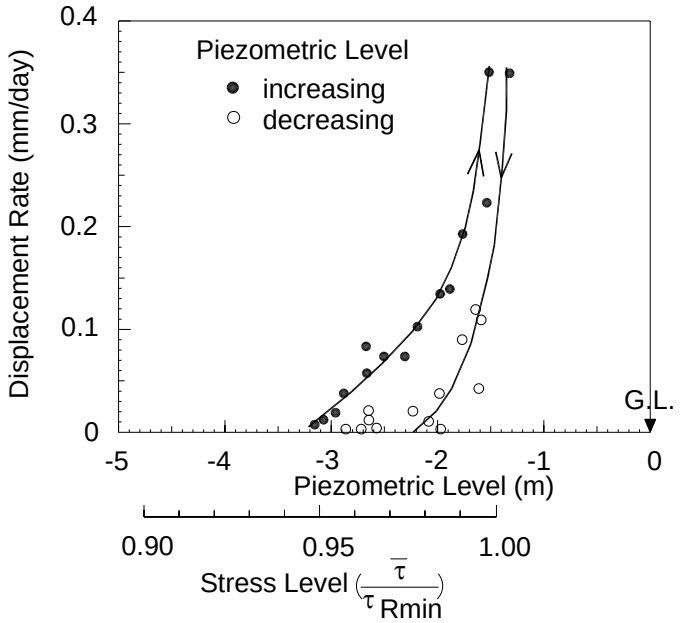

Figure 2-1: Relationship between the Displacement Rate and Water Level for the Fosso San Martino Slide (Modified after Picarelli and Russo, 2004).

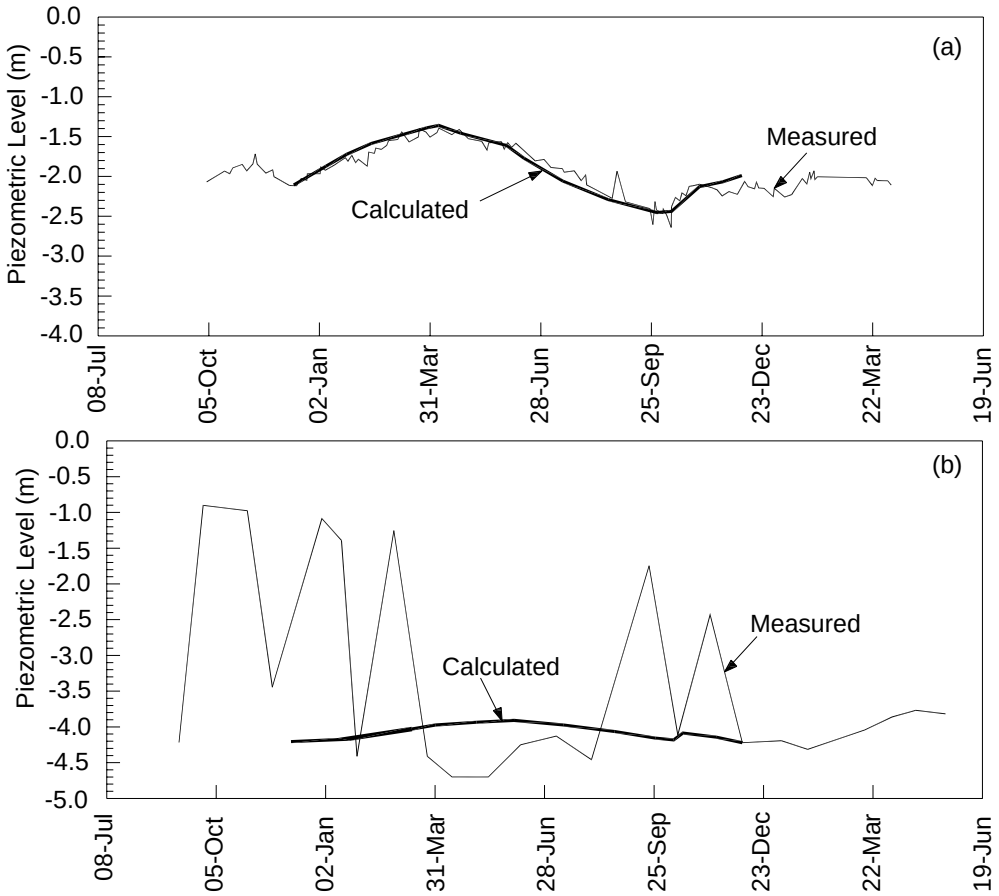

Figure 2-2: Calculated and Measured Pore Pressures in: (a) Low Active and (b) High Active Parts of the Masseria Marino Mudslide (Modified after Comegna et al., 2004)

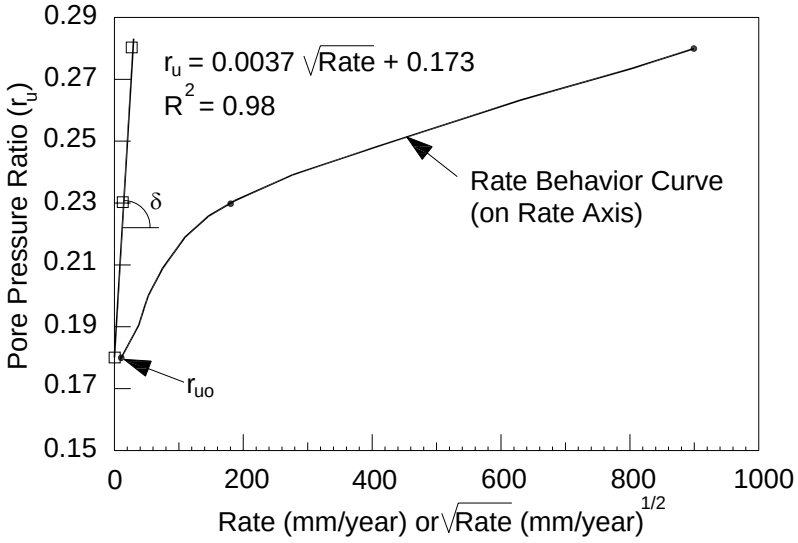

Figure 2-3: Square Root of Movement Rate with Pore Pressure Ratio (r_u) Increasing (Modified after Eshraghian et al., 2007)

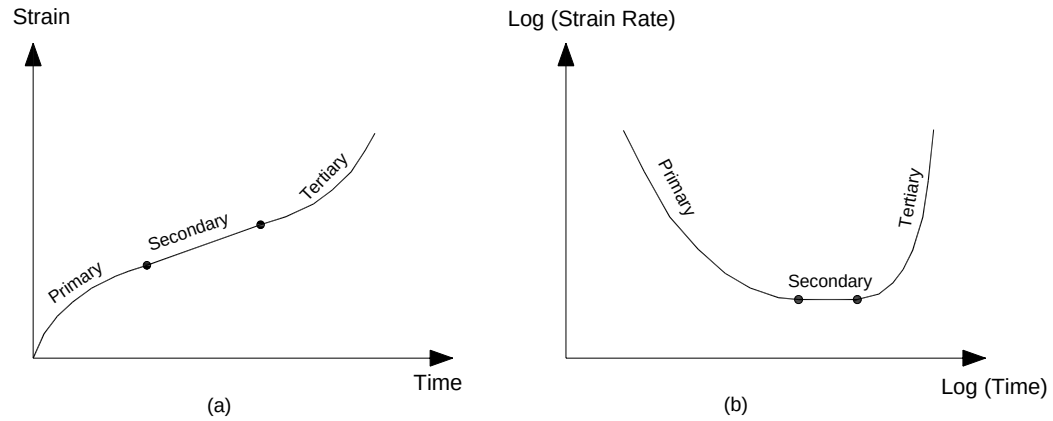

Figure 2-4: Primary, Secondary and Tertiary Creep Stages from a Typical Triaxial Test shown on both: (a) Arithmetic and (b) Logarithmic Scales (Modified after Augustesen et al., 2004)

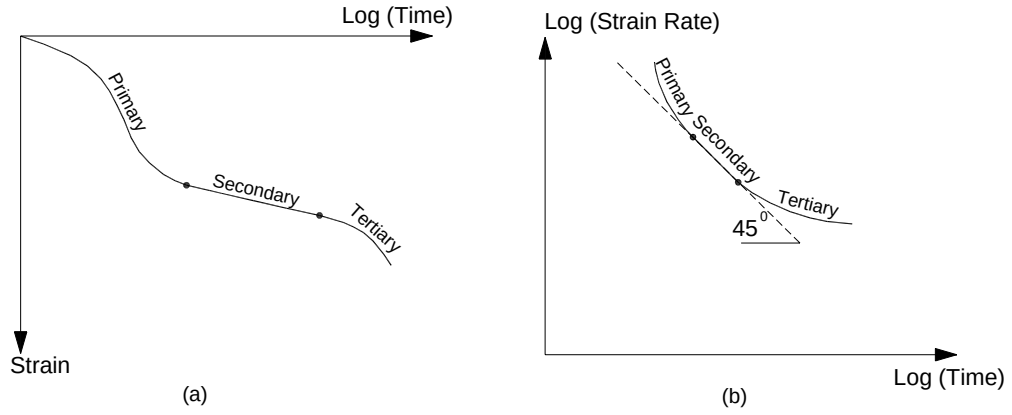

Figure 2-5: Primary, Secondary and Tertiary Compression Stages in an Odometer Test; (a) Strain-Logarithm of Time Plot, and (b) Logarithm of Strain Rate-Logarithm of Time Plot (Modified after Augustesen et al., 2004).

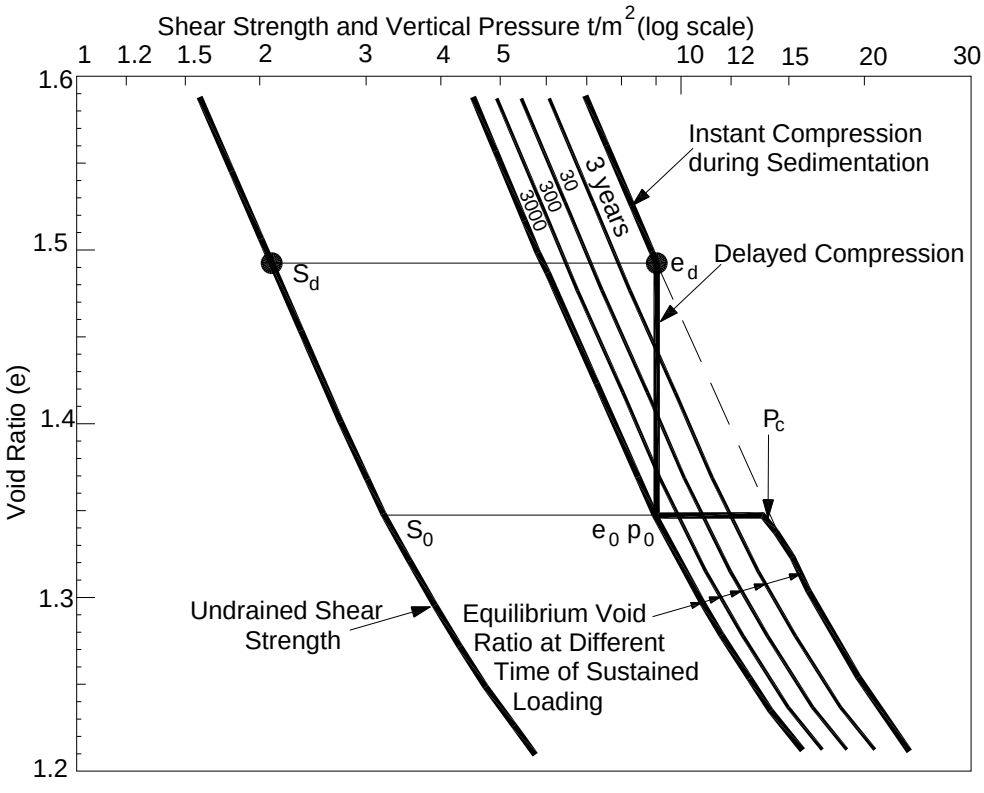

Figure 2-6: Compressibility and Shear Strength of Clay Exhibiting Delayed Consolidation (Modified after Bjerrum, 1967)

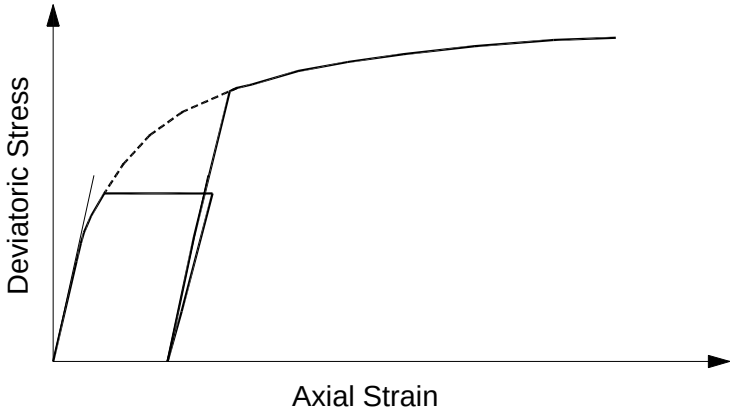

Figure 2-7: Superposition of Deviatoric Loads after Undrained Loading (Modified after Kavazanjian and Mitchell, 1980)

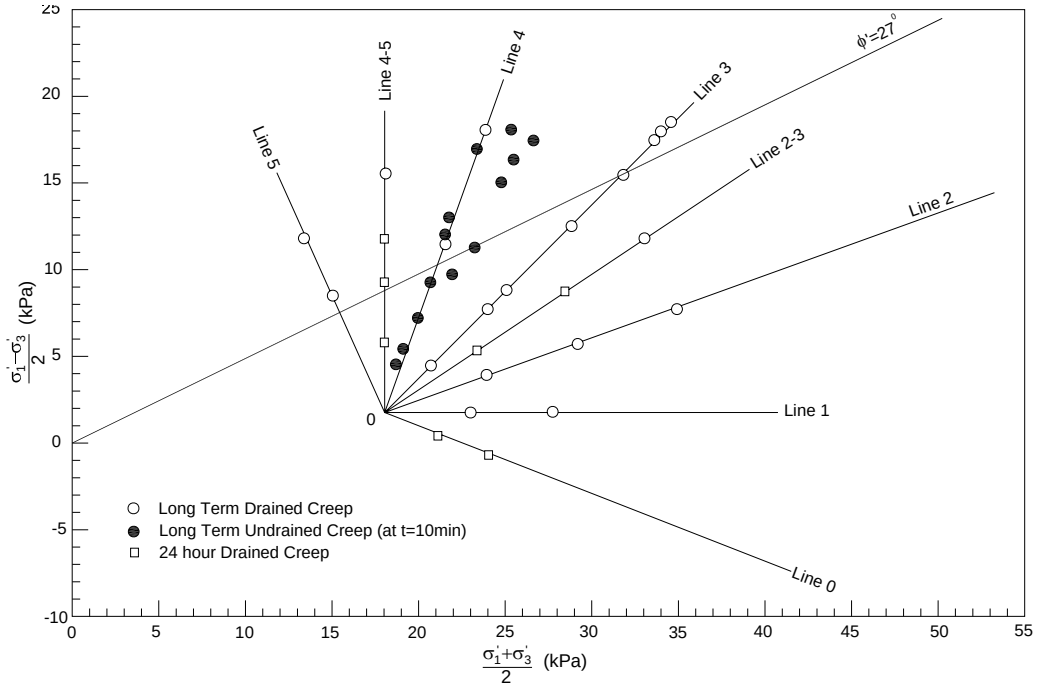

Figure 2-8: Stress Conditions for Drained and Undrained Creep Tests (Modified after Tavenas et al., 1978)

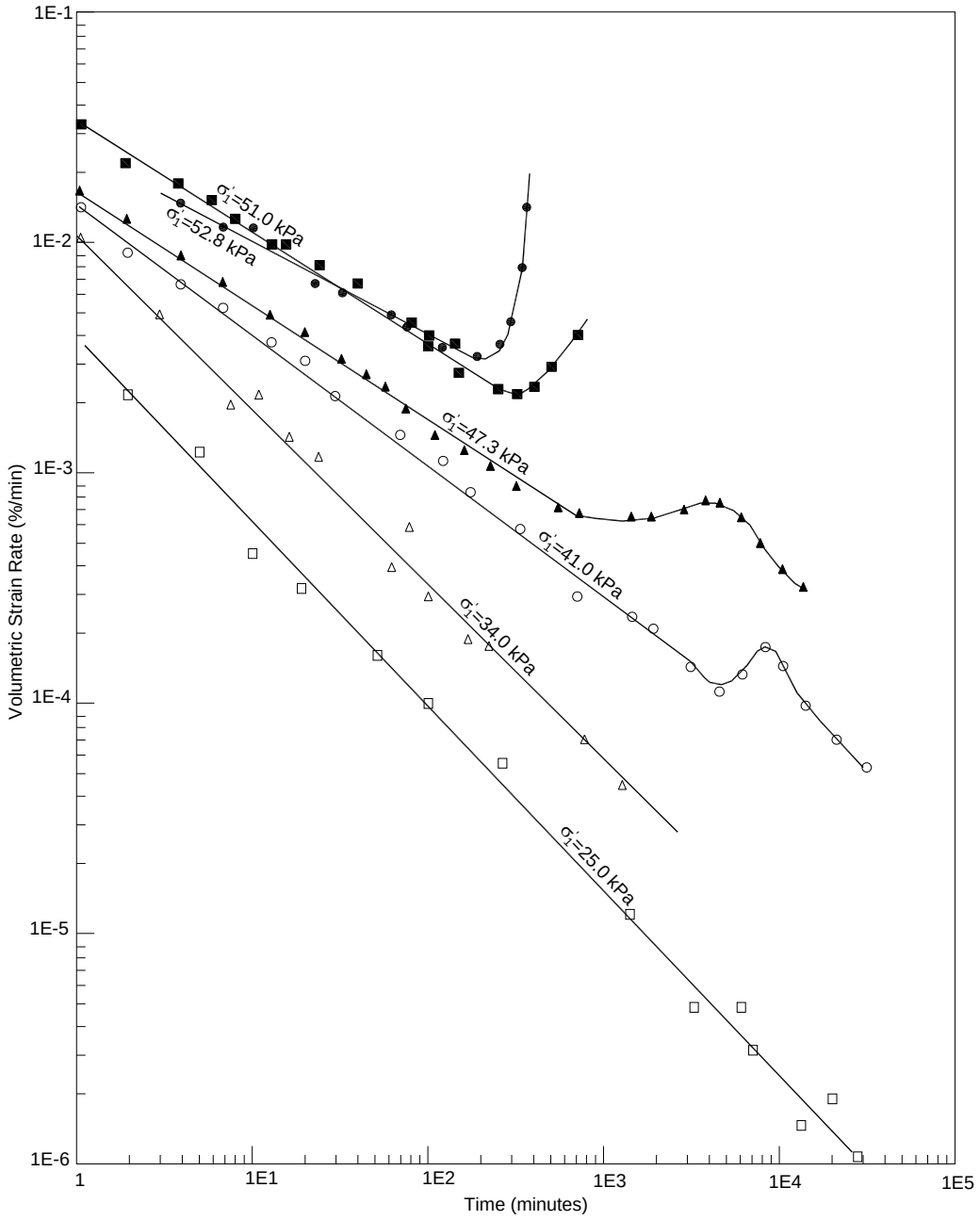

Figure 2-9: Volumetric Strain Rate – Time Relationship for Drained Tests on Lightly Overconsolidated Clays at σ'_3=16.5 kPa (Modified after Tavenas et al., 1978)

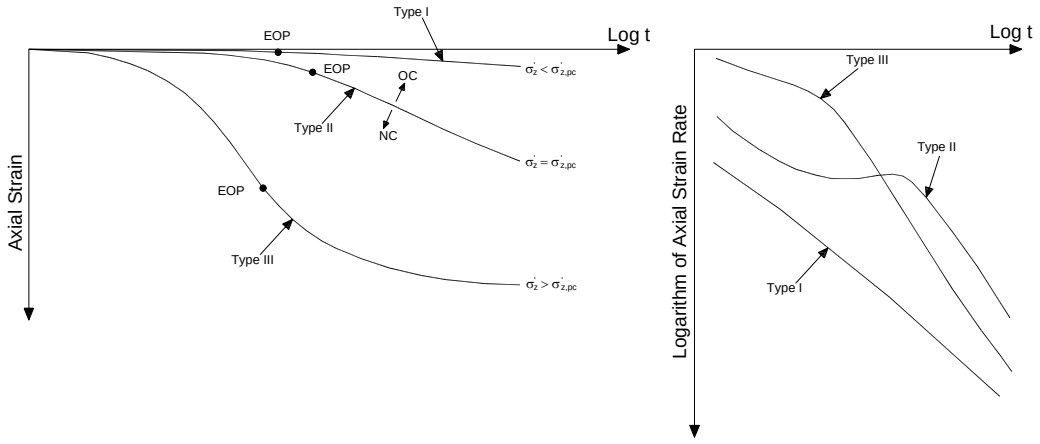

Figure 2-10: Strain Rate Behaviour of Clayey Soils having Different Stress Histories. Type I Corresponds to an Overconsolidated Sample. Type II Corresponds to a Sample where the Stress is Close to the Preconsolidation Stress. Type III is a Normally Consolidated Sample (Modified after Augustesen et al., 2004)

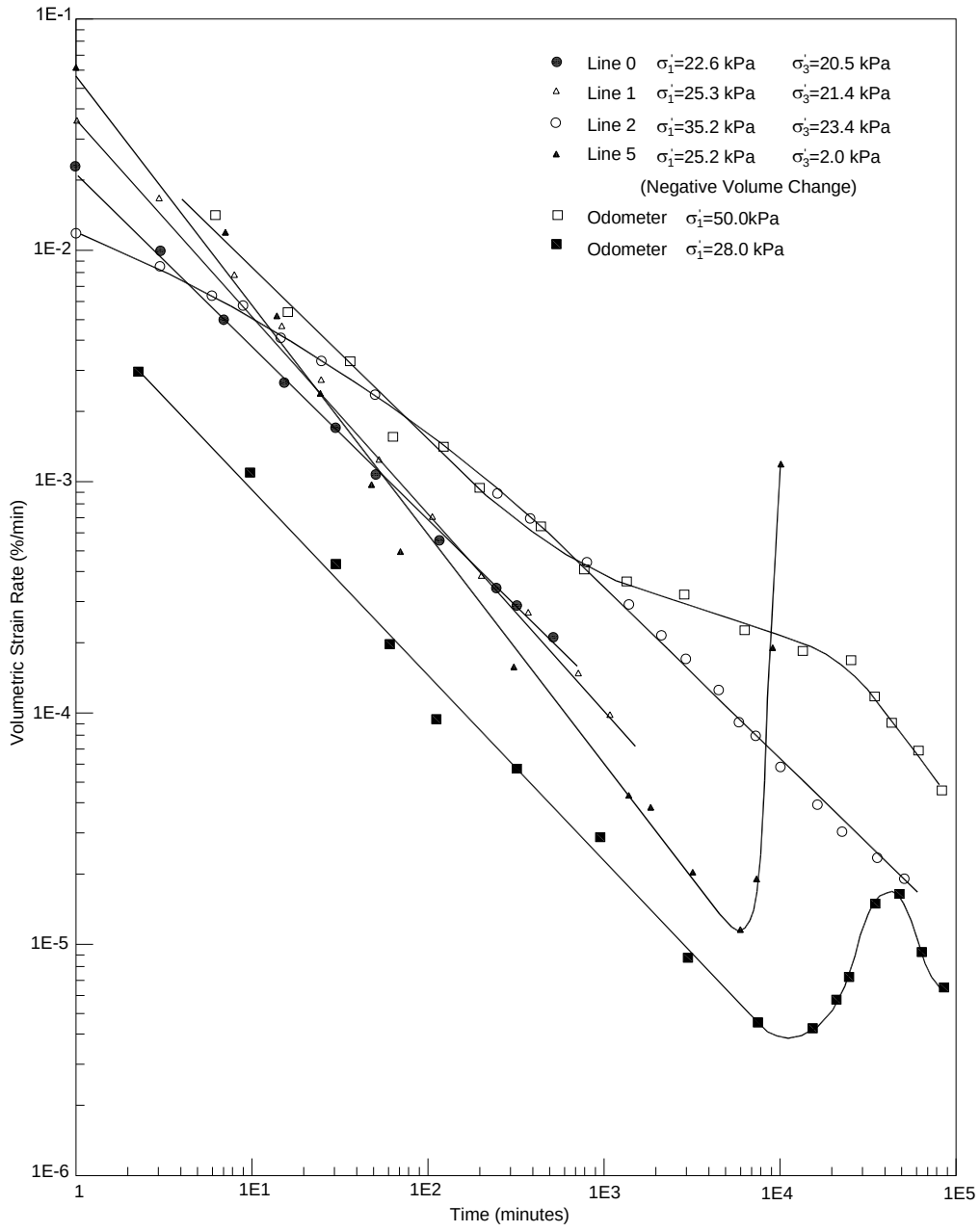

Figure 2-11: Volumetric Strain Rate – Time Relationship for Drained Tests under Various Stress Conditions (Modified after Tavenas et al., 1978).

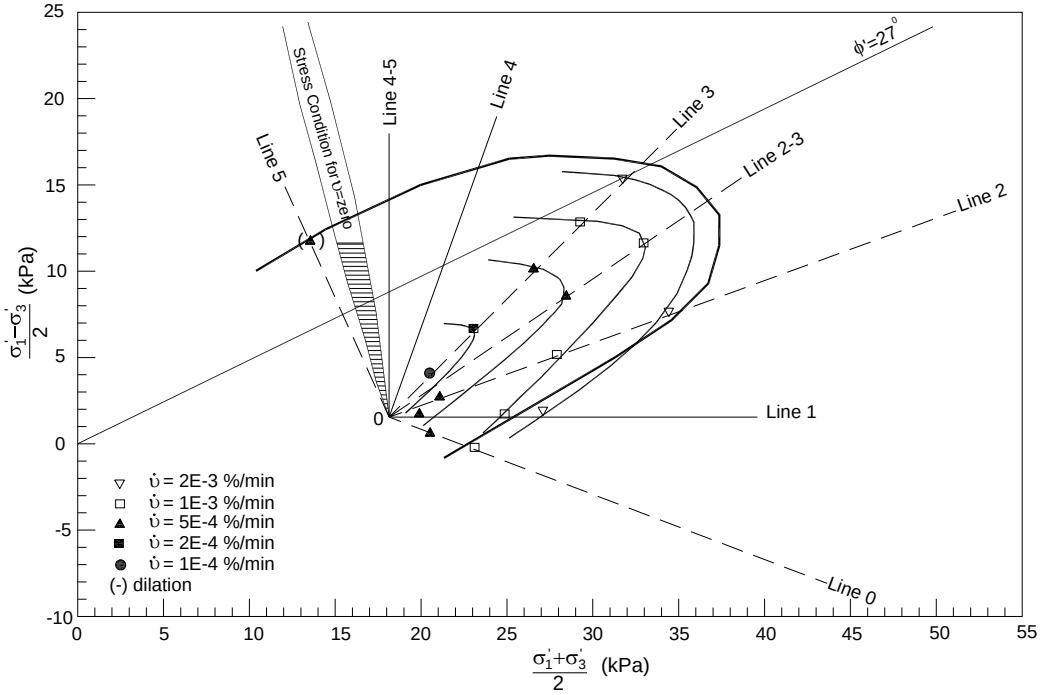

Figure 2-12: Lines of Equal Volumetric Strain Rate at t=100 min in the Stress Space for Drained Tests (Modified after Tavenas et al., 1978)

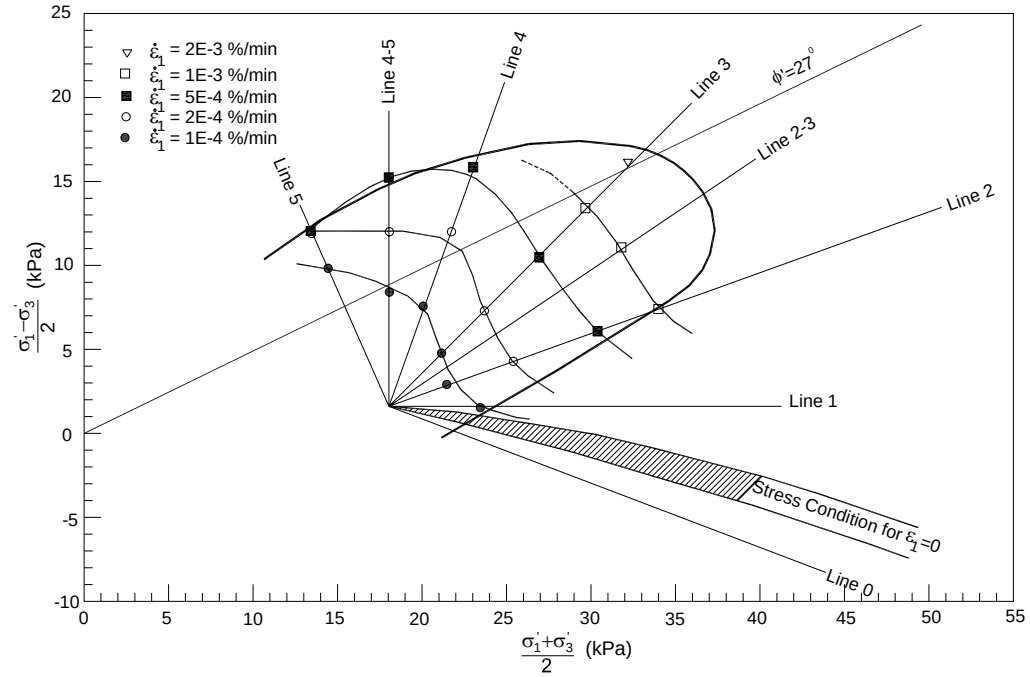

Figure 2-13: Lines of Equal Axial Strain Rate at t=100 min in the Stress Space for Drained Tests (Modified after Tavenas et al., 1978)

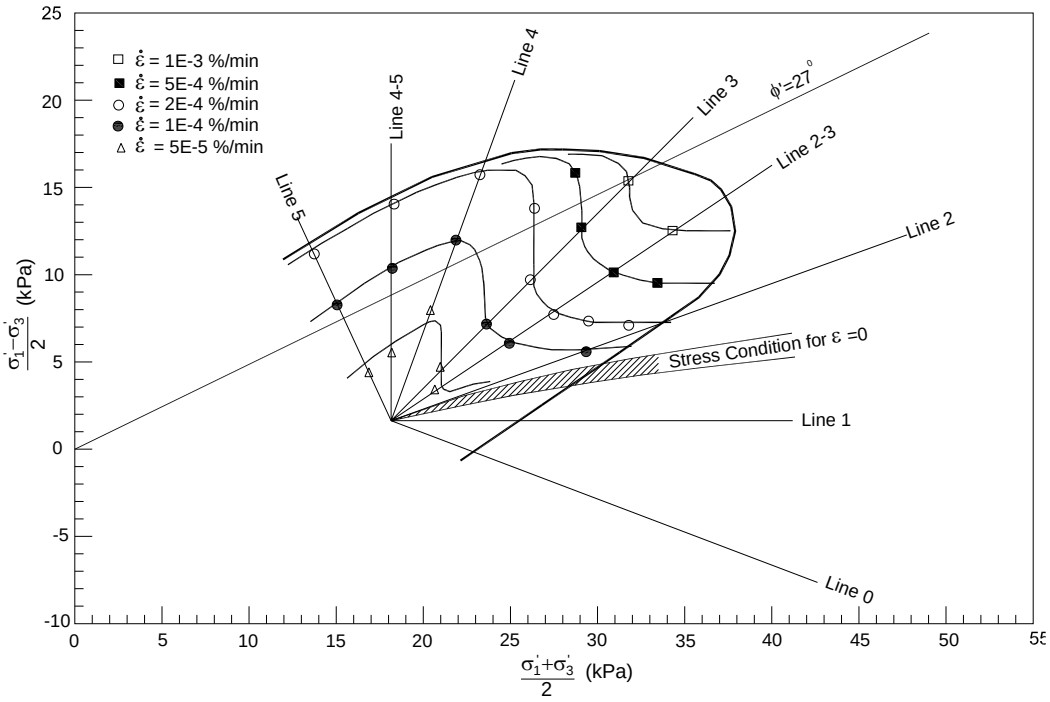

Figure 2-14: Lines of Equal Shear Strain Rates at t=100 min in the Stress Space for Drained and Undrained Tests (From Tavenas et al., 1978).

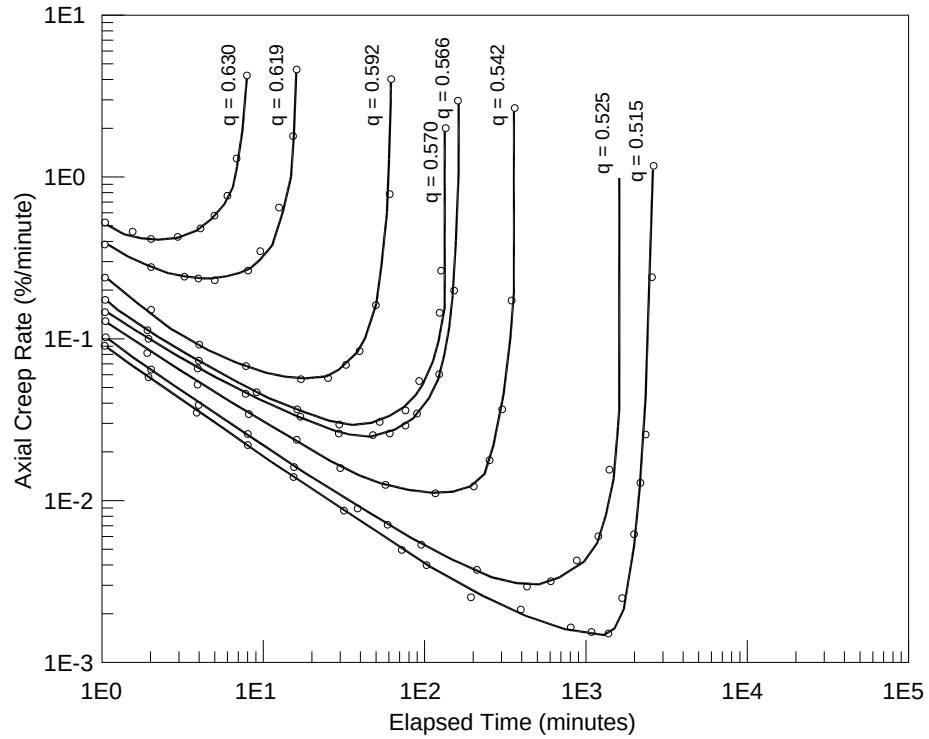

Figure 2-15: Sample of Results of Creep Rate versus Time Plots for the Isotropically Consolidated Specimen at Different Deviatoric Stress Levels (Modified after Campanella and Vaid, 1974)

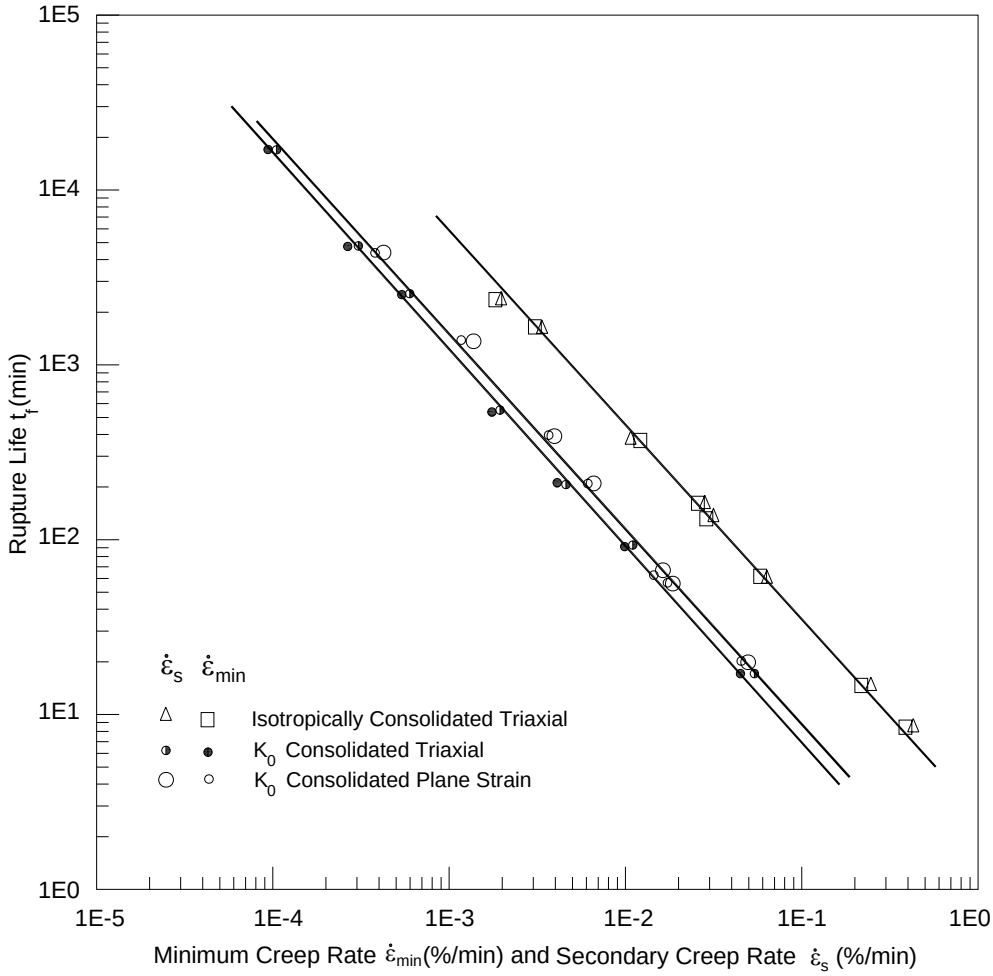

Figure 2-16: Relationships between the Creep Rupture Life and the Minimum Creep Rate (Modified after Campanella and Vaid, 1974).

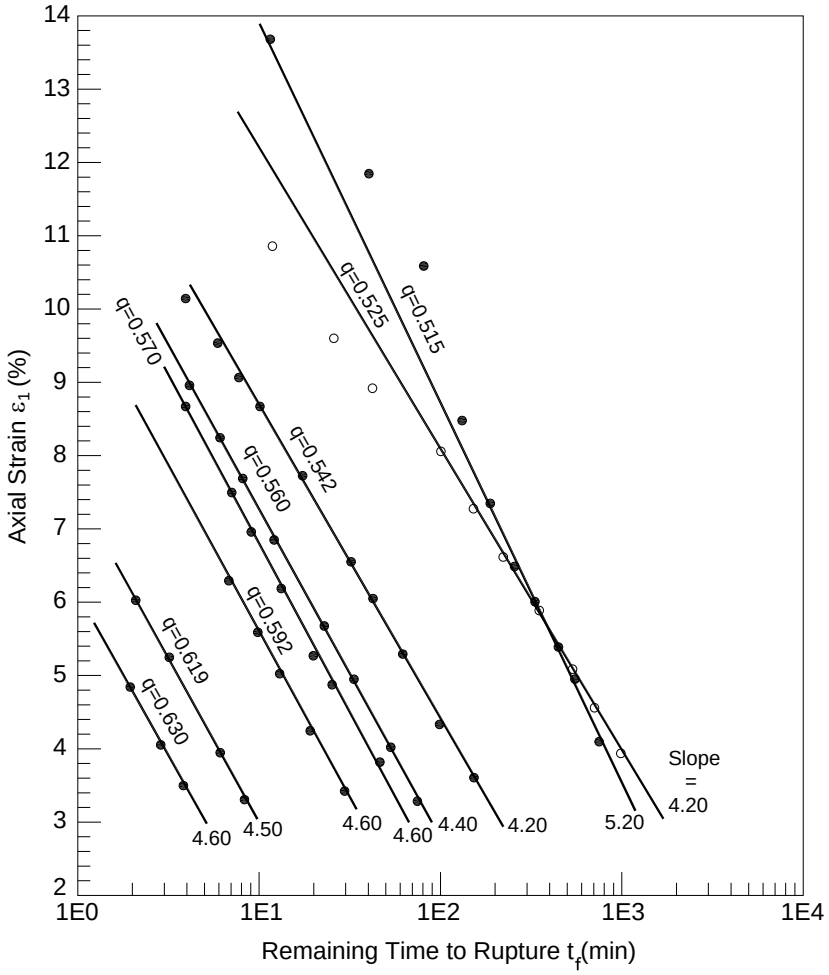

Figure 2-17: Relationship between the Remaining Time to Rupture during Tertiary Creep and Axial Strain for the Isotropically Consolidated Triaxial Test (Modified after Campanella and Vaid, 1974)

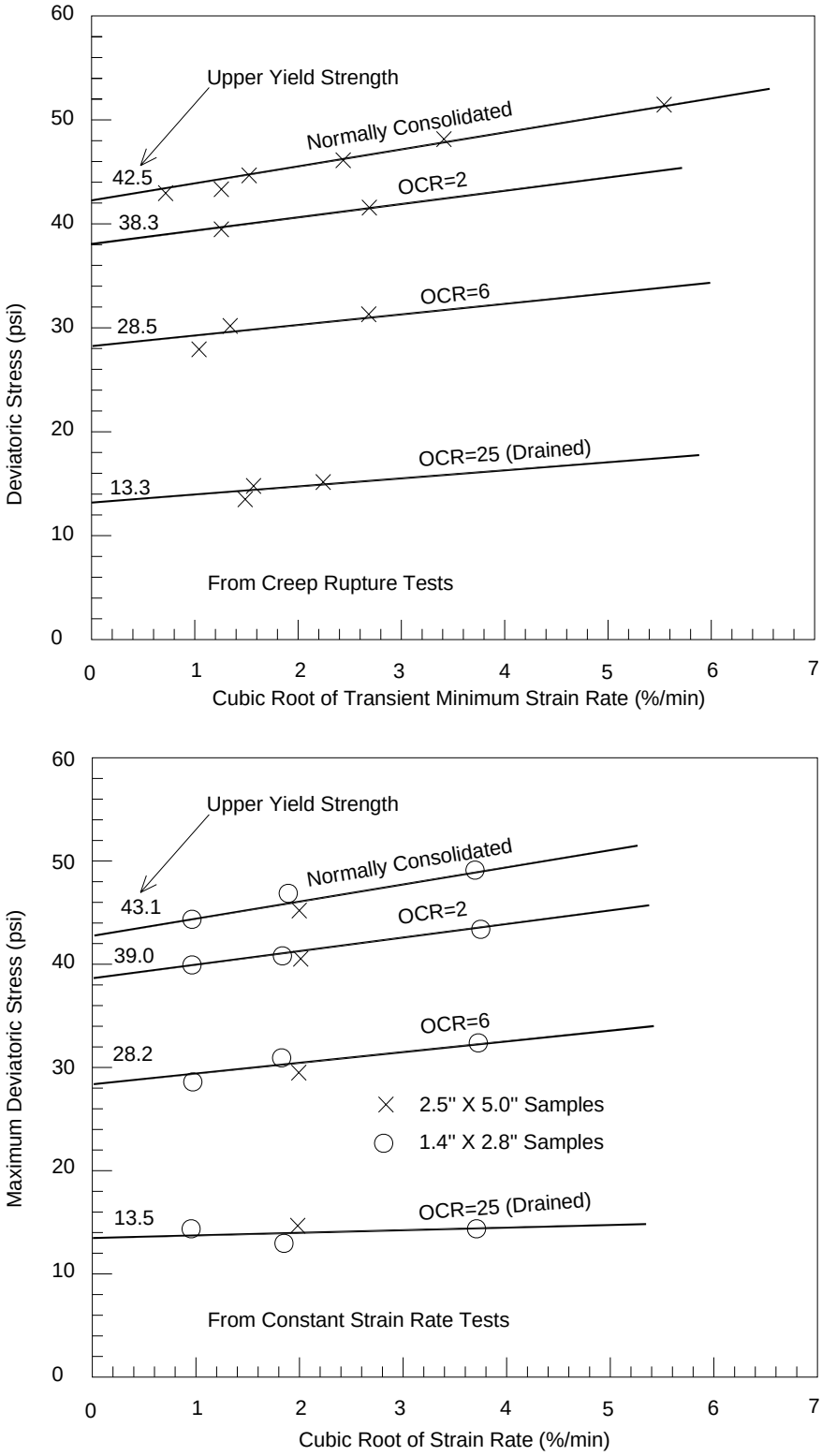

Figure 2-18: Determination of Upper Yield Strength using the Proposed Method (Modified after Finn and Snead, 1973)

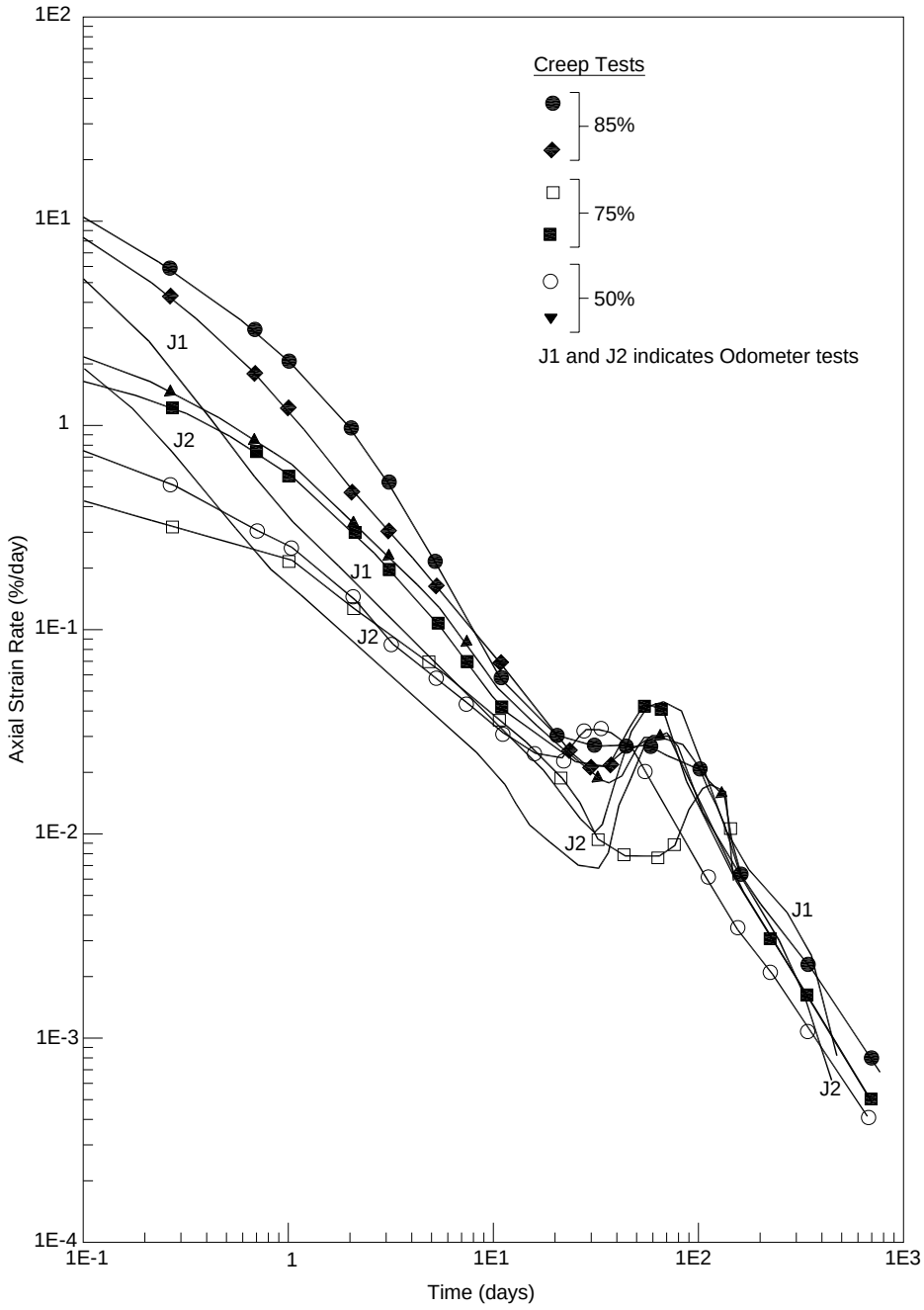

Figure 2-19: Axial Strain Rate versus Time for Normally Consolidated Pancone Clay (Modified after Bishop and Lovenbury, 1969)

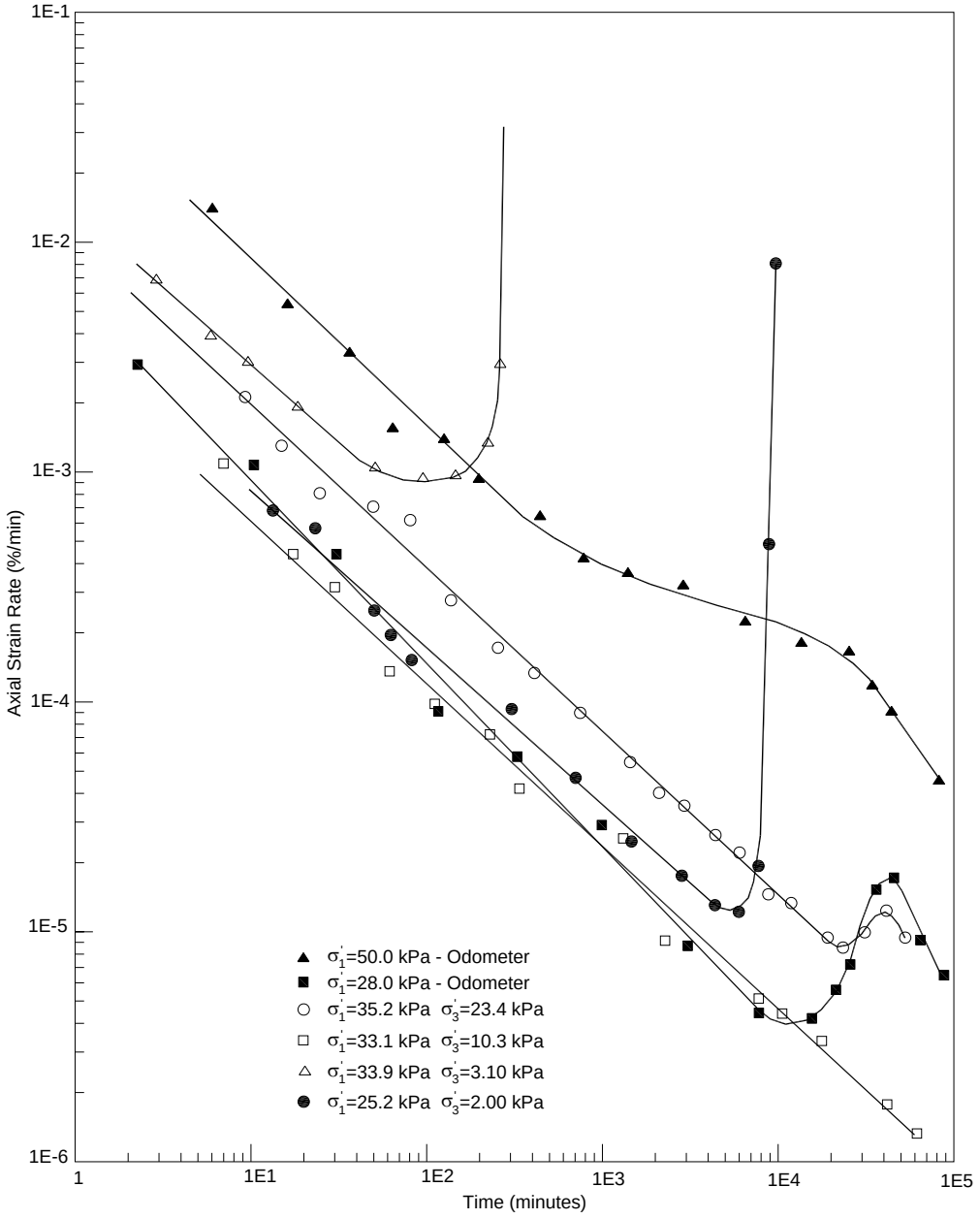

Figure 2-20: Axial Strain Rate versus Time Plots for Drained Tests under Various Stress Conditions (Modified after Tavenas et al., 1978)

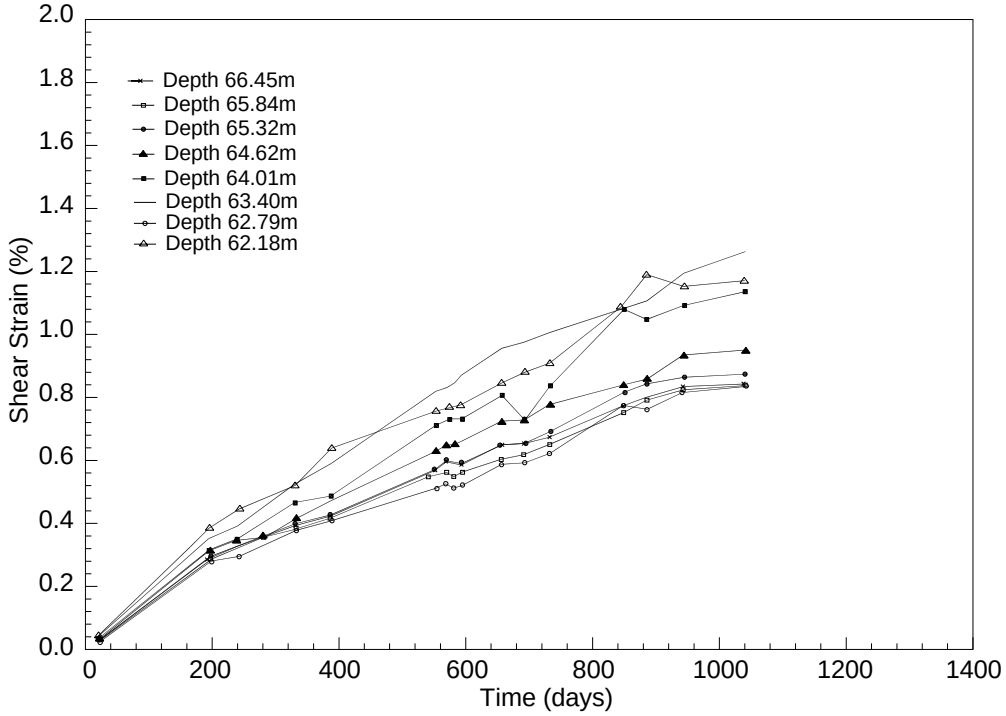

Figure 2-21: Shear Strain versus Time at Different Depths for the Upper Half of Clay from One of the Inclinometers (Modified after Watts, 1981)

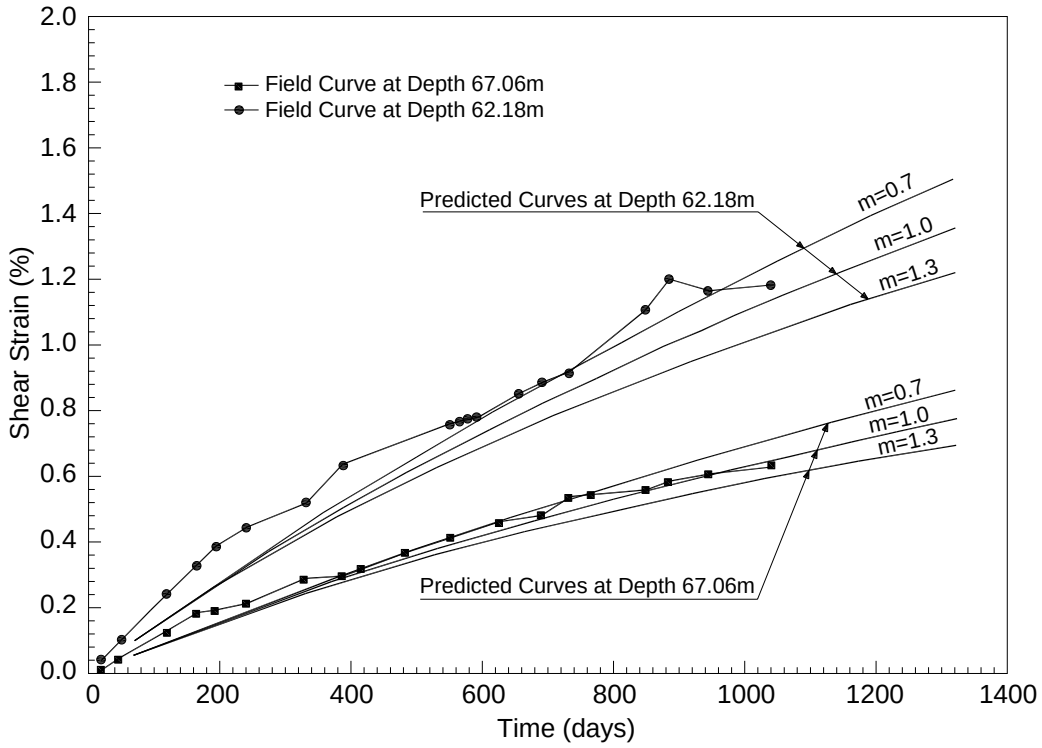

Figure 2-22: Actual and Predicted Field Shear Strain Values (Modified after Watts, 1981)

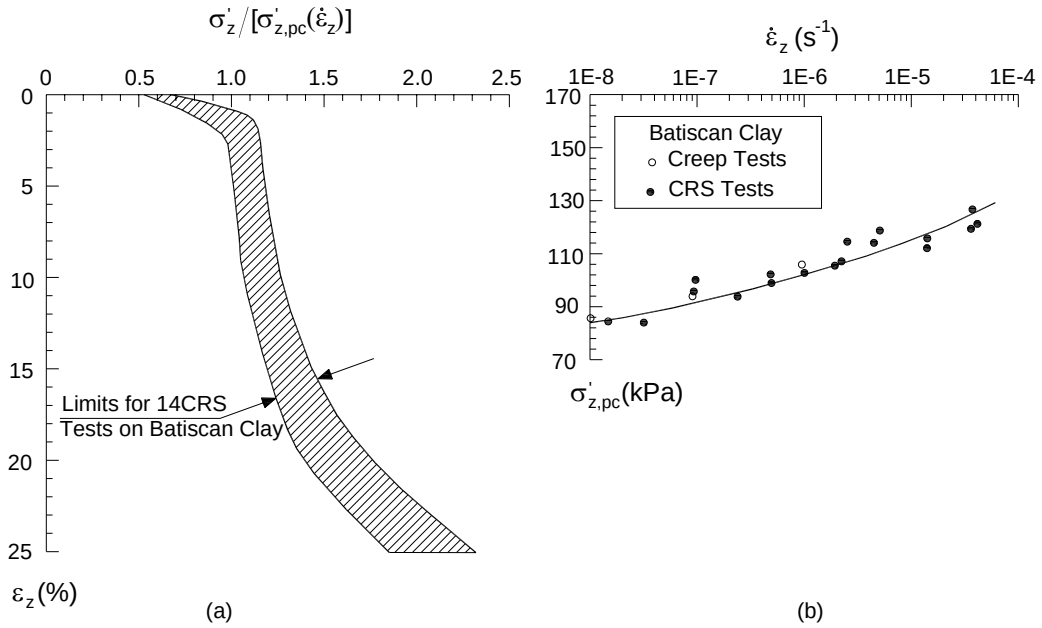

Figure 2-23: (a) Normalized Effective Stress Strain Relationship from Constant Rate of Strain Odometer Tests and (b) Variation of the Preconsolidation Pressure with Strain Rate (Modified after Leroueil et al., 1985)

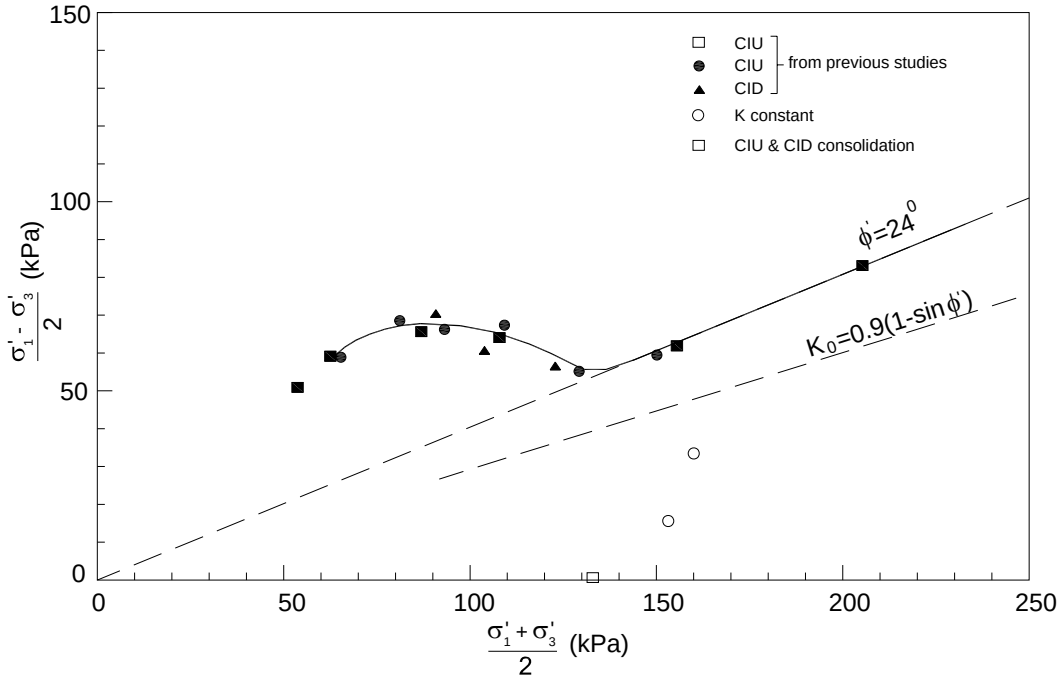

Figure 2-24: Yield Loci from Many Triaxial Tests (Modified after Tavenas and Leroueil, 1977)

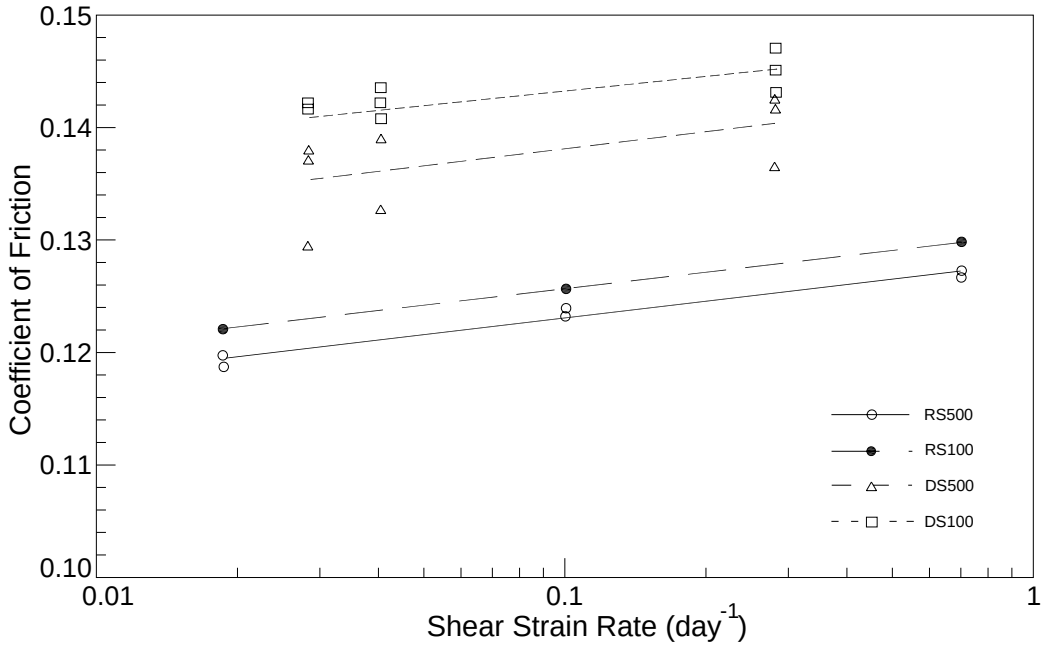

Figure 2-25: Variation of Coefficient of Friction with the Logarithm of Shear Strain Rate (Modified after Wedage, 1995)

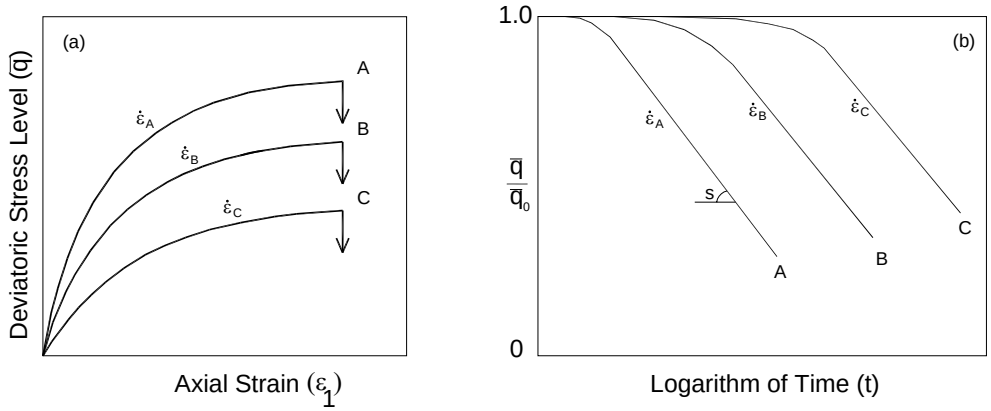

Figure 2-26: Schematic Representation of Typical Stress Relaxation Test Results (Modified after Augustesen et al., 2004)

3 Vulnerability to Slow Moving Slides

3.1 Introduction

Vulnerability is the degree of loss for a given element at risk resulting from the occurrence of a natural phenomenon like landslides (Varnes, 1984). Vulnerability to a landslide can be assessed by comparing the value of damages to the actual value of the vulnerable facility (Remondo et al., 2004). The increased population in the world has led to a considerable rise in urban development in landslide-prone areas. Urban landslides are triggered mainly by seasonal hydrological, environmental and anthropogenic changes like rainfall, earthquakes and human activities. Human activities include grading slopes, loading slope crests and increasing groundwater pressures by irrigation, from septic systems and/or by deforesting, which helps to increase the infiltration rate to the soil. The adverse effect of the problem of urban landsliding has become more severe because of the uncontrolled population growth in hillside areas in some countries. Therefore, the hazards that arise from urban development in landslide-prone areas are increasing despite the progress in the application of mitigation measures.

While the losses resulting from rapid landslides like debris flows, mud flows and rock falls are the highest and the most severe, slow moving slides also have adverse effects on nearby facilities. The accumulation of slow movement can lead in some cases to a total disruption of the serviceability of these facilities. Loss of life may result as well. According to Cruden and Varnes (1996), slow slides fall into three classes:

1. Extremely slow moving slides: This class includes slides moving at rates ranging from zero to 16mm/yr.
2. Very slow moving slides: This class includes slides moving at rates ranging from 16mm/yr to 1.6m/yr.
3. Slow moving slides: This class includes slides moving at rates ranging from 1.6m/yr to 160m/yr (~13.3 m/month).

This chapter uses the available literature to discuss the degree of damage caused by the different classes of slow slides to different facilities. The vulnerable facilities include urban and suburban settlements, highways and railways, bridges, dams and linear infrastructure such as pipelines. The main information required from each of the reviewed cases is the movement rate and the degree of damage it caused. Moreover, the different attributes of the reviewed cases, such as the type of the materials controlling the movement, the method of measuring the movement and the likely trigger(s) of movement, are highlighted. Some useful statistics with important implications are presented.

It became possible at the end of the review to develop “damage-extent scales” describing the expected degree of damage from a certain movement rate. The scales are developed for each group of the surveyed facilities. The developed

scales are damage-extent scales rather than vulnerability scales because case histories are usually poor with regard to reporting the original value of the vulnerable facility and the cost of repairing the damage. The degree of damage resulting from a certain slide velocity is the most common information mentioned in case histories.

3.2 Characteristics of Slow Moving Slides

More than sixty cases of slow moving slides are reviewed in this study. Fifty two of the studied cases contain complete information about the movement rate and the degree of damage. Both attributes are important in developing the required scales. The cases cover instabilities in many countries in the world: Canada, USA, Brazil, Ecuador, Costa Rica, Australia, New Zealand, Italy, United Kingdom, Switzerland, Norway, Croatia, Yugoslavia, Germany, Greece, Austria, Turkey, China, Japan, Malaysia, Korea and Sri Lanka. Some of the surveyed slides affect more than one type of facility, e.g., urban areas and highways or highways and linear infrastructure. A brief description of each of the reviewed cases is provided in Appendix A.

In addition to the rate of movement and the degree of damage, important information regarding the method of the displacement measurement, the type of the slide material and the main trigger(s) of movement is presented in the following subsections. These attributes are summarized in Table 3-1. The simple statistics presented are intended to be helpful to geotechnical engineers dealing with slow moving slides.

3.2.1 Displacement Measurement Method

About forty five cases indicated the method of displacement measurement. Some of the surveyed slides were monitored by utilizing more than one type of measurement. Inclinometers were used to record the movement in about 56% of the studied cases. However, due to the shearing-off of inclinometer casings when displacements reach around 100 mm, inclinometers were not used to measure the displacements of slides moving at rates of more than 590 mm/yr. In the upper range of very slow slides and in the range of slow slides, other measurement methods such as surface surveying, remote techniques and the use of geomorphologic evidence become more reliable due to their ability to measure larger displacements over longer periods of time. The low accuracy of these methods may not enable them to accurately record extremely slow movements. Remote techniques such as Synthetic Aperture Radar Interferometry (IN-SAR) and Terrestrial Laser Scanning (TLS) were used in only 9% of the studied slides. These techniques have developed recently, and the reliance on them should increase in the future as they provide coverage of large areas and overcome some of the disadvantages of inclinometers. However, the increased application of in-

place inclinometers will overcome the present issues. Figure 3-1 shows the percentages of use of each of inclinometers, surface surveying, remote techniques, extensometers and geomorphology in measuring the displacements of slow slides. The sum of the percentages of the different methods is more than 100% because more than one method of displacement measurement was utilized in some of the surveyed cases, as mentioned above.

3.2.2 Materials Hosting the Rupture Surface

Forty nine cases stated explicitly the type of the material hosting the rupture surface. More than half of these slides (53%) have their rupture surfaces in soil materials, mainly clays and silts. About 27% of the surveyed cases have their rupture surfaces in weak rocks like clay shales. The rupture surfaces run along the interface between the soil and the underlying rock in 12% of the reviewed cases, and the rest have their rupture surfaces in rock materials. The sum of the percentages is also slightly higher than 100%.

This comparison may show that the expected hazards from rock slopes may be rock falls or toppling rather than sliding on a well defined rupture surface. On the other hand, more than half the studied cases have their rupture surfaces in soil. While this fact does not necessarily indicate that sliding is the dominant mode of failure of earth slopes, it can be postulated that enough documentation is available for earth slides which helps to understand their behaviour. Figure 3-2 shows the percentages of slides having their rupture surfaces in soil, rock, weak rock and at the interface between soils and rocks.

3.2.3 Trigger(s) of Movement

Some of the studied cases have more than one trigger of movement although the majority have single triggers. Forty eight cases report the trigger(s) of the slow movement of slides. Rainfall is the main trigger of movement in 67% of the reviewed slides. This finding draws attention to the importance of designing and installing drainage measures for facilities constructed in heavy rainfall areas. Toe erosion and human activities are the triggers (or one of the triggers) of movement in about 40% of the surveyed slides. Reservoir filling and reservoir level seasonal fluctuations seem to be threatening slopes that lie upstream of dams as these factors trigger the movement of about 10% of the studied cases. Other triggers like earthquakes, snowmelt and mining activities have minor effects on the slow movement of natural slopes. Figure 3-3 shows the percentages of the contribution of different triggers to slow slide movements.

3.2.4 Type of the Vulnerable Facility

The vulnerable facilities include the five categories mentioned above: urban and suburban settlements, highways and railways, bridges, dams and linear infrastructure. Forty three percent of the vulnerable facilities are urban and suburban communities. This high percent is expected due to the direct threat posed to human life when towns are built close to natural moving slopes. The vulnerability of highways and railways is documented in 27% of the studied cases. Similarly, highway and railway hazards are life-threatening to passengers. The level of threat is, however, less than that in urban communities. Figure 3-4 shows the relative citations of the different types of vulnerable facilities among the studied cases.

3.3 Degree of Damage Scales

Twenty five cases of slow moving slides describe actual damages to urban and suburban communities. The cases are sorted in the ascending order of the slide velocities starting from a measured rate of 5mm/yr up to 51m/yr. A brief description of each case is provided in Section A-1 of Appendix A. Five more cases are not rich in movement data and are mentioned at the end of Section A-1.

Table 3-2 presents a more refined summary of these cases, focusing on the degree of damage resulting from different slide velocities. All the cases are compiled to form a new scale describing the vulnerability of urban communities to slow moving slides. The scale defines the expected degree of damage to urban communities from different slide velocities lying in the range of slow, very slow and extremely slow slides. The developed scale is presented in Table 3-7.

Similarly, Table 3-3 through Table 3-6 summarize the degree of damage resulting from the different movement rates of slides adversely affecting highways and railways, bridges, dams and linear infrastructure, respectively. The reviewed cases are described in more detail in Section A-2 through Section A-5 of Appendix A. Table 3-8 through Table 3-10 show the developed scales for the expected degree of damage from different slide velocities to highways and railways, bridges and dams, respectively. Unlike the cases describing urban communities' damages, the cases summarized in Table 3-3 through Table 3-5 do not reveal a wide spectrum of movement rates. Therefore, during the development of the damage-extent scales for highways and railways, bridges and dams, some limits among different levels of damage have been set according to the limits among extremely slow, very slow and slow movement rates.

Pipelines and water service pipes are examples of linear infrastructure. Only four cases are available with sufficient data. A fifth one has a qualitative description of the threat posed by a slow moving earth slide to a pipeline. The limited number of

available cases makes it difficult to develop a scale for the extent of damage caused by slow moving slides to pipelines and water service pipes.

3.4 Conclusions

The literature survey presented in this chapter allows for the development of four new scales describing the expected degree of damage versus movement rate for urban communities, highways and railways, bridges and dams threatened by extremely slow, very slow and slow moving slides. The four scales are shown together in Figure 3-5. The various degrees of damage to each of the studied facilities are categorized into minor, moderate, major and severe. The tabulated scales shown in Figure 3-5 are shown schematically in Figure 3-6. A minor degree of damage is assigned a green colour, a moderate degree is assigned an orange colour, a major one is assigned a yellow colour, and, finally, a severe degree of damage is assigned a red colour. Figure 3-6 reveals that buildings and residential houses may tolerate higher slide velocities than other facilities before experiencing serious damage. On the other hand, bridges are the least tolerant facilities, for movement rates as low as 100mm/yr may cause severe damages. Such low rates may cause only moderate damage to urban communities. The proposed scales can be enhanced by the inclusion of more cases.

Since the quantification of vulnerability is a major entry towards the evaluation of the specific risk, the various degrees of damage are assigned numeric values for the consequence factor. The consequence factors of 0.1, 0.4, 0.7 and 1.0 correspond to minor, moderate, major and severe degrees of damage, respectively. The study has an important practical significance for geotechnical engineers as it provides a way of predicting the degree of damage based on preliminary estimates of movement rates. Hence, the proper field investigation program can be planned, and successful remedial measures can be implemented. In addition, alarm systems can be designed based on the measured movement rates in the field.

Table 3-1: Summary of the Reviewed Cases

Case Number	Reference	Material Hosting the Rupture Surface	Displacement Measurement Method	Movement Rate (mm/yr)	Trigger	Vulnerable Facility
1	Cascini et al. (2008b)	Quaternary deposits	Differential Synthetic Aperture Radar Interferometry (D-InSAR)	5	Rainfall	A 489 km^2 next to Liri-Garigliano and Volturno Rivers in Italy (urban development)
2	Wasowski et al. (2008)	Clay	Persistent Scatterers Interferometry (PSI)	8	Rainfall and Construction activity	Casalnuovo Monterotaro and Pietramontecorvino towns in Italy
3	Ortigão and Kanji (2004)	Clays	-	<10	Rainfall and seismic activity	Town of Santiago de Puriscal in Costa Rica
4	Bonnard et al. (2008)	Clay shale	Surface surveying techniques	10	-	Triesen and Triesenberg villages in eastern Switzerland
5	Jworchan et al. (2008)	Colluvium and Interface between residual soils and bedrock	Inclinometers	12	Rainfall	A slope proposed for residential development in the West Pennant Hills, Sydney, Australia
6	Barton and McCosker (2000)	Rock	Inclinometers	12	Rainfall	Coastal cliff in Afton Down, UK
7	HBT AGRA Limited (1992)	Preglacial lake clays and clay shale	Inclinometers	14	-	Town of Peace River, Alberta, Canada
8	Calcaterra et al. (2008)	Rock	Permanent Scatterers Synthetic Aperture Radar Interferometry (PS-InSAR) and inclinometers	16	Rainfall	Buildings of the Moio della Civitella village in Salerno, Italy
9	Buccolini and Sciarra (1996)	Marly clays	Inclinometers and surface monuments	19 – 26	Rainfall	Dwelling houses and a highway in the Abruzzo region, Italy
10	Ortigão and Kanji (2004)	Interface between soil and bedrock	Surface surveying	30	Rainfall	Town of Cuenca, Ecuador
11	Blikra (2008)	Rock	Extensometers, GPS, total station and Inclinometers	30 – 100 (up to 365)	Seasonal changes (mostly rainfall)	The Aknes rockslide in Norway may generate tsunamis that killed people before

12	Bressani et al. (2008)	Interface between overlying colluvium and clayey siltstone	Inclinometers	34 (up to 80)	Rainfall	Urban slope in Santa Cruz do Sul, Brazil
13	Fort et al. (2000b)	-	Inclinometers and surface surveying	91	Coastal erosion and rainfall	Seawall structures, roads and footpaths in Lyme Regis town, UK
14	Bunza (2000)	Gravel and silt	Extensometers	92	Rainfall, snowmelt and erosion	Tiefenbach village near Oberstdorf, Germany
15	Clifton et al. (1986)	Clay shale	Inclinometers	108	River erosion	Regina beach in Saskatchewan, Canada
16	Wang et al. (2008)	Colluvium	GPS and extensometers	180	Rainfall and reservoir level fluctuations	Village located on the slope of the Shuping landslide, China
17	Mihalinec and Ortolan (2008)	Clay	Comparison of topographic maps	152 – 300	Rainfall	Urban communities in Zagreb, Croatia
18	Oppikofer et al. (2008)	Rock	Terrestrial Laser Scanning (TLS)	60 – 70 (up to 200)	Rainfall, Earthquakes, mining operations and snow melt	The Aknes rockslide in Norway may generate tsunamis that killed people before
19	Esser (2000)	Plastic lacustrine clay	Inclinometer	306	Construction activities	Residential complex in Ohio, USA
20	Fort et al. (2000a)	Stiff, fissured overconsolidated Barton clay	Surface surveying	861	Toe erosion and rainfall	Buildings on top of a cliff at Barton-on-Sea shore in Hampshire, UK
21	Zhou (2000)	Soil rock interface	-	2000 (a maximum of more than 4000)	-	Sichuan city in China
22	Spizzichino et al. (2004)	Clay	Air photos	4000	Rainfall and human activity	Crago village in Italy
23	Ibadango et al. (2005)	Sedimentary rocks	Differential GPS	6000	Construction activities	Urban settlements on the elongated valley of the Loja basin in Ecuador
24	Fujisawa et al. (2007)	Earth slide	Extensometers and inclinometers	9100	Rainfall	Buildings and water service pipes collapsed and a part of a

						highway heaved in Japan
25	Mantovani et al. (2004)	Quaternary terrain	Surface surveying	51100	Rainfall	A house affected by movement of “La Maina” landslide around the Sauris reservoir in north eastern Italy
26	Beaumont and Forth (1996)	Glacial deposits of sands and gravels overlying boulder clay	Inclinometers	13.8	Mining activities	Railway embankment in the county of Durham, UK
27	Kalteziotis et al. (1993)	-	Inclinometers	13 – 19	-	The national road from Athens to Sounion
28	Clementino et al. (2008)	Pre-sheared bentonitic clay shale and sandstone	Inclinometers	35	Water ponding on the slope	Highway east of the town of Drayton in Alberta, Canada
29	Cascini et al. (2008a)	Softened clay	Inclinometers	44	Rainfall	A major road and the Rome-Florence railway
30	Ceccucci et al. (2008)	Quaternary deposits and dislocated bedrock	Inclinometers	65	Rainfall	Collapse of a long stretch of a national road, the Serre La Voute landslide, North West Italy
31	Hayley (1968)	Clay shale	Inclinometers and surface monuments	100	River erosion	Highway 49 and the Little Smoky bridge in Alberta, Canada
32	D’Elia et al. (2000)	Interface between weak and competent rock	Inclinometers	132	Rainfall	The Ionic coast, Italy
33	Sun et al. (2000)	Volcanic saprolite	Air photos and topographic maps	450	Rainfall	A roadside cutslope above Lai Ping Road, Sha Tin, China
34	Lee and Clark (2000)	Glacial till	Surface surveying	560	Rainfall and erosion	Coastal cliff instabilities along the Scarborough Coast, UK affected a road
35	Fuchsberger and Mauerhofer (1996)	Shaley graphite	Inclinometers	590	Construction activities	A motorway in the Austrian Alps
36	Nichol and Lowman (2000)	Interface between till and mudstones and siltstones	-	600 – 6000	Rainfall	The A5 Trunk road between London and Dublin, UK

37	Chandler and Broise (2000)	Sandy silt and clayey silt colluvium	Air photos	5600	Rainfall	Major railway corridor from Colombo to Bodalla, Sri Lanka
38	Malone et al. (2008)	Rock	Total station and photogrammetric surveys	7000	Rainfall	New highway in Malaysia
39	Lokin et al. (1996)	Weathered marly clay	Inclinometers	10	Toe erosion	SLOBODA bridge in Novi Sad, Yugoslavia
40	Carson et al. (1991)	Bentonitic layers	-	23	River downcutting	An ancient bridge in the county of Shropshire, England
41	Bonnard et al. (2000)	-	Surface surveying and inclinometers	60	Rainfall	Polmengo bridge near Faido, Switzerland
42	Brooker and Peck (1993)	Clay shale	Personal estimates	90 – 120	Toe erosion, precipitation and horizontal forces from the bridge anchor	Peace River suspension Bridge and a water pipeline, British Columbia, Canada
43	Brooker and Peck (1993)	Clay shale	-	100	Bridge construction	The Bismarck Bridge across the Missouri River, USA
44	Kang et al. (2000)	Incompetent shales	-	240	Bridge construction	The Sugock Bridge in Andong, Korea
45	Moore et al. (2006)	Clay	Inclinometers and surface monuments	10 – 14	Reservoir level fluctuations and rainfall	Mica Dam, British Columbia, Canada
46	Wu et al. (2008)	Coal beds with sandstones and mudstones	Inclinometers	57	Underground coal mining	Hancheng power station, China
47	Catalano et al. (2000)	Clay	Inclinometers	127	Reservoir filling	Trinita Dam, Italy
48	Catalano et al. (2000)	Softened clay layer	Topographic monuments	110	Reservoir filling	Casanuova Dam, Italy
49	Gillon and Saul (1996)	Sandy silt clay gouge	Aerial survey data	180	Rainfall	Clyde Dam, New Zealand
50	Bai et al. (2008)	Fine grained material	-	730	Reservoir filling	Lijiaxia hydropower station, China
51	Brooker and Peck	Clay shale	Inclinometers	100	Rainfall	Oil well casing, Swan Hills,

	(1993)					Alberta, Canada
52	Barlow (2000)	Clay shale	Geomorphologic evidence	188	Stream incision	Pipeline, Fort McMurray, Canada

Table 3-2: Summary of the Case Histories on the Vulnerability of Urban Communities to Slow Moving Slides

Case Number	Location	Degree of Damage	Movement Rate (mm/yr)	Soil Type	Remarks
1	Italy	No exact statement of damage but could be minor	5	Quaternary deposits overlying upper Miocene bedrock	
2	Italy	Cracks in buildings	8	Clay	Cracks might be from buildings subsidence
3	Costa Rica	Cracks on the ground and in some buildings	<10	Residual soils overlying cohesive saprolitic soils underlain by weathered igneous rock	
4	Switzerland	Minor damage to village houses and infrastructure	10	Clay shales	Development in the village is not affected by slope movements
5	Australia	Cracks in an embankment within the site in addition to some bent trees	12	Colluvium over residual soils overlying bedrock	
6	United Kingdom	It is considered that there could be a threat to a coastal road in a town	12	Well jointed rock with no shear surfaces	
7	Peace River town, Canada	Removal of a portion of a street and structural distress to some houses	14	Glacial deposits overlying preglacial lake clays over clay shale	
8	Italy	Open cracks, wall disjunction and badly working casings	16.2	Rock	Authors classified this damage as light to moderate
9	Italy	Damage to dwelling houses	26	Marly clay	
10	Ecuador	10^0 tilting in the walls of a farmhouse	30	Soil over bedrock	

11	Norway	Minor damages could occur to residential settlements and towns	30 – 100	Rock	A wide scale study. A warning system was designed where the recorded rate lies in the green range (safe and no damages expected)
12	Brazil	Cracked pavements in streets and damages to houses	80	Interface between colluvium and clayey siltstone	
13	United Kingdom	Cracks in roads and footpaths of a town and damage to seawall structures	91	-	
14	Germany	The slides threatens a village by debris flow	92	Gravel and silt	
15	Regina beach, Canada	Rupture of service utilities, ground cracking. No damage to concrete sidewalk	108	Bentonitic clay shales	The study concluded that 100mm/yr is enough to break a municipal water line
16	China	Cracks in roads and houses of a residential settlement on a slope	170 – 240	Colluvium	
17	Croatia	Houses suffered damage (not specified)	150 – 300	Clay	
18	Norway	Minor to moderate damage may occur to residential settlements	200 – 365	Rock	
19	USA	Cracks in houses Walls buckling Bending of doors and windows Damage of the rear wall of a garage by downslope movement	306	Plastic lacustrine clay	

20	United Kingdom	Movement led to major slope failures below a hotel building	861	Stiff, fissured overconsolidated Barton clay	
21	China	Cracks in a slope within a residential complex Severe damage to the backwall of a building	2000 (a maximum of more than 4000)	Soil rock interface	Due to the implementation of a warning system, the buildings were evacuated and no life losses took place
22	Italy	Severe damage to Crago village buildings	4000	Clay	
23	Ecuador	Parts of some houses of the city of Loja were separated by 1m in 2 months	6000	Sedimentary rocks	
24	Japan	Collapse of a car repair factory	9100	Earth slide	
25	Italy	Partial collapse to a house in a residential complex	51100	Quaternary terrain	

Table 3-3: Summary of the Case Histories on the Vulnerability of Highways and Railways to Slow Moving Slides

Case Number	Location	Degree of Damage	Movement Rate (mm/yr)	Soil Type	Remarks
26	United Kingdom	Cracks in road pavement Road needed re-pavement every 3 or 4 years	13.8	Glacial deposits overlying boulder clay	
27	Greece	Cracks in the pavement of a major highway	13 – 19	-	
9	Italy	Traffic disruption to a highway	26	Marly clay	
28	Alberta, Canada	Cracks in a highway that needed patching once or twice a year	35	Presheared bentonitic clay shale over sandstone	
29	Italy	Damage not specified	44	Softened clay	A previous reactivation caused lots of damage and has interrupted a major road and highway
31	Alberta, Canada	Cracks in highway 49 Patching performed once a year	Minimum of 15 and up to 100	Till overlying preglacial lake clay and clay shale	
30	Italy	Damage not specified but not severe	65	Quaternary deposits in addition to dislocated bedrock	A previous reactivation led to the collapse of a long stretch of a national road
32	Italy	Undefined threat to a road and a railway	132	Intensely fissured clay shale and limestone over a bedrock	
33	China	No quantification of damage reported	450	Volcanic saprolite over competent bedrock	Severe rainstorm events cause road blocking
34	United kingdom	No damage reported to a coastal raod This rate was recorded after remedial	560	Sedimentary rocks overlain by glacial till	

		measures have been installed		
35	Austria	Development of large fissures and failures in the cut slopes of a motorway A major traffic disruption expected if no drainage measures were adopted	590	Intensely sheared shaley graphite layer
36	United kingdom	Traffic obstruction of a trunk road Breach of the boundary between the road and the rear garden of a residential property	600 – 6000	Glacial till overlying a sequence of mudstones and siltstones
37	Sri Lanka	Severe disruption to a railway corridor	5600	Sandy silt and clayey silt colluvium
38	Malaysia	Disruption to a highway construction	7000	Rock (schist)
24	Japan	Upheaval of a part of a highway	9100	Earth slide

Table 3-4: Summary of the Case Histories on the Vulnerability of Bridges to Slow Moving Slides

Case Number	Location	Degree of Damage	Movement Rate (mm/yr)	Soil Type	Remarks
39	Yugoslavia	No actual damage to the SLOBODA bridge but there is a threat. Mitigation plans are set for probable distress in the future	10	Weathered marly clay	
40	United Kingdom	Continuous movement of abutment and piers	23	Bentonitic clays	
41	Switzerland	Numerous cracks in the abutment of a bridge caused by a very high flood	60	-	
42	British Columbia, Canada	Displacement of one of the Peace River suspension bridge anchors led to the bridge collapse	90 – 120	Clay shale	
31	Alberta, Canada	The Little Smoky bridge west pier needs continuous extension to accommodate movements	100	Till overlying clay shale	
43	USA	The Bismarck bridge pier needs continuous extension to accommodate movements	100	Clay shale	
44	Korea	Bridge suffered severe deformations	240	Alternating competent sandstones and incompetent shales	

Table 3-5: Summary of the Case Histories on the Vulnerability of Dams to Slow Moving Slides

Case Number	Location	Degree of Damage	Movement Rate (mm/yr)	Soil Type	Remarks
45	British Columbia, Canada	Minor or no damage to Mica Dam	10 – 14	Rock slide moving on thin clay gouges	
46	China	Serious damage to the Hancheng power station structures	57	Coal beds with sandstones and mudstones	
48	Italy	Fissures and cracks observed in Casanuova dam	110	Softened clay layer	
47	Italy	Damage to the electric cabin and the guardian's house of Trinita Dam No damages to the dam	127	Highly permeable formation over a weathered clay formation	
49	New Zealand	Slide volume is enough to block the Clyde dam reservoir The slide generated waves are expected to be higher than the free board	180	Planar rock slide moving over slickensided sandy silt clay gouge	
50	China	Failure of localized disintegrated loose slide mass on the surface of the slope Slide generated waves may endanger the hydropower station	730	Fine grained material with a clay percent sometimes over 90%	

Table 3-6: Summary of the Case Histories on the Vulnerability of Linear Infrastructures to Slow Moving Slides

Case Number	Location	Degree of Damage	Movement Rate (mm/yr)	Soil Type	Remarks
51	Alberta, Canada	Bending of oil well casing (Swan Hills Oil Field)	100	-	
42	British Columbia, Canada	Break down of a pipeline	90 – 120	Clay shale	
52	Fort McMurray, AB, Canada	Displacement of pipelines	188	Glacial deposits overlying Cretaceous sedimentary clay shale over oil sands	
24	Japan	Rupture to a water service pipe	9100		

Table 3-7: Degree of Damage Expected from Slow Moving Slides to Urban Communities versus Movement Rate

Movement Rate (mm/yr)	Degree of Damage
0 – 10	- Minor or no damage
10 – 100	- Cracks in streets, footpaths and nearby embankments - General signs of distress like bent trees - House walls disjunction and badly working casings - May cause damage to small dwelling houses
100 – 300	- Cracks are wide to the extent that houses start to suffer a noticeable damage - Rupture of service utilities
300 – 800	- House walls buckling, bending of doors and windows and various damages in houses
800 – 4000	- Severe damage and failures to slopes or retaining walls supporting buildings - If no warning system implemented, human losses may occur
>6000	- Complete collapse of buildings

Table 3-8: Degree of Damage Expected from Slow Moving Slides to Highways and Railways versus Movement Rate

Movement Rate (mm/yr)	Degree of Damage
0 -10	- Minor or no damage
10 – 100	- Cracks start to appear - Developed cracks need patching once or may be twice a year - Needs re-pavement once every 3 or 4 years - May cause traffic disruption
100 – 160	- Wider cracks in pavements - Need patching at intervals less than one year
160 – 1600	- Development of large fissures in embankment slopes - Failure may occur to embankment slopes - A major traffic disruption is expected if no drainage measures were implemented
> 1600	- Severe collapse to the highway or the railway - Traffic obstruction - May lead to life losses

Table 3-9: Degree of Damage Expected from Slow Moving Slides to Bridges versus Movement Rate

Movement Rate (mm/yr)	Degree of Damage
0 -10	- Minor or no damage
10 – 30	- Movement of piers and abutments take place but cracks may be very small - Mitigation plans should be set for probable future distress
30 – 100	- Numerous cracks start to appear - There is a continuous need to extend the bridge piers and abutments to accommodate movements
> 100	- Deformations become severe and pose a real threat to the bridge safety - Suspension bridges may collapse if the bridge anchors lied in the movement zone

Table 3-10: Degree of Damage Expected from Slow Moving Slides to Dams versus Movement Rates

Movement Rate (mm/yr)	Degree of Damage
0 – 16	- No reported damage
16 – 160	- Serious damages to the hydropower structures - Fissures and cracks may be observed in earth and rock fill dams
> 160	- Failure of loose masses on the slope surface and hence the reservoir may be blocked - Slide generated waves may overtop the dam crest

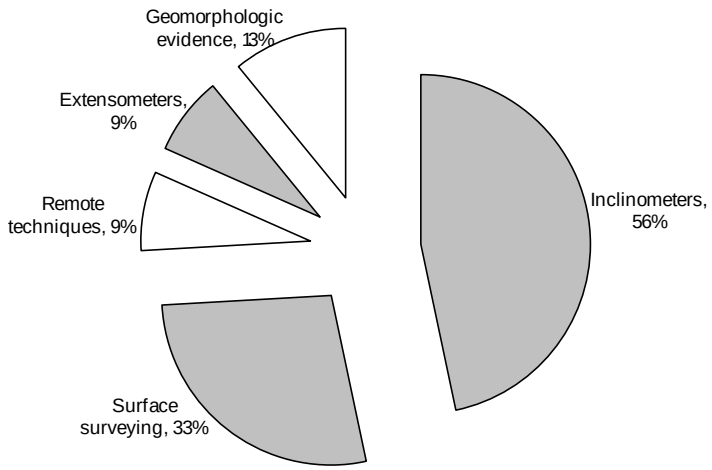

Figure 3-1: Percentages of Different Methods of Displacement Measurement

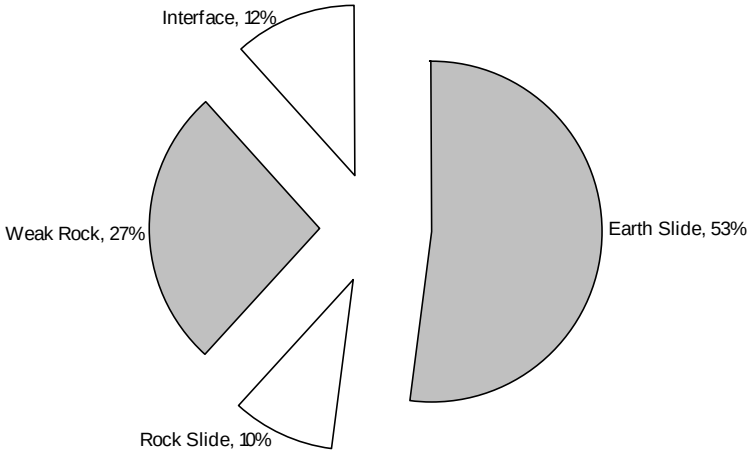

Figure 3-2: Percentages of Different Material Types Hosting the Rupture Surface

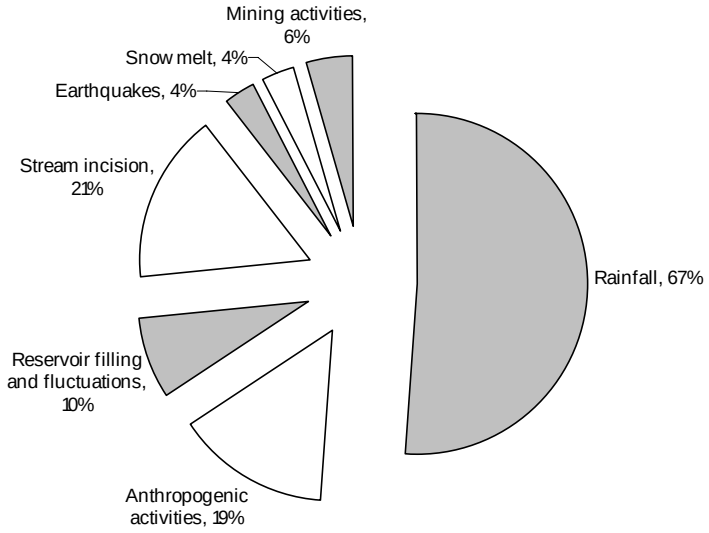

Figure 3-3: Percentages of Different Triggers of Movement

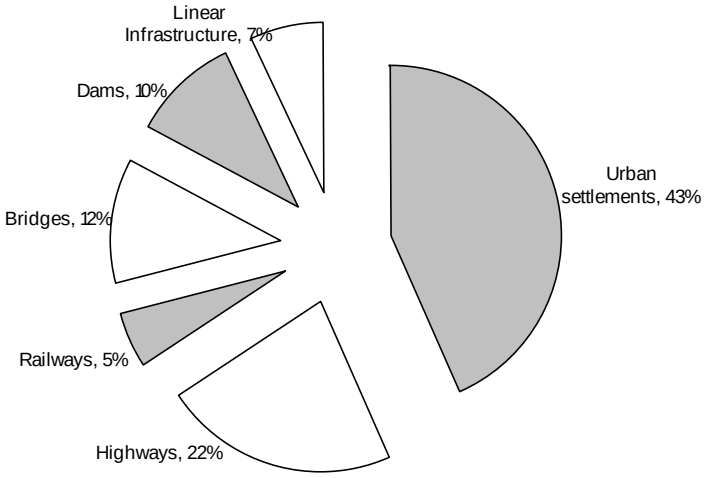

Figure 3-4: Percentages of Citation of Different Vulnerable Facilities in the Reviewed Literature

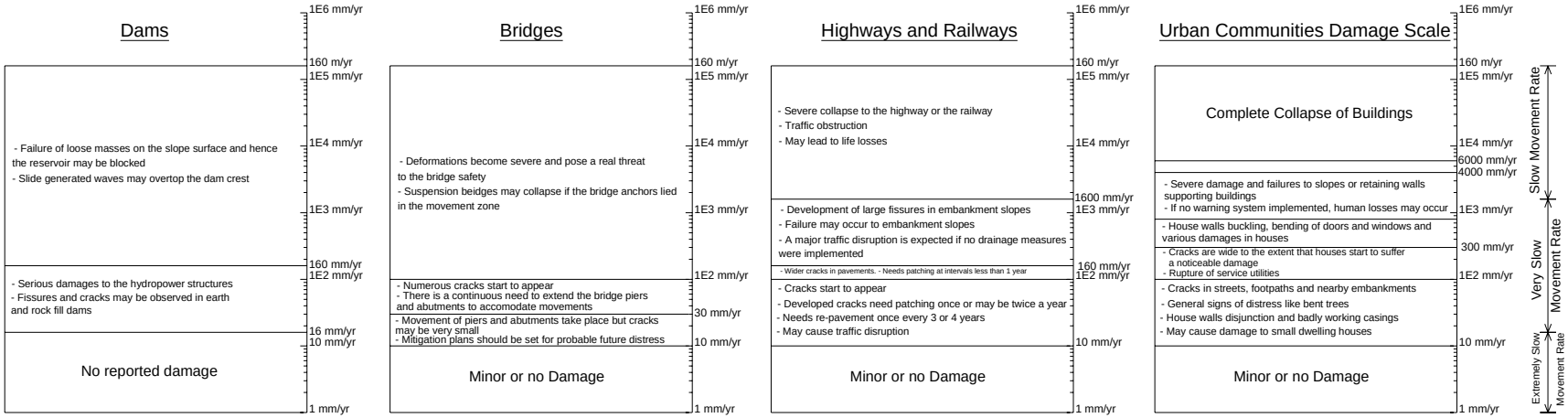

Figure 3-5: Damage Extent of Different Facilities to Slow Moving Slides shown together with the Movement Classification as Slow, Very Slow or Extremely Slow

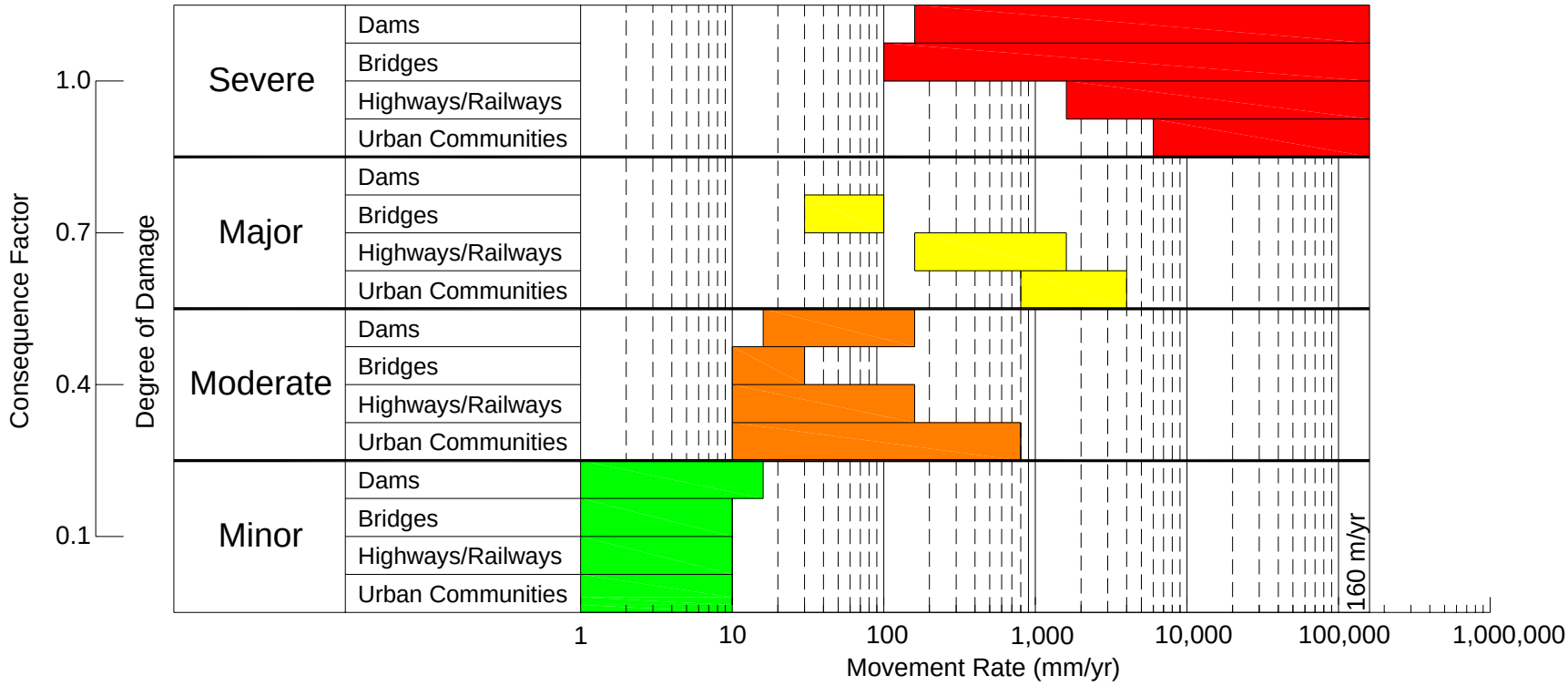

Figure 3-6: Schematic Representation of the Developed Scales showing the Degree of Damage and the Consequence Factor versus Movement Rate

4 The Instability at the Little Chief Slide

4.1 Introduction

The 800 million m^3 Little Chief Slide is on the north-west side of the former Columbia River valley in the Monashee Mountains, about three kilometers upstream (north) of Mica Dam. The valley at this location is about 1350 – 1425m deep and has an average slope of about 30º. The width of the slide is approximately 1800m along the former Columbia River, and the horizontal distance from the toe to the crest is approximately 2700m. The construction of the Revelstoke and Mica Hydroelectric projects on the former Columbia River resulted in considerable rises in water levels behind the dams. These rises caused the inundation of the toes of many ancient rockslides like the Checkerboard Creek Slope, Downie Slide, Dutchman's Ridge and the Little Chief Slide. Both the Downie Slide and Dutchman's Ridge have been stabilized by using drainage tunnels and drain holes. The stability of these slides is a major design, reservoir operation and safety requirement. Figure 4-1 shows a map location of both the Mica Dam and the Little Chief Slide, and Figure 4-2 shows an aerial view of the dam and the slide.

The current rate of movement in the Little Chief Slide is around 10 to 14 mm/year (0.027 – 0.038 mm/day). The slide is thus classified as an extremely slow slide according to the classification by Cruden and Varnes (1996). The first-time slide appears to have occurred thousands of years ago, and the current movements are post-failure movements. The Little Chief slide is presumably moving as one entity, as evidenced by the equal rate of movement observed at many surface monuments along the slide. The movement zones support depths of rock ranging between 100 and 300 meters (Moore et al., 2006).

The site has been under investigation since the 1960's and more recently since 2004. This chapter presents the history of site investigation of the Little Chief Slide, followed by an explanation of the site geology. The groundwater flow regime at the Little Chief Slide is simulated numerically by using the SEEP/W finite-element-based code (Krahn, 2004). The available historical information about the slide suggests that seasonal pore pressure changes have minimal effects on movement and that creep deformations of the materials forming the movement zones represent an appreciable percent of the total movement. An analysis of the field movement records at six movement zones is carried out, and the results suggest that the total movement results from both creep deformations and seasonal hydrologic changes. Creep deformations may account for about 73% on average of the total movement of the Little Chief Slide.

The quantification of creep deformations is an important outcome of studying the instability at the Little Chief Slide. In all the studies reviewed in the previous

chapter, no attention was paid to creep as a component of movement. The previous studies correlated, qualitatively or quantitatively, the total movement to one or more triggers like rainfall or toe erosion. Creep is the movement that proceeds during the periods of zero pore pressure changes or constant effective stresses. Hence, creep must be quantified in order to assess the effectiveness of the implemented mitigation options.

The creep behaviour of the slide materials of the Little Chief Slide is also investigated in the laboratory, and the results of the experimental testing program are presented. The laboratory strain rates are compared to the available records from the field.

4.2 Previous and Current Investigations

4.2.1 Early Investigations

The Little Chief slide was identified during an airphoto study of the proposed Mica Dam reservoir in 1961. The initial investigation of the site started in 1968 and 1969 during the construction of the Mica Dam (1968 – 1970). The investigation involved drilling boreholes DH901, 902, 903, 904 and 906 as shown in Figure 4-3. A further field investigation was carried out in 1976 and another investigation in 1985 (DH85-24) as part of the nearby Dutchman's Ridge investigation. The 1985 investigation aimed at exploring the slope movements and groundwater pressures, and determining if the characteristics of the slides at Dutchman's Ridge and the Little Chief Slide were similar. However, some of the installed casings were too short to penetrate the slide base. This problem was evident by comparing the movement rate from the inclinometers with the movement rate of the surface monuments installed at the same locations. The inclinometer installations from 1969 to 2004 showed that the slide is moving extremely slowly at a rate of 4 – 14mm/year even after the reservoir filling (1973 – 1976). However, prior to 2004, there were no functioning piezometers. Some water levels were measured in leaky inclinometer casings. During the initial investigation, there was a concern that the toe of the Little Chief Slide was resting on liquefiable sand. However, the subsurface investigation and the monitoring program showed that such sand did not exist beneath the toe (Rapp, 2006; and Moore et al., 2006).

4.2.2 Recent Investigations

BC Hydro found that the previous investigation program gave neither a complete image of subsurface conditions, nor did it provide sufficient information to predict the slope's behaviour. Consequently, a new extensive subsurface investigation and monitoring program was started in 2004. The recent

investigation by BC hydro was aimed at studying the stability under seismic loading, reducing the uncertainty of the geologic and hydrologic models, understanding the mechanics of slope movements and determining the risk of failure (Rapp, 2006; and Moore et al., 2006).

A new borehole, DH04-01, was drilled to a depth of 265m in 2004 (see plan location in Figure 4-3). This borehole is equipped with a multi-point piezometer and a data logger. In addition, five surface survey monuments and helipads were constructed in order to monitor the movement in the upper half of the slope. The in-place inclinometers (IPI's) previously installed in boreholes DH901 and 906 were replaced and refurbished as well.

The 2005 field investigation program began in the fall of 2005 and involved drilling seven new boreholes (DH05-01, DH05-02A, DH05-03, DH05-04, DH05-05, DH05-06 and DH05-07) with an average depth of 325 meters in addition to the seven already existing boreholes. The locations of the boreholes drilled during 2005 are shown in Figure 4-3. The 2005 program involved installing inclinometer casings in boreholes DH05-03, 04, 05, 06 and 07 as well as in-place inclinometers in these five boreholes. The IPI's were installed after reviewing the inclinometer measurements taken in spring 2006. The program also involved conducting piezometric profile testing (PPT) in boreholes DH05-01, 03, 04 and 05. Continuous piezometric pressures have been monitored in boreholes DH05-01 and DH05-02A by installing multi-point piezometers and data-logging systems. In addition, the field program involved installing 15 surface survey monuments to monitor surface movements. The detailed core logs of the borehole installed in 2004 and the seven boreholes installed in 2005 are shown in Figure B-1 through Figure B-8 in Appendix B.

An adequate hydro-geological model must allow for the determination of the effect of reservoir filling and weather cycles on the ground water pressures and, hence, the stability. The presence of low permeable shear zones caused pressure differentials of up to 75 meters between the overlying and the underlying materials. As mentioned above, numerical analyses simulating the initial groundwater conditions before the construction of the Mica Dam, the effects of the reservoir filling and the effects of rainfall and reservoir level fluctuations are conducted as part of this research. The available pore pressure data and their seasonal changes are presented in Section 4.6.

4.3 Quaternary and Structural Geology and History of Movement

The toe of the slide had overridden Quaternary deposits of glacial till and granular materials (sand and gravel), as the investigation of boreholes DH903 and DH904 revealed. The stratigraphy in one of the two drill holes shows two glacial till units separated by a 22 meters thick layer of rock-slide deposits. The previous

geological interpretation revealed that the slide occurred at the end of the most recent Fraser glaciation and overrode the glacial deposits. This interpretation implies that the slide occurred less than 11000 years ago. However, the current geological investigation suggests that the overridden till, which lies below the valley floor and rests directly on bedrock, is more likely associated with an older glaciation that ended approximately 60000 years ago. This is attributed to the presence of deep tills in boreholes DH903 and DH904 that are 85 to 100 metres below the drowned channel of the Columbia River. Hence, it is suggested that these tills were deposited in an ancestral Columbia River valley prior to the Fraser glaciation. The slide debris that overlies these tills refers to an earlier phase of activity associated with the Olympia inter-glaciation period, 60,000 – 25,000 YBP (Friele and Clague, 2006).

Some surface ash deposits (Mazama ashes) in the relaxed zone above the head scarp whose age dates back 7700 YBP had not been disturbed by the slide movements. In the eastern part of the slide, however, some slide movements have taken place since the last 7700 years evidenced by the burial of the Mazama ashes by the landslide debris in this area and the lack of Mazama ashes on the debris surfaces. Hence, it is currently believed that the first slide movement started at least some 60000 years ago, and that no substantial movement has occurred for 7700 YBP (Friele and Clague, 2006; Moore et al., 2006; and Rapp, 2006).

Moore et al. (2006) presented a brief summary of the structural geology of the Little Chief Slide. The materials encountered at the slide are Upper Proterozoic metasediments that have been deformed possibly four times. The metamorphism of these materials has led to the formation of minerals between garnet and sillimanite grade. A regional normal fault trends along the toe of the slope under the valley bottom. This fault might have caused a 1500m offset in the stratigraphy. The faults underlying the base of the Little Chief Slide have possibly been formed due to the potential existence of the regional normal fault.

Evidence is available for only two of the four possible deformations recognized regionally. The first deformation is evidenced by the pervasive foliation. The second one is evidenced by a regional antiform adjacent to the northeast scarp and by minor folds elsewhere. The second deformation is also associated with lineations that usually plunge nearly downslope. However, some lineations plunge towards the opposite direction within an area that extends to about one third the slide width along the reservoir shoreline. This observation implies the possible occurrence of block rotation within the slide. Joints usually dip along micaceous foliations and run parallel to the lithological boundaries. An exposure of a major tectonic fault was observed at the reservoir level downstream from the slope. Another one was identified at the head scarp. Both dip steeply into the slope and may significantly alter the groundwater flow regime.

4.4 Nature of the Slide Materials

The high quality drilling techniques used in the 2005 site investigation program enabled a better characterization of the slide deposits, which range from soft, sheared micaceous material to hard fractured rock different from the underlying rock. Foliations within some blocks were uniform, indicating limited internal deformations. The occasional similarity of these blocks to the underlying rock led to the termination of drilling at depths shallower than the depth of the main shear zone, and this caused some misinterpretations.

The shear zone materials are mainly soft, granular or micaceous, enclosing some hard rock fragments. Shear zones containing thin clay layers are characteristic of the soft zones. The main rupture surface, or the basal detachment, is identified by the presence of slickensides and clay from a few millimetres to about 200 mm thick, followed by a suddenly-increased-quality rock. Although the underlying rock is sometimes fractured and sheared, these fractures and shears are tightly interlocked or intact. Figure 4-4 shows one of the main movement zones at a depth range of 242 – 245m in Borehole DH05-01.

4.5 Previous Laboratory Testing

4.5.1 Introduction

Various laboratory tests were carried out on samples from the soft zones of the Little Chief Slide. Some of these tests were carried out by the project consultants and were included in the BC Hydro 2005 field investigation report (Rapp, 2006). These tests are summarized in this section. Other tests have been carried out as part of this present research and are presented in Section 4.7.3.

The previous laboratory tests include the following:

- Grain size distribution analyses.
- Direct shear and index testing.
- Consolidated-Undrained triaxial testing and index testing.
- X-ray diffraction.

4.5.2 Grain Size Distribution

Grain size distribution analyses were carried out on 23 samples of colluvium, lodgment till and ablation till. The samples of colluvium were collected from the surface, and till samples were collected from the surface and from boreholes DH903 and 904. The purpose of these analyses was to distinguish among colluvial debris, lodgment till and ablation till. Lodgment till contains erratics in

addition to fine contents. Ablation till is, however, distinguished from colluvium only by the presence of erratics with striations (Friele and Clague, 2006). The grain size distributions for the 23 acquired samples are shown in Figure 4-5.

Grain size distribution analyses were also carried out on samples obtained from deep soft zones. Figure 4-6 shows the grain size distribution curves for two samples taken from boreholes DH05-04 and DH05-05 at approximate depths of 158.7 and 228.9m, respectively (Bhuyan, 2006). More grain size distribution analyses have been carried out as part of this research. These are shown in Section 4.7.3.

4.5.3 Index Testing

Index tests were carried out on one sample taken from borehole DH05-05 at a depth of 228.80 – 229.00m, but the results were missing from the BC Hydro 2005 field investigation report (Rapp, 2006).

4.5.4 X-ray Diffraction

X-ray diffraction analyses were carried out for 15 samples from different boreholes (McLeod, 2006). Table 4-1 summarizes the samples' information and the results of the analyses. High Montmorillonite content, indicating low shear strength, was found in the sample taken from depth 203.9m in borehole DH903. The strength values are provided in the next section.

4.5.5 Direct Shear Testing

Displacement controlled direct shear tests were carried out on 12 samples under vertical consolidation pressures that ranged between 2 and 6MPa. Each sample was subjected to four forward and reverse cycles. During the first forward cycle, the displacement rate was 0.4mm/hr until the maximum reached horizontal displacement was 6 – 9mm. The rate was increased to 4mm/hr in the next reverse cycle until a maximum displacement of 3mm more than the previous cycle was attained. The fast rate of 4mm/hr was maintained during the following forward cycle until a maximum displacement of 6mm was reached. A fourth and final reverse cycle was run under a displacement rate of 0.4mm/hr until a maximum displacement of 6mm was attained. Table 4-2 presents a summary of the direct shear tests results for the 12 samples. High Montmorillonite content was encountered in one sample taken from borehole DH903, as evident by the X-ray diffraction results. The residual friction angle of this sample was equal to 10^0. No other evidence of Montmorillonite was present in any of the drill cores, and Rapp (2006) concluded that it was a localized seam. Since our testing program includes triaxial drained creep and consolidated drained tests on samples taken from

borehole DH05-07, as is detailed in Section 4.7.3, the shear stress-horizontal displacement diagram for the sample taken from DH05-07 at depth 328.8 is shown in Figure 4-7.

4.5.6 Consolidated Undrained Triaxial Testing

Eight consolidated-undrained triaxial tests were carried out to determine the shear strength of the softer materials. The majority of the tested samples yielded residual friction angles between 22^0 and 31^0. The peak strengths were either the same as the residual strengths or slightly higher (Moore et al., 2006). The strength plots for this type of test were not available in the BC Hydro 2005 field investigation report (Rapp, 2006).

4.6 Ground Water Flow Modeling of the Little Chief Slide

4.6.1 Introduction

As mentioned in the previous section, an adequate hydro-geological model must enable the determination of the effects of the reservoir filling and weather cycles on the ground water pressures and, hence, the stability. Therefore, a ground water flow modeling for the Little Chief Slide is carried out to explore the effects of the reservoir filling as well as rainfall and reservoir level fluctuations on the ground water flow regime. The Little Chief Slide is investigated by using the SEEP/W finite-element-based software (Krahn, 2004) with the purpose of establishing the initial conditions before the reservoir filling, simulating the effect of the reservoir filling and then introducing the effects of both the reservoir level fluctuations and rainfall on the pore pressures inside the slide.

4.6.2 Available Data

4.6.2.1 Hydraulic Conductivity

Reliable values of the saturated hydraulic conductivity must be used for a proper ground water flow model to be established. In addition, the variation of the hydraulic conductivity with increased suction should be defined by using an adequate K-function so the transient effect of hydrological boundary condition changes can be modeled correctly.

In situ falling head tests (Piezometric Profile Testing) were performed inside boreholes DH05-01, DH05-03, DH05-04 and DH05-05 at different depths (Rapp, 2006). Figure 4-8 shows the available conductivity data from borehole DH05-01. Similar plots for boreholes DH05-03, DH05-04 and DH05-05 are included in

Appendix B (Figure B-9). Every two points having the same hydraulic conductivity value represent the depth interval over which the measurement was taken.

The amount of data is obviously limited. In order to assign each element in the proposed finite element mesh a representative hydraulic conductivity value, the available data have been correlated with the rock weathering condition available from the core logs, as shown in Table 4-3. Obtaining correlations between the saturated hydraulic conductivity and the depth below the ground surface or the Rock Quality Designation (RQD) was not possible. Hence, the hydraulic conductivity values are plotted against the rock weathering condition as shown in Figure 4-9. The bedrock with weathering conditions F, F-FS and FS is assigned a saturated hydraulic conductivity of 1.9 X 10^{-6} m/sec; the bedrock that is FS-SW is assigned a saturated conductivity of 5.4 X 10^{-6} m/sec; and all the materials that are more weathered than FS-SW are assigned a saturated conductivity of 3.2 X 10^{-5} m/sec. It is assumed, then, that the whole domain can be divided into three layers with different conductivities.

Cross-section A of the Little Chief Slide (see its location in Figure 4-3) is considered for analysis, for it passes through boreholes DH05-04, DH05-01, DH05-05 and DH04-01, which are well instrumented and provide good means for evaluating the numerical analyses results. Some useful data are available about the water level before and during reservoir filling in borehole DH902. Borehole DH05-02A lies about 90 meters north of the cross-section, so it is considered as well. Hence, more data to compare with the numerical analyses results are available for cross-section A than for cross-section B. As shown in Figure 4-10, the thickness of the middle layer is small and decreases downslope and upslope of boreholes DH05-05 and DH05-04, respectively. The upslope boundaries of the middle layer were extrapolated until they intersected. The boundary between the upper and lower layers was drawn parallel to the ground surface upslope of borehole DH05-04. The weathering conditions of the bedrock encountered in borehole DH05-02A confirm the position of the upper-lower layers boundary as being parallel to the ground surface. However, the stratigraphy of borehole DH04-01 shows a succession of slightly, moderately and highly weathered strata down to the end of the borehole at depth 265m. Hence, the upper-lower layers boundary at this location is modified as shown in Figure 4-10.

4.6.2.2 Pore Pressure Data

The piezometric data are available from three sources:

1. Falling head in-situ tests which were carried out at boreholes DH05-01, DH05-03, DH05-04 and DH05-05 at the depths indicated in Table 4-3. These tests are called Piezometric Profile Testing or PPT. This set of data is shown in Figure 4-11.

2. Some recent records of pore pressure fluctuations with time for the eleven multi-point piezometers (MP) installed in boreholes DH04-01, DH05-01 and DH05-02A. These data are shown in Figure 4-12 through Figure 4-14.
3. Some drill hole water levels before and during the reservoir filling at boreholes DH906 (DH05-05) and DH902. These data are shown in Figure 4-15, which shows the variation of the drill hole water level with the rise or drop of the reservoir level. Figure 4-15 reveals that the water level in DH906 (DH05-05) was almost unaffected by the rise or the drop of the reservoir level. On the other hand, the water level in DH902 rose from elevation 731.5m to 751.6m when the reservoir level rose from elevation 688.8m to 751.6m.

The available data from the PPT indicates that the pressure heads recorded in the lower layer in borehole DH05-01 are lower than those recorded in the upper layer. This may be attributed to the relatively higher conductivity of the upper layer, which consists of moderately to highly weathered rock, and, hence, the layer is more responsive to hydrological boundary condition changes, like rainfall and reservoir level fluctuations, than the lower layers. Therefore, it is assumed that the piezometric heads recorded in the underlying low conductivity layer correspond to the initial case before the reservoir filling. The validity of this assumption is supported by the observed match between the recorded value of the pressure head before the reservoir filling in borehole DH05-05 (formerly DH906) and the pore pressures recorded in 2005 in the underlying low conductivity layer (see Figure 4-11 and Figure 4-15). This match increased our confidence in this understanding.

4.6.3 Seepage Analysis

4.6.3.1 Introduction

Based on the above discussion, the seepage analysis of the Little Chief slide proceeded in four steps:

1. Steady state analysis: The head boundary conditions were: (i) the former Columbia River level, (ii) the average pore pressures recorded in the underlying low permeability rock at the locations of boreholes DH05-04, DH05-01 and DH05-05 (see Figure 4-11), and (iii) the drill hole water level recorded in DH902 (see Figure 4-15).
2. Transient analysis to simulate the reservoir filling.
3. Two transient analyses to simulate the effects of both the rainfall and reservoir level fluctuations on the pressure heads. Although each of the two effects is studied separately, the results are presented in the same subsection.

4.6.3.2 Material Properties

A transient seepage analysis requires a clear definition of the volumetric water content and the hydraulic conductivity variation with suction. A preliminary steady state analysis shows that both the middle and lower layers are mostly fully saturated. Hence, the volumetric water content and hydraulic conductivity functions are defined for the upper layer only. The definition of the two suction functions is not possible from laboratory experiments, and, hence, predictive tools are used. Grain size distribution analyses of 23 samples from lodgement till, debris and ablation till are available from the previous studies and are shown in Figure 4-5 (after Friele and Clague, 2006). The average grain size distribution is calculated and shown in Figure 4-16, and then, using the Ayra and Paris (1994) method, a volumetric water content function is developed. The saturated void ratio is assumed to be ~0.43 (like that of a sandy material), so the saturated volumetric water content is equal to 0.3. The coefficient of volume compressibility is set to 10^{-5}kPa^{-1}. Fredlund et al.'s (1994) method is used to predict the hydraulic conductivity versus the suction function from the calculated volumetric water content function. The predicted volumetric water content and hydraulic conductivity functions for the upper layer are shown in Figure 4-17.

As shown in Figure 4-17, the hydraulic conductivity drops down to extremely low values, 10^{-32} m/sec at the maximum suction 10^{6}kPa. Some issues can arise when using such extremely low values, especially when applying infiltration, since the maximum intensity of the rainfall recorded at the nearest weather station is around 10^{-7}m/sec. Hence, the rainfall may cause a full saturation of the system, an outcome which the measured data do not support. In addition, convergence problems are expected to arise due to the steep nature of the hydraulic conductivity function. Therefore, it is proposed to run the steady state analysis three times, each with a different volumetric water content and hydraulic conductivity function for the upper layer:

1. Purely horizontal function; i.e., assuming the upper layer remains saturated with increased suction. This case represents one extreme. The volumetric water content function in that case is assumed to be horizontal as well.
2. The predicted functions from the Ayra and Paris (1981) method and the Fredlund et al. (1994) method. This case represents the other extreme.
3. An estimated or assumed function that represents an intermediate case between the two extremes. The conductivity function is constructed by assuming that the hydraulic conductivity value drops to 10^{-10}m/sec (a typical clay conductivity value) at the maximum suction (10^{6}kPa). The volumetric water content is assumed to drop to 10% of its saturated value at the maximum suction (10^{6}kPa).

The three hydraulic conductivity and volumetric water content functions are shown in Figure 4-18 and Figure 4-19, respectively. For the middle and lower layers, both the volumetric water content and the hydraulic conductivity functions are assumed to be constant with increased suction due to the full saturation

condition of the two layers based on a preliminary steady state analysis, as mentioned above. Since the rock is relatively intact in these two layers and because preliminary analyses have showed the results to be insensitive to changes in the saturated volumetric water content, a very low value of 5% is assumed for the saturated volumetric water content. The coefficient of volume compressibility is set to 5 X 10^{-8} kPa^{-1}.

4.6.3.3 Steady State Analysis

The former Columbia River level defines the right head boundary condition of the domain. The recorded pore pressures in the underlying non-weathered bedrock at the locations of boreholes DH05-04, 05-01 and 05-05 as well as the drill hole water level recorded in DH902 before the dam construction define some pressure head boundary conditions. After running the steady state analysis, the shape of the phreatic surface to the left of borehole DH05-04 was completely horizontal. This shape is clearly attributable to the lack of any boundary conditions identified in this area. Although the area upslope of borehole DH05-04 is not of a primary interest because no measurements were taken in that area, reasonably defining the phreatic line shape in that area is necessary. It is found from the steady state analysis that the phreatic line runs approximately parallel to the ground surface in the upper half of the slope. Therefore, the resulting phreatic line is extrapolated from the upslope of borehole DH05-04, and a new set of fixed head boundary conditions are identified along a section located approximately 340m upslope of borehole DH05-04. In addition, the head boundary conditions are also defined at the left boundary of the domain. The analysis is carried out three times for the cases of the horizontal, estimated and predicted volumetric water content and conductivity functions. The shape of the mesh together with the resulting phreatic surface for the predicted function case is shown in Figure 4-20 as a sample result. The red dots represent the head boundary conditions used to identify the problem.

In order to assess the reliability of each model, the predefined pressure heads are compared to the calculated height of the phreatic line above the measurement point. This comparison or model calibration is essential to evaluate the reliability of the values used for the saturated hydraulic conductivity of different units. The results of the model calibration are summarized in Table 4-4, which reveal that the horizontal function greatly overestimates the phreatic line position at the location of borehole DH05-05 and downslope, and greatly underestimates its position upslope. The predicted function seems to replicate more accurately the field conditions than the estimated function, especially at the two higher boreholes (DH05-04 and DH05-01). However, the total absolute error is 63.1% for the predicted function versus 75.4% for the estimated function. As mentioned above, however, the use of the predicted function during the rainfall analysis may cause convergence problems. Therefore, it is decided to exclude the horizontal function (for the upper layer) from the remaining analyses and to carry out each of the reservoir filling, rainfall and reservoir fluctuations analyses once by using the predicted function and a second time by using the estimated one.

In order to gain more confidence in the assigned values of the saturated hydraulic conductivity, the same analysis is repeated but by lowering the value of the saturated hydraulic conductivity of the upper layer by one order of magnitude, i.e., 3.2 X 10^{-6} m/sec. In other words, the defined functions points, either the predicted or the estimated, are shifted down by one order of magnitude. The resulting phreatic line for the case of the predicted functions is shown in Figure 4-21 as an example. The use of the estimated functions yields a similar shape. The predefined pressure heads at each borehole are compared to the calculated height of the phreatic line above the measurement point after using different values for the hydraulic conductivity. The comparison is shown in Table 4-5. In addition, it is attempted to lower the saturated hydraulic conductivity of the lower layer by one order of magnitude as well, i.e., 1.9 X 10^{-7} m/sec. A similar comparison is carried out and the results are shown in Table 4-6.

A comparison of the error percentages in Table 4-4, Table 4-5 and Table 4-6 shows that the use of the first set of conductivity values replicates more reasonably the initial groundwater conditions at the Little Chief Slide. Unreliable results are obtained when the hydraulic conductivity contrast is changed by only one order of magnitude. Freeze (1977) carried out numerical modeling of the groundwater conditions at the Downie slide. He concluded after a series of analyses that the average hydraulic conductivity of the geologic materials encountered at the Downie slide was 10^{-7} m/sec. He concluded as well that the contrast of hydraulic conductivities between the low-conductivity shear zones and the high-conductivity layers was at most two orders of magnitude, i.e., 10^{-6} to 10^{-8} m/sec. Field conditions were found to be reasonably represented either by a homogeneous slide (K_{sat} = 10^{-7} m/sec) or a layered slide where the conductivities ranged from 10^{-6} to 10^{-8} m/sec.

The absolute values of the conductivities that are assigned to the different layers of the Little Chief Slide in the steady state analyses might be a bit higher than what would be expected for these kinds of materials. This discrepancy is due to the composition of the water in the drillhole that contains drilling additives (Rapp, 2006). Since the main aim is to simulate the field pore pressures and not the flow rates, the behaviour of the system becomes primarily dependent on the ratios between the conductivity values of different layers and not the absolute values. The chosen contrast between the conductivities of the different units is considered to practically represent the initial pore pressures in the field.

4.6.3.4 Reservoir Filling Analysis

The reservoir was filled between 1973 and 1976. In terms of seepage analysis, the right head boundary condition value is raised from the former Columbia River level to the minimum reservoir level, i.e., at El. 740m. The water level is assumed to rise from the old former Columbia River level to the minimum reservoir level in a period of two months and then to stay constant for a period of 360 months or

30 years, which represents the time period from the filling up of the reservoir until the time the recent measurements were taken. The initial conditions for this transient analysis are the output of the previous steady state analysis.

In order to accurately model the reservoir filling process, the time steps are chosen so as to be as small as practically reasonable during the filling and after reaching the minimum reservoir level and then are increased until the end of the studied time range. The rise of the Columbia River level to the minimum reservoir level is modeled by ten time steps; each is 0.2 months, or six days. The next ten time steps have the same increment of six days. The rest of the studied time period (356 months) is modeled by 89 time steps; each is four months long. The total time steps for modeling the transient effect of the reservoir filling process are 109 steps. As the minimum pressure head at any of the locations of interest (Table 4-4) is around 52m, excluding the results at borehole DH902, the tolerance value of the residual pressure head during the iterative process of the numerical solution is set to six meters (approximately 10% of the minimum expected value).

The analysis starts by using the estimated volumetric water content and hydraulic conductivity functions. Figure 4-22 shows the phreatic surface location for both the initial conditions (the same as the output of the previous steady state analysis) and after the reservoir filling. Figure 4-22 reveals that the effect of the reservoir filling extends for about 995m inside the slope from the slope toe (the intersection of the minimum reservoir level and the ground surface). Using the predicted volumetric water content and hydraulic conductivity functions, the effect of the reservoir filling extends back up the slope for ~960m. The steep nature of the predicted hydraulic conductivity function caused non convergence in the solution in the sixth time step only, i.e., during the reservoir filling. The residual pressure head is 6.6 meters. No convergence issues appeared in the other time steps or when using the estimated functions.

The results of the numerical analysis are compared to the available pore pressure measurements before and after the reservoir filling. At borehole DH902 (see Figure 4-15), the recorded data indicate a rise in the pore pressure head due to the reservoir filling by 20.1m. The model predicts a phreatic surface rise by 19m for both the estimated and predicted functions. At the location of borehole DH05-02A, the minimum recorded water surface depth below the ground surface in 2005 was 24m (see Figure 4-14). The numerical model locates the water surface after the reservoir filling at depths 27 and 29m for the estimated and predicted functions, respectively. Borehole DH901 is about 140m from the reservoir shoreline although it does not lie on section A. The recorded rise in the piezometric head due to the reservoir filling is 31.5m (see Figure 4-23), and the numerical model results indicates a rise of 30 and 36m when using the estimated and predicted functions, respectively. At the location of borehole DH05-05 (formerly DH906), the recorded pore pressures before and after the reservoir

filling were not changed. However, the numerical model indicates rises of 7 and 8m for the estimated and predicted functions, respectively.

The comparison between the model results and the actual data shows that the model can accurately simulate the filling of the Mica Dam reservoir at the locations of the four boreholes mentioned above. The only location at which the model cannot replicate the field conditions is borehole DH04-01. The ground surface elevation at DH04-01 is 902m. As shown in Figure 4-12, a deeper piezometer installed at DH04-01 indicates a water level fluctuation of 10meters (EL 788 – 798m). These fluctuations were recorded since 2005 and are assumed to be due to both rainfall effects and reservoir level fluctuations effects. The minimum water table should then be the water table after reservoir filling. This assumption is supported by the recorded data at the location of borehole DH05-05. The piezometric head fluctuated between 938 and 945m during 2005 and 2006 (see Figure 4-24). The minimum elevation (938m) is only 0.8m above the piezometric head elevation that was recorded before and after reservoir filling (see Figure 4-15). Hence, the piezometric elevation 788m at DH04-01 is considered the water table elevation after the reservoir filling. The numerical analysis results show, however, that the water table elevation after the reservoir filling is 843m. It is considered that the model overestimated the location of the phreatic surface for the steady state conditions, and, hence, the calculated water table elevation after the reservoir filling is higher than the actual value. The reason for this overestimation may be the presence of inward dipping shear zones, which caused pressure differentials up to 75m to occur along borehole DH04-01 (Moore et al., 2006). A shallower piezometer showed a fluctuation of 4m only (El. 860 – 864m) since 2005. The effect of this low conductivity dipping shear band cannot be modeled due to the very small thicknesses of the shear bands relative to the large dimensions of the studied domain.

The numerical analysis results (as shown in Figure 4-22) show that the pore pressures at the locations of boreholes DH05-04 and DH05-01 remained essentially constant, and that the steady state conditions were not exceeded; i.e., no effect of the reservoir filling occurred at these locations. As shown in Figure 4-24, the pressure head difference recorded in borehole DH05-01 between April and July of 2006 is 7 meters. As illustrated above, the minimum piezometric elevation (El. 1148) would correspond to the water table after the reservoir filling. Figure 4-11 clearly reveals that this elevation is essentially equal to the minimum pressure heads recorded in the lower layer. Therefore, the available data suggest that no noticeable effects occurred at this location as a result of the reservoir filling. This conclusion is supported by the results of the numerical analysis.

4.6.3.5 Rainfall and Reservoir Level Fluctuations Effects

The recorded changes in pore pressures over an annual cycle are mostly attributable to the amount and rate of infiltration in addition to the effect of the reservoir level fluctuations. Both effects are studied in this subsection although

they are investigated separately in the numerical model. The results are viewed separately and then compared with the recorded pore pressure changes. The tip elevations of the eleven multi-point piezometers (MP) installed in boreholes DH04-01, DH05-01 and DH05-02A are shown in Table 4-7. The measured piezometric elevations together with the reservoir level fluctuation cycle are shown in Figure 4-12 through Figure 4-14, as indicated above.

The nearest weather station is the Mica Dam Station (52.05^0 N, 118.59^0 W and Elevation 579.1m). The ground surface elevation at the location of borehole DH05-04 (the highest borehole of interest) is 1396.8m. There was a concern that the rainfall at the slope toe could be snow upslope. However, an altitude difference of ~820m is expected to make a temperature drop of 5^0 to 6^0 C (a similar temperature gradient has been reported in a BC Hydro report on the probable maximum water input in the Downie slide, Revelstoke project, Report no. DD121, 1978). Therefore, rainfall with variable intensity is applied at the ground surface from the location of borehole DH05-04 down to the slope toe. Figure 4-25 shows the input mesh used in simulating the rainfall effect.

The rainfall records at the Mica Dam weather station are available both hourly and daily. As it is proposed to simulate the rainfall process since 1976 (after the end of reservoir filling), hourly and daily rainfall distributions with time are expected to cause convergence problems due to the steepness of the input infiltration function. Hence, the monthly rainfall data were used as input to the proposed infiltration function. Two problems are encountered while trying to assign a representative infiltration rate function:

1. The amount of water that infiltrates into the soil is a quotient of the recorded precipitation due to the effects of evapo-transpiration and surface runoff. It is assumed in the analysis that all the precipitation infiltrates into the soil. This assumption should give an upper bound solution to the pore pressure increase due to infiltration.
2. The falling rain during the winter months (from the beginning of December to the end of March) does not actually penetrate into the soil but can be considered to cause wetting of the existing snow cover. In the spring, the snow starts to melt and this melting causes significant amounts of water to infiltrate through the soil. Therefore, it is assumed in the analysis that the infiltration rate during the winter months is essentially zero. The total amount of the recorded precipitation during these months is equally divided and added to the reported rainfall during the spring months (April to June). For example, if the total precipitation from the beginning of December until the end of March is 150mm in a certain year, the recorded rainfall in each of the spring months is increased by 150/3 = 50mm before using in the input infiltration function. The rainfall data recorded during the summer and fall months (July to November) is used unchanged in the input infiltration function.

Figure 4-26 shows the distribution of the recorded monthly rainfall from the beginning of 1976 until the end of 2006 based on Environment Canada records, and Figure 4-27 shows the redistributed infiltration rate function. To simulate the reservoir level fluctuation cycle and rainfall variation with time effects accurately and practically, the time step chosen for the reservoir fluctuations analysis is one day and is set to half a month while analyzing the rainfall effect since the data are available monthly. 1216 and 740 time steps are used for the reservoir fluctuations and rainfall analyses, respectively. The phreatic surface of the last time increment in the reservoir filling analysis is imported to represent the initial conditions before introducing the transient functions. As mentioned above, each of the two analyses is carried out twice, once by using the estimated volumetric water content and hydraulic conductivity functions, and a second time by using the predicted functions.

The simulation of the reservoir fluctuations effect shows that both the estimated and predicted functions yield similar results. However, the use of the predicted functions to simulate the rainfall effect causes convergence problems, and the residual pressure head significantly exceeds the predefined tolerable value (six meters) in many iterations. The analysis was stopped after 50 time steps, and the results are considered unreliable. Hence, the results of simulating the rainfall effect are shown based on using the estimated material functions only as an input. The shape of the phreatic surface throughout the different time steps of the rainfall analysis using the estimated and predicted functions is shown in Figure 4-28 and Figure 4-29, respectively. The values of the residual pressure head in the non-converged time steps using the predicted functions in the rainfall analysis are illustrated in Figure 4-30.

The pressure head is queried at the points closest to the locations of the multi-point piezometers. Table 4-8 shows the coordinates of the queried nodes. Due to the big dimensions of the slope, the average element dimension is around 15 – 20m. This geometrical setting accounts for the difference in position between the multi-point piezometers and the queried points.

Figure 4-31 and Figure 4-32 show the results of the numerical simulation of the reservoir fluctuations and rainfall effects, respectively, at borehole DH04-01. The results of the reservoir fluctuations simulation show that the model predicts the piezometric elevations 30 – 45 meters higher than the actual measurements at the locations of MP47 and MP02. Similar observations are found from the results of simulating the reservoir filling in the previous subsection. The disregard of the two dipping shear zones in the numerical analysis may account for this elevation difference. The elevations of the two dipping shear zones, the elevations of the three multi-point piezometers and the measured piezometric head elevations are shown in Figure 4-33. The numbers in brackets refer to the recorded fluctuations. MP20 shows, however, the occurrence of artesian pressures, and the piezometric elevation predicted by the model is around 26m below the measured data.

The model predicts the piezometric head changes due to the reservoir fluctuations between April and August 2007 at the locations of MP47, MP20 and MP02 to be 5, 7 and 4 metres, respectively. The numerical model results indicate a less than one meter rise in the piezometric elevation due to infiltration during the same period at each of the three piezometers. The measured fluctuations at the three locations are, however, 6.5, 6 and 13 metres, respectively. The results suggest that the numerical model is capable of predicting practical values of the pore pressure fluctuations down to the elevation of the lower dipping shear zone. The results also suggest that the occurrence of artesian pressures at MP20 is due to the confinement of the zone around the piezometer with the very low permeability shear zones.

The results of the numerical analysis at the location of borehole DH05-01 are shown in Figure 4-34 and Figure 4-35. The difference in elevation between MP46 and MP40 is 15m, and the average width of the triangular elements in the finite element mesh is around 15 – 20m, as mentioned above. This small elevation difference led to the representation of both piezometers by the same node. The numerical simulation shows that the reservoir level fluctuations do not have any effect on the piezometric elevation at borehole DH05-01, when using either the estimated or the predicted functions. This conclusion is supported by comparing the actual measurements to the results of the numerical simulation of the rainfall effect (see Figure 4-35). It is clear that the trend of the variation of the calculated piezometric elevations due to rainfall matches to a great extent the trend of the measured data, i.e., a steep rise in the piezometric elevation during the spring and a relatively flat drop during the summer and fall months. However, the magnitude of the rise is significantly underestimated by the model. The calculated rise in the piezometric elevation due to rainfall in the period between March and June of 2006 is two meters at all the queried locations. The measured data show, however, a rise of 6 meters between April and July of the same year at MP74, MP46 and MP40. The rise is 9 meters at MP34.

The calculated piezometric elevations at MP34 and MP40 due to the applied infiltration function are about 10meters lower than the measured elevations. At MP74 however, the difference increases to 55m. This discrepancy is due to the observed difference between the calculated and measured initial heads. This difference at borehole DH05-01 was 22.5m which is equal to 10.8% of the measured head (see Table 4-4).

The third borehole to compare the numerical model with is DH05-02A. The pore pressure responses to both the reservoir level fluctuations and rainfall are shown in Figure 4-36 and Figure 4-37, respectively. Figure 4-37 clearly reveals that the calculated pressure head changes due to rainfall are less than one meter, and, hence, the total calculated piezometric elevation follows the same trend as that resulting from the simulation of the reservoir fluctuations effect. This result is supported by the observed similarity between the trends of the measured piezometric elevation cycles (see Figure 4-36) and the reservoir level fluctuation

cycle. The measured rises in the piezometric elevations at the locations of MP86, 66, 35 and 12 during the period from April to August 2006 are 24, 21, 20 and 18 metres, respectively. The calculated rises in the piezometric elevations due to the reservoir level fluctuations at the same locations and during the same time period are, however, 10, 10, 13 and 13 metres, respectively. At higher piezometric points, the model predicts only 40 to 50% of the measured value. This ratio increases to 65 and 72% at the lower measurement points.

4.6.4 Conclusions

The following conclusions are drawn from the results of the numerical simulation of the ground water flow at the Little Chief Slide:

1. The model could replicate the initial in-situ piezometric elevations before the construction of the Mica Dam.
2. The chosen ratios between the saturated hydraulic conductivity of the different units seem to be acceptable considering that the purpose of the analysis is to simulate the field pressure heads, not the flow rates.
3. The reservoir filling process does not affect the water table for locations further than 1000 meters from the reservoir shoreline.
4. The extent of the reservoir filling effect is verified by the piezometric data recorded at the locations of boreholes DH05-01, DH05-05 (DH906), DH902, DH05-02A and DH901.
5. The presence of inward dipping shear bands at borehole DH04-01 causes a significant difference between the measured and calculated piezometric heads before and after the reservoir filling.
6. Regarding the simulation of the reservoir fluctuations and rainfall effects, although the model is considered to predict only 30 to 65% of the measured ranges in the field, the model is capable of correctly simulating the trend of the piezometric elevation variation with time and, hence, of detecting the zones where the pore pressure response is dominated by either the reservoir level fluctuations or rainfall. The results of the numerical analysis show that the reservoir level fluctuations have a dominant effect on the pore pressure response at locations near the slope toe. At locations far upslope, however, pore pressures are dependent mainly on the infiltration rate.

4.7 Movement Behaviour of the Little Chief Slide

4.7.1 Introduction

As mentioned in Section 4.2.2, the 2005 program involved installing inclinometer casings in boreholes DH05-03, 04, 05, 06 and 07. Manual recordings of data have been available since the fall of 2005 and until the summer of 2007 on approximately semi-annual time intervals. In-place inclinometers (IPI's) were installed in these five boreholes after reviewing the inclinometer measurements taken in the spring of 2006. Hence, continuous records of the movement data at different movement zones have been available since the fall of 2006.

This section presents the results of analyzing the field measurements taken at the IPI's. The contribution of creep to the total movement is filtered out. This separation has some practical implications that are highlighted. A triaxial drained creep testing program is carried out in order to investigate the creep behaviour of the soft zones in the laboratory and to compare the field and laboratory creep behaviours.

4.7.2 Analysis of Field Inclinometer Measurements

4.7.2.1 Available Data for the Analysis

All the information related to the movement zones where the IPI's were installed is included in Table 4-9. The movement zones characterization is obtained from the BC Hydro 2005 field investigation report (Rapp, 2006). The widths of the movement zones and the records of movement were provided by BC Hydro in summer 2008. Figure 4-38 through Figure 4-43 show the continuous movement records at different movement zones as detected by the IPI's. The movement rate is calculated based on a one-month time interval and expressed in units of mm/yr in order to have large and sensible numbers. The rates are shown as numeric values on the plots. The sensor installed in borehole DH05-04 failed in April 2008, and the string was pulled out for repair. The data taken at borehole DH05-05 show a high noise and does not show a clear trend, unlike the other movement zones. Therefore, these data are not considered in the analysis. Scanned images of both the IPI and the manual inclinometer measurements at borehole DH05-05 are shown in Appendix B: Figures B-10 and B-11.

4.7.2.2 Analysis of Data

The plot shown in Figure 4-38 indicates that the movement at depth 210.9m in borehole DH05-03 proceeded during the period from the beginning of September 2006 to the end of April 2007 at an average rate of 4.5mm/yr. The movement accelerated afterwards from the beginning of May until the end of August 2007 at

an average rate of 17.1mm/yr. The slide velocity then decreased back to 4.1mm/yr on average during the period from the beginning of September 2007 until the end of May 2008. The available data from September 2006 to September 2007 represent a complete annual cycle of movement and therefore are chosen for study. Borehole DH05-03 lies at a distance more than 1000m from the reservoir shoreline, and, hence, the pore pressure changes would be mainly driven by rainfall rather than reservoir fluctuations, as concluded from the seepage analysis. As the infiltration rate during the period of the fall, winter and early spring is very low, the pore pressure changes during this period are essentially zero; i.e., the effective stress is constant. Hence the recorded rate of 4.5mm/yr from September 2006 to April 2007 would represent a creep deformation of the movement zone. Creep does actually persist for the whole year, but it is obscured during the spring and summer months by the effects of seasonal hydrologic boundary conditions changes like infiltration and/or reservoir level fluctuations, and by the effects of changes in the forces acting on the slide like lateral water pressures inside tension cracks and/or water ponding. Hence, the movement recorded from the beginning of May 2007 to the end of August 2007 represents a superposition of creep and seasonal movements. Therefore, creep at this movement zone would account for 4.5mm out of a total of 8.8mm of movement from the beginning of September 2006 until the end of August 2007. It follows then that the viscous properties of the movement zone at depth 210.9m in borehole DH05-03 are responsible for about 51% of the total movement occurring at this zone.

The IPI sensor installed in borehole DH05-04 failed in April 2008, as mentioned above. The sensor malfunction is evidenced by the change in the direction of the movement component “B” since the fall of 2007 (see Figure 4-39). This led to an unreasonable recorded rate of 38mm/yr in January 2008. Therefore, the studied period of the displacement-time curve is chosen to be from September 2006 to September 2007. The movement continued from the beginning of September 2006 to the end of April 2007 with an average rate of 1.5mm/yr. During the remaining four months of the studied period, the superposition of the creep deformation and the seasonal movements gave rise to an equivalent displacement rate of 14.3mm/yr. Therefore, creep accounts for 1.5mm out of a total annual movement of 5.8mm; i.e., creep contributes to about 26% of the total movement of this soft zone.

The creep movement at borehole DH05-04 is approximately one third the creep movement at borehole DH05-03. This difference may be attributed to the higher rock fragment content in the movement zone of DH05-04 than DH05-03 as indicated by the core logging and evidenced by the values of RQD. The seasonal movement occurring in both boreholes is 4.3mm. This match is due to their location at approximately equal distances from the reservoir shoreline (see Figure 4-3). The results of the numerical modeling of the groundwater conditions presented in the previous section show that the groundwater regime in the vicinity of borehole DH05-04 is not affected by the reservoir filling and the reservoir level fluctuations. It is expected that borehole DH05-03 is not affected as well. Hence,

the movement occurring in excess of the creep deformation would be due to pore pressure changes due to rainfall in addition to any possible seasonal forces acting on the slide. The creep and seasonal movements of the soft zones in boreholes DH05-03 and DH05-04 are illustrated in Figure 4-44 and Figure 4-45, respectively. The maximum seasonal movement rate is attained in June when the infiltration is the highest due to the added effect of snow melt. If the seasonal movement results from a reservoir level rise, the maximum rate would be attained around August (the time of the maximum reservoir level). The possibility of movement acceleration due to reservoir drawdown is excluded at these two movement zones because the movement rate drops to its minimum value during the period of the reservoir level drop (from August to April).

Figure 4-40 and Figure 4-41 show the movement records of the two movement zones at the depths of 171.3m and 233.8m, respectively, in borehole DH05-06, which lies very close to the reservoir shoreline, as shown in Figure 4-3. This figure shows that the movement trend of the upper movement zone (Figure 4-40), unlike the two previous zones, does not follow a clear annual cycle. The maximum recorded movement rate is 5.0mm/yr. In the spring of 2007, movement rates as low as 0.5 and 0.3 mm/yr were recorded. The movement accelerated to 4.6mm/yr during May 2007 and then was almost constant until the end of October 2007. Hence, the movement did not accelerate during either the period of the maximum infiltration (spring months) or the reservoir level rise (April to August). Therefore, the movement was not affected by any seasonal changes during the period from September 2006 until the end of October 2007 although the upper movement zone lies very close to the reservoir shoreline. The detailed core logging of this movement zone suggests that it is composed of very soft clay followed by moist silty clay and underlain by rock fragments within a soft micaceous matrix (Rapp, 2006). The zone might be of a very low permeability and, hence, does not respond to the seasonal hydrologic boundary conditions changes. This suggests that creep represents 100% of the total movement of this zone. Since January 2008 and until June 2008, however, the movement persisted with an average rate of 4.0mm/yr. While this movement acceleration may be attributed to a drop in the reservoir level, the movement proceeded during the same period in the previous year (January to June 2007) at an equivalent annual rate of 1.9mm/yr. The overall rate of movement recorded at this zone during the period from the beginning of September 2006 to the end of May 2008 was 2.0mm/yr.

The conditions at the lower movement zone (Figure 4-41) are quite different. The average movement rate during the period from the beginning of September 2006 to the end of April 2007 was 2.4mm/yr (assuming that the rate during September 2006 was zero). During the next four months, the average rate rose to 3.1mm/yr and then dropped back to 2.5mm/yr during the period from the beginning of September 2007 to the end of November 2007. Surprisingly the movement later accelerated to an average rate of 5.7mm/yr. This acceleration might be attributable to a reservoir level drawdown effect. However, the movement did not

accelerate with the same value during the same period in the previous year. Therefore, the movement behaviour of the lower zone of borehole DH05-06 followed an annual cycle trend until the end of November 2007. The difference between the lower and upper zones is that the lower zone has higher granular content and is therefore more permeable. This feature allows the effects of the seasonal changes to be clearer. Creep represents 2.4mm of the total annual movement. The total recorded movement was 2.6mm from the beginning of September 2006 to the end of August 2007. Therefore, creep represents 92% of the total movement.

Figure 4-42 and Figure 4-43 show the movement records at the two movement zones at the depths of 126.8m and 331.6m, respectively, in borehole DH05-07, which is 110m apart from the reservoir shoreline, as shown in Figure 4-3. The analysis of the movement records of the upper movement zone (depth 126.8m) shows it to follow an annual cycle trend, as do boreholes DH05-03, DH05-04 and the lower movement zone of borehole DH05-06. The period from the beginning of November 2006 to the end of October 2007 is considered representative of a typical annual cycle and, hence, is chosen for analysis. The investigation of the displacement versus time curve during the spring and summer of 2007 shows that maximum displacement rates of 9.3 and 7.7 mm/yr were recorded in June and July; i.e., the movement acceleration followed the rise of the reservoir level to its maximum in August. The rate started decreasing when the reservoir level dropped after August. The average movement rate from the beginning of May to the end of August 2007 was 6.6mm/yr. Therefore, it is considered that the seasonal movement of this zone follows the rise and drop of the reservoir level rather than the rainfall. During the rest of the studied period, the average movement rate was 2.6mm/yr. This persisting movement during the periods of minimum reservoir level is considered a creep movement. The total movement during the studied period equals 3.9mm. Therefore, the creep contribution to the total movement is around 67%. The negative movement rate recorded during January 2008 is considered an erroneous reading and, therefore, is not considered in the analysis.

The lower movement zone (Figure 4-43) shows a similar behaviour to that of the upper zone of borehole DH05-06. The core logging of the lower movement zone of borehole DH05-07 shows that it is composed of dark green clay underlain by a light gray green matrix with small rock fragments. The value of the RQD equals 36%. On the other hand, the upper movement zone of borehole DH05-07 contains high granular and rock fragment content. The value of the RQD equals 6%. This comparison suggests that the lower zone might have a lower permeability that makes it unaffected by the seasonal hydrologic boundary conditions changes. This implication is supported by the observed halting of movement during the month of June 2007 (a high movement rate should be expected from either rainfall or reservoir level fluctuations). The overall movement rate during the studied period since the beginning of November 2006 was 2.4mm/yr.

4.7.2.3 Discussion

The analysis of the movement records of the movement zones in boreholes DH05-03, DH05-04, DH05-06 and DH05-07 shows that the total movement at any of the movement zones is generally composed of creep and seasonal movements. Creep is equal to the total movement during periods of zero pore pressure changes. Seasonal movements generally result from pore pressure changes due to rainfall and reservoir level fluctuations, in addition to changes in the forces acting on the slide, like lateral pressures of the water filling the tension cracks and surface water ponding. The available piezometric and hydrologic data enabled correlating the seasonal movements only to pore pressure changes resulting from rainfall and reservoir fluctuations rather than other seasonal forces affecting the slide.

The results of the analysis are summarized in Table 4-10, which reveals that creep of the shear zones may account for about 73% on average of the total movement. The summary also shows that creep accounts for 90% on average of the total displacement at locations close to the reservoir shoreline. At far locations, however, seasonal movements may account for 50 – 75% of the total movement. The results summarized in Table 4-10 have an important practical implication. As mentioned above, creep deformation contributes to 73% on average of the total movement of the Little Chief Slide. This finding means that any mitigation measures, like drainage ditches, installed to control the movement may be successful in stopping only about 27% on average of the total movement. The use of drainage measures will be more efficient at upslope locations where the seasonal displacements contribute to 50 – 75% of the total movement. Thus, the creep behaviour of the slide materials of the Little Chief Slide must be investigated. An experimental creep testing program has been carried out and is outlined in the next section.

4.7.3 Drained Triaxial Creep Testing Program

4.7.3.1 Introduction

The creep properties of fine geotechnical materials have been studied in detail in the literature. Singh and Mitchell (1968) developed an equation that describes the strain rate as a function of time and deviatoric stresses. The equation is adequate to describe the creep behaviour of clay whether it is normally or overconsolidated, disturbed or remolded, wet or dry, or drained or undrained. The equation is applicable as well for a range of deviatoric stress levels from 30% to 90%. The majority of the data used to develop the three-parameter Singh-Mitchell (1968) equation involved low deviatoric stresses, which are normally encountered in the near surface geotechnical problems. The only exception, as mentioned above in Chapter 2, was the two creep tests performed by Campanella (1965) on samples of dry Illite, which were subjected to deviatoric stresses of approximately

11MPa. However, these tests were part of a study concerned with the rate process theory.

Therefore, the experimental program carried out as part of this present research aims at verifying the phenomenological Singh-Mitchell equation under the level of stresses encountered at the Little Chief Slide. The laboratory creep strain rates are then compared to the field values. The following subsections explain the testing equipment and the testing procedure. The available samples for testing and the testing plan are presented afterwards. The results of the experimental creep testing program are then analyzed, followed by a comparison of the field and laboratory behaviours.

4.7.3.2 The Testing Equipment

An ISCO Series D (model 100DX) single syringe pump is utilized to apply the required high stresses to the tested samples. The pump can be operated in either a pressure or a flow mode. The advantage of the flow mode is the ability to gradually increase the stress to the design value without overshooting the desired pressure value. The deviatoric stress pump capacity is 103ml. The maximum flow rate that can be applied is 60 ml/min, and the minimum rate is 10^{-5} ml/min. The displacement rate is related to the applied flow rate through the relation

$$\dot{\delta} = \frac{10 * q}{A}, \qquad \text{4-1}$$

where
q is the flow rate (ml/min),
A is the hydraulic cylinder effective area (cm^2), and

$\dot{\delta}$ is the displacement rate (mm/min).

Equation 4-1 is the simple relationship between the flow rate and velocity. The right hand side is multiplied by 10 for unit conversion. The maximum and minimum rates of displacement that can be applied are 29.6 and $5X10^{-6}$ mm/min, respectively. The resulting axial load is measured by using a load cell. The maximum pressure that can be applied by the pump is 10000 psi (~69MPa).

4.7.3.3 Testing Procedure

The suitable cores for testing were frozen and then cut and trimmed to the required dimensions. The samples were then placed in a triaxial cell and subjected to a 500kPa back pressure. The samples were left over the night to allow the degree of saturation to approach 100%. The B-test was carried out for each sample by raising the confining pressure by increments of 50 – 60kPa and

monitoring the developed pore pressure. The achieved value of Skempton's parameter B ranged between 0.96 and 0.98 for all samples. It was considered then that the samples had achieved a full saturation condition.

The applied confining stresses for the tested samples ranged between 1.5 and 4.6MPa, as is detailed in the next subsection. The required confining stress was applied through increments that started from 125 – 150kPa and then were doubled up to the required value. Each increment was applied for 24 hours to allow for full primary consolidation. The next step was applying the deviatoric stress. Since the aim of the experimental program is to study the creep properties of the slide materials, each deviatoric increment was applied for a period of one to three weeks.

4.7.3.4 Available Samples for Testing and the Applied Stresses

The cores provided by BC Hydro were examined to identify the suitable samples for testing. Some of the slide materials were in a disturbed loose state and were not chosen for testing. The tested cores were taken from borehole DH05-07 at depths of 125.00 to 126.25m and 158.70 to 159.00m, and borehole DH05-06 at depth of 171.05 to 171.25m.

The ground surface elevation at borehole DH05-07 is 779.21m. The actual recorded water table elevation in borehole DH901 (the same location as borehole DH05-07) fluctuates between elevation 730 and 752m. The fluctuations are due to the reservoir level changes. The values of the total stresses, minimum recorded pore pressures, and, hence, the effective stresses for the soft materials cores encountered in borehole DH05-07 are shown in Table 4-11.

The available undisturbed core from the depth of 125.00 to 126.25m is sufficiently large to cut and trim three samples to the standard dimensions. Doing so allows for exploring the effect of varying the confining stress value on the creep behaviour of this movement zone. Hence, it is decided to apply 1.5, 2.0 and 3.0MPa confining stresses for the three samples available from this depth range at borehole DH05-07.

The effective vertical stress at the depth of 158.70 – 159.00m in borehole DH05-07 is 3.21MPa. Since this level of stress is already included in the above mentioned stress range, and in order to study the creep behaviour under a wider range of stresses, the applied confining stress for this sample is taken to be equal to its total stress: 4.3MPa.

Regarding borehole DH05-06, the ground surface elevation is 765.72m. No piezometric data is available to calculate the pore pressure. In order to study the creep behaviour under a wide range of stresses and because this sample represents a detachment surface between soft materials and an underlying hard rock so that it can be assumed that the pore pressure within the core at this depth is very low, the

sample is subjected to a confining stress of 4.6MPa. Table 4-12 presents a summary of the tested samples locations and the applied confining stresses.

4.7.3.5 Results

(i) Borehole DH05-07 – Depth 125.00 to 126.25m

Figure 4-46 shows a photo of the drilled core between the depths of 125.00 and 126.25m, and Figure 4-47 shows the grain size distribution curves of samples 1 through 3. Samples 1 and 3 are nearly identical with regard to grain sizes while sample 2 has a higher fine content. The cores were frozen and then cut and trimmed to a standard height to a diameter ratio of 2. The bulk unit weights are calculated by knowing the mass and volume of the samples. The initial moisture contents are determined for the trimmings, and, hence, the initial void ratios are calculated. Table 4-13 presents a summary of the first three samples geometrical and physical properties. The creep test on sample #1 was carried out prior to my involvement in the project. Some of the sample information is not available.

The first step to test the applicability of the Singh-Mitchell equation (Singh and Mitchell, 1968) is to plot the axial strain rate versus time on a logarithmic scale for different deviatoric increments. The deviatoric stress increments shown in Table 4-14 are chosen so the stress levels range between 20 and 90%. An approximate value of 30^0 is assigned for the residual friction angle based on the direct shear and consolidated undrained tests carried out previously by BC Hydro (Rapp, 2006; and Moore et al., 2006). The actual friction angle is determined at the end of each test by loading to failure, as is detailed below. During the consolidation phase of sample #3, leakage was observed from the cell. When the cell was drained to check the setup, a distinctive shear plane was observed. It was decided to re-constitute the sample by compacting it to its initial moisture content and density and then leaving it in the moisture room to mature and be ready for testing. Therefore, the presented results of sample #3 are for a re-constituted sample.

Figure 4-48 through Figure 4-51 show the results of the axial strain rate versus time plots for the first three samples. As shown in the figures, the logarithm of the axial strain rate decreases mostly linearly with the logarithm of time except at early testing times (<10 minutes), and when tertiary creep is observed. Deviation form the linear behaviour at early testing times is attributable to the more dominant effect primary consolidation has on the specimen deformation than primary creep during early stages of deviatoric stress application. The slope of the axial strain rate – time plots, the creep parameter m, was determined by linear regression for the range between t=10 minutes and the onset of tertiary creep, if any. The value ranged from 1.04 to 1.31 for sample #1, from 0.87 to 1.15 for sample #2 and from 0.83 to 0.92 for sample #3. The values of the parameter m lie in the expected range for most soils, 0.7 – 1.3, as pointed out by Singh and Mitchell (1968).

The samples were loaded to failure after the end of each test. Since the slide is moving at an extremely slow rate (10 – 14 mm/yr), the loading to failure is carried out in a drained condition. Stress strain data for sample #1 are not available, but the friction angle at failure is equal to 27^0. Therefore, the deviatoric stress at failure for sample #1 is 2.49MPa. The variation of the deviatoric stress with time to failure for sample #2 is shown in Figure 4-52. The drop and jump in the plot are due to a sudden power shutdown that affected the data-reading instruments. The maximum deviatoric stress at failure is 5.61MPa. The shape of the failure surface for sample #2 is shown in Figure 4-53. The inclination of the failure surface and the value of the deviatoric stress at failure indicate that the friction angle is equal to 35.7^0. The variation of the deviatoric stress with time for sample #3 is shown in Figure 4-54. The sample does not show a distinctive shear plane. The observed failure deviatoric stress corresponds to an angle of internal friction 37.4^0. After determining the failure deviatoric stresses, the actual deviatoric stress levels for each of the creep stages are calculated. The values are listed in Table 4-14.

The next step in validating the Singh-Mitchell (1968) equation is to plot the axial strain rate versus the deviatoric stress level at different time periods. The plots are shown in Figure 4-55 through Figure 4-57 for samples 1 through 3. These figures show that the logarithm of the axial strain rate generally increases linearly with the deviatoric stress level on an arithmetic scale except at early testing times, mostly due to the dominating effect on deformation of primary consolidation, as pointed above. Hence, the axial strain rates increase mostly exponentially with the deviatoric stress level. The slope of the straight line is the creep parameter $\bar{\alpha}$. The values of the creep parameter $\bar{\alpha}$ ranged from 1.87 to 3.16 for sample #1, from 0.73 to 3.20 for sample #2 and from 0.61 to 3.34 for sample #3.

The results of the triaxial drained creep experiments carried out on samples 1 through 3 can be summarized in two main points:

1. The axial strain rate decreases with time possibly according to a power function in the primary creep range, excluding the results at early testing times (<10minutes) when the primary consolidation process may have a dominant effect on the specimen deformation.
2. The axial strain rate increases possibly exponentially with the deviatoric stress level, except at early testing times as pointed above.

The above two points approach the main features of the Singh-Mitchell (1968) equation. Therefore, the creep behaviour of the movement zones at the Little Chief Slide may be explained by this equation. In order to evaluate all the parameters of the equation, the axial strain rate at zero deviatoric stress level at unit time, parameter A, was determined for the three samples. The Singh-Mitchell (1968) creep equation parameters for the three samples are listed in Table 4-15, which shows that there is no clear trend for the variation of the creep equation parameters with the confining stress. Generally, more than three samples need to

be tested in order to be able to develop a modified Singh-Mitchell equation with confining stress dependent parameters.

Watts (1981) studied the creep behaviour of the Tar Island clay foundation of the Syncrude tailings dyke both in the laboratory and in the field, as mentioned earlier in Chapter 2. The parameters m, $\bar{\alpha}$ and A determined in the laboratory by Watts were found to be 1.13 (unitless), 3.0 (unitless) and 0.18%/min, respectively. The parameter m was assumed to be equal to unity in the field analysis in order to facilitate the calculation of the initial time. The value of the parameters $\bar{\alpha}$ was equal to 5.1 (unitless), and the value of the parameter A was not determined in the field analysis. The values of the parameters m and $\bar{\alpha}$ for the Little Chief Slide movement zones are comparable to those of the Tar Island clay layer parameters determined in the laboratory. However, the values of the parameter A for samples #1 and 3 are about two orders of magnitude lower than those of the Tar Island clay layer. The value of the parameter A of sample #2 is, however, comparable. The big difference in the value of the parameter A can be attributed to differences in the structure and stiffness of the two materials. The match between the parameters m and $\bar{\alpha}$ indicates that the strain rate variation with the time and stress level is similar irrespective of the initial strain rate value.

(ii) Borehole DH05-06 – Depth 171.05 – 171.25m (Sample #4)

The results of the creep tests of samples 1 through 3 show that the creep behaviour of the movement zones of the Little Chief Slide may obey the equation developed by Singh and Mitchell (1968). Therefore, the two remaining samples are tested in order to investigate more aspects of the time dependent behaviour of the slide materials at the Little Chief Slide.

Sample #4 is chosen from borehole DH05-06 at a depth of 171.05 to 171.25 meters. The sample was intended to be loaded isotropically to its in-situ stress value (4.62MPa), then loaded to failure in order to investigate the effect of sustained periods of creep loading on the strength of the slide materials. The sample height is 123.45mm with a diameter of 63.74mm and a mass of 904.93 gm. The initial moisture content and initial void ratio are 14.1% and 0.34, respectively. No grain size analysis was performed for this sample. The sample was consolidated to the design confining stress in increments as above. However, during the last increment, 2500 to 4620kPa, leakage was observed from the cell, and it was necessary to replace it. When the sample was removed, two distinct planes of failure were found. The sample lies at a detachment surface between rock-slide deposits and a soft clay seam. Therefore, although the loading was isotropic, the material was not isotropic in response due to its heterogeneity. The shape of the sample before and after testing is shown in Figure 4-58.

(iii) Borehole DH05-07 – Depth 158.70 – 159.00m (Sample #5)

The sample height is 129.53mm with a diameter of 62.53mm and a mass of 947.11 gm. The initial moisture content and the initial void ratio are 10.3% and

0.25, respectively. The fines content by weight equals 28%. One of the purposes of testing sample #5 is to investigate the creep behaviour under very low deviatoric stress levels. Singh and Mitchell (1968) indicated that creep strains under deviatoric stress levels of less than 30% are of a little practical importance. However, these researchers based their conclusion on tests carried out under relatively low confining stresses. Sample #5 was subjected to very low deviatoric increments of 500 and 1000kPa. The results of the axial strain versus time for the D=1000kPa increment were very noisy and suggested the occurrence of a technical problem with the LVDT. Figure 4-59 shows the axial strain rate versus the time plot for the D=500kPa increment. The value of the creep parameter m is well below the expected range for most soils (Singh and Mitchell, 1968). In addition, the value is very close to 0.5 which is characteristic of primary consolidation. This suggests that the movements at very small stress levels are mainly the result of primary consolidation and cannot be explained by the Singh-Mitchell (1968) equation. It can also be concluded that no apparent threshold stress level exists below which "movement" (which is not necessarily creep) cannot occur. A similar conclusion was made by Bishop and Lovenbury (1969).

Figure 4-49 reveals the occurrence of tertiary or accelerated creep deformations at a deviatoric stress of 3.7MPa (stress level 65.9%) for sample #2. The occurrence of tertiary creep may infer the onset of failure plane development in the sample. In that plot shown in Figure 4-49, the test duration should have been extended to see whether the strains will continue accelerating or will decelerate after a while. Therefore, sample #5 was subjected to a deviatoric stress level as high as 70% for two weeks. The axial strain and axial strain rate versus time plots for that increment are shown in Figure 4-60 and Figure 4-61, respectively. The two figures show that the primary creep stage is followed by a tertiary creep stage where the strains accelerate, marking the onset of shear plane development in the sample (see Figure 4-62 for the shape of the sample after test termination). However, the strains start to decelerate back again to the same levels as before the tertiary stage. The deceleration of the strains implies the sample is gaining strength, or the stress has dropped due to the large strain.

4.7.3.6 Field versus Laboratory Strain Rates

The laboratory strain rates are compared to the field strain rates resulting from the IPI installed at depth 126.8m (416 ft) in borehole DH05-07. As summarized in Table 4-10, the creep deformation at the depth of 126.8m in borehole DH05-07 is equal to 2.6mm during a period of one year (November 2006 to October 2007). The width of the movement zone at this location is 1.8m. The field shear strain rate is therefore equal to $\frac{2.6}{1800} * 100 * \frac{1}{365 * 24 * 60} = 2.7 \text{ X } 10^{-7}$ %/min. The minimum axial strain rates encountered in the laboratory during testing samples 1 through 3 (Figure 4-48 through Figure 4-51) are 9.0 X 10^{-7} %/min, 1.4 X 10^{-6} %/min and 1.0 X 10^{-6} %/min for samples #1, 2 and 3 under deviatoric stress levels of 20%, 32% and 30%, respectively. The in-situ creep strain rate is within

an order of magnitude lower than the axial strain rates encountered in the laboratory. This comparison implies that laboratory testing for this kind of material is somewhat representative of the field behaviour. The in-situ strain rates could have been replicated from the laboratory testing if the testing period was extended to two or three weeks. However, the initial time of creep testing in the laboratory is always set to unity while, when considering the field behaviour, it is equal to the time since the initiation of the field creep movements until the time the measurements were taken. In addition, this conclusion is arrived at by comparing the field and laboratory creep rates of one movement zone only. The limited number of the available cores for testing did not enable comparing the field and laboratory behaviours at other movement zones.

Although the field results from the in-place inclinometers show the distribution of the field shear strain rate with time, and the Singh-Mitchell (1968) equation describes an axial strain rate function, the comparison of the laboratory axial and shear strain rates variation with time indicated that they both vary in a similar manner and are of the same order of magnitude.

4.7.4 Discussion

Samples 1 through 3 were loaded to failure after the end of the last creep increment. Table 4-16 summarizes the values of the principal stresses at failure as well as the internal friction angles. The summary indicates that the average friction angle at failure of the slide plane materials at borehole DH05-07 at the depth of approximately 126m equals 31.4^0, excluding the results of the re-constituted sample (Sample #3). The ground surface and the inferred slide plane inclinations at the location of borehole DH05-07 are approximately 16.8^0 (Rapp, 2006). Assuming infinite slope conditions and zero pore pressure at this movement zone; i.e., assuming that the movement zone has such a low conductivity that the effective stress equals the total stress, the shear stress level in the field would be 49.4%, and the factor of safety against slope failure would be around 2.0. However, based on the minimum recorded pore pressures that correspond to the creep movement (u=0.75MPa at depth 125.6m), the stress level equals 65.2% and the safety factor equals 1.53.

Figure 4-49 indicates that strains accelerate for the sample subjected to a confining stress of 2MPa at a stress level of 65.9%. Therefore, the actual stress level in the field is equal to the stress level that caused strain acceleration in the laboratory. The laboratory minimum strain rate is equal to 3.4×10^{-6} %/min, i.e., one order of magnitude higher than the field value. The testing time in the laboratory is considerably shorter than the time since the initial creep movement occurred in the field as mentioned above. Figure 4-63 shows a plot of the laboratory and field creep rates against the time and deviatoric stress level.

Therefore, based on the field and laboratory behaviours of this particular movement zone, the minimum pore pressure conditions correspond to a stress level that may promote movement acceleration, as is evidenced by the match between the actual strain rate in the field and the minimum strain rate attained in the laboratory after which strain acceleration took place. However, previous investigations of drained creep behaviour (Tavenas et al., 1978; and Bishop and Lovenbury, 1969) and our test on sample #4 (see Figure 4-60) indicate that strain acceleration in drained creep testing is transient and is followed by a stage of strain deceleration where the material can sustain higher deviatoric stresses before failure.

The above conclusions are based on studying the field and laboratory behaviours of one movement zone only, as mentioned above. These conclusions cannot be generalized to predict the behaviour of the whole slide because they imply that the implementation of the right mitigation measure in the field to limit the pore pressures to their minimum values may not be sufficient to prevent movement acceleration even if transient. More laboratory testing and field investigations are needed to draw a firm conclusion.

The comparison between the field and laboratory creep behaviours has another important implication that may prove valuable in infinite slope stability problems involving significant creep deformations. The conventional design safety factor of 1.5 corresponds to a stress level of approximately 67%. Creep strains acceleration, even if transient, may take place approximately around that stress level. Hence, a design factor of safety of 1.5 in such a case would provide only a marginal protection against any probable movement acceleration caused by the persisting creep movements. The increase of the design factor of safety to 1.8 or 2.0 in infinite slope stability problems involving significant creep deformations would bring the stress level down to 50 – 56%. Such levels would ensure that the strain rates are always decreasing. This conclusion cannot be generalized to slopes involving finite slip surfaces because the local factor of safety varies from a point to another.

4.8 Conclusions

The conclusions drawn from the study of the instability at the Little Chief Slide are summarized in the following points:

1. The groundwater conditions at the Little Chief Slide are simulated using a two-dimensional continuum seepage model. The model is successful in establishing the initial conditions and in simulating the reservoir filling effect. Regarding the effects of the reservoir level fluctuations and rainfall, the model can predict the extent of influence of each of them and the trend of the pore pressure variation. The model, however, predicts only about 30 – 65% of the pressure head changes occurring due to either the reservoir fluctuations or rainfall. The pore pressure changes at the locations near the

reservoir shoreline are more affected by the reservoir level fluctuations than by rainfall. The pore pressure changes seem to result solely from infiltration for locations further than 1000m from the reservoir shoreline. Due to the big dimensions of the slope, the model cannot simulate the localized effects of thin low permeability shear zones on the pore pressure regime.

2. Creep represents a significant fraction of the total movement of the soft zones. It accounts for about 73% on average of the total movement. Movement also results from seasonal changes in pore pressures due to infiltration and/or reservoir level fluctuations, and from seasonal changes in other forces acting on the slide like lateral water pressures in tension cracks and surface ponding. The available piezometric and hydrological data enabled correlating the seasonal movements only to pore pressure changes resulting from rainfall and reservoir level fluctuations.
3. The contribution of creep to the total movement at locations far upslope ranges from 25 – 50% and is about 90% at locations near the shoreline.
4. The high contribution of creep to the total movements indicates that the use of drainage measures may stop only 27% on average of the total movement. Hence, drainage measures should be installed at upslope locations where the contribution of the creep to the total movement is lower.
5. The creep behaviour of the movement zones of the Little Chief Slide may be represented by the three-parameter Singh-Mitchell (1968) equation. Therefore, the equation developed by Singh and Mitchell (1968) could be successfully applied under high stresses.
6. The in-situ creep strain rates match the laboratory values within an order of magnitude although the time since the initiation of the creep in both cases is considerably different.
7. The calculated stress level in the field at one of the movement zones based on the minimum pore pressure is approximately equal to the laboratory stress level that caused strain rate acceleration after attaining a minimum value. Hence, there is a possibility of movement acceleration in the field even if the applied mitigation measures could keep the piezometric levels at minimum values. However, this conclusion is based on comparing the field and laboratory behaviours of one zone only and should not be generalized to the whole slide unless more laboratory testing and field investigations confirm this conclusion.
8. In infinite slope stability problems involving significant creep deformations, the conventional design safety factor of 1.5 brings the stress levels to a limit where strain acceleration may take place after long periods of decreased movement rate. It is suggested that the design safety factor in these problems be raised to 1.8 or 2.0.

Table 4-1: Results of X-Ray Diffraction Analysis (McLeod, 2006)

Borehole	Depth (m)	1	2	3	4	5	6	7	8	9	10	11	12	13	14
DH05-07	318.9		V. Min.												Abun.
DH903	202.2		Mod.			Abun.						Mod.	Mod.		
DH903	203.9	V. min.	Min.						Abun.	Mod.	Mod.				
			Min.						Abun.	Mod.		Min.			
DH04-01	252.5	Mod.	Mod.	Min.			V. Min.		V. Min.	Min.					
DH05-01	126.0	Abun.		Mod.	V. Min.		V. Min.								
DH05-01	139.5	Abun.		Abun.					?						
DH05-03	56.9	Min.		Abun.											
DH05-03	117.4	Mod.			Min.						Mod.				
DH05-03	128.7	Mod.		Mod.											Mod.
DH05-03	136.9	Mod.			Min.										Abun.
DH05-03	325.5	Mod.		Abun.			Mod.	Min.							
DH05-02A	214.2	Mod.		Abun.	V. Min.										
DH05-04	169.6	Abun.		Min.			Min.				Mod.				
DH05-05	63.9	Mod.				Mod.								Abun.	
DH05-05	145.5	Abun.		Min.	Min.					Mod.					

1: Quartz
2: Calcite
3: Muscovite
4: Chlorite
5: Clinochlore
6: Albite
7: Microcline
8: Montmorillonite
9: Kaolinite
10: Magnesioriebeckite
11: Talc
12: Anthophyllite
13: Dravite
14: Laumontite
Abun: Abundant
Mod.: Moderate
Min. and V. Min.: Minor and Very Minor

Table 4-2: Summary of the Direct Shear Testing Results (Bhuyan, 2006)

Borehole	Depth (m)	Description	Applied Normal Stress (MPa)	Maximum Friction Angle (Degrees)	Remarks
DH05-01	243.69 – 244.00	Green clay layer	4.8	26	Sheared along clay-rock interface
DH05-02A	206.50 – 206.6	Sheared clayey soil	3.4	23	Evidence of previous staining
DH05-03	304.80	Thin clay layer	5.8	29	Sheared through thin clay layer
DH05-04	158.65 – 158.80	Green clayey silt embedded with rock particles	3.4	34	Grinding of rock particles
DH05-05	228.80 – 229.00	Green clay	2.4	21	Relatively flat direct shear surface
			4.8	20	Sample extrusion observed along direct shear surface
DH05-05	242.20 – 242.70	Clay and rock	5.0	30	Relatively flat direct shear surface
DH05-06	234.75 – 234.85	Black thin clay layer	3.9	31	Sheared through thin clay layer
DH05-07	328.80	Green clay	5.4	26	Soft fractured rock and green clay matrix
DH903	201.78	Hard dried flakes and powder	3.3	18	Peak friction angle of 20^0 during initial forward cycle
DH903	202.08 – 202.38	Hard fragment and flakes	3.3	26	Relatively flat direct shear surface
DH903	203.91	Hard flakes and fragments	3.3	13	Peak friction angle of 16^0 during initial forward cycle. Residual friction angle of one sample was 10^0 due to a high Montmorillonite content

Table 4-3: Hydraulic Conductivity Data and the Corresponding Rock Weathering Condition

Borehole	Weathering Condition*	K (m/sec)	Depth Interval (m)		Average Depth (m)
			From	To	
DH05-05	F-FS	1.84E-07	153.57	169.16	161
DH05-05	SW-MW	1.84E-07	153.57	169.16	161
DH05-04	SW-FS	3.18E-05	97.16	103.63	100
DH05-04	SW-MW	3.18E-05	97.16	103.63	100
DH05-04	FS	2.18E-06	161.17	187.45	174
DH05-04	FS	5.24E-07	188.60	202.62	196
DH05-04	FS	8.68E-07	231.27	256.03	244
DH05-03	SW-FS	5.41E-06	108.75	124.81	117
DH05-03	FS	6.23E-06	154.45	169.00	162
DH05-03	F	9.92E-07	204.15	219.15	212
DH05-03	F	2.14E-06	230.65	246.73	239
DH05-03	F	3.33E-06	249.26	260.45	255
DH05-01	FS-HW	8.54E-06	93.50	111.10	102
DH05-01	FS-MW	1.28E-06	116.65	124.82	121
DH05-01	F-minor FS	1.28E-06	257.15	287.88	273
DH05-01	F	1.28E-06	257.15	287.88	273

* F: Fresh
FS: Fresh Stained
F – minor FS: Fresh with minor fresh stains
SW: Slightly Weathered
MW: Moderately Weathered
HW: Highly Weathered

Table 4-4: Summary of the Steady State Analyses

Borehole	Predefined Pressure Head Boundary Condition (m)	Predicted Function		Estimated Function		Horizontal Function	
		Height of Phreatic Line (m)	Error (%)	Height of Phreatic Line (m)	Error (%)	Height of Phreatic Line (m)	Error (%)
DH05-04	118.61	128.3	8.2	106.4	-10.3	70.3	-40.7
DH05-01	207.89	194.5	-6.4	185.4	-10.8	186.8	-10.1
DH05-05	52.35	74.9	43.2	73.6	40.6	126.6	141.9
DH902	3.42	3.24	-5.3	2.95	-13.7	4.78	39.8

Table 4-5: Summary of the Steady State Analysis Results after Lowering the Upper Layer Conductivity by one Order of Magnitude

Borehole	Predefined Pressure Head Boundary Condition (m)	Predicted Function		Estimated Function	
		Height of Phreatic Line (m)	Error (%)	Height of Phreatic Line (m)	Error (%)
DH05-04	118.61	138	16.3	135	13.8
DH05-01	207.89	253	21.7	254	22.2
DH05-05	52.35	157	200.0	159	203.7
DH902	3.42	20	484.8	18	426.3

Table 4-6: Summary of the Steady State Analysis Results after Lowering the Lower Layer Conductivity by one Order of Magnitude

Borehole	Predefined Pressure Head Boundary Condition (m)	Predicted Function		Estimated Function	
		Height of Phreatic Line (m)	Error (%)	Height of Phreatic Line (m)	Error (%)
DH05-04	118.61	48	-59.5	44	-62.9
DH05-01	207.89	148	-28.9	118	-43.2
DH05-05	52.35	40	-23.6	28	-46.5
DH902	3.42	2.40	-29.8	2.42	-29.2

Table 4-7: Elevations of the Eleven Multi-point Piezometers Installed since 2005

Borehole	G.S. Elevation (m)	Multi-Point Piezometer	Piezometer Tip Elevation (m)
DH04-01	902.0	MP47	732.2
		MP20	684.9
		MP02	643.5
DH05-01	1290.0	MP74	1126.1
		MP46	1063.0
		MP40	1047.8
		MP34	1032.5
DH05-02A	766.5	MP86	666.45
		MP66	617.68
		MP35	539.35
		MP12	478.39

Table 4-8: The locations of the Nodes that the Pressure Heads were queried at

Borehole	Multi-Point Piezometer	Piezometer Tip Elevation (m)	Nearest node coordinates (m)	Stratigraphic Layer
DH04-01	MP47	732.2	2407, 728	Upper layer
	MP20	684.9	2416, 681	Upper layer
	MP02	643.5	2425, 650	Upper layer
DH05-01	MP74	1126.1	1576, 1126	Middle layer
	MP46	1063.0	1584, 1049	Boundary of middle and lower layer
	MP40	1047.8	1584, 1049	Boundary of middle and lower layer
	MP34	1032.5	1573, 1026	Lower layer
DH05-02A	MP86	666.45	2725, 658	Upper layer
	MP66	617.68	2725, 617	Upper layer
	MP35	539.35	2723, 535	Lower layer
	MP12	478.39	2738, 469	Lower layer

Table 4-9: Summary of Field Inclinometer Measurements Locations and Material Characterization

Borehole	Movement Zone $\begin{pmatrix} \text{ft} \\ \text{m} \end{pmatrix}$	Characterization (After Rapp, 2006)	IPI Installed at (ft, m)	Remarks
DH05-03	682 – 698 207.9 – 212.8	• Thin clay layer underlies soft mica with disoriented rock fragments. This overlies rock fragments in soft micaceous matrix. • Piezometric head is higher by 45m than the head recorded at the bottom of the borehole. • RQD = 0%, Recovery = 99%.	692, 210.9	
DH05-04	570 – 582 173.7 – 177.4	• Clayey zone with some mica and rock fragments. More rock is present towards bottom with less matrix. • Piezometric head is higher by 21m than the head recorded at the bottom of the borehole. • RQD = 13%, Recovery = 97%.	578, 176.2	IPI sensor has failed in April 2008
DH05-05	738 – 742 224.9 – 226.2	• Numerous foliation joints and soft rocks. • RQD = 0%, Recovery = 100%	738, 224.9	High noise of data was detected and the borehole was excluded from the analysis
	774 – 782 235.9 – 238.4	• 10mm dark green clay, followed by a rock fragments matrix. • RQD = 9%, Recovery = 100%	777, 236.8	
	808 – 816 246.3 – 248.7	• Soft micaceous clayey layer. Quality improves abruptly at depth 248.2m • RQD = 6%, Recovery = 100%	810, 246.9	
DH05-06	560 – 564 170.7 – 171.9	• Very soft clay flowed to box shape followed by moist silty clay; underlain by rock fragments within soft micaceous matrix • RQD = 0%, Recovery = 100%	562, 171.3	No piezometric data was available
	764 – 770 232.9 – 234.7	• Soft micaceous clay with granular content overlies rock with soft zones.	767, 233.8	

		• RQD = 0%, Recovery = 100%		
DH05-07	410 – 416 125.0 – 126.8	• Soft micaceous zone with granular content. Very low content of rock fragments present. This is followed by rock fragments containing granular material. • RQD = 6%, Recovery = 98%	416, 125.0	No piezometric data was available
	1080 – 1090 329.2 – 332.2	• Dark green clay underlain by a light gray green matrix with small rock fragments. • RQD = 36%, Recovery = 100%	1088, 331.6	

Table 4-10: Summary of the Analysis of Movement Data

Borehole	Movement Zone $\begin{pmatrix} \text{ft} \\ \text{m} \end{pmatrix}$	Studied Period	Total Annual Movement (mm)	Creep Component (mm)	Percent of Creep Contribution (%)
DH05-03	682 – 698 207.9 – 212.8	Sep06 to Aug07	8.8	4.5	51
DH05-04	570 – 582 173.7 – 177.4	Sep06 to Aug07	5.8	1.5	26
DH05-06	560 – 564 170.7 – 171.9	Sep06 to Aug07	1.5	1.5	100
	764 – 770 232.9 – 234.7	Sep06 to Aug07	2.6	2.4	92
DH05-07	410 – 416 125.0 – 126.8	Nov06 to Oct07	3.9	2.6	67
	1080 – 1090 329.2 – 332.2	Nov06 to Oct07	1.8	1.8	100

Table 4-11: Total, Pore and Effective Stresses for the Cores taken from Borehole DH05-07

Depth (m)	Total Stress (MPa)	Pore Pressure (MPa)	Effective Stress (MPa)
125.00	3.38	0.74	2.64
126.25	3.41	0.76	2.65
158.70	4.28	1.07	3.21

Table 4-12: Summary of Samples Information

Sample Number	Borehole	Depth (m)	Confining Stress (MPa)
1	05-07	125.00 – 125.25	1.50
2	05-07	125.50 – 125.75	2.00
3	05-07	126.00 – 126.25	3.00
4	05-06	171.05 – 171.25	4.62
5	05-07	158.70 – 159.00	4.30

Table 4-13: Summary of the First Three Samples Information

Sample #	Height (mm)	Diameter (mm)	Initial Moisture Content* (%)	Bulk Density (kN/m^3)	Initial Void Ratio** (unitless)
1	130.38	63.17	-	-	-
2	132.07	63.83	13.4	21.83	0.375
3	132.49	62.98	12.4	22.13	0.345

* Initial Moisture Content was taken as the average of 2 samples from the trimmings
** Initial void ratio was calculated based on a specific gravity of 2.7

Table 4-14: Applied Deviatoric Increments and Deviatoric Stress Levels for Samples 1 through 3

Sample #	Confining Stress (MPa)	Applied Deviatoric Increments (MPa)	Applied Deviatoric Stress Levels (%)
1	1.5	0.5, 1.0, 1.6, 2.2	20, 40, 64, 88
2	2.0	1.0, 1.8, 2.7, 3.7	18, 32, 48, 66
3	3.0	2.8, 3.6, 4.4, 5.2	30, 39, 48, 56

Table 4-15: Summary of Curve Fitting Parameters for Samples 1 through 3

Sample number	Confining Stress (MPa)	m			A (%/min)	$\bar{\alpha}$		
		Range	Avg.	SD		Range	Avg.	SD
1	1.5	1.04 1.19 1.31 1.19	1.18	0.11	0.0022	3.16 2.08 1.87	2.37	0.69
2	2.0	1.06 1.15 1.00 0.87	1.02	0.12	0.0724	0.73 3.20 2.46	2.13 (2.83 if lower value omitted)	1.27
3 (Re-constituted)	3.0	0.88 0.83 0.92 0.92	0.89	0.04	0.0048	1.60 3.34 0.61	1.85 (2.47 if lower value omitted)	1.38

Table 4-16: Summary of Failure Stresses and Friction Angles Values for Samples 1 through 3

Sample #	Confining Stress (MPa)	Deviatoric Stress Levels Applied During Creep Testing (%)	Deviatoric Stress at Failure (MPa)	Maximum Applied Deviatoric Stress Level (%)	Major Principal Stress (MPa)	Friction Angle (^{0})
1	1.5	20, 40, 64, 88	2.5	88	4.0	27.0
2	2.0	18, 32, 48, 66	5.6	66	7.6	35.7
3 (Re-constituted)	3.0	30, 39, 48, 56	9.3	56	12.3	37.4

Figure 4-1: Location of the Little Chief Slide

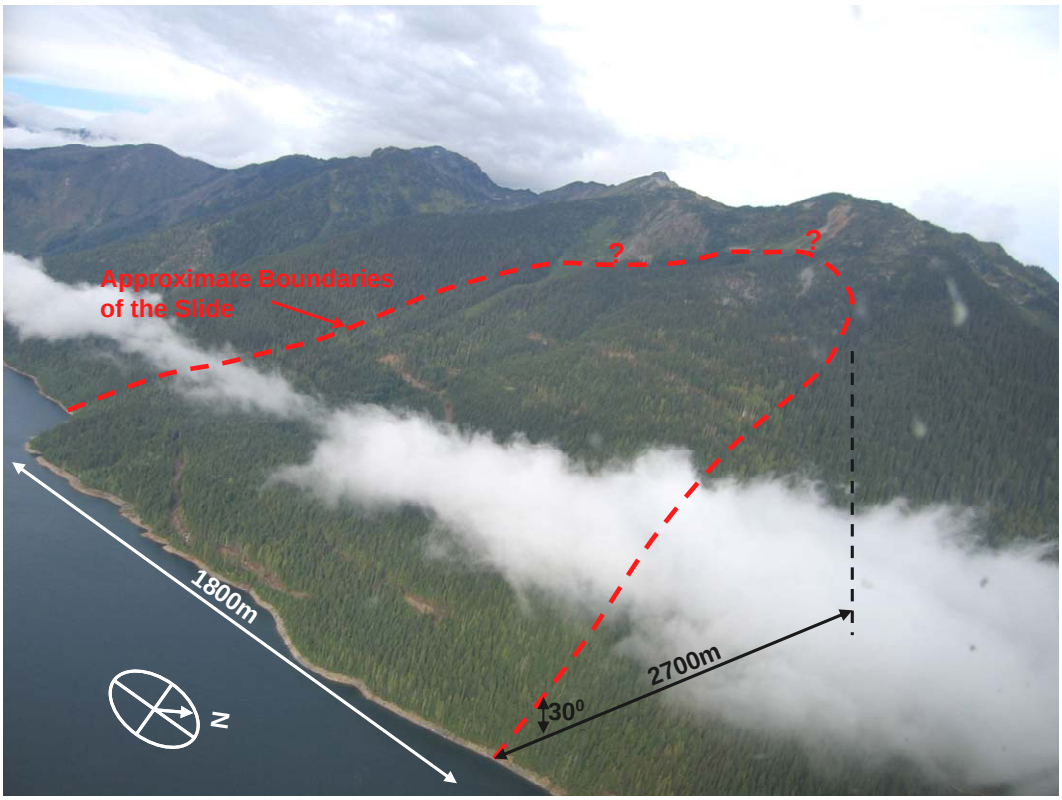

Figure 4-2: Aerial View of the Little Chief Slide Showing the Approximate Boundaries and the Dimensions of the Slide

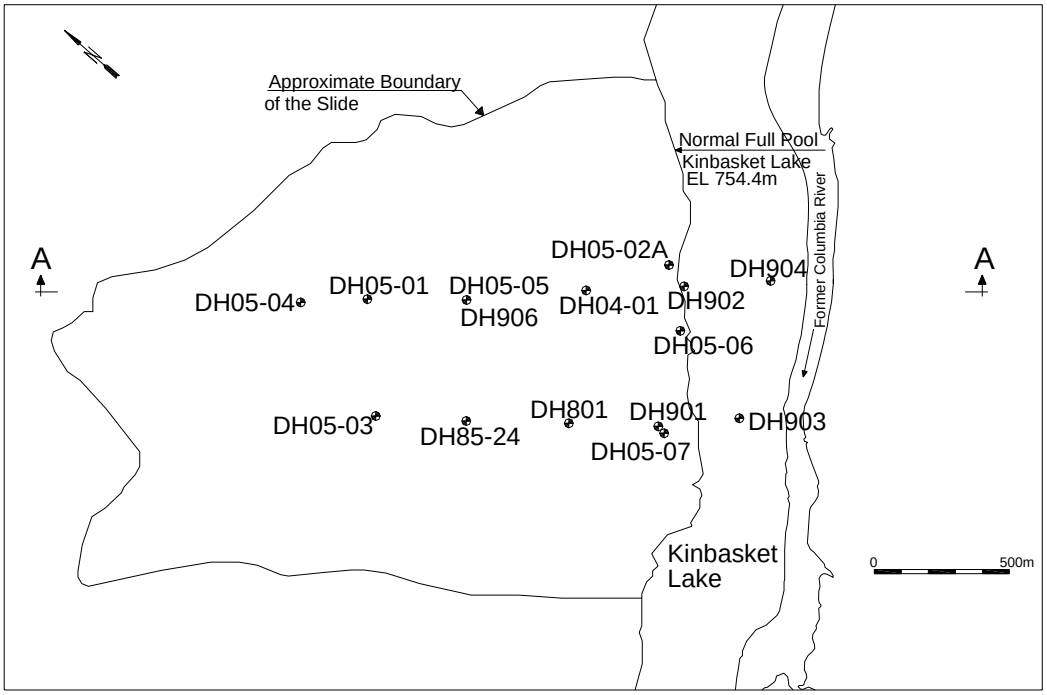

Figure 4-3: Locations of Boreholes, Slide Boundaries, Reservoir Shoreline and Former Columbia River (Modified after Rapp, 2006)

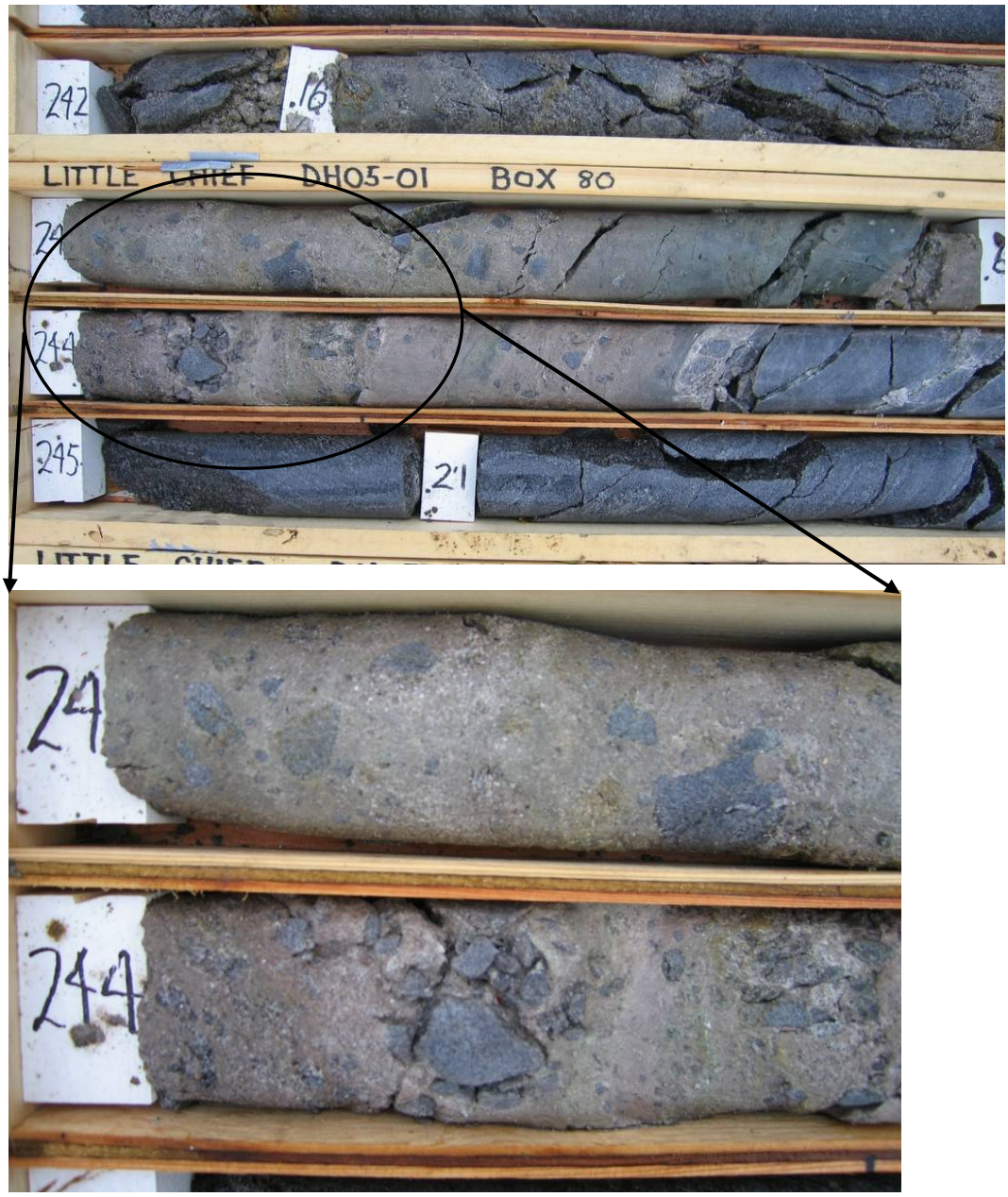

Figure 4-4: A Close-up of the Main Movement Zone at Depth Range 242 – 245m in Borehole DH05-01

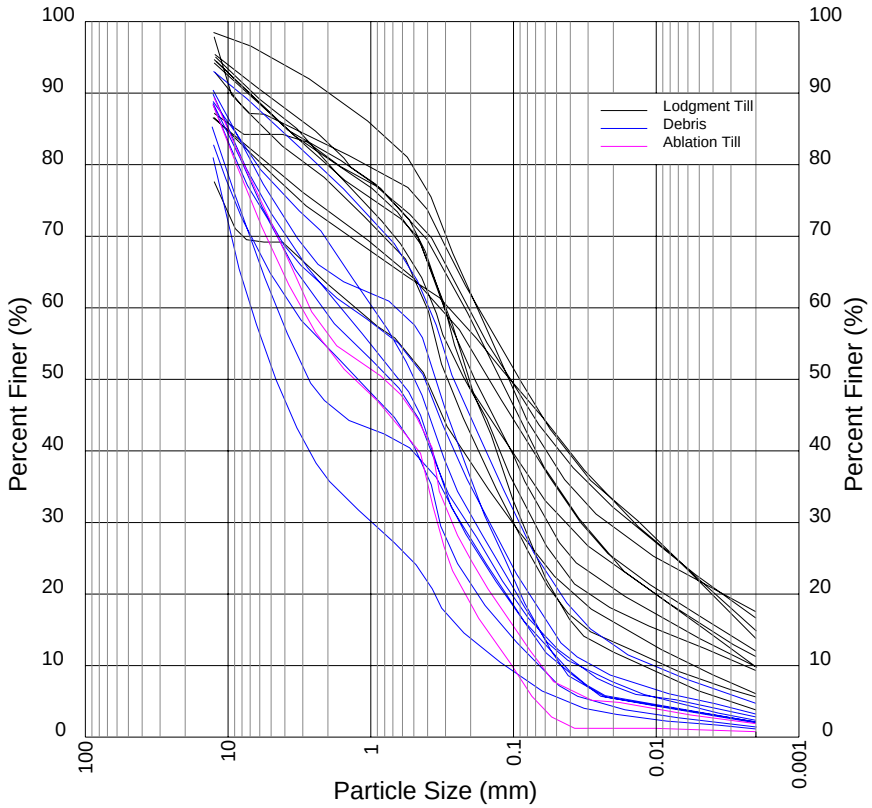

Figure 4-5: Grain Size Distributions for 23 Samples Representing Lodgment Till, Debris and Ablation Till (Modified after Friele and Clague, 2006)

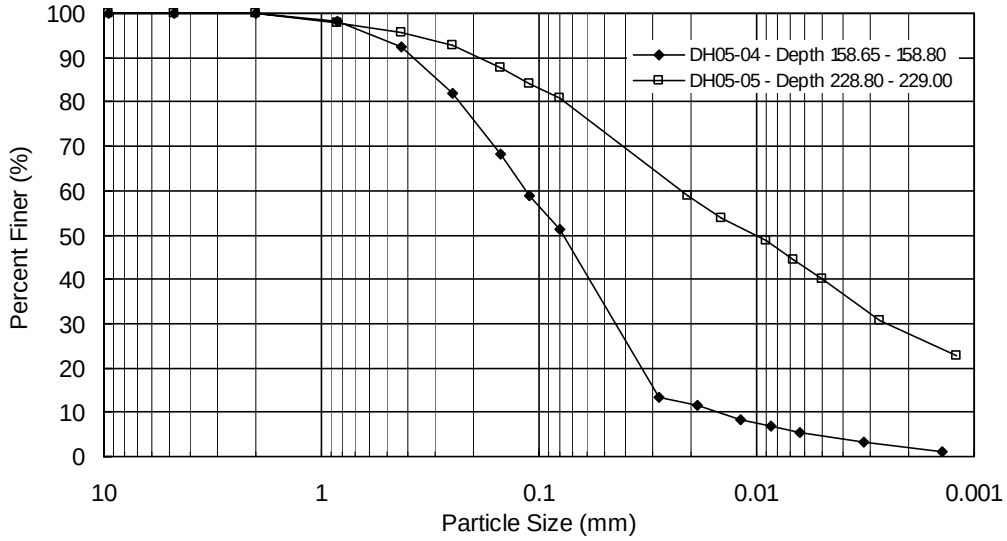

Figure 4-6: Grain Size Distribution Curves for Two Samples taken from Boreholes DH05-04 and DH05-05 (Bhuyan, 2006)

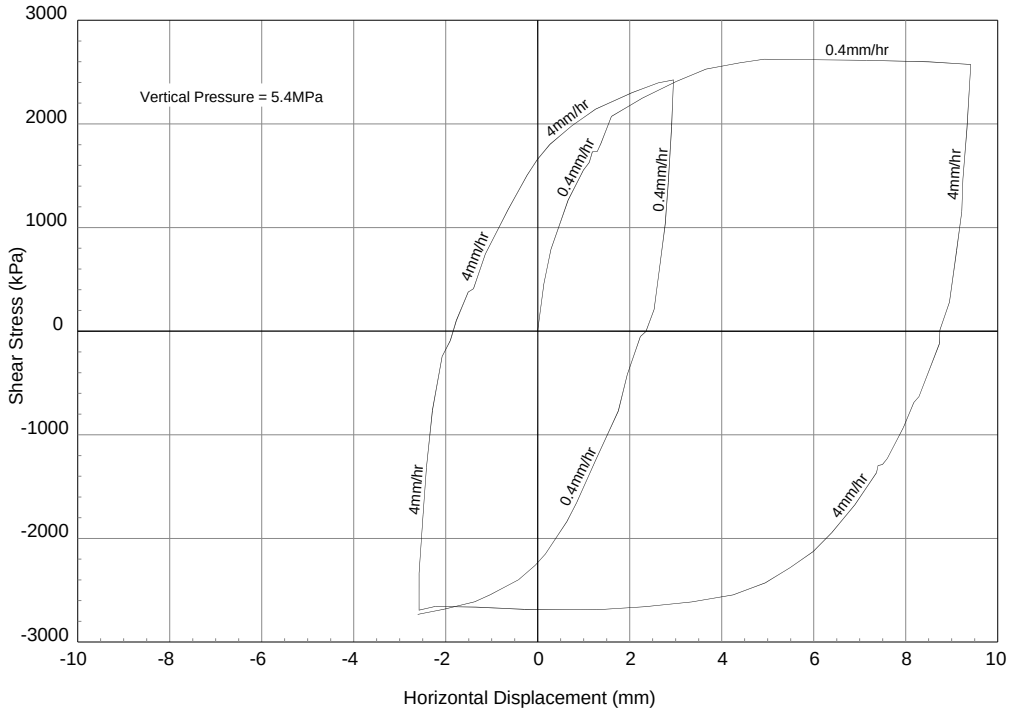

Figure 4-7: Shear Stress-Horizontal Displacement Plot for a Sample taken from Borehole DH05-07 at Depth 328.7 – 328.8m and Subjected to a Vertical Pressure of 5.4MPa (Bhuyan, 2006)

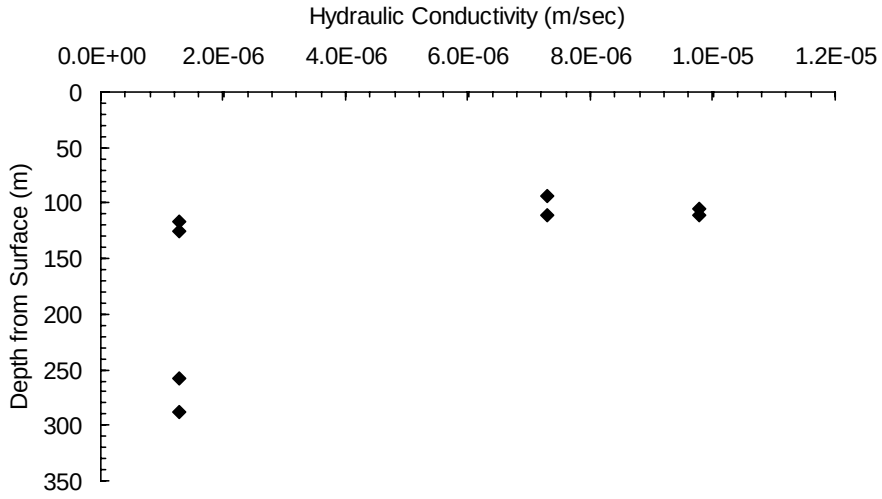

Figure 4-8: Records of Hydraulic Conductivity Measured in Borehole DH05-01 at the Indicated Depths

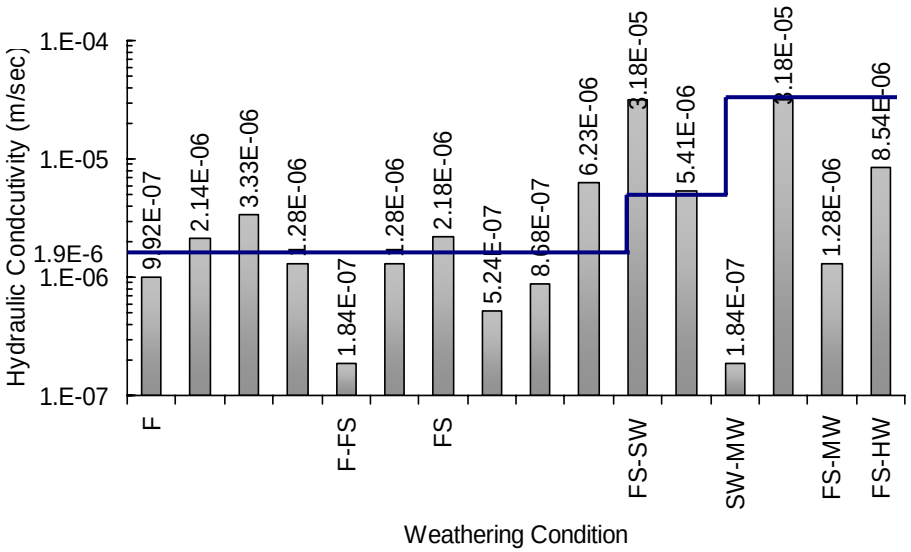

Figure 4-9: Hydraulic Conductivity Plotted against Rock Weathering Condition (F: Fresh, FS: Fresh Stained, F-FS: Fresh to Fresh Stained, SW: Slightly Weathered, MW: Moderately Weathered, HW: Highly Weathered)

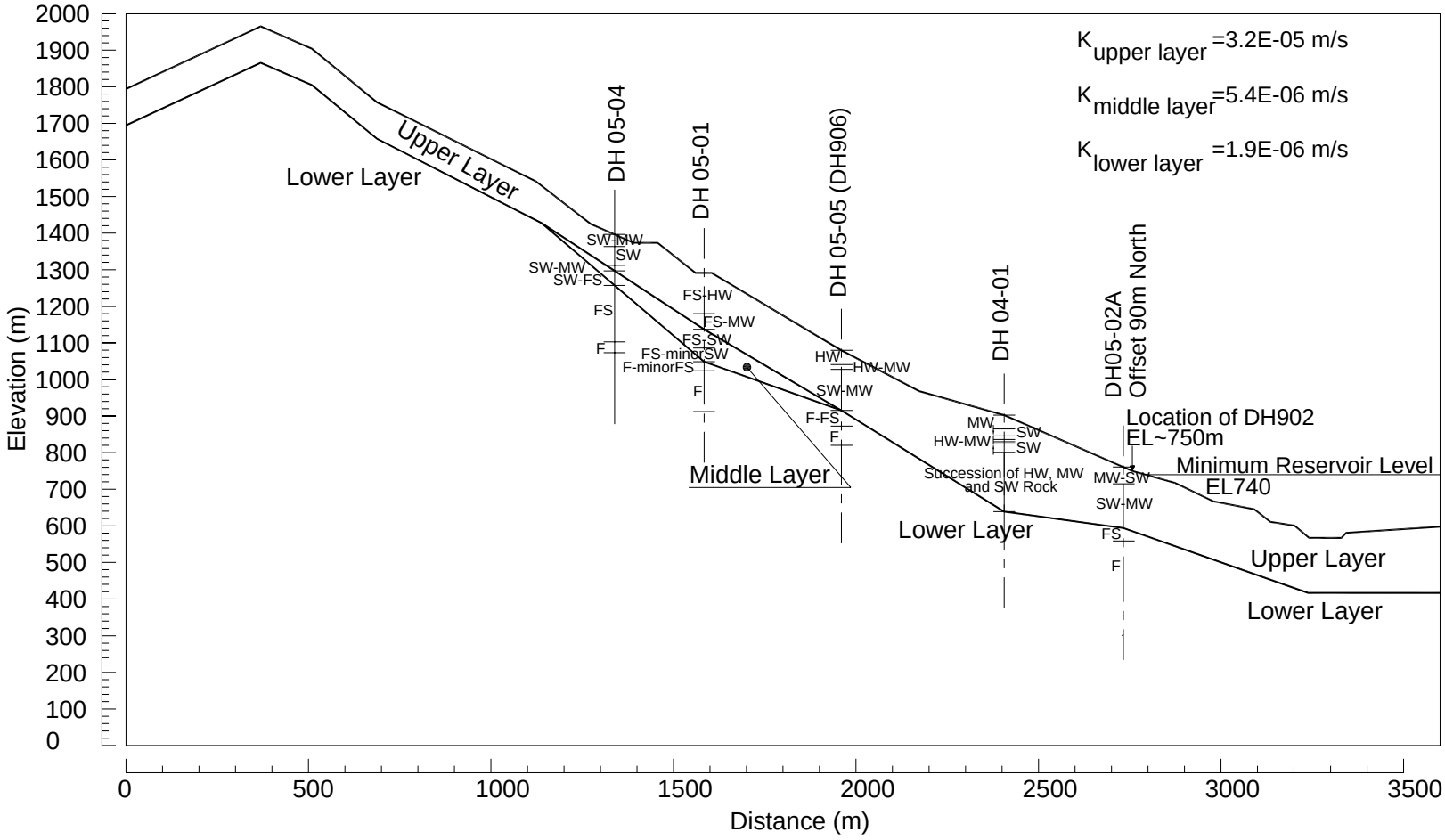

Figure 4-10: Cross Section A-A with the Assumed Boundaries between Different Layers

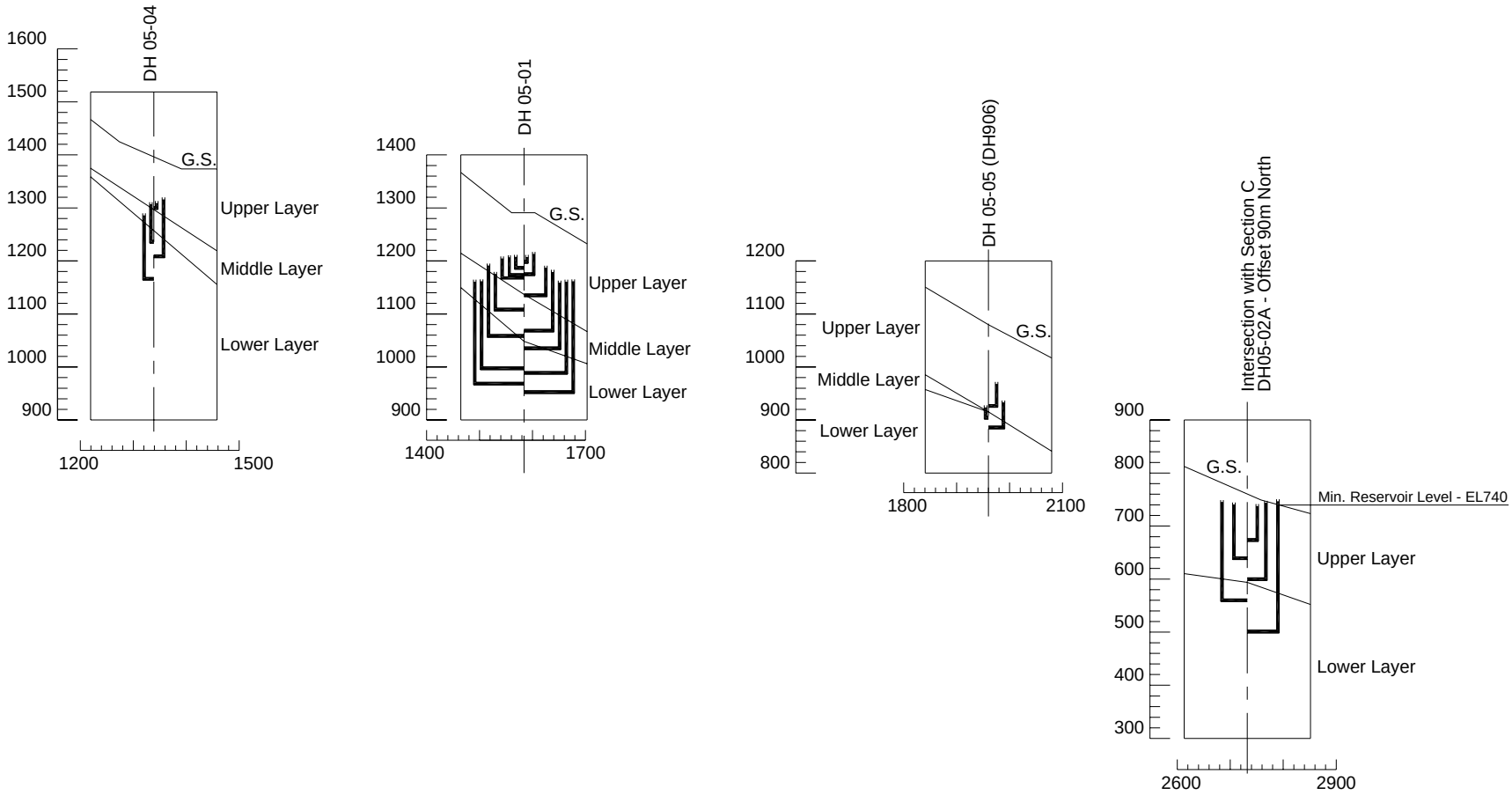

Figure 4-11: Piezometric Data Resulted from PPT for Boreholes DH05-04, DH05-01, DH05-5 and DH05-02A (Modified after Rapp, 2006)

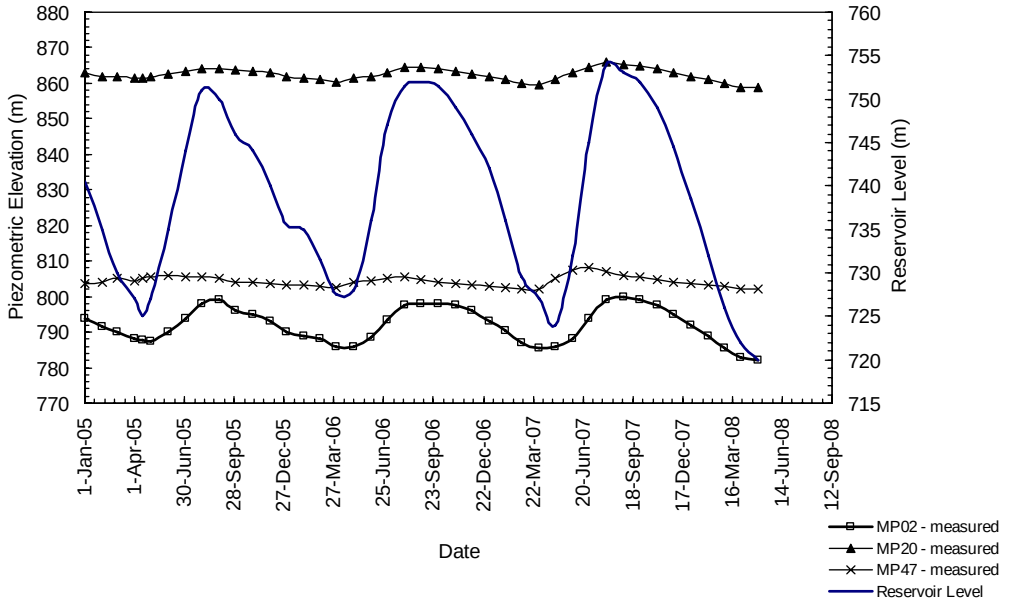

Figure 4-12: Measured Piezometric Elevations in Borehole DH04-01 together with Reservoir Fluctuation Cycle

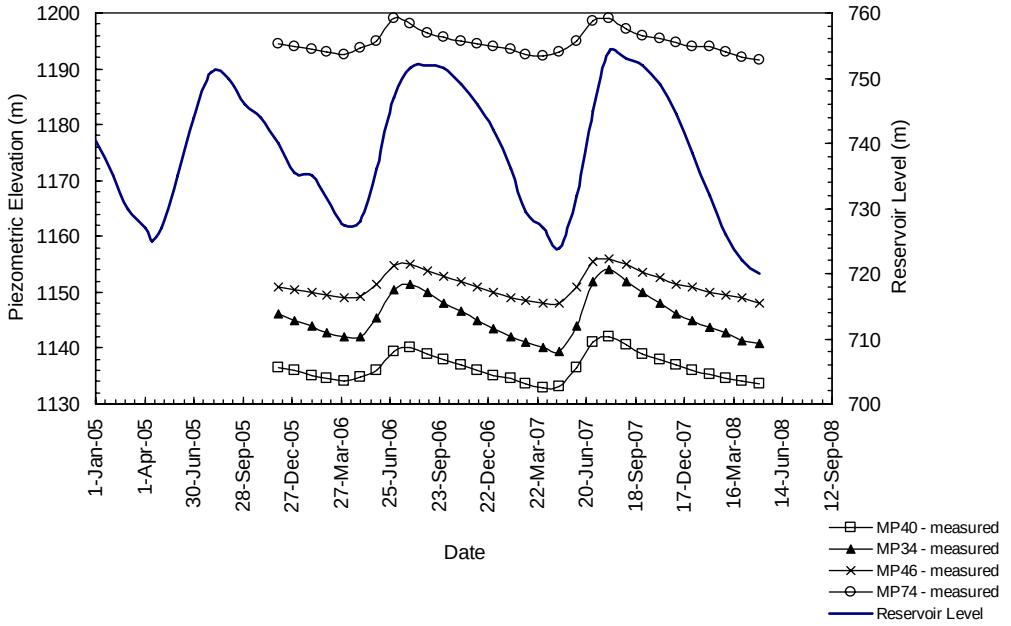

Figure 4-13: Measured Piezometric Elevations in Borehole DH05-01 together with Reservoir Fluctuation Cycle

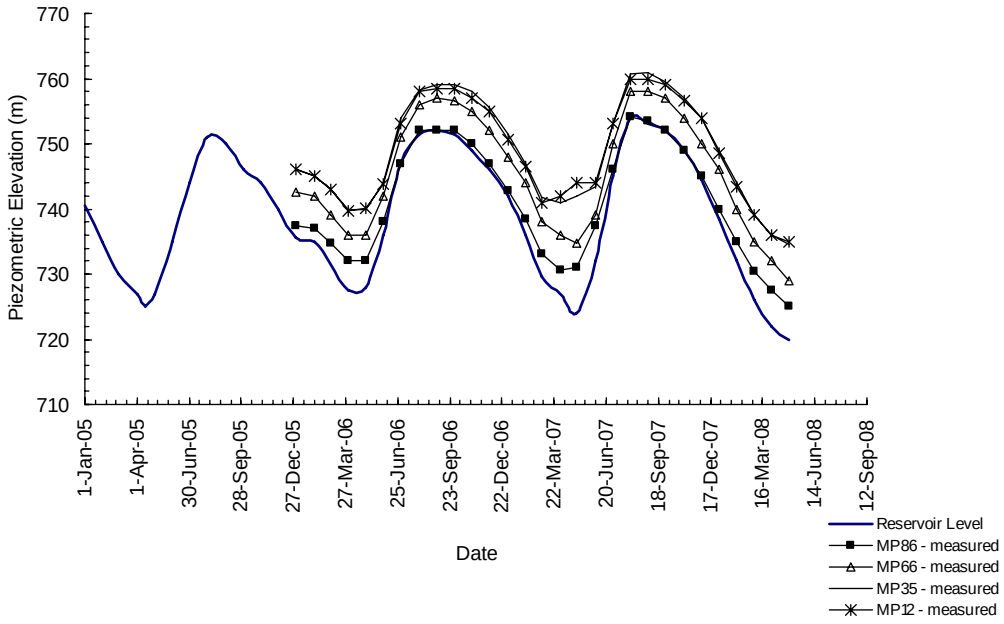

Figure 4-14: Measured Piezometric Elevations in Borehole DH05-02A together with Reservoir Fluctuation Cycle

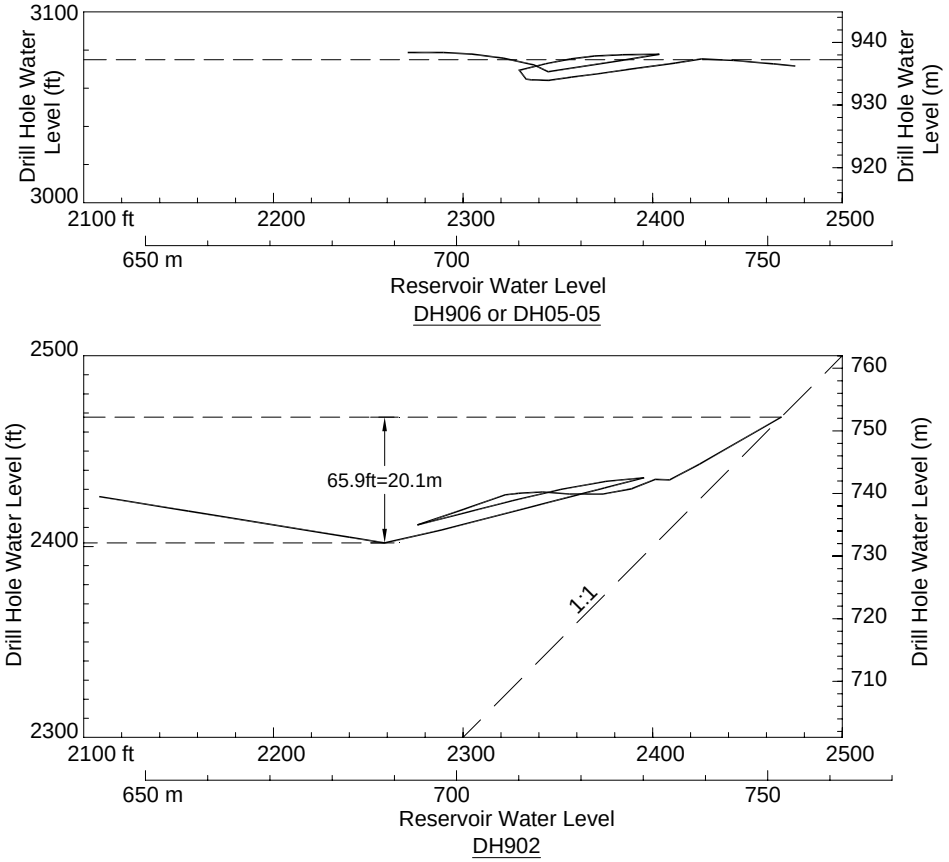

Figure 4-15: Drill Hole Water Levels before and during Reservoir Filling for Boreholes DH906 (DH05-05) and DH902 (Modified after Gavin, 1969)

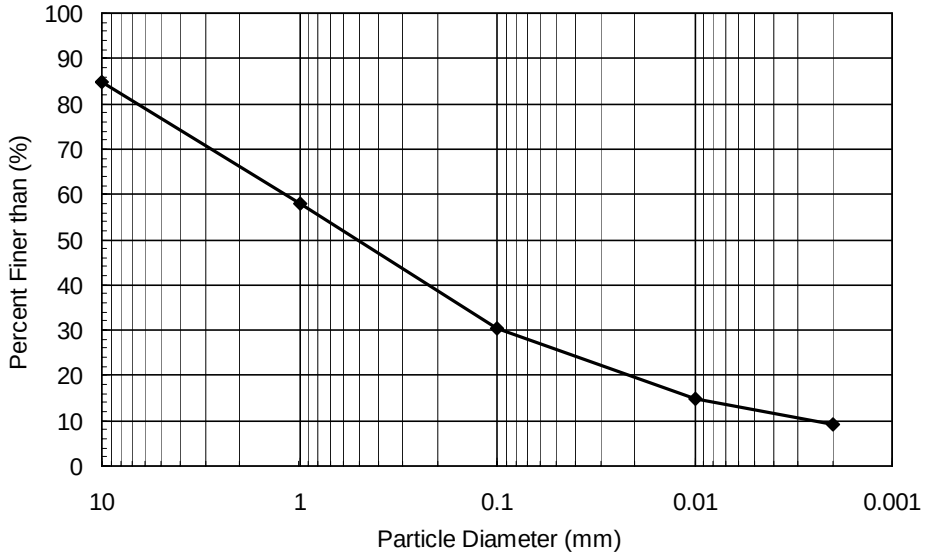

Figure 4-16: Average Grain Size Distribution Assumed for the Upper Layer

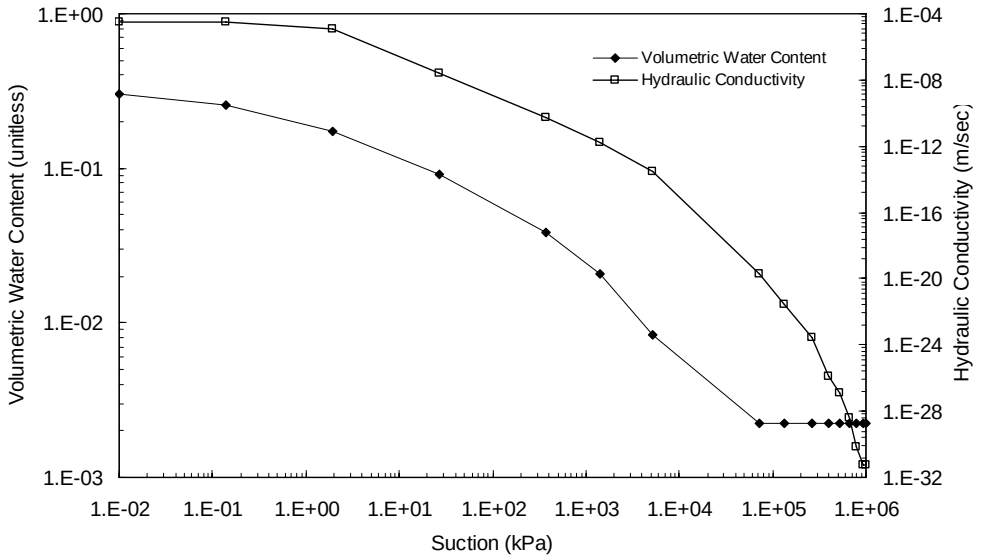

Figure 4-17: Volumetric Water Content and Hydraulic Conductivity Functions as Predicted for the Upper Layer

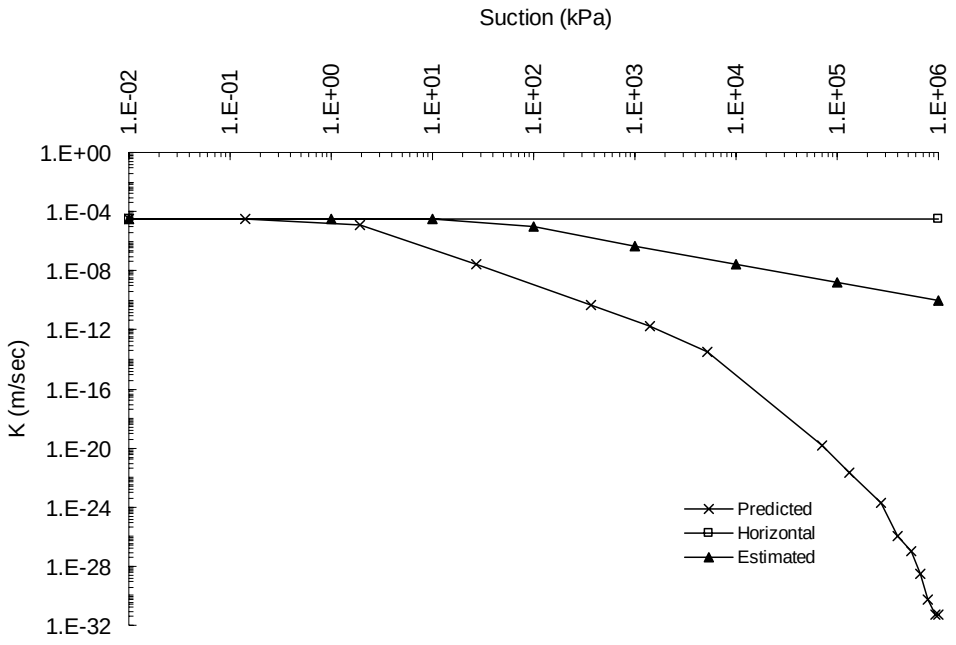

Figure 4-18: The Predicted, Horizontal and Estimated Hydraulic Conductivity Functions Used in the Analysis

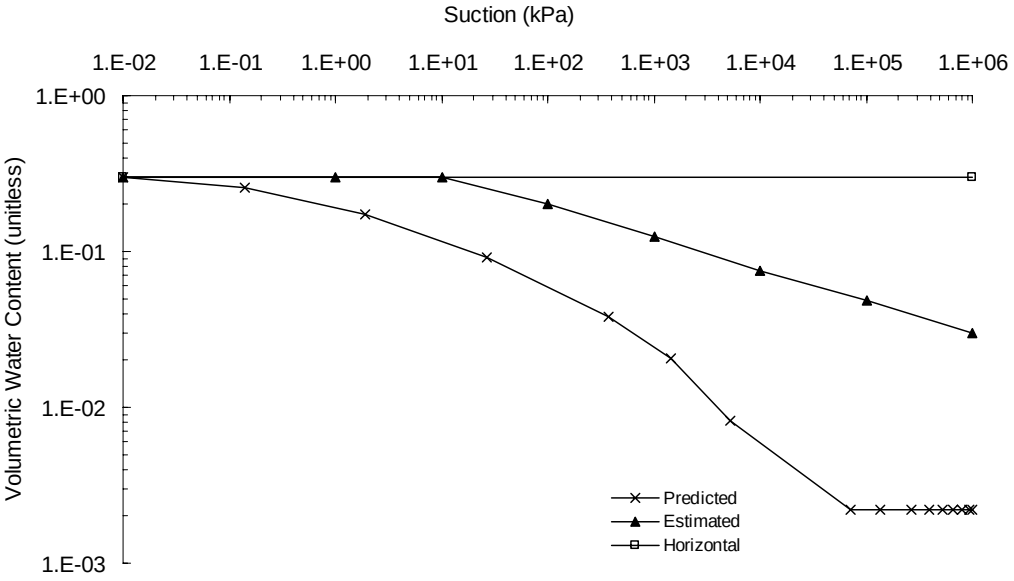

Figure 4-19: The Predicted, Horizontal and Estimated Volumetric Water Content Functions Used in the Analysis

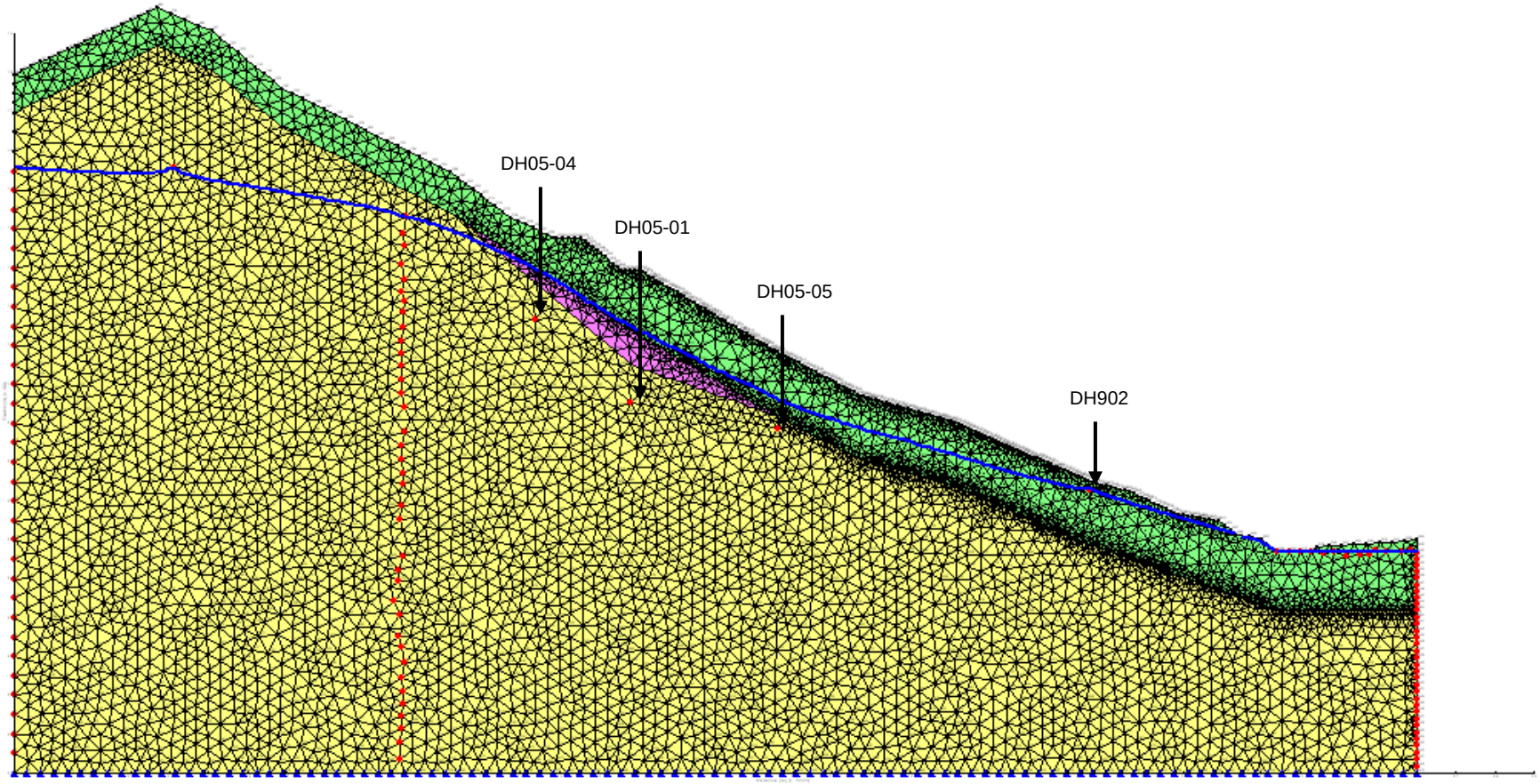

Figure 4-20: Shape of the Finite Element Mesh used in SEEP/W and the Resulted Phreatic Surface (Predicted Functions)

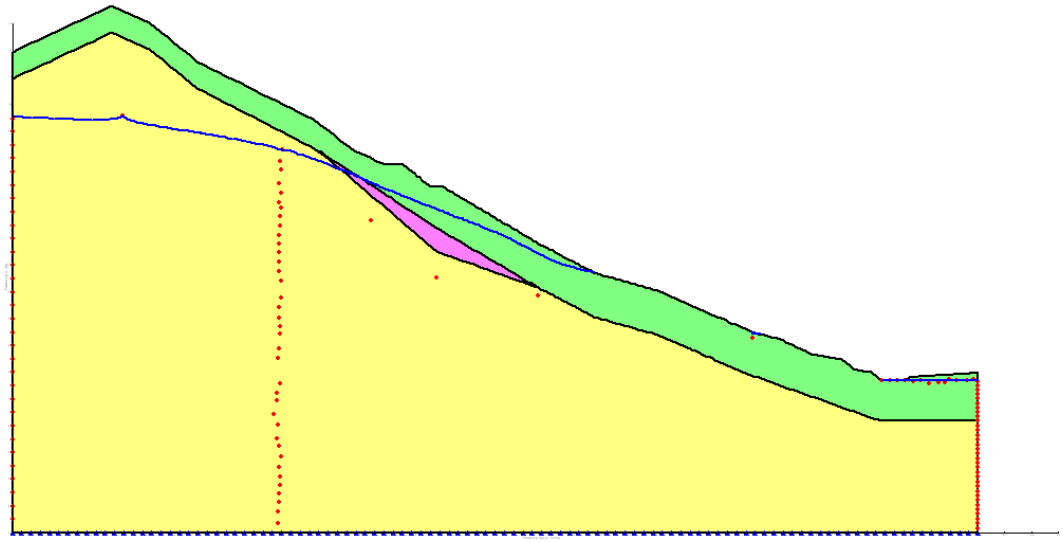

Figure 4-21: Shape of Phreatic Line after using one order of magnitude lower values for the Hydraulic Conductivity of the Upper Layer (Predicted Functions)

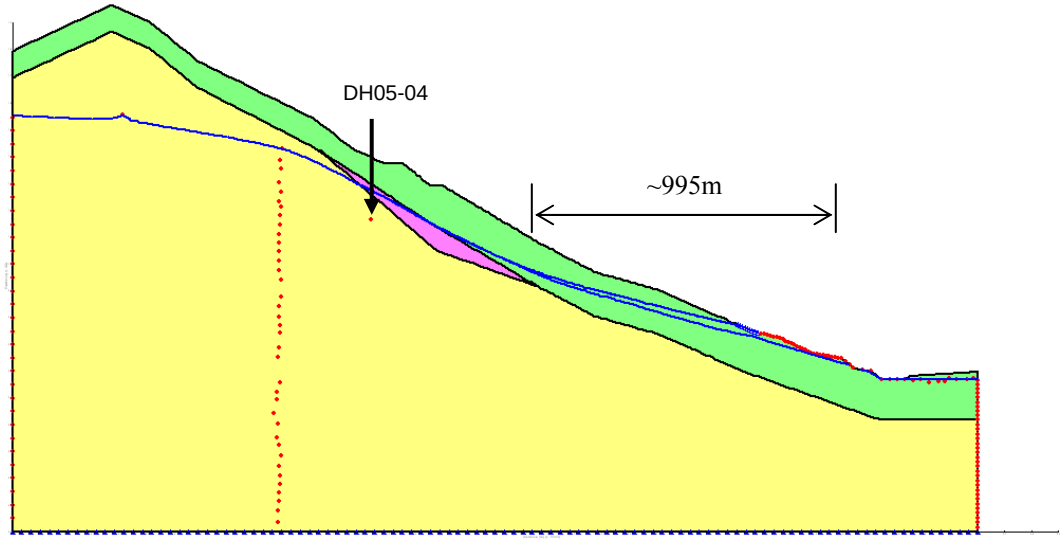

Figure 4-22: Phreatic Surface Location before and after Filling the Reservoir (Estimated Functions)

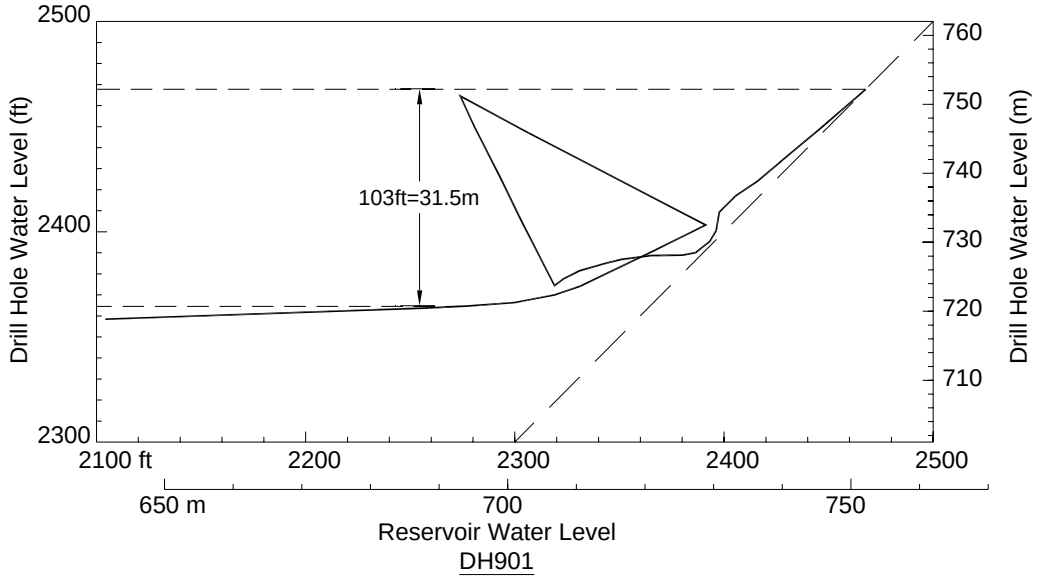

Figure 4-23: Drill Hole Water Levels in DH901 before and during Reservoir Filling (Modified after Gavin, 1969)

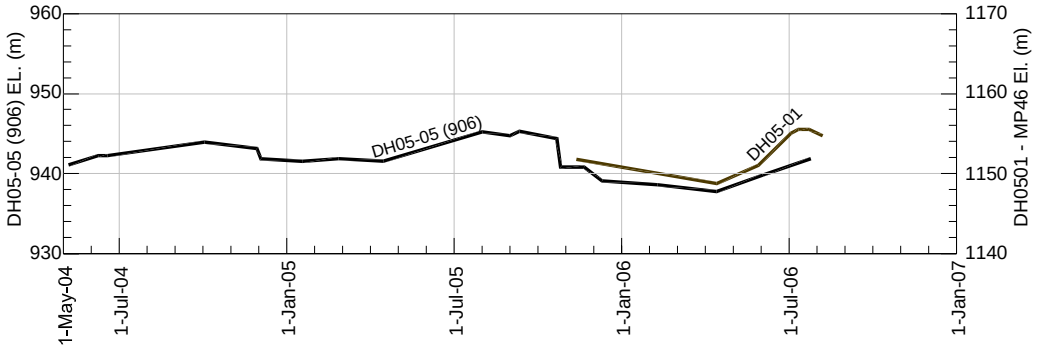

Figure 4-24: Piezometric Data Recorded in Boreholes DH05-05 (906) and DH05-01 (Modified after Moore et al., 2006)

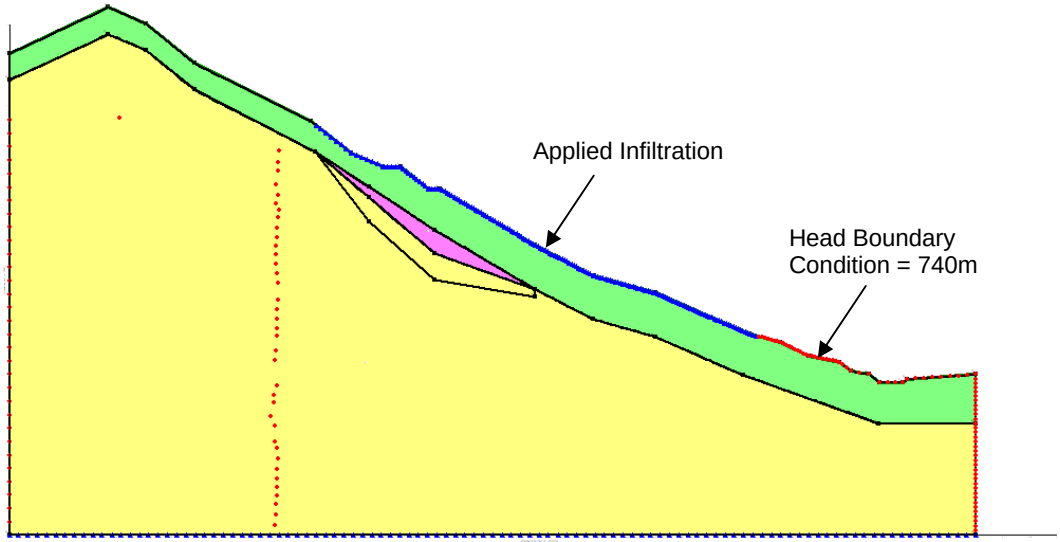

Figure 4-25: Shape of the Finite Element Mesh Used in Simulating Rainfall Effect

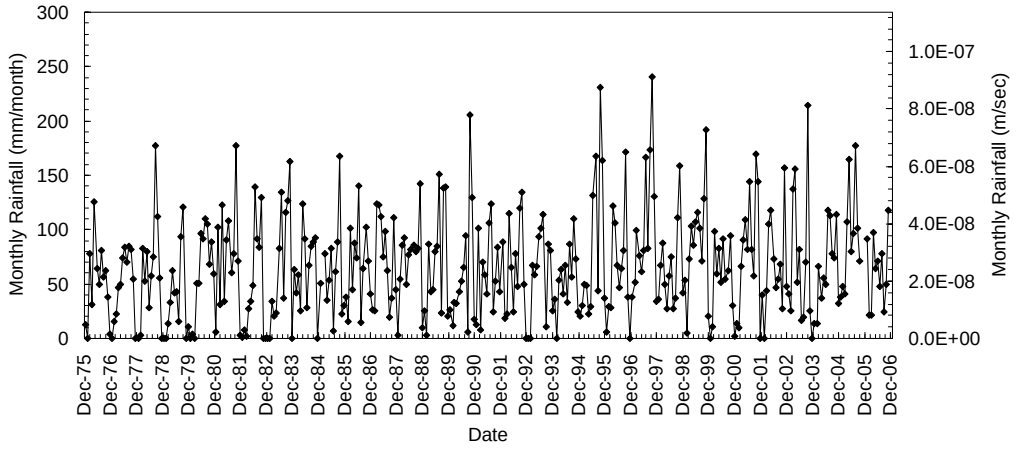

Figure 4-26: The distribution of Monthly Rainfall for a 30 Years Time Period Expressed in mm/month and m/sec

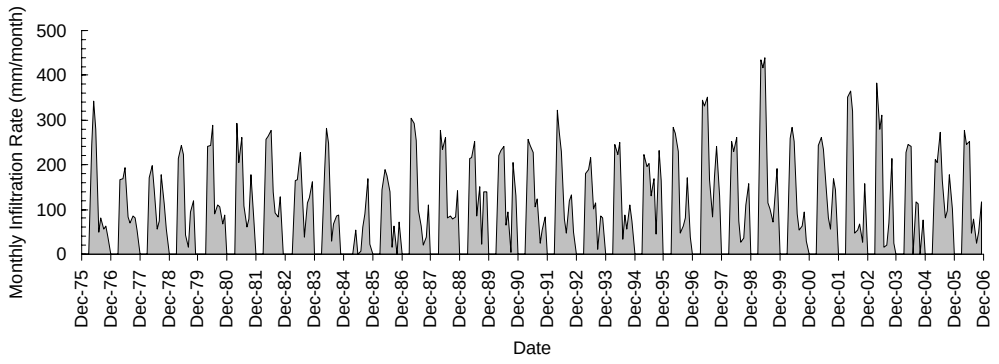

Figure 4-27: Redistributed Monthly Infiltration Rate Function

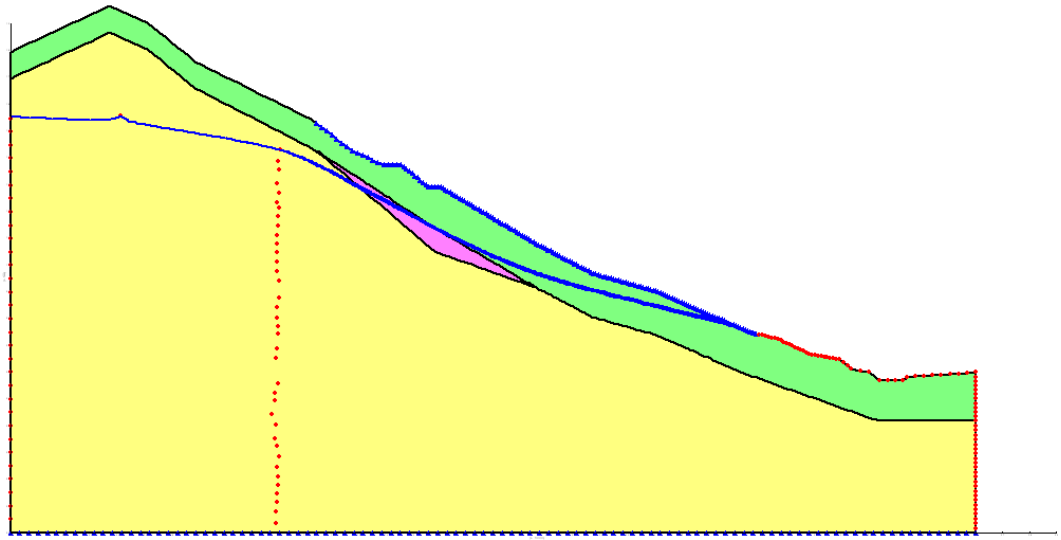

Figure 4-28: Phreatic Line Variation due to the Application of Rainfall for 30 years (Estimated Functions)

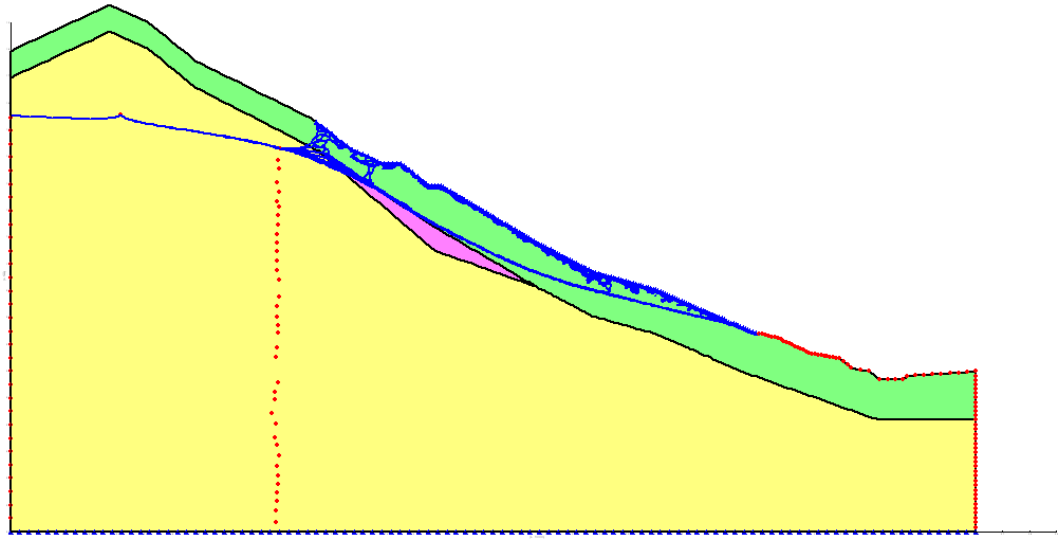

Figure 4-29: Phreatic Line Variation due to the Application of Rainfall for 30 Years (Predicted Functions)

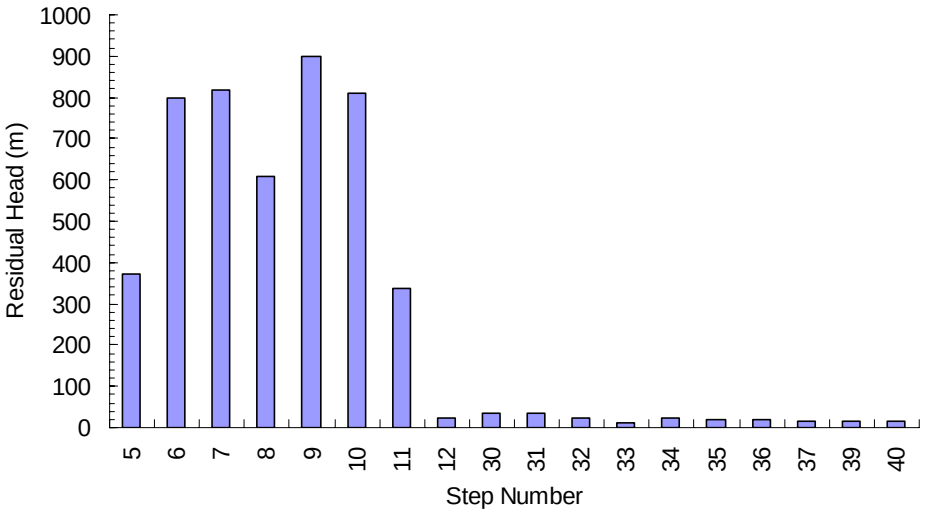

Figure 4-30: Residual Head Values in Non-Converged Time Steps (Using Predicted Functions)

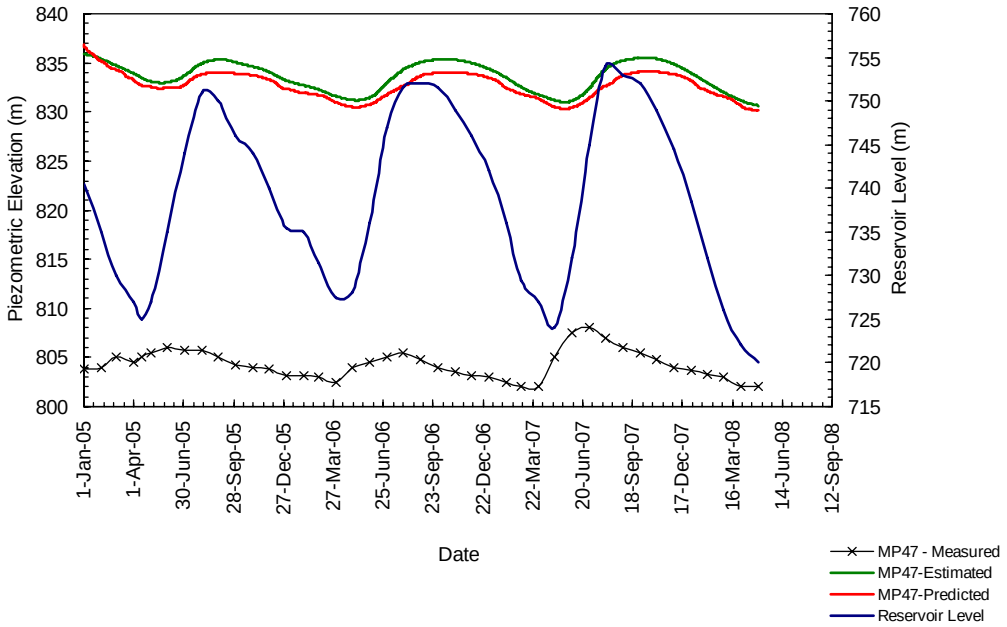

(a)

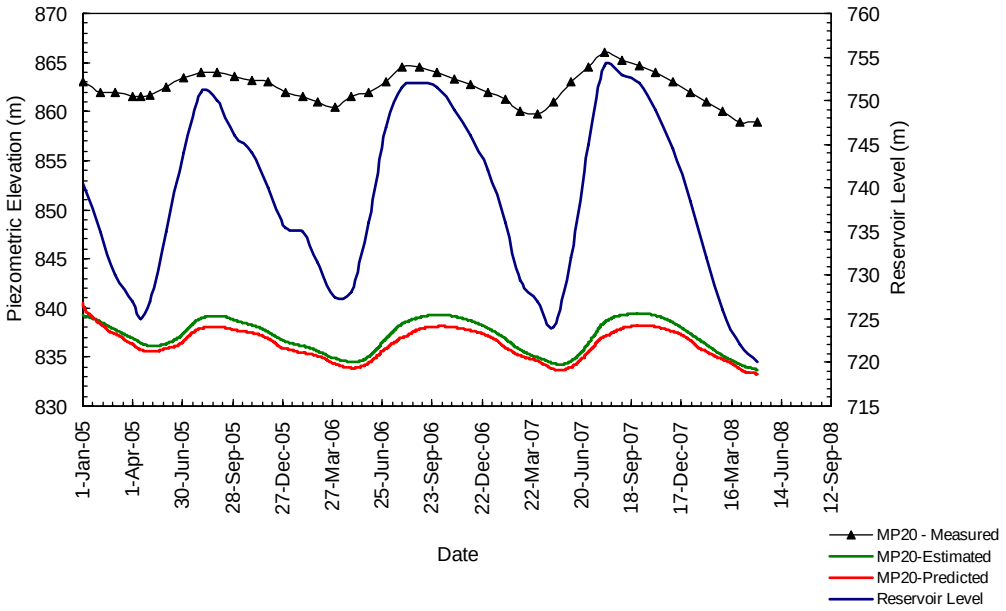

(b)

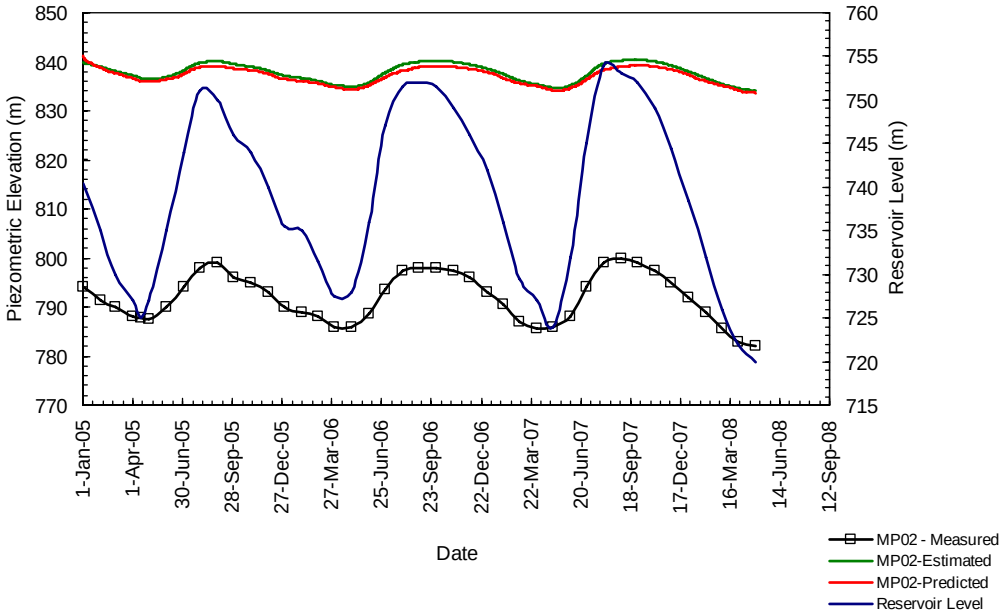

(c)

Figure 4-31: Results of the Numerical Simulation of Reservoir Fluctuations at the Location of Borehole DH04-01: (a) MP47, (b) MP20 and (c) MP02

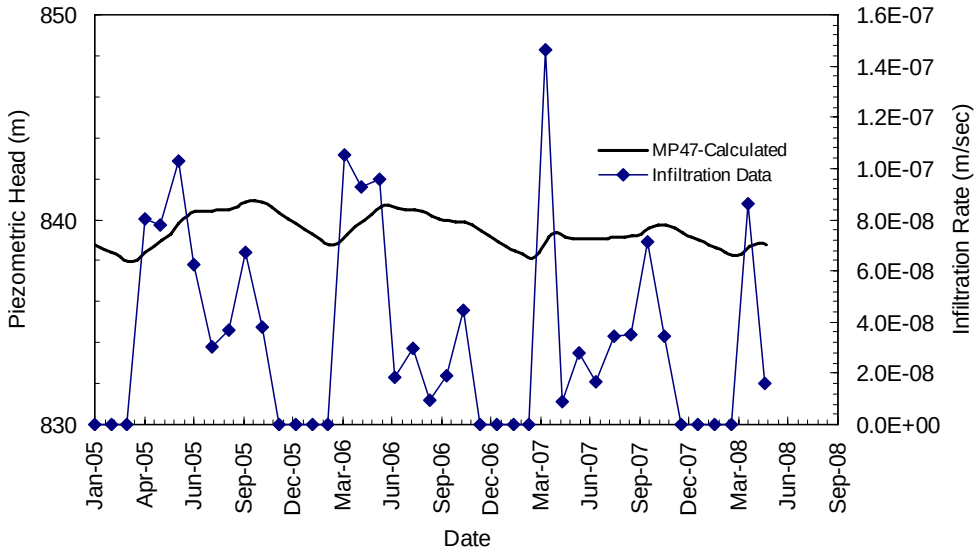
850
840
830
Piezometric Head (m)
1.6E-07
1.4E-07
1.2E-07
1.0E-07
8.0E-08
6.0E-08
4.0E-08
2.0E-08
0.0E+00
Infiltration Rate (m/sec)
MP47-Calculated
Infiltration Data
Jan-05
Apr-05
Jun-05
Sep-05
Dec-05
Mar-06
Jun-06
Sep-06
Dec-06
Mar-07
Jun-07
Sep-07
Dec-07
Mar-08
Jun-08
Sep-08
Date

(a)

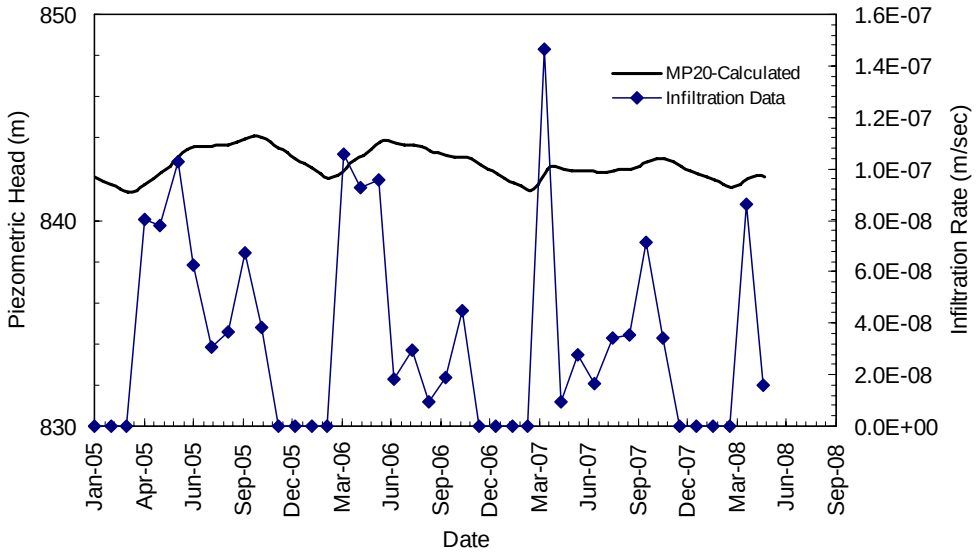
850
840
830
Piezometric Head (m)
1.6E-07
1.4E-07
1.2E-07
1.0E-07
8.0E-08
6.0E-08
4.0E-08
2.0E-08
0.0E+00
Infiltration Rate (m/sec)
MP20-Calculated
Infiltration Data
Jan-05
Apr-05
Jun-05
Sep-05
Dec-05
Mar-06
Jun-06
Sep-06
Dec-06
Mar-07
Jun-07
Sep-07
Dec-07
Mar-08
Jun-08
Sep-08
Date

(b)

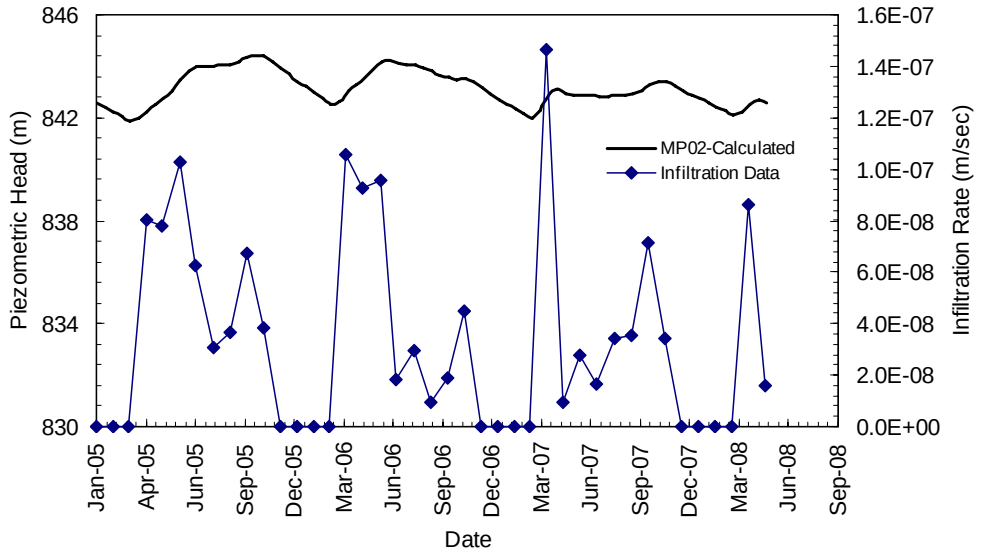

(c)

Figure 4-32: Results of the Numerical Simulation of Rainfall Effect at the Location of Borehole DH04-01: (a) MP47, (b) MP20 and (c) MP02 (Estimated Functions only)

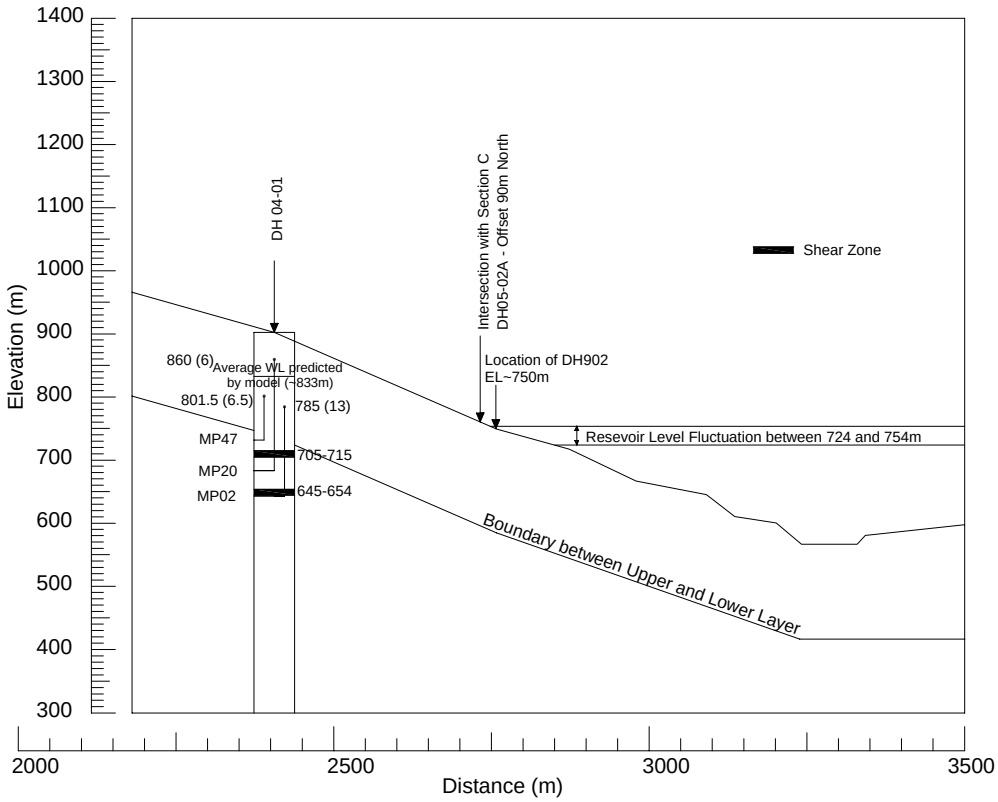

Figure 4-33: Locations of the Dipping Shear Zones in Borehole DH04-01 together with Measured Data

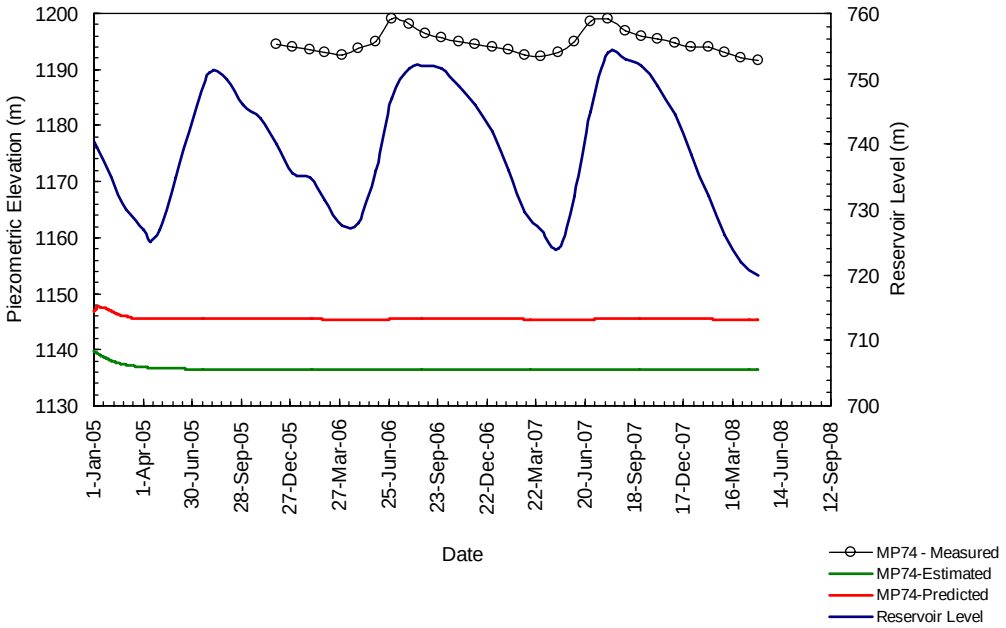
Piezometric Elevation (m)
Reservoir Level (m)
Date
1200
1190
1180
1170
1160
1150
1140
1130
760
750
740
730
720
710
700
1-Jan-05
1-Apr-05
30-Jun-05
28-Sep-05
27-Dec-05
27-Mar-06
25-Jun-06
23-Sep-06
22-Dec-06
22-Mar-07
20-Jun-07
18-Sep-07
17-Dec-07
16-Mar-08
14-Jun-08
12-Sep-08
MP74 - Measured
MP74-Estimated
MP74-Predicted
Reservoir Level

(a)

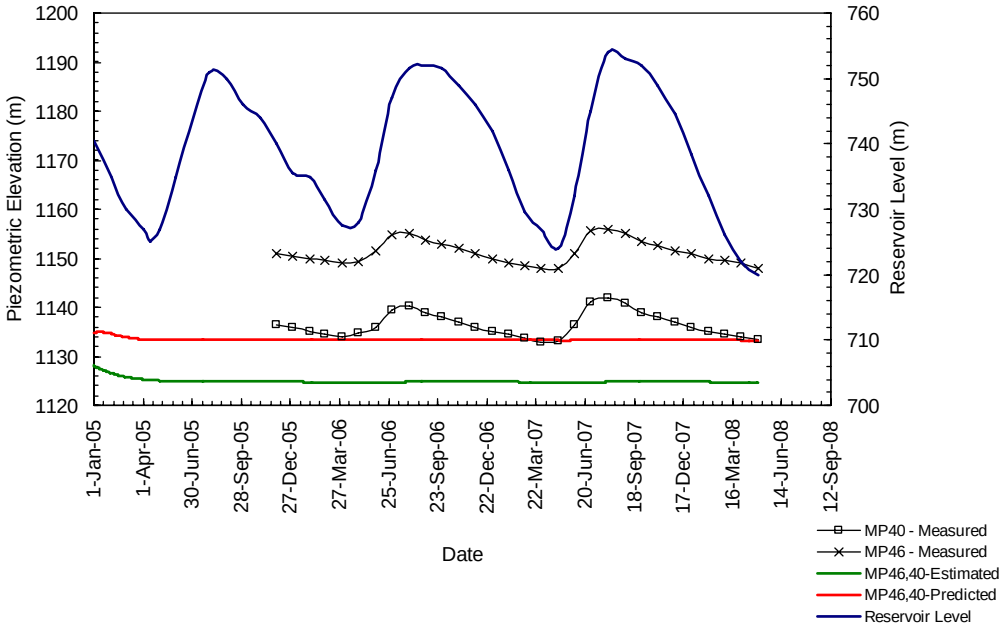
Piezometric Elevation (m)
Reservoir Level (m)
Date
1200
1190
1180
1170
1160
1150
1140
1130
1120
760
750
740
730
720
710
700
1-Jan-05
1-Apr-05
30-Jun-05
28-Sep-05
27-Dec-05
27-Mar-06
25-Jun-06
23-Sep-06
22-Dec-06
22-Mar-07
20-Jun-07
18-Sep-07
17-Dec-07
16-Mar-08
14-Jun-08
12-Sep-08
MP40 - Measured
MP46 - Measured
MP46,40-Estimated
MP46,40-Predicted
Reservoir Level

(b)

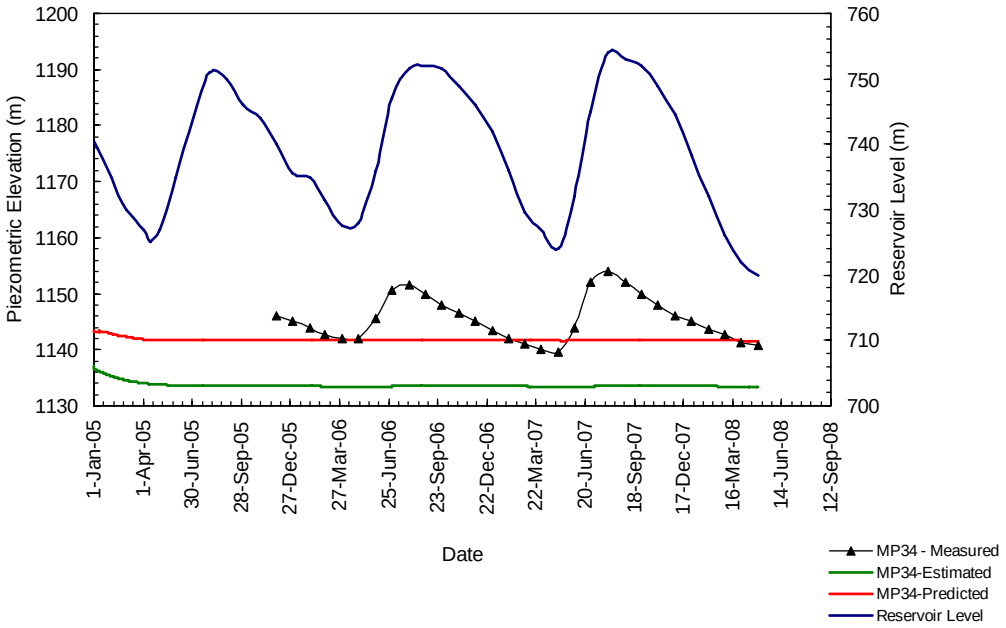

(c)

Figure 4-34: Results of the Numerical Simulation of the Reservoir Fluctuations Effect at the Location of Borehole DH05-01: (a) MP74, (b) MP46 and 40, and (c) MP34

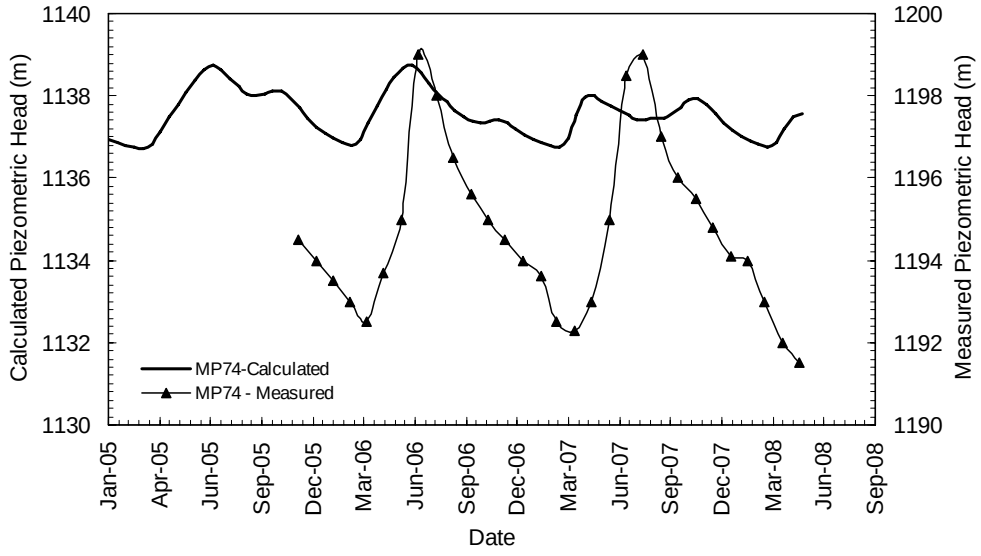

(a)

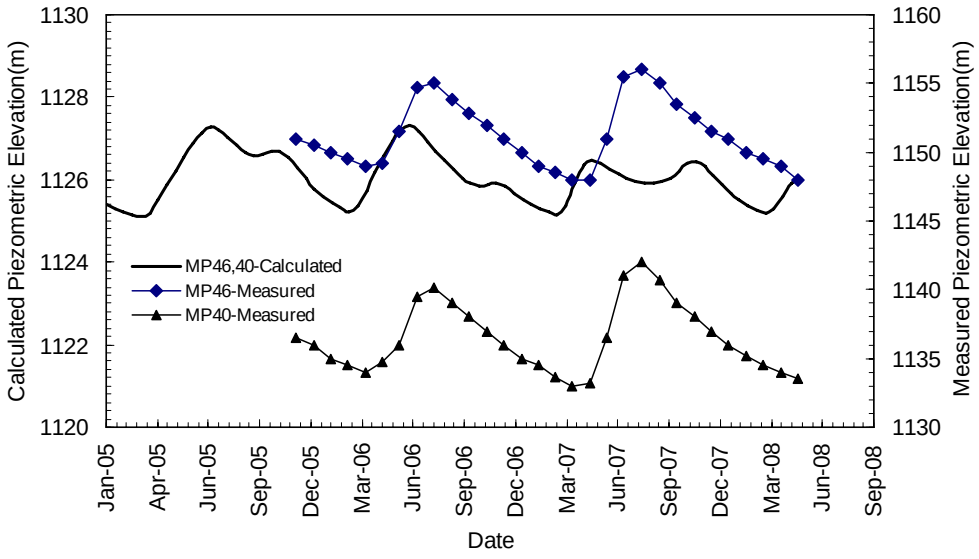

(b)

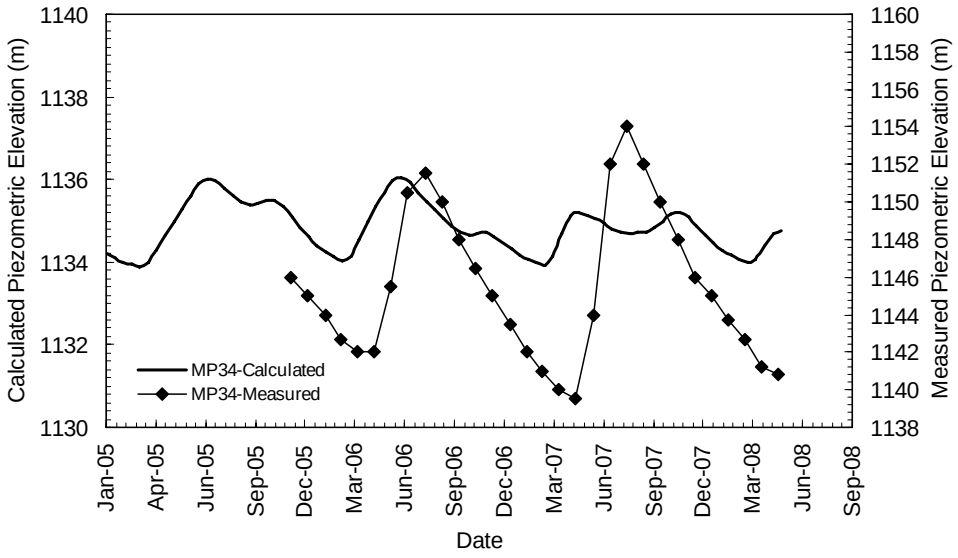

(c)

Figure 4-35: Results of the Numerical Simulation of Rainfall Effect at the Location of Borehole DH05-01: (a) MP74, (b) MP46 and 40, and (c) MP34 (Estimated Functions Only)

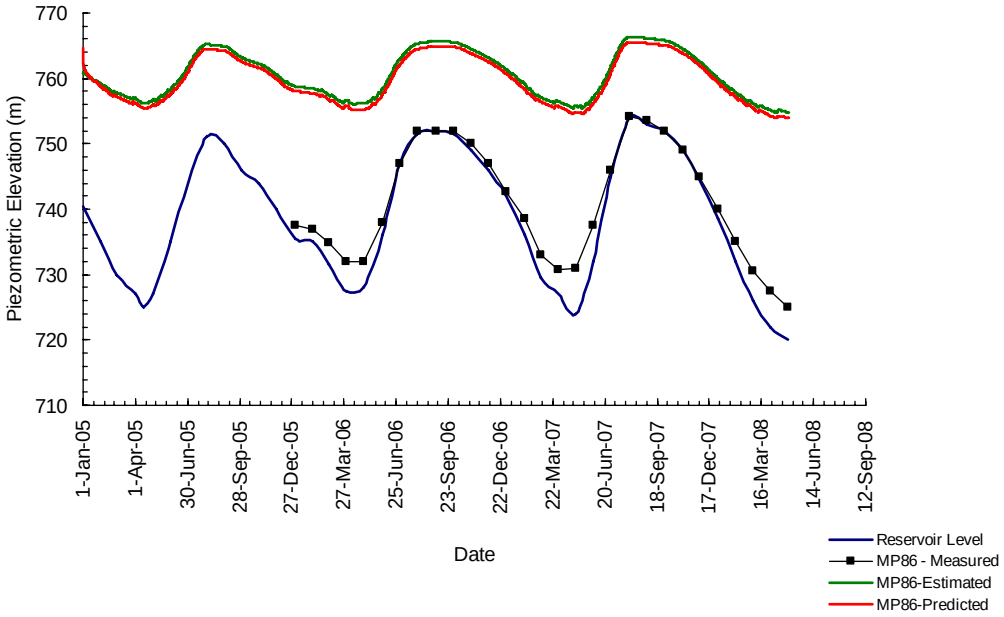
770
760
750
740
730
720
710
Piezometric Elevation (m)
1-Jan-05
1-Apr-05
30-Jun-05
28-Sep-05
27-Dec-05
27-Mar-06
25-Jun-06
23-Sep-06
22-Dec-06
22-Mar-07
20-Jun-07
18-Sep-07
17-Dec-07
16-Mar-08
14-Jun-08
12-Sep-08
Date
Reservoir Level
MP86 - Measured
MP86-Estimated
MP86-Predicted

(a)

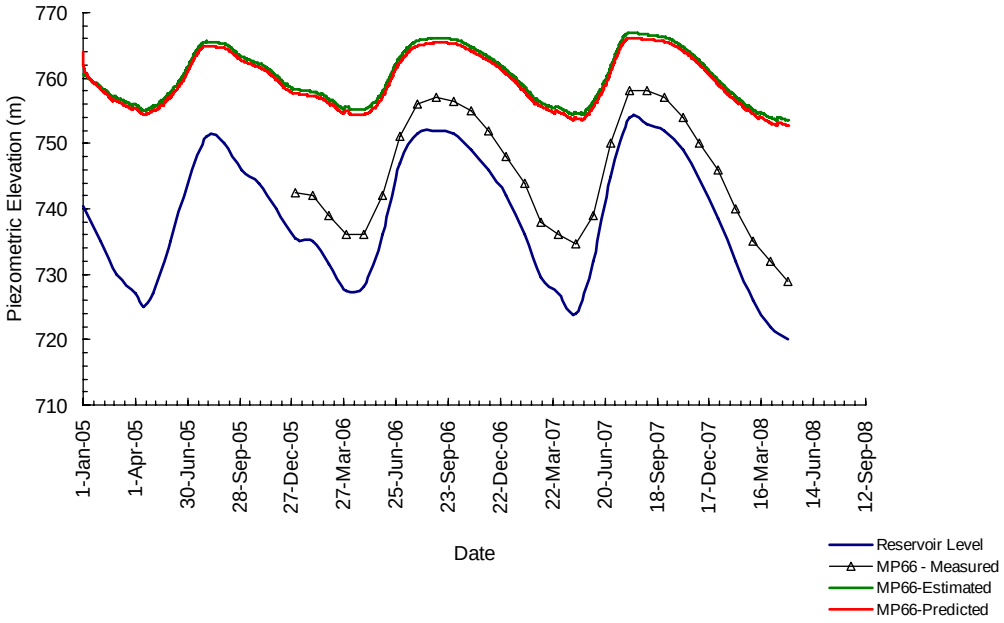
770
760
750
740
730
720
710
Piezometric Elevation (m)
1-Jan-05
1-Apr-05
30-Jun-05
28-Sep-05
27-Dec-05
27-Mar-06
25-Jun-06
23-Sep-06
22-Dec-06
22-Mar-07
20-Jun-07
18-Sep-07
17-Dec-07
16-Mar-08
14-Jun-08
12-Sep-08
Date
Reservoir Level
MP66 - Measured
MP66-Estimated
MP66-Predicted

(b)

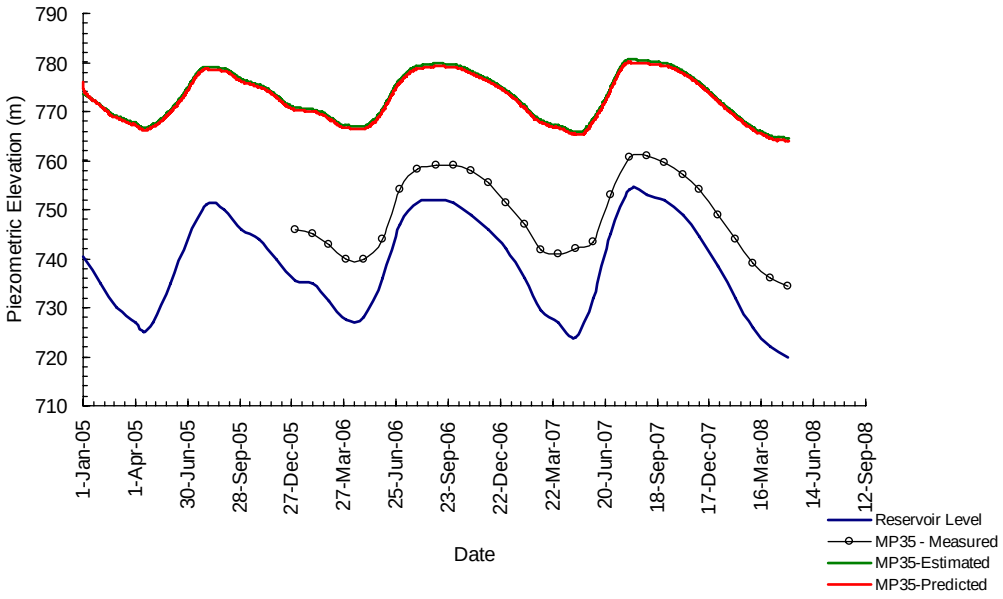

(c)

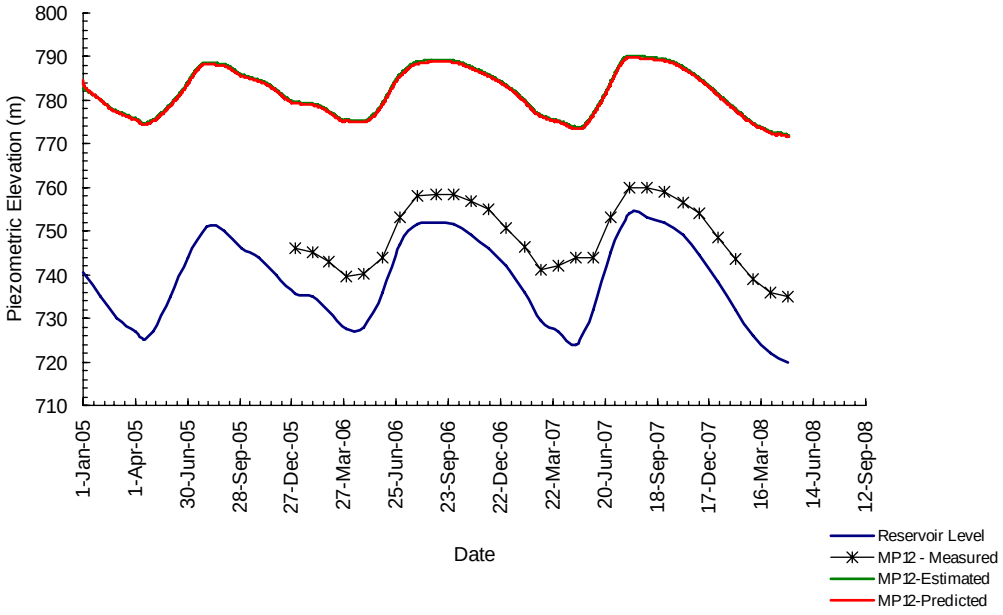

(d)

Figure 4-36: Results of the Numerical Simulation of Reservoir Fluctuations at the Location of Borehole DH05-02A: (a) MP86, (b) MP66, (c) MP35 and (d) MP12

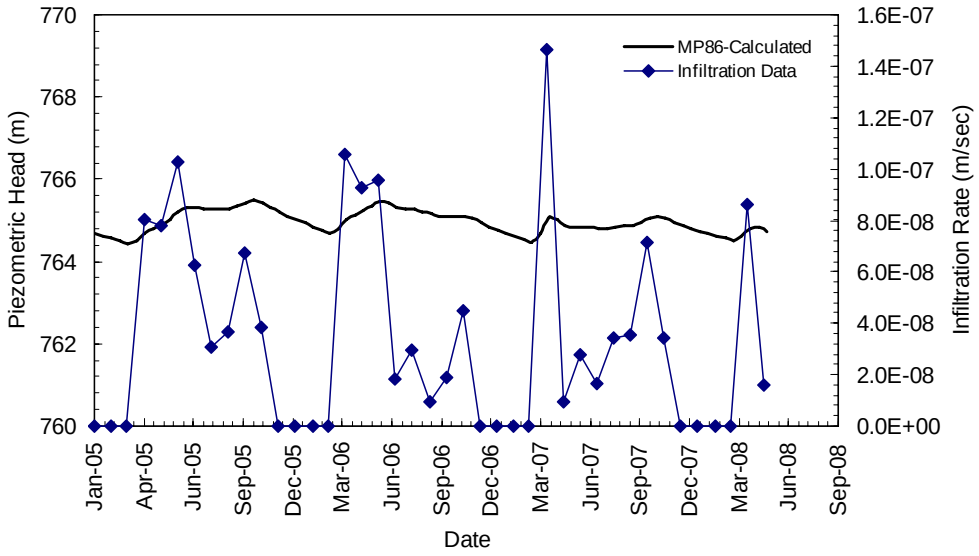
MP86-Calculated
Infiltration Data
Piezometric Head (m)
Infiltration Rate (m/sec)
Date
770
768
766
764
762
760
1.6E-07
1.4E-07
1.2E-07
1.0E-07
8.0E-08
6.0E-08
4.0E-08
2.0E-08
0.0E+00
Jan-05
Apr-05
Jun-05
Sep-05
Dec-05
Mar-06
Jun-06
Sep-06
Dec-06
Mar-07
Jun-07
Sep-07
Dec-07
Mar-08
Jun-08
Sep-08

(a)

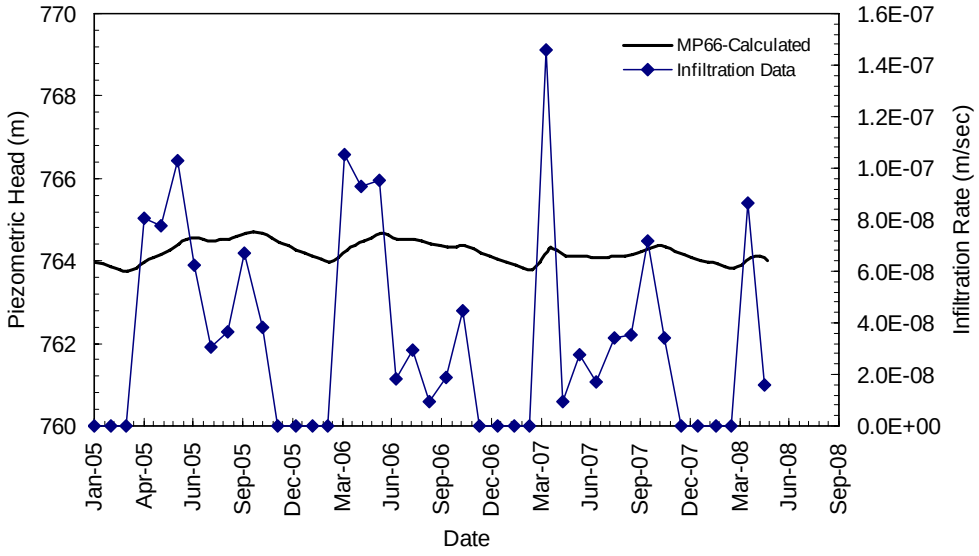
MP66-Calculated
Infiltration Data
Piezometric Head (m)
Infiltration Rate (m/sec)
Date
770
768
766
764
762
760
1.6E-07
1.4E-07
1.2E-07
1.0E-07
8.0E-08
6.0E-08
4.0E-08
2.0E-08
0.0E+00
Jan-05
Apr-05
Jun-05
Sep-05
Dec-05
Mar-06
Jun-06
Sep-06
Dec-06
Mar-07
Jun-07
Sep-07
Dec-07
Mar-08
Jun-08
Sep-08

(b)

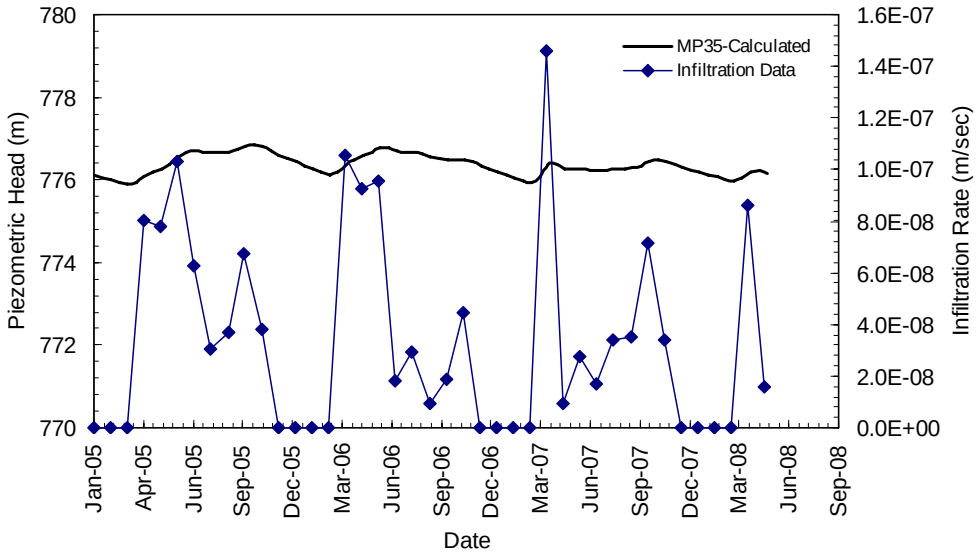

(c)

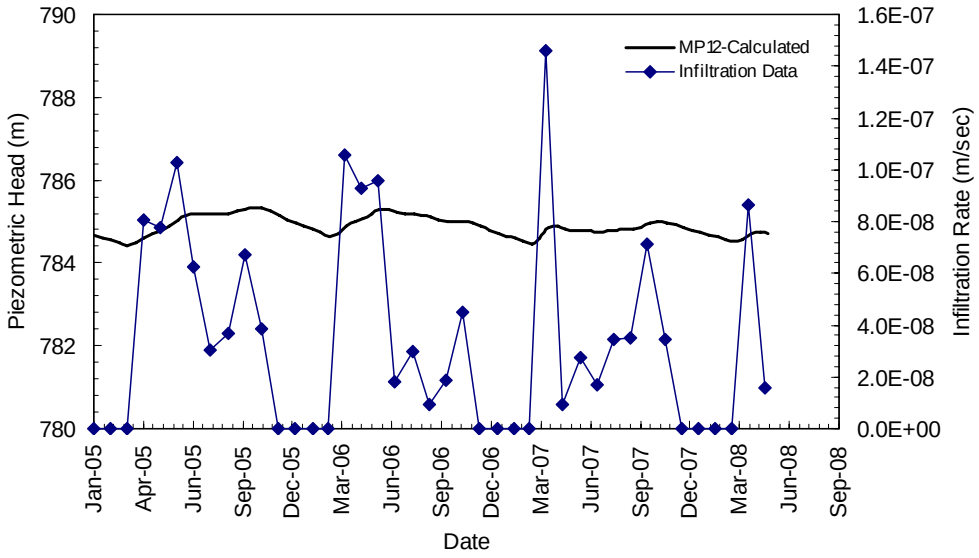

(d)

Figure 4-37: Results of the Numerical Simulation of Rainfall Effect at the Location of Borehole DH05-02A: (a) MP86, (b) MP66, (c) MP35 and (d) MP12 (Estimated Functions Only)

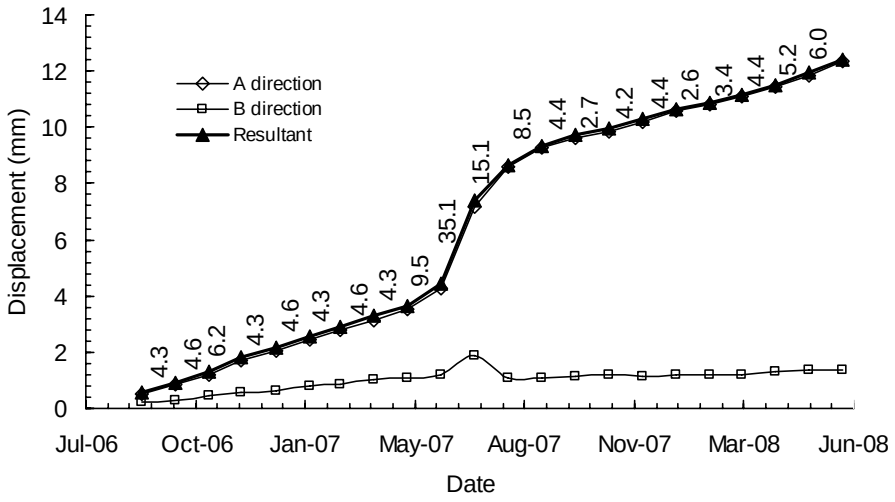

Figure 4-38: Displacement versus Time Plot Resulted from the IPI Installed at Depth 210.9m in Borehole DH05-03

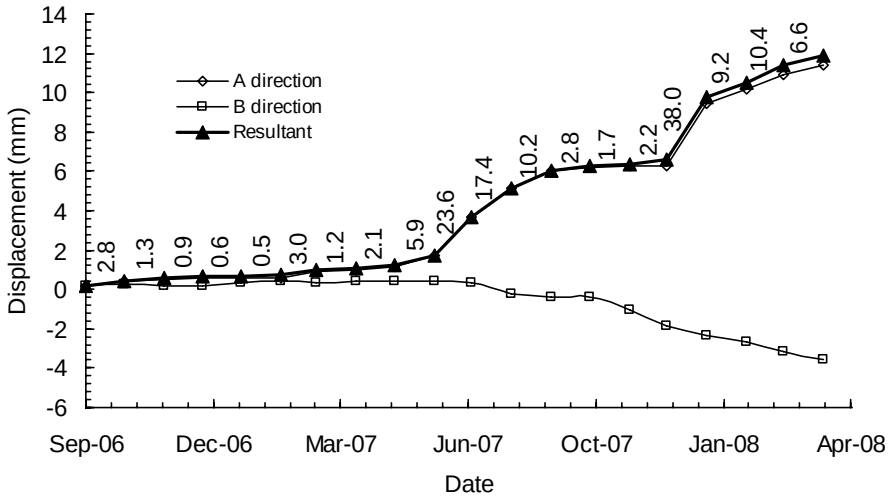

Figure 4-39: Displacement versus Time Plot Resulted from the IPI Installed at Depth 176.2m in Borehole DH05-04

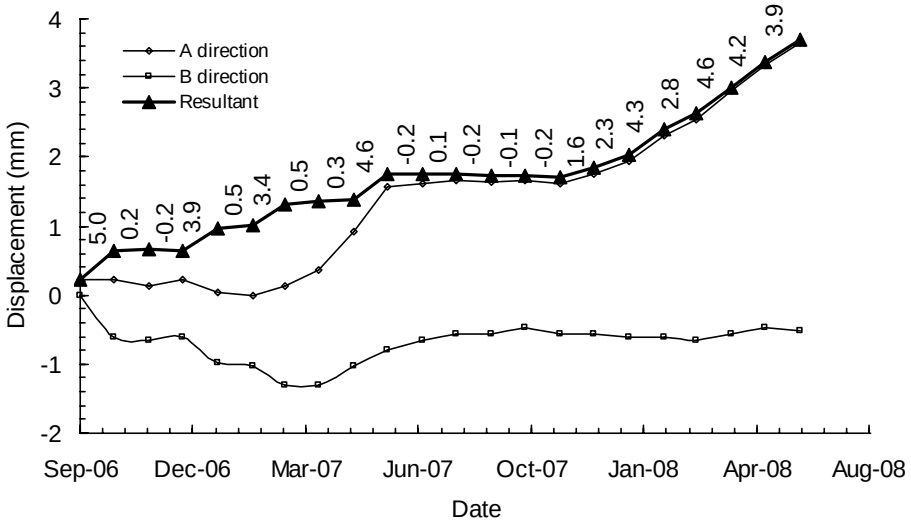

Figure 4-40: Displacement versus Time Plot Resulted from the IPI Installed at Depth 171.3m in Borehole DH05-06

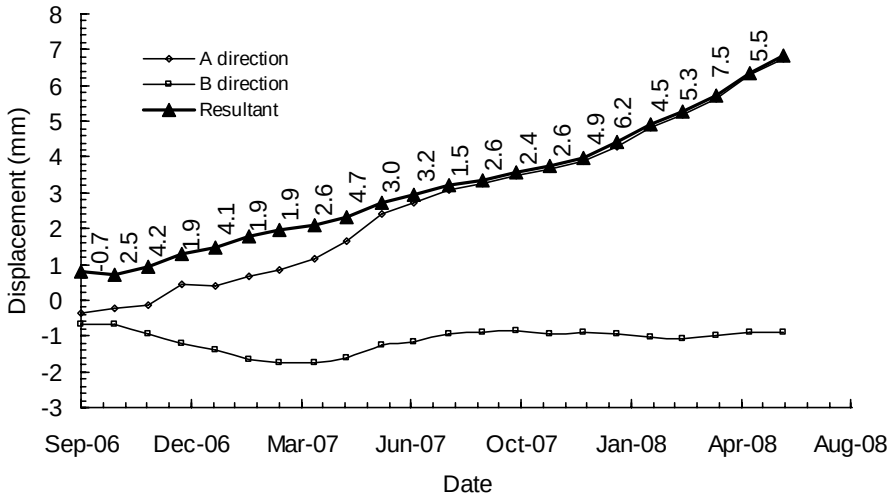

Figure 4-41: Displacement versus Time Plot Resulted from the IPI Installed at Depth 233.8m in Borehole DH05-06

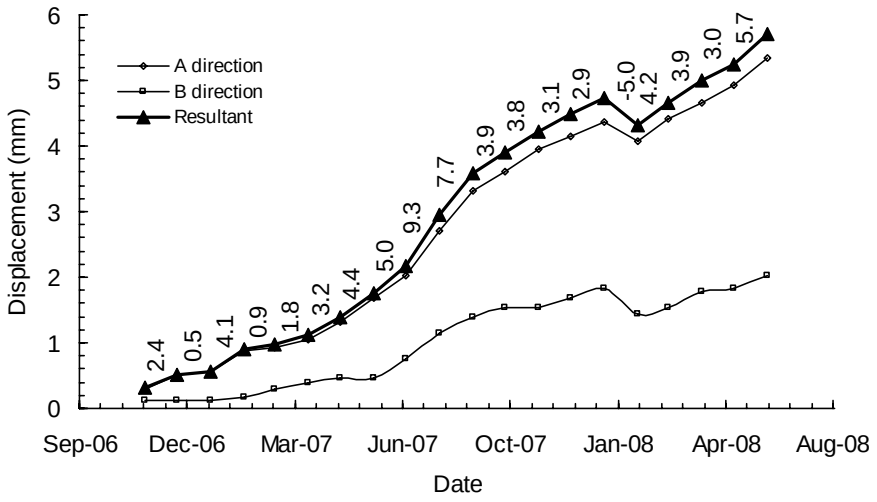

Figure 4-42: Displacement versus Time Plot Resulted from the IPI Installed at Depth 126.8m in Borehole DH05-07

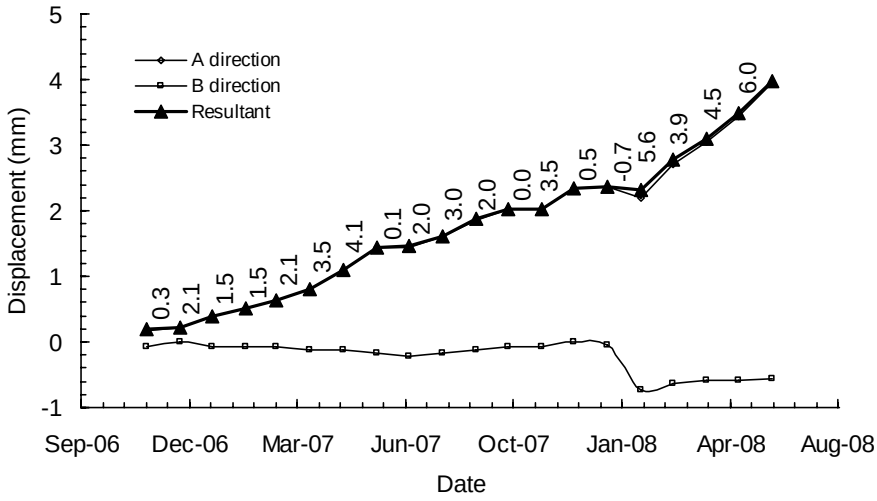

Figure 4-43: Displacement versus Time Plot Resulted from the IPI Installed at Depth 331.6m in Borehole DH05-07

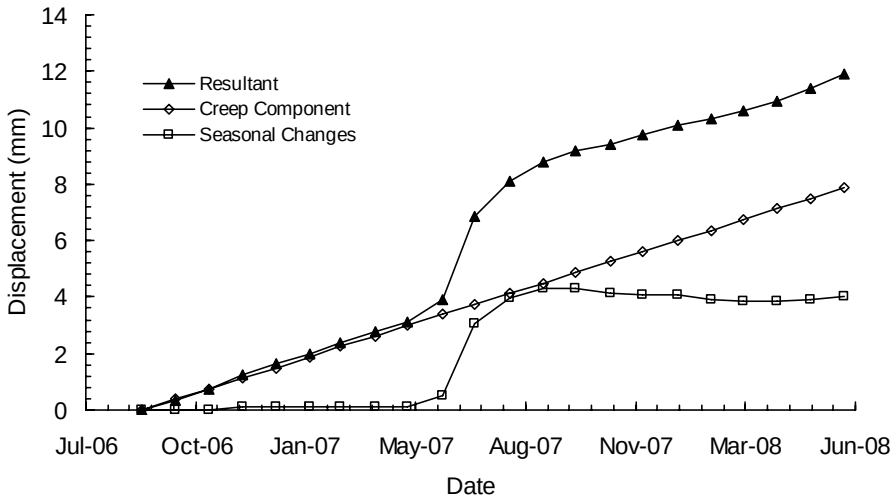

Figure 4-44: Different Components of Movement at Depth 210.9m in Borehole DH05-03 Referenced to the Recorded Movement in September 2006

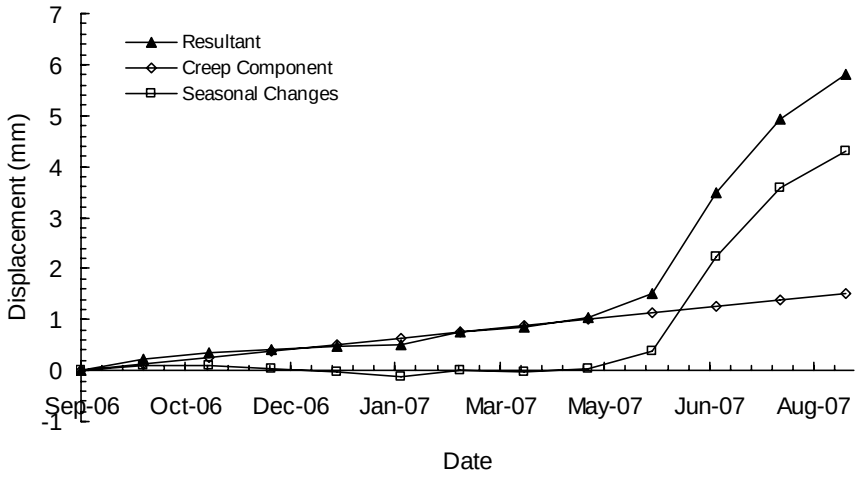

Figure 4-45: Different Components of Movement at Depth 176.2m in Borehole DH05-04 Referenced to the Recorded Movement in September 2006

Figure 4-46: Photo of the Samples taken from DH05-7 between Depths of 125 and 126.50m

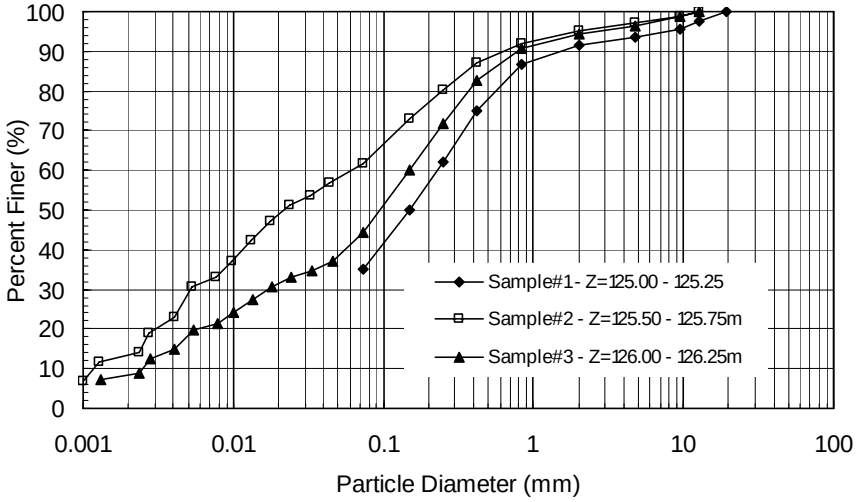

Figure 4-47: Grain Size Distribution Curves for Samples 1 through 3

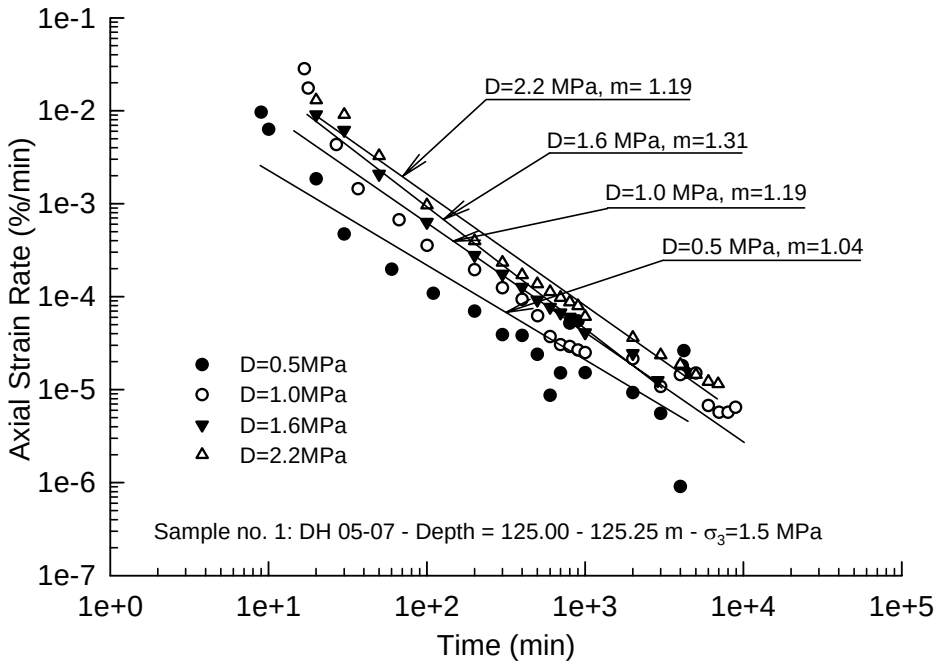

Figure 4-48: Axial Strain Rate versus Time for Sample #1

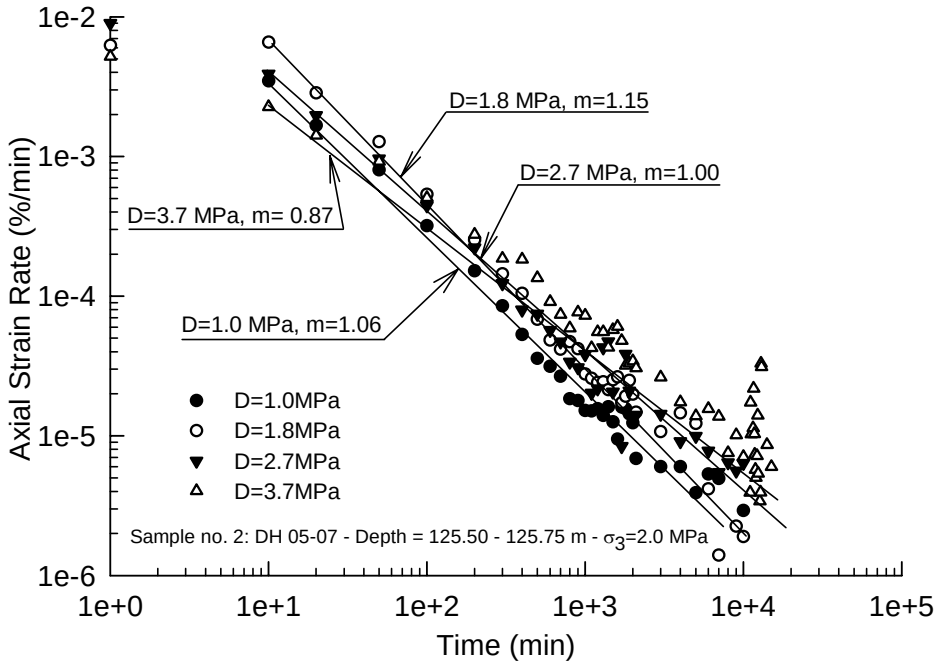

Figure 4-49: Axial Strain Rate versus Time for Sample #2

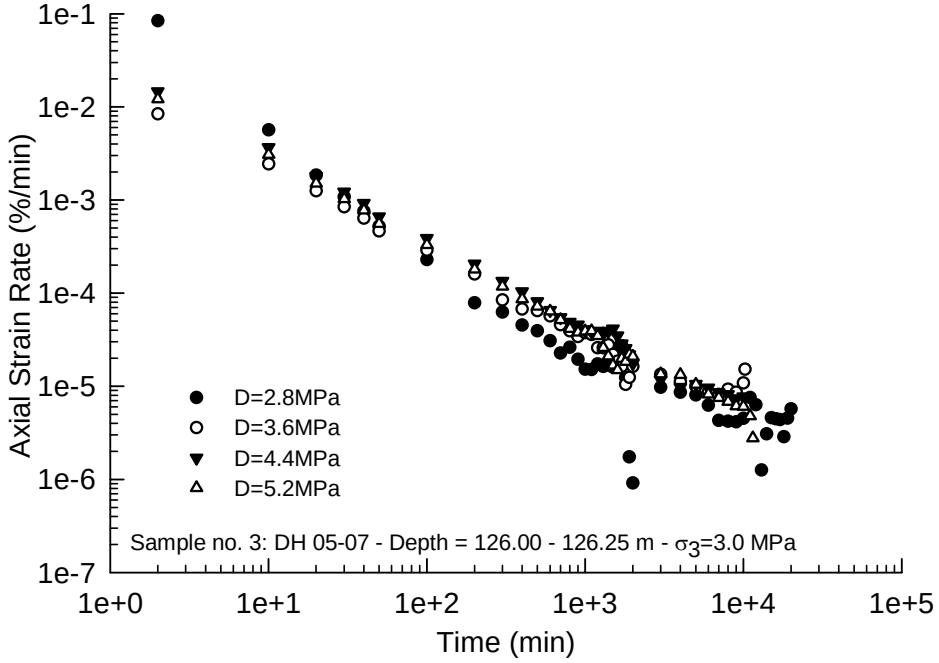

Figure 4-50: Axial Strain Rate versus Time for Sample #3

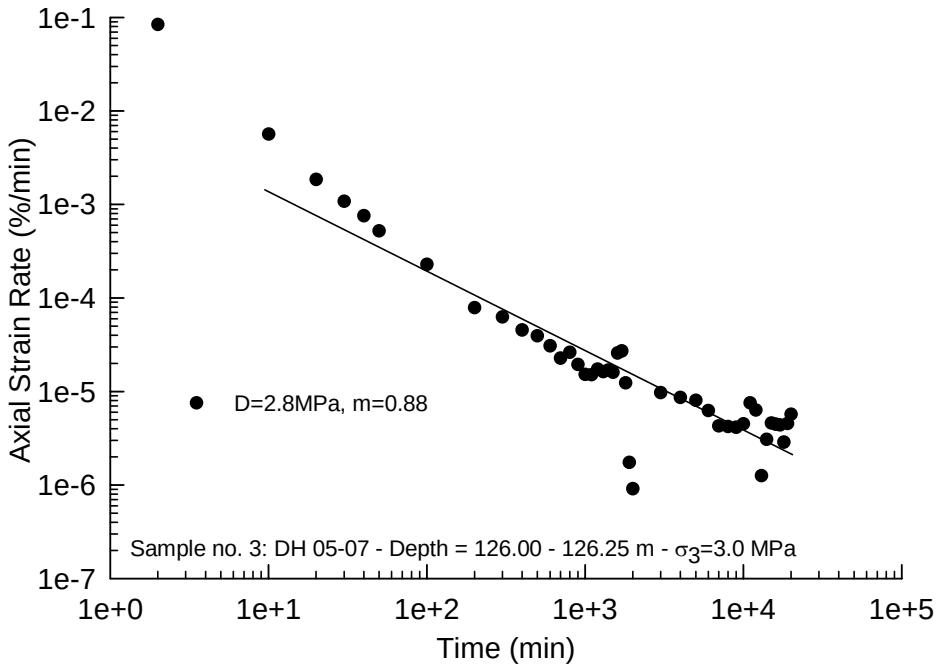

(a)

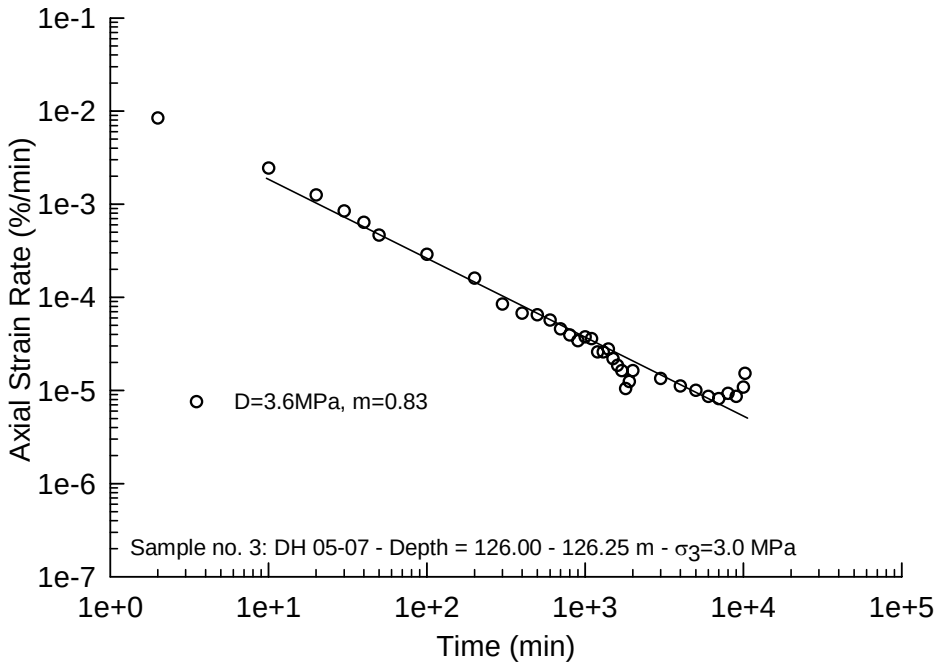
1e-1
1e-2
1e-3
1e-4
1e-5
1e-6
1e-7
Axial Strain Rate (%/min)
D=3.6MPa, m=0.83
Sample no. 3: DH 05-07 - Depth = 126.00 - 126.25 m - σ3=3.0 MPa
1e+0
1e+1
1e+2
1e+3
1e+4
1e+5
Time (min)

(b)

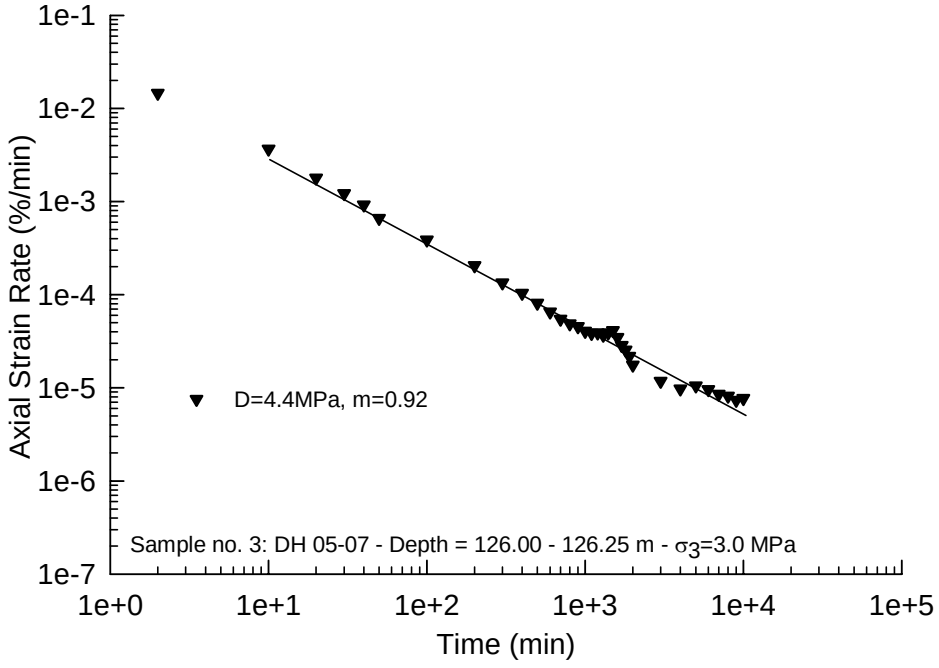
1e-1
1e-2
1e-3
1e-4
1e-5
1e-6
1e-7
Axial Strain Rate (%/min)
D=4.4MPa, m=0.92
Sample no. 3: DH 05-07 - Depth = 126.00 - 126.25 m - σ3=3.0 MPa
1e+0
1e+1
1e+2
1e+3
1e+4
1e+5
Time (min)

(c)

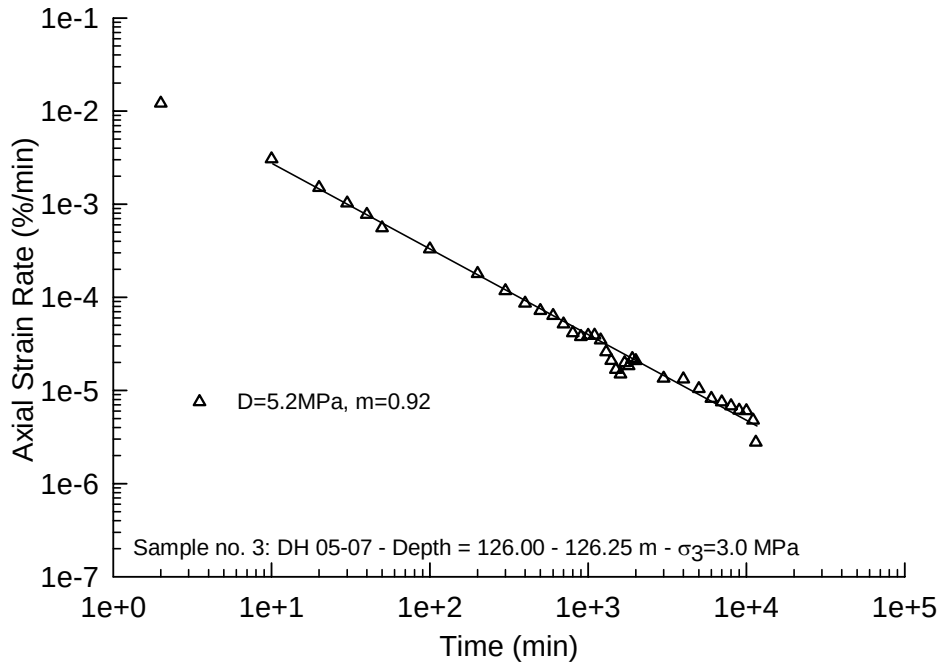

(d)

Figure 4-51: Linear Regressions for Axial Strain Rate versus Time Plots for Sample #3: (a) Deviatoric Stress 2.8MPa, (b) Deviatoric Stress 3.6MPa, (c) Deviatoric Stress 4.4MPa, and (d) Deviatoric Stress 5.2MPa

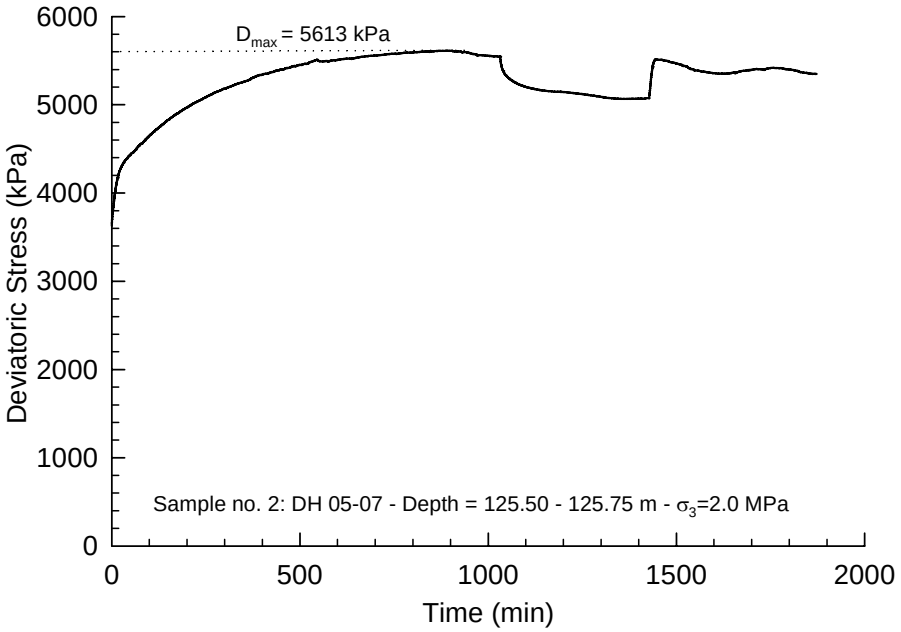

Figure 4-52: Deviatoric Stress Variation with Time after Loading to Failure (Sample #2)

Figure 4-53: Sample #2 after Failure

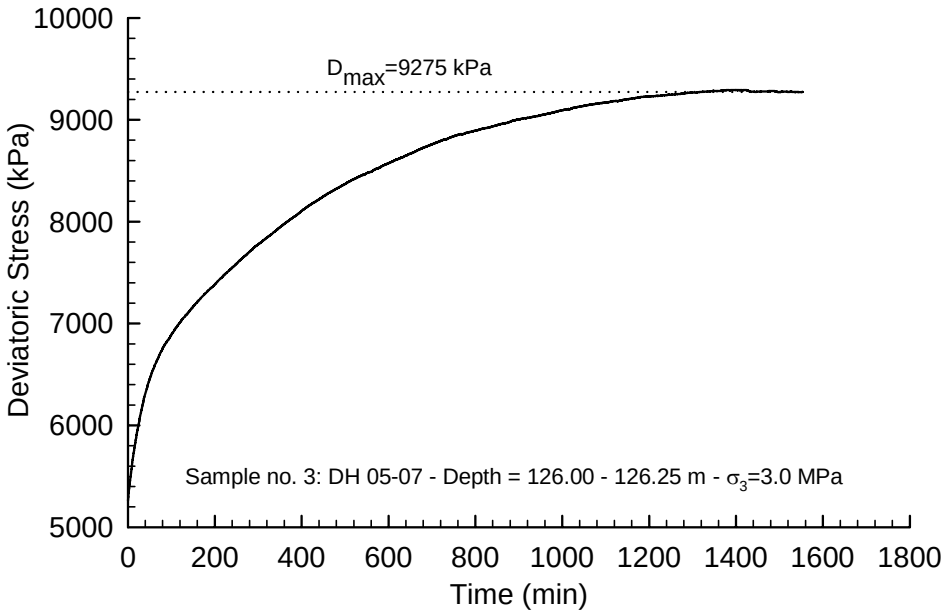

Figure 4-54: Deviatoric Stress Variation with Time after Loading to Failure (Sample #3)

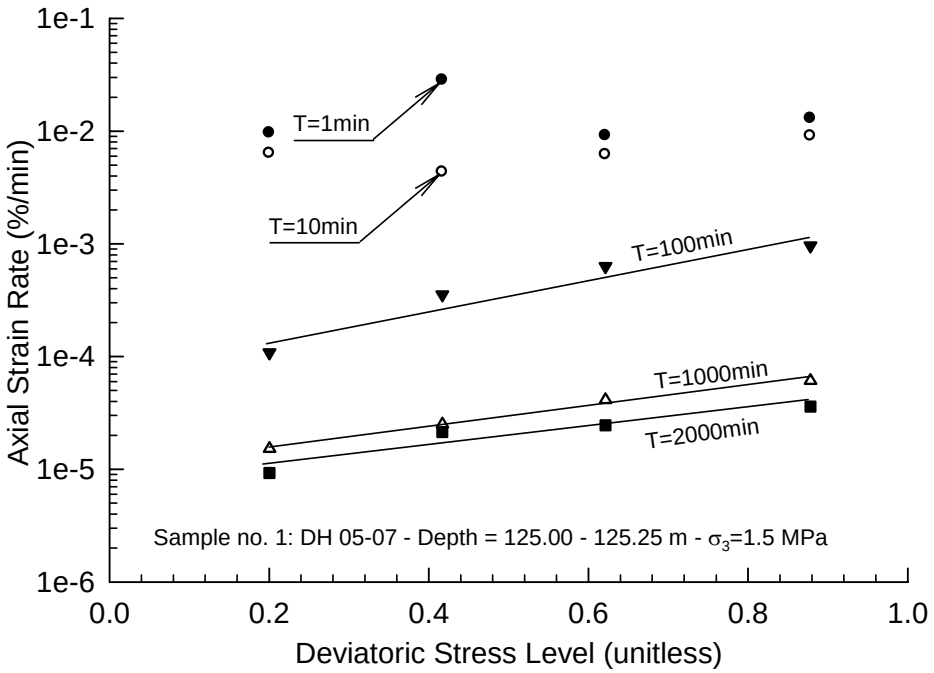

Figure 4-55: Axial Strain Rate versus Deviatoric Stress Level (Sample #1)

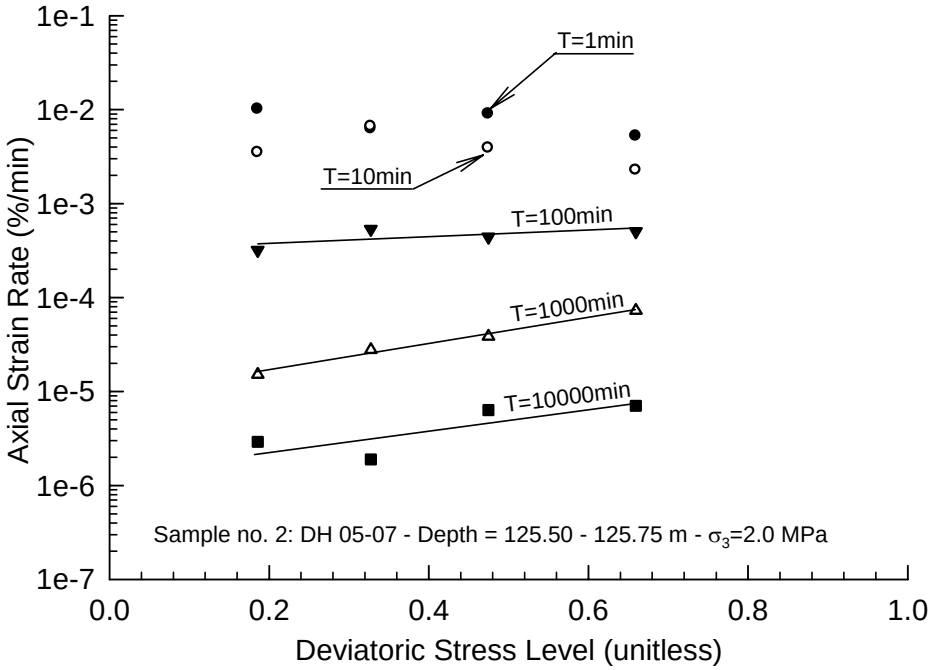

Figure 4-56: Axial Strain Rate versus Deviatoric Stress Level (Sample #2)

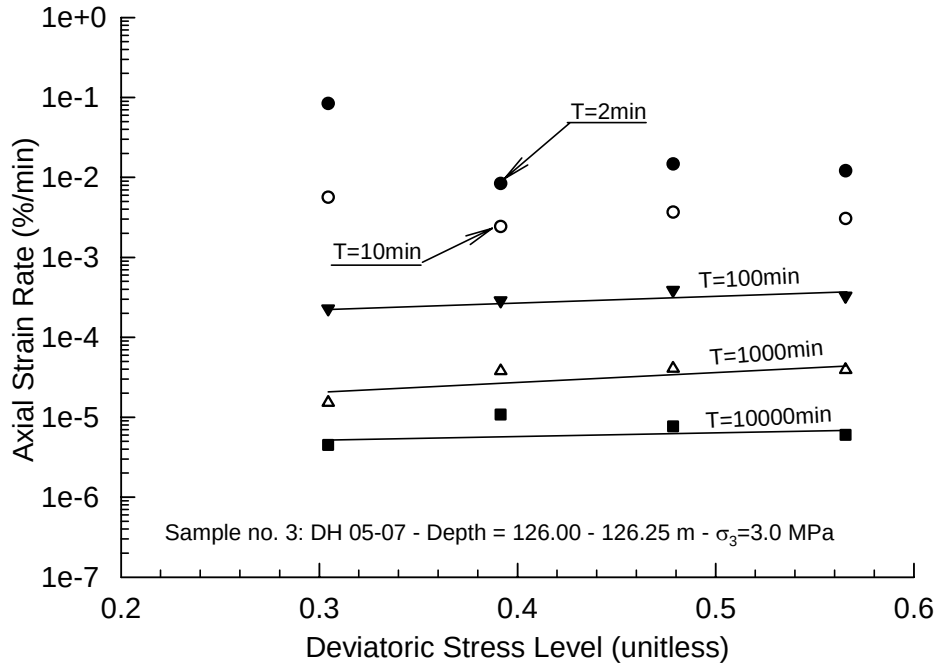

Figure 4-57: Axial Strain Rate versus Deviatoric Stress Level (Sample #3)

(a) Before testing

(b) After test termination

Figure 4-58: Shape of Sample #4 before and after Testing

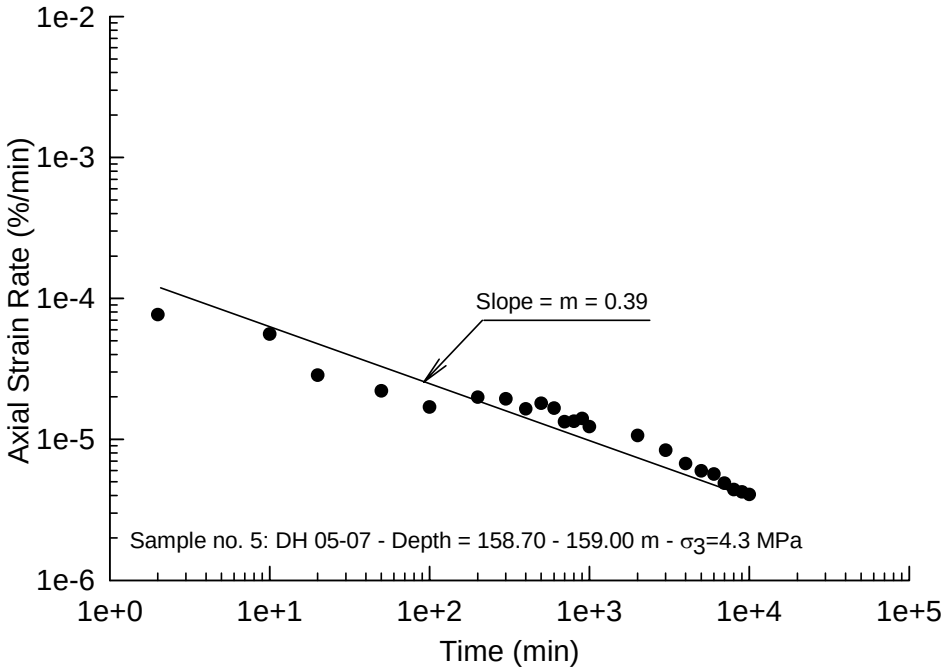

Figure 4-59: Axial Strain Rate versus Time for Sample #5 under a Deviatoric Stress 0.5MPa.

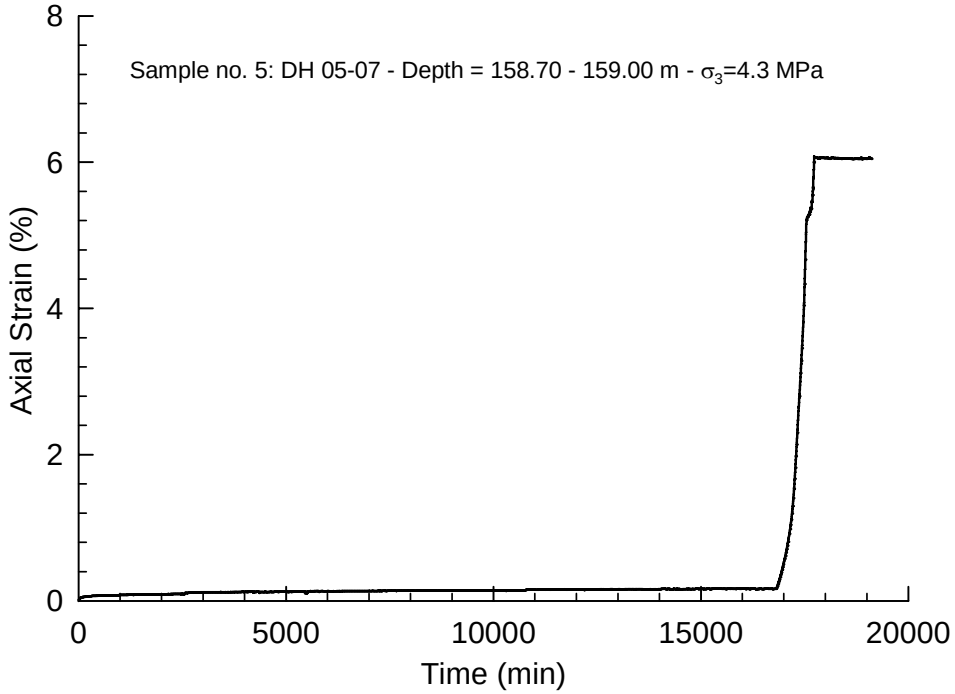

Figure 4-60: Axial Strain versus Time for Sample #5. Borehole DH05-07: Depth 158.70 – 159.00, Deviatoric Stress = 8.4MPa (~70% Stress Level)

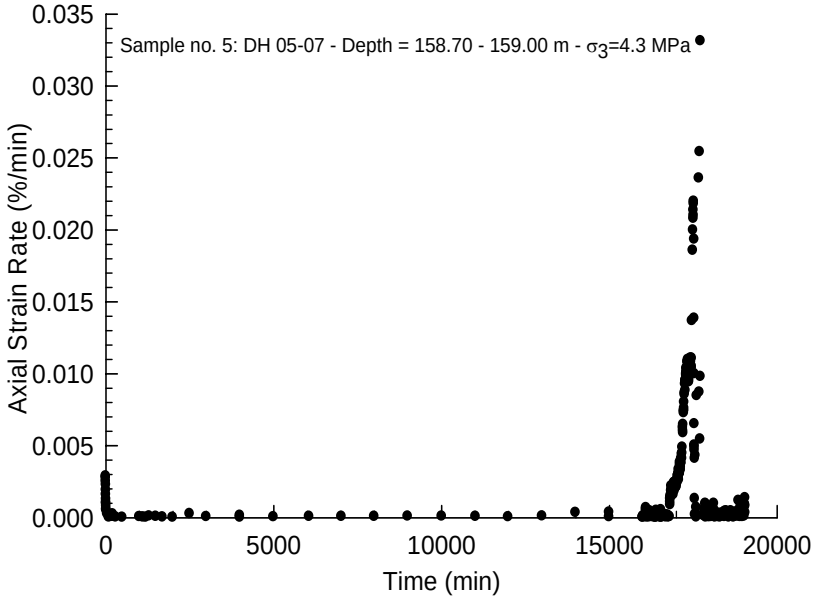

Figure 4-61: Axial Strain Rate versus Time for Sample #5. Borehole DH05-07: Depth 158.70 – 159.00, Deviatoric Stress = 8.4MPa (~70% Stress Level)

Figure 4-62: Sample #5 after Loading to 70% Stress Level

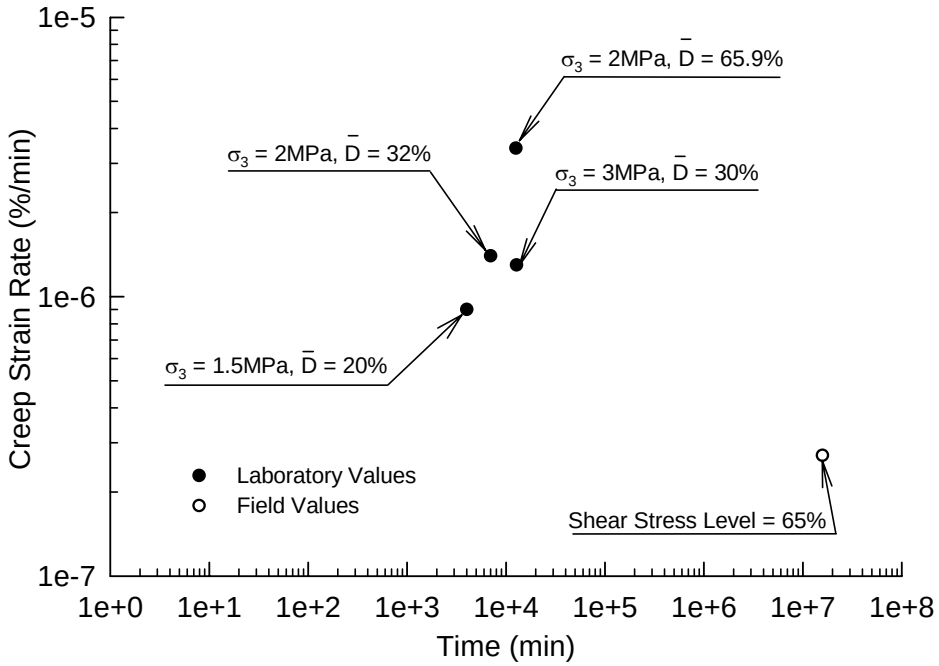

Figure 4-63: Comparison between Field and Minimum Laboratory Creep Strain Rates

5 The Triggers of the Movements of the Little Smoky Slides

5.1 Introduction

The Little Smoky Slides are located at the intersection of the Little Smoky River and Highway 49 about 48 km north of Valleyview in north-western Alberta (Figure 5-1). The bridge carrying Highway 49 across the north flowing river was completed in 1957. The river valley at this location is about 90m deep and has an average slope of 7^0. The steel truss bridge crossing the river is 271m long. The bottom level of the bridge deck is at an elevation of approximately 496m, and the minimum river level is at an elevation of approximately 487.5m (Hayley, 1968; Thomson and Hayley, 1975; Alberta Infrastructure, 1998; and Skirrow et al., 2005). Movements of the west abutment and pier were noticed soon after construction and have continued. The movements have been and still are posing a threat to the bridge safety. Hayley (1968) and Thomson and Hayley (1975) investigated the stability of the west slope, which lies downstream and west of the bridge. Movement rates up to 100mm/yr have been recorded. The bridge's west pier and abutment needed continuous extensions in order to accommodate the movements. Movements of both the south and north slopes have been monitored semi-annually from 2001 to 2005. The south and north slopes were found to move at rates of 30 and up to 70 mm/yr, respectively. The most recent investigation took place between 2007 and the end of 2008 and involved monitoring the pore pressures and movements of the west, south and north slopes at intervals as short as two weeks during the period of movement acceleration. The locations of the west, south and north slopes are shown in Figure 5-2.

The following sections present a description of the regional setting, a review of the previous investigations and their outcomes. The results of the most recent investigations are then presented, followed by an analysis of the movements, pore pressures and hydrological records. At the end of the study, the movement behaviours could be described and the different triggers of movement could be defined. The contribution of each trigger is quantified. The resolution of the total movement into individual components has important implications with regard to the choice of the relevant hazard mitigation options.

5.2 Regional Setting

During the Tertiary Period, before glaciation, the Peace River drainage basin area was characterized by broad valleys cut into rocks of the Upper Cretaceous age. The preglacial valley at the Little Smoky site was cut mainly through flat-lying sandstones and shales of the Wapiti Formation. However, preglacial river erosion eroded this layer and exposed a member of the Smoky Group, the Puskwaskau

formation, which has been described as “soft grey fissile shales of marine origin” (Hayley, 1968).

Liverman et al. (1989) showed that the surface till in this region of west central Alberta is Late Wisconsin in age and represents only the Laurentide glaciation. As Cruden et al. (1993) pointed out, the Late Wisconsin Laurentide ice sheet blocked the regional drainage while advancing up the regional gradient of the area. Hence, preglacial lakes were formed in the broad preglacial valleys. The clay till and the preglacial lake clays that were formed in some locations reflect the composition of the poorly indurated Smoky Group shales over which the ice advanced. After ice retreat, the melt water incised through the Pleistocene deposits to form the current relatively steep-sided valleys around the Peace, Smoky, and Little Smoky Rivers.

The river bed consists mainly of coarse boulders (Hayley 1968). The rivers in the early Pleistocene carried gravels, and some were deposited on the river terraces. These preglacial Saskatchewan sands and gravels originated in the foothills of the Rocky Mountains. They contain quartzites, cherts and sandstones, and, in some locations, lie between bedrock and the overlying till. Other boulders in the river channel were eroded from the till (Rennie, 1966).

The condition of the clay shale differs according to its depth from the ground surface (Hayley, 1968). At a depth of 12 feet (3.7m) or less, it is soft and badly fractured. However, the clay shales at depths of 60 feet (18.3m) or more are generally hard and intact (Hayley, 1968).

5.3 Previous Investigations

5.3.1 The West Slope Investigation

The west slope of the Little Smoky Slide was investigated in the late sixties by Hayley (1968). The monitoring program involved ten installed inclinometers (five installed by Hayley and five installed previously) and a number of surface survey monuments to capture the movements, two installed piezometers to monitor the ground water pressures, and five drilled boreholes to obtain representative samples. The surface monuments were installed along line A and line B as shown in Figure 5-3. This figure also shows the locations of the slope indicators installed by Hayley (LS6 through LS10).

Grain size analyses and index tests were carried out on some samples of the drilled boreholes. The results are shown in Table 5-1 and Table 5-2, respectively. The variation of the movement with time at the locations of inclinometers LS6, LS7, LS8, LS9 and LS10 is shown in Figure 5-4. Movement occurred on both a deep horizontal rupture surface and secondary movement planes. Hayley (1968)

noticed from the movement profiles and the shape of the movement versus time curves that the rate of movement was the highest at points near the toe of the slide and decreased upslope. The results of surface surveying confirmed that observation. Hence, the movement of the west slope was considered retrogressive. The area under study lies at an outside meander of the river, and, hence, the erosion at the toe is intense. It was then considered that toe erosion is the main trigger of the retrogressive movement. The only exception to that behaviour was inclinometer LS9, which showed a higher movement rate than that of LS10 although LS9 is more distant from the toe. Hayley (1968) mentioned that inclinometer LS9 is located at an area of intense river erosion.

Triaxial and direct shear tests were carried out to determine the peak and residual strengths, respectively, of the materials forming the west slope. The peak and residual friction angles of the shale were found to be 32^0 and 14^0, respectively. The residual friction angle of one sample of remoulded till was determined from direct shear tests and was equal to 18.5^0. There was no cohesion intercept.

Limit Equilibrium Analyses (LEA) were carried out by Hayley (1968) in order to verify the movement mechanism. The main and secondary failure planes were located based on the inclinometer movement profiles. However, some of the secondary planes locations were determined based on the ground surface profile. Hayley (1968) considered the movement to take place among seven blocks. The downslope block starts moving after being eroded by the river. Next, the upslope block loses its passive support and starts moving. While analyzing an intermediate block, Hayley (1968) assumed that the passive force exerted by the downslope block is vertical. He found that inclined and zero passive forces would give excessively high and low safety factors, respectively. The blocks were analyzed by using the wedge method developed by the U.S. Corps of Engineers (U.S.C.E., 1960).

Thomson and Hayley (1975) analyzed each block individually by using the Morgenstern and Price (1965) method, which does not allow for using more than one failure plane in the same analysis. When an intermediate block was being analyzed, the part of the slip surface extending from the toe of the block to the river bank was assigned a nominal shearing angle of 2^0. The choice of this small shearing resistance angle was found to give factors of safety close to unity. The geometry of the seven blocks as interpreted by Thomson and Hayley (1975) is shown in Figure 5-5. The safety factors of the blocks involved in the slide as determined by using the wedge method (Hayley, 1968) and the Morgenstern and Price method (Thomson and Hayley, 1975) are shown in Table 5-3. Thomson and Hayley (1975) mentioned that some refinements were made regarding the locations of the secondary failure planes over those interpreted by Hayley (1968). These refinements may explain the slight differences between the factors of safety resulting from the two methods.

Based on the concept proposed by Thomson and Hayley (1975), a series of LEA is carried out, as part of this present research, by using the Morgenstern and Price method for the seven blocks forming the retrogressive slide on the west slope. The results are shown in Table 5-4. The values are close to Thomson and Hayley's values. The maximum difference is 11.5%. The blocks that showed the highest safety factors in Thomson and Hayley's analyses (blocks 3, 5 and 6) show as well the highest safety factors in the current analysis. The purpose of this comparison is to validate the use of the Morgenstern and Price method to analyze retrogressive slides.

5.3.2 The South and North Slopes Investigations

The portion of Highway 49 that crosses the Little Smoky valley was at one time Highway 43 and was previously named Highway 34. These changes in numbering as well as institutional changes in record keeping make it difficult to retrieve archived data acquired since the sixties. More than 35 slope indicators have been installed in the Little Smoky Slide. However, most of these records are not available (Skirrow et al., 2005).

Alberta Infrastructure and Transportation (AIT) started an investigation program for the south and the north valley slopes in 2001. This program involved drilling four test holes into the north slope to examine the stratigraphy. Three of these holes were equipped with inclinometer casings, and two were equipped with pneumatic piezometers. In addition, four boreholes were drilled into the south slope. Inclinometer casings were installed in all of them, and pneumatic piezometers were installed in only two boreholes. The locations of the boreholes containing the slope indicators and piezometers are shown in Figure 5-6. Boreholes SI31A, SI32, SI35 and SI96-2 are previously installed slope indicators that have enough movement to be included in this review. Readings were taken semi-annually from the beginning of 2001 and until the end of 2005 when most of the slope indicators had failed.

Figure 5-7 shows a cross-section through the south slope and the cumulative displacement profiles from the inclinometer monitoring. The borehole logging (Proudfoot and Tweedie, 2002) indicated the presence of clay till overlying a clay layer underlain by clay shale in boreholes SI01-6 and SI01-2. The clay layer could be preglacial lake clay. The material properties for this layer, however, were not determined. In borehole SI01-7, another clay layer overlies clay till, suggesting that this clay layer is post-glacial. The clay till directly overlies the clay shale in borehole SI01-9. The line joining the points, where the maximum displacements take place, forms the main failure plane. The main failure plane runs almost at the interface between the clay shale and the overlying deposits. Morgenstern (1987) suggested that "glacial drag forces", which form as a result of the weakness of the top layers of clay shales and their interference with the overlying till, are responsible for the presence of the main slide plane at the

interface. Hence, the residual shear strength in the vicinity of the slide plane would be very low. The implication of this observation is discussed in Section 5.4.5 in more detail. The displacement versus time plots for the four inclinometers installed in the south slope are shown in Figure 5-8.

Figure 5-9, which presents a cross-section through the north slope, shows the stratigraphy, the ground water table and the movement zones detected at different depths as interpreted by Proudfoot and Tweedie (2002). The stratigraphy shows a layer of varved clay between the clay till and clay shale layers. Proudfoot and Tweedie (2002) indicated that slickensides were sometimes observed in the varved clay layer. The layer could then be preglacial lake clay. The soil parameters were determined based on correlations with the Atterberg limits and experience. Proudfoot and Tweedie (2002) performed a back analysis for the slide as one block. The residual friction angles for till and clay shale were assigned values of 12.5^0 and 9.5^0, respectively. These values are lower than those determined by Hayley (1968). Proudfoot and Tweedie (2002) found that an operational strength of the varved clay of 9.5^0 corresponded to a factor of safety of unity. Their analysis, however, ignored the presence of the secondary failure planes that were detected by the inclinometers. The displacement versus time plots for the inclinometers installed in the north slope are shown in Figure 5-10.

5.4 The 2007 – 2008 Field Investigation Program Results

5.4.1 Overview

The investigation of the south and north slopes of the Little Smoky valley from 2001 until the end of 2005 was successful in defining the locations of the failure planes, the geological cross-sections that show the materials forming the slide, a general sense of the groundwater regime and the global annual movement rates. However, the frequency of monitoring was too low to allow for the examination of the variation of the movement rates with pore pressures and, hence, with the hydrological boundary conditions changes like rainfall and river level fluctuations. Therefore, it was necessary to increase the frequency of monitoring the displacements and pore pressures in order to get a more detailed picture of the likely triggers and their impact on movement. As all the inclinometer casings that were installed in 2001 had been sheared off by 2005, a new program was started in early 2007 and involved drilling new boreholes and installing new inclinometer casings and vibrating wire piezometers.

Three new boreholes were drilled at three locations in the west (TH07-W), south (TH07-S) and north (TH07-N) slopes in 2007. A track-mounted auger drill rig was used to obtain samples from the overlying till in January 2007, and a track-mounted wet rotary drill rig was used to obtain cores from the underlying clay shale in March 2007 (Bala and Proudfoot, 2007). A plan showing the locations of

all the old and new boreholes is shown in Figure 5-11. Core logging and visual description of the materials encountered in the three boreholes are carried out at the University of Alberta with the kind help of Professor John Shaw, and, hence, the cross-sections through the three slopes are updated. The findings are presented in Section 5.4.2.

Each of the three boreholes is equipped with an inclinometer casing and one vibrating wire piezometer, except for the borehole at the north slope, which is equipped with two vibrating wire piezometers. In addition, two additional holes were drilled at the same location in each of the west and south slopes to install two additional vibrating wire piezometers. One more hole was drilled next to the north slope borehole to install a third vibrating wire piezometer. A total of nine vibrating wire piezometers are equally divided among the west, south and north boreholes (Bala and Proudfoot, 2007). The borehole and instrumentation information are summarized in Table 5-5.

The 2001-2005 investigation indicated that the movement accelerates during the spring and summer and slows down during the fall and winter months. Hence, the frequency of readings was chosen based on the annual movement cycle. A few readings were taken during the rest of 2007 in April, October and November. From March 2008 until the end of June 2008, movement and pore pressure measurements were taken every two weeks. During July and August 2008, readings were taken every three weeks. The frequency of readings was reduced to one month from the beginning of September 2008 until November 20th 2008 when the last set of readings was taken. With the appreciated help of some colleagues, the author visited the site on October 4th 2007, October 18th, November 22nd 2007, January 24th 2008, March 28th, April 10th, April 25th, May 8th, May 25th, June 4th, June 19th, July 3rd, July 23rd, August 14th, September 4th, October 8th and November 20th 2008 in order to monitor the displacements and piezometric heads at the locations of the three boreholes.

Subsections 5.4.2 through 5.4.6 present the results of the 2007/08 field investigation program of the west, south and north slopes. The geological cross-sections are updated, and the influencing factors on the movement are highlighted. The contribution of each single causal factor is separated on a quantitative basis. Hence, important conclusions regarding the relevance of different mitigation options are drawn.

5.4.2 Stratigraphy

The samples and the cores obtained from the three drilled boreholes in 2007 were brought in wooden boxes to the University of Alberta by personnel from the University of Alberta and Thurber Engineering Ltd. All the obtained cores were visually inspected, and the resulting logs of boreholes TH07-W, TH07-S and TH07-N are shown in Figure 5-12 through Figure 5-14. The logs include the

locations of the movement zones, the depths of the piezometers' tips and the maximum recorded fluctuations in the piezometric levels over the whole monitoring period. The analysis of the movement and pore pressure records is presented in the following subsections.

An updated cross-section through line B of the west slope is shown in Figure 5-15. The minimum piezometric level measured during the recent investigation is only one metre higher than the level inferred from Hayley (1968) analysis. The recent logging revealed a smaller thickness of till than that in the previous interpretation. The depth of the main failure plane resulting from the recent monitoring matches the old interpretation. However, a secondary movement zone is detected in borehole TH07-W. This secondary movement zone is expected to shift the location of the secondary failure plane of block two of the west slope. The location of the secondary failure plane of block 2 was determined by Hayley (1968) based on the ground surface profile.

A similar updated cross-section through the south slope is shown in Figure 5-16. The lowest piezometric level measured in borehole TH07-S is lower by less than 0.5m than the phreatic surface elevation determined during the 2001-2005 investigation. The recent borehole logging suggests that the interface between the clay layer (thought to be deposited in a preglacial lake) and the underlying clay shale is higher by about four metres than the previous interpretation. The recent movement monitoring also suggests that the depth of the main failure plane is also about four metres lower than that in the previous interpretation. No secondary movement zones are detected in the most recent monitoring or during the 2001-2005 monitoring. The boundaries between the clay till, clay and clay shale are located based on both the previous and the most recent borehole logs. The suggested boundaries indicate the presence of a thin clay layer (less than 6 metres thick) above the clay till in the region between SI01-6 and SI01-2. This clay layer is thought to be post-glacial lacustrine clay. The clay layer that lies between the clay till and the clay shale is mostly preglacial lake clay. The main failure plane runs almost at the interface either between the clay till and the clay or between the clay and the clay shale for the region between SI01-6 and SI01-2. This situation is also present at borehole SI01-9. However, at the location of TH07-S, the main failure plane is about four meters below that interface and lies in the clay shale layer. The preglacial clay layer is hatched in the cross-section shown in Figure 5-16.

The updated cross-section through the north slope is shown in Figure 5-17. The phreatic surface determined from previous investigations coincides with the piezometric elevation measured at a depth of 66.1m. The main movement zone detected in borehole TH07-N is an exact extension of the previous investigation's failure plane. The varved clay layer (thought to be preglacial) is also present in borehole TH07-N. However, this layer was not present at the location of borehole SI01-3. This layer is hatched in the updated cross-section.

The investigations of the previous and the current interpretations of stratigraphy lead to an important conclusion. The locations of the main rupture surfaces of the Little Smoky Slides are controlled by one of three stratigraphic settings:

1. The preglacial lake clays as in the north slide,
2. The interface between the overlying till or preglacial clays and bedrock as in the south slide, or
3. The upper layer of the clay shale, which is usually weakened by weathering as in the west slide.

This conclusion is in accordance with the observations of Scott (1989) and Cruden et al. (1993).

5.4.3 Material Physical Properties

The visual inspection of the north slope borehole (TH07-N) confirms the presence of preglacial lake clays above the preglacial sands and gravels that overlie bedrock. The Atterberg limits were determined at different depths in borehole TH07-N and for samples thought to be clay shale in borehole TH07-S. The results are shown in Figure 5-18 and Figure 5-19, respectively. The values of the Atterberg limits of the materials encountered at the Little Smoky valley are compared to the values reported by Hayley (1968) for the clay shales of the west slope and the reported values in the literature of the Atterberg limits of some Upper Cretaceous clay shales and preglacial lake clays. Table 5-6 shows typical values of the Atterberg limits of Upper Cretaceous clay shales taken from Morgenstern and Eigenbrod (1974). The Atterberg limits of the preglacial lake clays at the Eureka River landslide, the Attachie landslide, the Dunvegan creek landslide, the Montagneuse River landslide and the Saddle River landslide were summarized by Miller and Cruden (2002) and are listed in Table 5-7. All the previous and the current values of the Atterberg limits of clay shales and preglacial lake clays are plotted on the two plasticity charts shown in Figure 5-20 and Figure 5-21, respectively. Some of the Atterberg limits values determined for the clay shale as part of the current investigation are very close to those determined by Hayley (1968) and to some values from the literature. Figure 5-21 also indicates that the Atterberg limits values of the preglacial lake clays of the north Little Smoky Slide are close to those of the Attachie and the Eureka River landslides. Miller and Cruden (2002) evaluated the residual friction angle of the preglacial clays of the Eureka River landslide according to Skempton (1985) and based on a clay fraction of 40% and PI of 21%. The value ranged from 8.2^0 to 13.1^0. The plasticity indices of the preglacial lake clay samples of the north slope at depths of 53.9, 54.9 and 56.1m are 21.6, 11.5 and 14.1%, respectively. The corresponding clay fractions are 43, 29 and 30%, respectively. Therefore, the residual friction angle of the preglacial clays of the north slope is expected to lie in the same range of 8.2^0 to 13.1^0. This range is close to the value reported by Proudfoot and Tweedie (2002).

5.4.4 The Triggers of Movement of the West Slope

The field monitoring program at the location of borehole TH07-W in the west slope involved measuring the variation with time of each of the horizontal displacements and pore pressures. The depths of the inclinometer casing and the piezometers' tips are mentioned in Table 5-5. The initial inclinometer readings were taken on January 24th 2008, and the last set of readings was taken on November 20th 2008.

The cumulative displacement profiles at different monitoring times are shown in Figure 5-22. A secondary movement zone exists at a depth of approximately 14.6m from the ground surface. The main movement zone lies at the depth range of 36.0 – 37.8m. The horizontal displacement of the main movement zone is plotted against time in Figure 5-23. The displacement rate is calculated between each two consecutive measurements and is displayed in units of mm/year.

Figure 5-23 reveals that the movement continued at a rate of 16.1mm/yr from the time of the initial reading until approximately the end of the winter season (March 28th 2008). The rate increased after that during the period from March 28th until July 3rd, which is just after the end of spring. The rate reached values as high as 59mm/yr between April 25th and May 8th. The velocity decreased again after July 3rd and until the end of the monitoring period to values close to the rate recorded between January 24th and March 28th 2008.

The movement apparently accelerates in spring and slows down to a minimum rate during the summer, fall and winter. The spring time usually exhibits the largest variations in pore pressures due to river level fluctuations and/or rainfall. Pore pressures at three different depths were recorded at different times in order to investigate the effect of pore pressure changes on the movement rate. The pore pressure variation with time at three different depths is shown in Figure 5-24 through Figure 5-26. One set of pore pressure measurements was taken by the project consultant at that time (Thurber Engineering Ltd.) in October 2007, and a few readings were taken by another consultant (Karl Engineering Ltd.). Figure 5-24 through Figure 5-26 reveal that the maximum range of the piezometric levels changes is 0.25m. This small range of pore pressure changes may imply a small impact of pore pressure changes on the movement rate. The piezometric levels decreased since July 23rd 2008 and were either constant or slightly decreasing during the period from October 4th 2007 to March 28th 2008, except at the depth of 33.3m where the piezometric level increased during that period. Hence, the effective stress was constant or slightly increasing during these periods, which coincided with the periods when the movement continued at a minimum rate. Therefore, the movement that continued at a minimum rate during the periods of constant effective stresses would be a creep deformation. Hence, creep is taken to be equal to $\frac{16.1+14.3+15.1+16.3+16.1+15.8}{6} = 15.6\,\text{mm/yr}$. The total movement can then be resolved into creep that becomes equal to the total

movement during the periods of constant or slightly increasing effective stress, and a seasonal movement that results generally from pore pressure changes, toe erosion and/or changes in the forces acting on the slope like lateral water pressures in tension cracks and water ponding. The available piezometric and hydrological data of the Little Smoky Slides allow only for correlating the seasonal movements to pore pressure changes and toe erosion. It is important to note that other triggers of the seasonal movement exist as well. The analysis of the displacement records of the west slide at the location of borehole TH07-W suggests that the seasonal movement is superimposed on creep during the spring months. The variation of the creep and seasonal movements are plotted in Figure 5-27.

The seasonal movement is plotted together with the piezometric depth below the ground surface against the time in order to investigate the impact of the pore pressure changes on the movement rate. The plots of the three piezometers are shown in Figure 5-28 through Figure 5-30. The behaviour at the piezometric depths of 20.2m and 45.2m reveals that the piezometric level started rising on April 10th 2008 and continued rising until June 4th 2008. This rise was accompanied by a noticeable increase in the seasonal movement. The drop in the piezometric depth on June 4th slightly decreased the seasonal movement rate. After June 19th 2008, the piezometric head elevations at the depths of 20.2m and 45.2m decreased until the end of the monitoring period (November 20th 2008). The seasonal movement remained constant after that date.

The pore pressure behaviour at the depth of 33.3m is quite different from that of the other two piezometers. Figure 5-29 shows that the piezometric head continuously decreased from March 28th to June 5th 2008 except for a slight rise on May 25th. However, the seasonal displacement continued increasing during that period. This different trend may be attributable to the proximity of this piezometer to the main movement zone, and, hence, the behaviour may be affected by the negative pore pressures that develop during shearing. This behaviour can also be attributable to the possible movement triggering by a river level drawdown mechanism. In order to investigate this possibility, the river level is plotted together with the seasonal movement against time as shown in Figure 5-31. This figure shows that the rise in the river level coincides with the increase in the seasonal movement rate. This observation excludes the possibility of the movement being triggered by a river level drawdown mechanism. River level drawdown was found to control the movement rates along the Thompson River valley in British Columbia (Eshraghian et al., 2005) where the preglacial lake clay layer hosting the rupture surface is underlain by preglacial sands that act as an aquifer. No preglacial sands are encountered in the west Little Smoky Slide. Moreover, the piezometric heads reported by Eshraghian et al. (2005) fluctuated by one to two metres. The fluctuations in the west Little Smoky Slide are less than 0.25m, as mentioned above.

The records of rainfall and the river level during 2008 were acquired from Environment Canada and plotted against time together with the pore pressure records. The plots are shown in Figure 5-32 through Figure 5-34. The peaks in the piezometric levels generally follow the peaks in the river level and daily rainfall, with a lagging time ranging from zero to up to 20 days. This time lag can be attributed partly to the relatively low conductivity of the west slope materials and partly to the time interval between every two consecutive readings, which was not less than two weeks. This behaviour is less pronounced at depth 33.3m. Therefore, the pore pressure changes are driven by both the river level fluctuations and rainfall.

It is concluded from the above results that creep accounts for about 15.6mm/yr on average of the total movement at borehole TH07-W. The total movement from January 24th until November 20th 2008 equals 18.7mm. The movement is expected to continue at a rate of approximately 15.6mm/yr from November 20th 2008 until January 24th 2009. Hence, the total annual movement at the location of borehole TH07-W in the west slope is approximately equal to 21.5mm. Therefore, creep accounts for about 72.6% of the total movement at borehole TH07-W. However, borehole TH07-W lies at about 196.5m from the slope toe. Since the movements at the west slope are retrogressive, the maximum total movement is expected to occur at locations closer to the toe. Hence, the contribution of creep to the total movement would be smaller at downslope locations.

In order to highlight the effect of the distance from the slope toe on the total movement rate, the total movement rate is plotted against the distance up the slope for both the recently installed slope indicator and the slope indicators installed previously by Hayley (1968). This plot is shown in Figure 5-35. The maximum total movement rate of the downslope block is 40.2mm/yr (at LS10), and, hence, the contribution of creep would be equal to 15.6 / 40.2, i.e., 38.8%. The rest of the movement would be triggered by either toe erosion, pore pressure rise, or other seasonal forces acting on the slide. The separation of these effects at the west slope is not possible at this stage of the analysis.

5.4.5 The Triggers of Movement of the South Slope

The field program of the south slope had the same objectives as the west slope. The variations with time of the horizontal displacements and pore pressures were recorded at the location of borehole TH07-S. The depths of the inclinometer casing and the piezometers' tips are presented in Table 5-5. The initial inclinometer readings were taken on April 25th 2007, and the last set of readings was taken on November 20th 2008.

The main movement zone width is approximately 1.8m, extending from a depth of 35.4m to 37.2m. The cumulative displacement profile is shown in Figure 5-36, the displacement versus the time plot is shown in Figure 5-37, and the

piezometric depths variations with time at the depths of 20.5m, 35.7m and 44.6m are plotted in Figure 5-38 through Figure 5-40. The movement continued from October 4th 2007 to January 24th 2008 at an average rate of 13.9 mm/yr. The movement rate was 16.6mm/yr during the period from October 8th to November 20th 2008. Hence, the minimum movement rate of the south slope is taken to be equal to $\frac{11.7+14.3+15.8+16.6}{4} = 14.6$ mm/yr. If it is assumed that the movement continues during the periods of nearly constant effective stress at an average rate of 14.6mm/yr, then the total movement can also be resolved into creep and seasonal movements in a similar way to the analysis of the west slope (see Figure 5-41).

Table 5-8 shows a simple comparison between the values of the total, creep and seasonal movements of the west and south slopes. The amount of the seasonal movement during the period from January 24th to November 20th 2008 is 5.1mm and 5.8mm in boreholes TH07-S and TH07-W, respectively, although borehole TH07-S lies at a closer location to the toe than borehole TH07-W (186.6m for TH07-S and 196.5m for TH07-W). This finding implies that erosion at the toe of the west slope is higher than that at the south slope. Hayley (1968) mentioned that the west slope lies at an outside meander of the Little Smoky River, and, hence, the erosion effect is pronounced. In addition, the west slope is located downstream from the Little Smoky Bridge, and intense toe erosion is expected. The values of the creep movements are 12.0mm and 12.9mm at TH07-S and TH07-W, respectively, over the monitoring period. This slight difference reflects the minor heterogeneities among the clay shales forming the main movement zones at the locations of boreholes TH07-S and TH07-W.

The seasonal movement is plotted together with the piezometric depths against time for the three piezometers installed at the location of borehole TH07-S in order to investigate the effect of pore pressure changes on the seasonal displacement. The plots are shown in Figure 5-42 through Figure 5-44. These figures indicate that the seasonal movement is driven by pore pressure changes, sometimes in a timely manner and, at other times, after a lag of approximately two weeks. This time lag can be attributed to the viscous nature of the slide materials, which delays the deformation associated with the pore pressure changes (Picarelli and Russo, 2004).

Only one exception to this trend occurred at the depth of 44.6m from October 18th to November 22nd 2007 when the piezometric level rose while the seasonal movement stayed constant. The river level is plotted together with the seasonal movement against time as shown in Figure 5-45. This figure shows that the periods of the seasonal movement acceleration coincide with the periods of rise in the river level. Hence, the possibility of the movement being triggered by a river level drawdown mechanism is also excluded.

Figure 5-46 through Figure 5-48 show the variation with time of each of the river level, daily rainfall and water level depths recorded in the three piezometers installed in borehole TH07-S. The three figures indicate that the pore pressures respond to both the river level and daily rainfall changes in a timely manner. However, the piezometric rise, which generally occurred since July 3rd 2008, was accompanied by a decrease in the river level down to a minimum value of 2.7m on August 23rd. The river level rose up to 3.4m on August 24th and then decreased again. On the other hand, small rises in the daily rainfall values up to 8mm/day occurred between July 3rd and the end of September, and a peak of 14.6mm/day occurred afterwards. Therefore, the piezometric head rise that occurred since July 3rd is attributed to the rainfall rather than river level fluctuations. At borehole TH07-W, however, the piezometric head generally decreased since July 3rd, as mentioned above. This finding indicates that the top till layer of the west slope is less permeable than the top layer of the south slope, and, hence, the effect of small values of daily rainfall on the south slope movement is more pronounced.

The analysis of the results of monitoring the slope indicator and the vibrating wire piezometers installed in borehole TH07-S indicates that the total movement can also be resolved into creep and seasonal movements. The seasonal movement is correlated to both toe erosion and pore pressure changes, which respond to the river level and/or daily rainfall changes. Creep can be evaluated by observing the movement rates during the periods of zero or very slight changes in the effective stress.

In order to verify the deduced values of the creep rates, a triaxial drained creep test was carried out on a core sample of the clay shale encountered in borehole TH07-S. Based on a total unit weight of 20kN/m^3 and on the recorded piezometric heads, the effective confining stress equals 560kPa. In order to investigate the possibility of strain acceleration, the applied deviatoric stress level equals 70%. The deviatoric stress value is calculated based on a residual friction angle of 14^0. The test duration was 70 days (more than 100,000 minutes). The variation of the axial strain rates with time on a logarithmic plot is shown in Figure 5-49. While the slope of the linear regression line is well below the range proposed by Singh and Mitchell (1968) for most soil types, the minimum attained strain rate equals 1.4 X 10^{-6} %/min. The field creep rate of the south slope equals 14.6mm/yr based on the field monitoring. This value corresponds to 1.5 X 10^{-6} %/min when divided by the width of the movement zone at borehole TH07-S (1.8m). This match does not necessarily indicate that laboratory creep rates can generally replicate field values, because the time since the initiation of creep is significantly different in both cases, as is the case in the Little Chief Slide.

Figure 5-8 and Figure 5-37 show that the effect of the distance up the slope on the total movement rate of the south slope is not as clear as that in the west slope. The average total movement rates recorded at SI01-6, SI01-7, SI01-2, SI01-9 and TH07-S are plotted against the distance from the south slope toe and are shown in Figure 5-50. No clear correlation similar to that found in the west slope exists

between the movement rate and the distance from the slope toe. In addition, the cumulative displacement profiles at inclinometers SI01-6, SI01-7, SI01-2, SI01-9 and TH07-S shown in Figure 5-7 and Figure 5-36 do not indicate the presence of any secondary movement zones in the south slope, whereas such zones are found in the west slope.

The above two observations imply that the slide at the south slope moves as one block. Therefore, a limit equilibrium analysis is performed for the whole south slide. The rupture surface follows the main movement zones detected by the previous and the current investigations, as shown in Figure 5-16. The highest piezometric levels recorded in boreholes SI01-6, SI01-2 and TH07-S are connected together. The river level is assumed to be at its highest elevation, i.e., about 2 metres above the minimum level. A back analysis is carried out according to the Morgenstern and Price (1965) method, and it is found that a friction angle of 8^0 would give a safety factor of 1.09. As mentioned in the previous section, the failure plane of the south slope runs almost at the interface between the clay shale and the overlying clays, and, hence, the glacial drag forces described by Morgenstern (1987) work to weaken this zone. The operational friction angle is, therefore, reasonable.

5.4.6 The Triggers of Movement of the North Slope

The access to borehole TH07-N was very difficult during the late fall of 2007 and the winter of 2008 due to the long distance between the highway and the borehole location (about 350m) and the relatively steep slope of the highway embankment. The thick snow cover during the winter made the process of mobilizing in and out almost impossible. Hence, the initial set of the pore pressure and inclinometer readings were taken on March 28th and April 10th 2008, respectively. The monitoring continued according to the same schedule outlined above. However, it was found when taking the September 4th set of readings that the inclinometer casing had sheared off. Hence, the available records of the movement extend from April 10th to August 14th. The piezometers installed at the depths of 35.6m and 50.6m functioned properly until the end of the monitoring program (November 20th 2008). However, the piezometer installed at the depth of 66.1m failed between June 19th and July 3rd 2008, probably because of the bending of the inclinometer casing as it approached failure.

The cumulative displacement profiles at different monitoring times are shown in Figure 5-51. The movement zone width is very small and lies between the depths of 56.1 and 56.7m. The main movement zone displacement variation with time is shown in Figure 5-52, with the movement rates expressed in units of mm/yr. Since no readings were taken during the late fall or winter months, all the recorded movement rates are higher than the minimum rates recorded at the west and south slopes (15.6 and 14.6mm/yr, respectively), which are attributable to creep deformation. The effect of the seasonal changes is the highest during the

monitoring period of this slope indicator. The shown movement record in Figure 5-52 is considered the superposition of the creep and seasonal movements without a clear distinction of the contribution of each of them.

The variations of the piezometric levels and the total movement with time for the three piezometers installed at the depths of 35.6m, 50.6m and 66.1m are shown in Figure 5-53 through Figure 5-55. Generally, the movement rate can be considered to correlate with the pore pressure changes with a two-weeks-time lag. This behaviour is confirmed at the upper piezometer and partially at the middle one, which sometimes shows a timely response to pore pressure changes. The behaviour is not clear at the lowest piezometer due to the short pore pressure monitoring period. The lag is also attributable to the viscous properties of the slide materials.

The possibility of the movement being triggered by a river level drawdown mechanism is investigated by plotting the total movement together with the river level against time, as shown in Figure 5-56. The movement acceleration clearly coincides with the river level drawdown period, except from May 8th to May 25th when the movement decelerated while the river level was falling. This finding suggests that the movement of the north slope is partially triggered by a river level drawdown mechanism, which was described by Eshraghian et al. (2005) as a controlling mechanism of the movement reactivation of some earth slides along the Thompson River valley in British Columbia. The stratigraphic profile of the north Little Smoky Slide is nearly similar to that of the Thompson River valley: preglacial gravels are overlain by a preglacial lake clay layer that hosts the rupture surface. Thus, the north slope crest may act as a recharge zone causing artesian pressures to develop in the gravel layer. When the river level rises, water seeps into the slide, but the pore pressure in the preglacial lake clay layer does not respond in a timely manner. Hence, the high river level condition tends to stabilize the slope. If the river level stays at the high elevation for a period of time, the pore pressures in the preglacial lake clay become equalized. When the river level drops afterwards, the slope loses the stabilizing pressures exerted by the water in the river, and the movement is reactivated. However, no pore pressure data for the preglacial lake clay and gravel layers of the north slope are available to verify this mechanism.

It should be noted however that the maximum recorded piezometric heads' ranges at the depths of 35.6, 50.6 and 66.1m are 0.11, 0.25 and 0.09m, respectively. These figures are considerably lower than the piezometric head changes at the Thompson River valley. Eshraghian et al. (2005) reported head changes ranging between 1 and 2 metres. Hence, the river level drawdown mechanism is not expected to have a major impact on the movement reactivation of the north Little Smoky Slide.

The recorded piezometric heads are also relatively smaller than the ranges recorded in boreholes TH07-W and TH07-S although the distance from borehole

TH07-N to the north slope toe, 177.5m, is slightly smaller than the distances between boreholes TH07-W and TH07-S and the toe. However, the movement rates recorded at TH07-N are noticeably higher than those recorded at TH07-W and TH07-S. Therefore, it is suggested that the recorded movements are the superposition of:

1. Creep that could be assumed to be an average value of the creep rate observed at the west and south slopes, i.e., 15.1mm/yr. Performing a creep test in the laboratory was not possible.
2. A seasonal movement driven by either pore pressure changes or a river level drawdown mechanism or both. This component is expected to be slightly smaller than the seasonal movements at boreholes TH07-W and TH07-S due to the relatively smaller variations of the piezometric levels in borehole TH07-N than in the other two boreholes.
3. A seasonal movement driven by toe erosion.

Seasonal movements may result as well from other forces acting on the slide like lateral water pressures in tension cracks and surface water ponding. Toe erosion at the north slope is expected to be higher than that at the other two slopes due to the presence of a confined flow condition resulting from the presence of two islands at the slope toe (Figure 5-2). The history of the formation of these islands is studied in order to learn more about the nature of the slope movement. The oldest map available for the site dates back to 1915 (Provincial Archives of Alberta – Map printed at the Office of the Surveyor General, June 1922). The width of the river at the location of the islands at that time was uniform, and no islands were indicated at that location. The width of the channel was around 148 metres. The rest of the available maps date back to only 1945 (Provincial Archives of Alberta), and the islands appear clearly on both the maps and the air photos available since 1945 (Air Photo Distribution Office, Edmonton). The presence of these two islands could be attributed to the occurrence of a big landslide in the past that might have dammed the river. Afterwards, water incised through the formed landslide dam over the years until now. The very small scale of the 1915 maps may render the reliability of this explanation questionable. However, the occurrence of a landslide dam in the past implies a rotational movement at least at the toe. The occurrence of a rotational movement at the toe was supported in a previous investigation by Thurber Engineering Ltd., which noticed some tilted trees at the toe of the north slope (Proudfoot and Tweedie, 2002). This explanation is further supported by the updated cross-section B-B shown in Figure 5-17, which indicates that a big segment of the main rupture surface lies within the preglacial lake clays. The majority of the Type 6 landslides that occurred in the Peace River Low-lands of western Canada have their rupture surfaces in preglacial lake clays (Cruden et al., 1993; Cruden et al., 1997; Hardy et al., 1962; Evans et al., 1996; and Miller and Cruden, 2002). Since the rupture surface of the Little Smoky north slope is hosted by preglacial lake clays, the likelihood of the occurrence of a landslide dam in the past with subsequent water incision through the formed dam is high.

A reconnaissance of the north Little Smoky Slide toe in August 2007 with Professor David Cruden from the University of Alberta included the viewing of the north bank from the west slope bank, looking north-east, as shown in Figure 5-57. This figure also shows the effect of erosion at the toe of the west slope. Figure 5-58 shows a closer view of the north slope toe. The tilting of the trees is very obvious. Standing at the toe of the north slope, Figure 5-59 and Figure 5-60 show exposures of the north slope toe. The exposure is composed mainly of unstratified till and sub-till clays. The terrace is overlain by alluvial sands and gravels that are deposited by the flowing water in the Little Smoky River. Chunks of the sub-till clays were cut, and closer views of these samples are shown in Figure 5-61 and Figure 5-62.

The occurrence of a landslide dam at the north slope necessitates that the main rupture surface emerges on the outside boundary of the island present at the slope toe. Hence, the main rupture surface detected in borehole TH07-N as well as from previous investigations was extrapolated downslope of borehole TH07-N and emerged on the outside boundary of the formed island. The updated cross-section B-B is re-constructed after adding the proposed rupture surface and is shown in Figure 5-63. The movement of the north slope is obviously retrogressive, as evidenced by the detection of secondary movement planes in boreholes SI01-3, SI96-3, SI35, SI34 and SI96-2. The observed cracks in the highway pavement may form the scarp of an additional secondary plane. This plane is shown by a dashed line in Figure 5-63. Another observed scarp upslope is believed to be the main scarp of the slide. This scarp is also shown by another dashed line in Figure 5-63.

In order to verify the location of the proposed rupture surface, a limit equilibrium analysis is carried out, as part of this present research, for the downslope block ABCD (see Figure 5-63). The residual friction angle of the overlying till is assumed to be 18^0 (Hayley, 1968; and Thomson and Hayley, 1975), and the residual friction angle in the vicinity of the rupture surface is assumed to be 9.5^0 according to Proudfoot and Tweedie (2002) and the correlations with the plasticity index and clay fraction. The method used in the analysis is the Morgenstern and Price method (1965). The safety factor is 1.08. Another location for the rupture surface is proposed by considering that the downslope block is bounded by points ABB'D. The safety factor of this block is 1.26. Hence, the assumption that the main rupture surface can be extrapolated downslope of borehole TH07-N along the segment B'CD is assumed valid.

The upslope block EFB is analysed in a similar way to that proposed by Thomson and Hayley (1975); i.e., by assuming that the friction angle along the segment BCD equals 2^0. The safety factor equals 0.49. Similarly, the safety factor of block GHF equals 0.40. The fourth block is assumed once to be bounded by the cracks in the highway (IJH) and another time by the observed scarp upslope (KJH). The safety factors for the two cases are 0.28 and 0.32, respectively. The very low factors of safety obtained for the second, third and fourth blocks may suggest that

a catastrophic failure may take place once the downslope block moves a sufficient displacement so that the upslope bocks completely lose their passive support. The segments of the secondary failure planes located inside the preglacial lake clay layer are assumed to have a friction angle of 9.5^0 in the analysis. This value is very low due to the anisotropic behaviour of this kind of material. The strength across the bedding is significantly higher than the strength along the bedding, which may offer another explanation for the very low safety factors of the upslope blocks.

As mentioned above, pore pressure changes account for a part of the seasonal movement. The variations of water levels in the three piezometers installed in borehole TH07-N, together with the river level and rainfall, are plotted against time in Figure 5-64 through Figure 5-66. The pore pressure changes show dependence on both the river level fluctuations and daily rainfall changes, with about a two-week time lag.

5.4.7 Rate Effects on Shear Strength

The effect of the loading rate on the residual shear strength of clays has been studied extensively in the literature, as detailed in Chapter 2. Leroueil et al. (1985) and Tavenas and Leroueil (1977) found that rate effects are negligible for strain rates slower than 1.7 X 10^{-8} sec^{-1} (or 1.02 X 10^{-6} min^{-1}). The highest displacement rate encountered in the recent investigation of the Little Smoky valley slopes is 138.8mm/yr at borehole TH07-N in the north slope. Given that the movement zone width equals 0.6m, the corresponding shear strain rate would be equal to $\frac{138.8}{600} * \frac{1}{365*24*60} = 4.4 \text{ X } 10^{-7}$ min^{-1}. The maximum field strain rate is thus lower than the loading rate range that would affect the residual shear strength.

The maximum field shear strain rate at borehole TH07-N corresponds to a laboratory displacement rate of 4.4 X 10^{-7} X 25.4 = 1.1 X 10^{-5} mm/min in the direct shear apparatus based on testing a 25.4mm thick sample. Skempton (1985) pointed out that the variations in the residual strength within the usual range of slow laboratory tests (e.g., 0.002-0.01 mm/min) are negligible. This conclusion by Skempton (1985) provides more evidence of the insignificant effect of the loading rates on the residual shear strength of the Little Smoky Slide materials.

As part of this present research, direct shear tests were carried out on clay shale samples taken from the main movement zone of the south slope in order to determine its residual shear strength and to investigate the effect of the displacement rate on the residual strength. The applied normal pressures are 200, 400, 600 and 800kPa. The slowest possible displacement rate of the direct shear apparatus is 10^{-4} in/min (2.54 X 10^{-3} mm/min), and, hence, this rate is used. The rate effects are investigated at a normal pressure of 700kPa by applying

displacement rates of 10^{-3} and 10^{-2} in/min (2.54 X 10^{-2} and 2.54 X 10^{-1} mm/min). The shear stress – normal stress plot is shown in Figure 5-67. The shear strength variation with normal stress under a displacement rate of 2.54 X 10^{-3} mm/min fits well to Mohr Coulomb failure envelope. The residual friction angle is equal to 15^0, which is only one degree higher than the value reported by Hayley (1968) and Thomson and Hayley (1975) for the clay shale of the west slope. However, the residual strength is unchanged when the rate is increased to 2.54 X 10^{-2} mm/min and is decreased by 22% when the applied displacement rate is 2.54 X 10^{-1} mm/min.

The results indicate that the actual movement rates in the Little Smoky Slide are below the range within which the residual strength is affected by strain rates. This conclusion matches the previous investigations. Augustesen et al. (2004) attributed the relatively higher strength at very slow rates (slower than $1X10^{-7}$ s^{-1}) to aging and structuration effects, which appear to account for any additional increase in stiffness.

5.5 Discussion

The investigation and analysis of the movement and pore pressure records measured at the locations of boreholes TH07-W, TH07-S and TH07-N lead to the conclusion that the total movement can be resolved into three main components:

1. Creep that contributes to about 15.6mm/yr of the west slope movement and 14.6mm/yr of the south slope movement. The contribution of creep to the total movement of the north slope is not clear because the monitoring period did not include times at which the effective stress is nearly constant. Therefore, an average value of the west and south slopes creep rates (15.1mm/yr) is assumed in the rest of this discussion.
2. A seasonal movement driven by pore pressure changes. Pore pressures generally respond to both the river level and daily rainfall changes, with a time lag ranging from zero to two weeks. This component exists in the three slopes with the same value as long as the distance of the point of interest from the slope toe is equal. This component could be due to a river level drawdown mechanism at the north slope.
3. A seasonal movement driven by toe erosion. This component exists in the three slopes with varying magnitudes. Toe erosion is higher in the west slope than in the south slope because the west slope lies downstream from the bridge. The confined flow condition at the toe of the north slope leads to a higher contribution of the toe erosion component than that at the other two slopes.

It is important to mention that seasonal movements may also result from changes in the forces acting on the slope like lateral water pressures in the tension cracks and water ponding. However, the available piezometric and hydrological data

enabled only correlating the seasonal movements to pore pressure changes and toe erosion.

It is attempted in this discussion to estimate the relative contribution of each component to the total movement based on the obtained results in addition to some reasonable judgements. The period from April 10th to August 14th 2008 is chosen for study since no records of movement are available for the north slope outside this period. Table 5-9 summarizes the values of the creep, seasonal and total movements recorded during this time period in boreholes TH07-W, TH07-S and TH07-N. The summary indicates that the seasonal movement of the west slope is more than three times that of the south slope although borehole TH07-S is 10 metres closer to the toe than TH07-W. This difference is attributed to the higher erosion at the toe of the west slope compared to that at the south slope since the west slope is located downstream from the bridge. Since the south slope was found to slide as a single block, it is considered that the net seasonal movement recorded at borehole TH07-S (1.5mm) is due only to the pore pressure changes that occur in response to the river level and/or daily rainfall fluctuations; i.e., the toe erosion effect is ignored at the south slope. By ignoring the distance effect and assuming that the pore pressure changes effect is the same at the two borehole locations, one can conclude that the difference in the seasonal movement between boreholes TH07-W and TH07-S, i.e., 5.2-1.5 = 3.7mm, would represent the amount of the seasonal movement occurring due to erosion at the toe of the west slope.

On the other hand, the seasonal movement of the north slope recorded at borehole TH07-N is considerably higher than that at the west slope. Although borehole TH07-N is closer to the toe than borehole TH07-W, this small distance difference cannot yield more than three times the seasonal displacement value. The high contribution of the seasonal movement of the north slope is attributed primarily to the confined flow condition encountered at the toe of the north slope due to the presence of the two islands. The contribution of the pore pressure changes to the total movement of the north slope is expected to be the same as that at the south slope, i.e., 1.5mm, if the distance from the toe effect is ignored. Hence, the seasonal movement occurring at TH07-N due to toe erosion would be equal to 16.5-1.5 = 15.0mm.

It is important to express the above deduced values in terms of annual rates. The studied period lasted for 126 days. Creep is known to persist for the whole year. Therefore, the creep rates of the west, south and north slopes are 15.6, 14.6 and 15.1mm/yr, respectively, as mentioned above. On the other hand, the seasonal movement does not persist for the whole year, but occurs only during the months of higher than minimum river level, rainfall and flow rate. These months are generally the spring and summer months. The distribution with time of the seasonal movement recorded at the location of boreholes TH07-W and TH07-S suggests that the seasonal movement persists from the beginning of March until the end of September, i.e., for 214 days.

The contribution of the pore pressure changes to the total movement is assumed to be the same for the three slopes by ignoring the distance from the toe effect. This value equals 1.5 mm in 126 days. Therefore, the pore pressure changes' contribution is assumed to be equal to $1.5 * \frac{214}{126} = 2.6$ mm/yr. The contribution of the erosion at the toe of the west slope is calculated in a similar way, i.e., $(5.2 - 1.5) * \frac{214}{126} = 6.2$ mm/yr. Finally, the contribution of the erosion at the toe of the north slope would be equal to $(16.5 - 1.5) * \frac{214}{126} = 25.4$ mm/yr.

The expected annual rates of all the movement components are summarized in Table 5-10. The resolution of the total movement into individual components has an important practical implication. It provides guidance for choosing the most suitable mitigation option. For example, the use of pore pressure relief measures on the north slope will be inefficient in arresting the movement because they will stop only about 3mm/yr out of 43mm/yr of the total movement, based on borehole TH07-N monitoring. The most suitable mitigation strategy would be toe armouring. On the other hand, both toe erosion and pore pressure changes at the south slope seem to have insignificant effects on movement (2.6 of 17.2mm/yr); i.e., seasonal effects contribute to only 15.2% of the total south slide movement.

It should be noted however that the main movement zone at the location of borehole TH07-W slides as part of the third block, according to Thomson and Hayley (1975) analysis and our verification. The seasonal movement of the first block is higher, as indicated above. Hence, the creep contribution at the downslope block becomes equal to $\frac{15.6}{40.2} * 100 = 38.8\%$, and the seasonal movements would account for up to 61.2% of the total movement of the west slope.

On the other hand, borehole TH07-N is located within the downslope block of the north slope, and, hence, the recorded rates are the maximum movement rates of the north slope. The south slope seems to slide as a single block, and, hence, the distance effect is nil.

The second important implication of quantifying the different components of movement is that the movement will <u>not</u> be arrested after the installation of toe armours and/or drainage measures. The movement will slow down to a minimum rate that is equal to the creep rate of the slide materials. The evaluation of the creep rate based on laboratory testing needs more investigation.

The interpretation of the deduced values of the seasonal movement needs great care since they depend more or less on the amount of the rainfall, river level and

flow rate in 2008. Significant changes in the hydrological boundary conditions may take place in other years and will yield different values of the seasonal movement, yet the creep deformation should remain unchanged. Therefore, the implementation of properly designed mitigation measures would help to reduce the movement of the Little Smoky valley slopes to a minimum rate of about 15mm/yr.

5.6 Summary and Conclusions

The west, south and north slopes of the Little Smoky valley move at very slow rates that adversely affect the serviceability of portions of Highway 49 as well as the Little Smoky Bridge. The stability of the west slope was studied in the late sixties (Hayley, 1968; and Thomson and Hayley, 1975). Slope movements and pore pressures were monitored and limit equilibrium analyses were carried out. The study concluded that the movement is retrogressive and is triggered by toe erosion. Alberta Infrastructure and Transportation started a field program in 2001 that involved monitoring the north and south slopes movements and pore pressures. Readings were taken semi-annually, so a general picture of the movement rates of these slopes and their acceleration times was drawn. The locations of the main and secondary movement zones were determined, and the groundwater flow regime was understood. However, no quantification of the effects on the movements of the different causal factors was obtained.

The most recent study started in 2007 as part of this present research. Three boreholes, each equipped with a slope indicator and three vibrating wire piezometers, were drilled into the west, south and north slopes. The purposes of the most recent investigation are to update the geological cross-sections available from previous studies, understand the movement trend by taking readings as frequently as possible, study the possibility of the presence of other triggers of movement in addition to toe erosion, and quantify the contribution of each component to the total movement. The samples and drilled cores were visually inspected, and the geological cross-sections were updated. Readings of slope indicators and piezometers were taken every two weeks during the spring of 2008, every three weeks during the summer, and every month or more during the fall and winter. A nearly complete annual cycle of readings is acquired. The movement and pore pressure records are plotted against each other and against the river level and daily rainfall records.

The investigation of the previous as well as the current interpretations of the stratigraphy has led to an important conclusion. The location of the main rupture surface is controlled by one of three stratigraphic settings:

1. The preglacial lake clays as in the north slope,
2. The interface between the overlying till or preglacial lake clays and bedrock as in the south slope, or

3. The upper layer of the clay shale that is usually weakened by weathering as in the west slope.

This conclusion is in accordance with the observations of Scott (1989) and Cruden et al. (1993).

The total movement of the Little Smoky valley slopes can be resolved into three main components:

1. A creep component that contributes to about 15.6 mm/yr of the west slope movement and 14.6 mm/yr of the south slope movement. The contribution of the creep to the total movement of the north slope is not clear because the monitoring period did not include times when the effective stress was nearly constant. Hence, an average value of the west and south slopes creep rates (15.1 mm/yr) is assumed.
2. A seasonal component driven by pore pressure changes occurring in response to the river level changes, the daily rainfall changes, or both, with a time lag ranging from zero to two weeks. This component exists with the same value in the three slopes as long as the distances of the points of interest from the slope toes are equal. This component might be due to a river level drawdown mechanism at the north slope. Based on the records of the movement, pore pressures and hydrological conditions in 2008, this component contributes to 6 – 15% of the total movement of the Little Smoky Slides.
3. A seasonal component driven by toe erosion. This component exists in different amounts in the three slopes. The toe erosion component is higher in the west slope than in the south slope because the west slope lies downstream from the bridge. The confined flow condition at the toe of the north slope causes a higher contribution of the toe erosion component than that at the west slope. Based on the records of the movement, pore pressures and hydrological conditions in 2008, this component contributes to 26% and 59% of the total movement of the Little Smoky west and north slides, respectively.

The available piezometric and hydrological data enabled correlating the seasonal movements to pore pressure changes and toe erosion as summarized above. However, seasonal movements may also take place in response to seasonal forces acting on the slide like lateral water pressures in the tension cracks and surface water ponding. While these effects are certainly reflected in the measured movement rates, the seasonal movements were compared to pore pressures and hydrological records.

The west and north slopes slide retrogressively. The south slope, however, slides as a whole block. The rate effects are negligible on the residual shear strength. The seasonal movements of the west, south and north slopes contribute to 61%, 15% and 65% of the total movement, respectively, based on the records of the movement, pore pressures and hydrological conditions in 2008. The application

of the suitable mitigation measures would serve to reduce the movements of the Little Smoky valley slopes to a minimum rate of about 15mm/yr.

Table 5-1: Grain Size Distributions of the Till and Shale Units (Modified after Thomson and Hayley, 1975)

Property	Soil Type		
	Till	Soft Shale	Hard Shale
%Sand sizes	23-60 (Sand Pockets)	5-6	-
%Silt sizes	31-40	51-57	-
%Clay sizes	9-35	38-43	-

Table 5-2: Summary of Atterberg Limits, Moisture Content and Unit Weights of Till and Shale (Modified after Thomson and Hayley, 1975)

Property	Soil Type		
	Till	Clay Shale	
		Soft	Hard
Natural Water Content (%)	21-22	21	15
Liquid Limit (%)	43-48	55	48
Plastic Limit (%)	18-21	31	23
Plasticity Index (%)	22-30	24	25
Bulk Density (kN/m^3)	19.50	21.78	-

Table 5-3: Safety Factors of the Seven Blocks Involved in the Retrogressive Slide at the West Slope (After Hayley, 1968 and Thomson and Hayley, 1975)

Block number	Safety Factor using the Wedge Method (Hayley, 1968)	Safety Factor using Morgenstern and Price Method (Thomson and Hayley, 1975)
1	-	1.03
2	1.0	1.09
3	1.0	1.30
4	1.4	1.03
5	1.4	1.30
6	1.2	1.27
7	1.1	1.03

Table 5-4: Verification of the Results of the Limit Equilibrium Analysis Carried out by Thomson and Hayley (1975)

Block number	Safety Factor	Remarks
1	0.92	
2	1.08	
3	1.14	
4	0.96	
5	1.15	The intermediate point of the secondary slide plane has been moved to the right by 5m. When it was in the original position, it gave “no solution”
6	1.15	
7	0.96	Main scarp has been moved by 5m. When it was in its original position, the safety factor was 0.511

Table 5-5: Summary of Borehole Information of the 2007/08 Program (Modified after Bala and Proudfoot, 2007)

Location	Borehole Depth (m)	Sampling	Slope Indicator Depth (m)	Piezometer Tip Depth (m)
West Slope	20.4	No	NA	20.2
	33.5	No	NA	33.3
	45.4	Yes	45.4	45.2
South Slope	20.7	No	NA	20.5
	36.0	No	NA	35.7
	45.1	Yes	45.1	44.6
North Slope	35.8	No	NA	35.6
	66.5	Yes	66.5	50.6
				66.1

Table 5-6: Typical Atterberg Limits for Clay Shales of Upper Cretaceous Age (Modified after Morgenstern and Eigenbrod, 1974)

Case Number	Geological Formation	Location	Depth (ft)	Moisture Content (%)	Plastic Limit (%)	Liquid Limit (%)	Plasticity Index (%)
1	Battle, Upper Cretaceous	Cyprus Hills, Alberta	60	16.7	21.1	50.7	29.5
2	Battle, Upper Cretaceous	Cyprus Hills, Alberta	60	21.2	25.7	50	24.3
3	Edmonton Formation, Upper Cretaceous	Edmonton, Alberta	15	17.2	17	180	163
4	Bearpaw Formation, Upper Cretaceous	Cyprus Hills, Alberta and South Saskatchewan	12	18-28	22.8	87	64.2
5	Gault Clay, Upper Cretaceous	England	-	21.9	14.9	68.5	43.6
6	Pierre Formation, Upper Cretaceous	Upper Missouri River, Montana	85	25.8	32.7	44.7	12
7	Clagget Formation, Upper Cretaceous	Upper Missouri River, Montana	450	13.5	27.8	89.8	62
8	Colorado Formation, Upper Cretaceous	Upper Missouri River, Montana	40	28.5	27.8	68	40.2
9	Marlboro Formation, Upper Cretaceous	Central Alberta	114	9	21	31.6	10.6
10	Belly River Formation, Upper Cretaceous		39	15	20.1	74.2	54.1
11	Dunvegan Formation, Upper Cretaceous	Western Alberta	15	28	30	45	15
12	Edmonton Formation, Upper Cretaceous	Central Alberta	10	25	33.4	57.3	23.9
13	Edmonton Formation, Upper Cretaceous	Central Alberta	35	28	32.8	107	74.2
14	Kootenay Formation, Upper Cretaceous	Southwest Alberta	200	40	-		
15	Edmonton Formation, Upper Cretaceous	Central Alberta	40	26.6	23	44	21

Table 5-7: Atterberg Limits of Preglacial Lake Clays in the Peace River Area (Modified after Miller and Cruden, 2002)

Location	P.L. (%)	L.L. (%)	P.I. (%)
Eureka River landslide	22.5	43.5	21.0
Attachie landslide	23.0	40.0	17.0
Dunvegan Creek landslide	14.0	47.0	33.0
Montagneuse River landslide	21.0	65.0	44.0
Saddle River landslide	25.0	73.0	48.0

Table 5-8: Comparison between Total, Creep and Seasonal Movements at Boreholes TH07-W and TH07-S in the Period from January 24th to November 20th 2008

TH07-W (West Slope)			
Date	**Total Movement (mm)**	**Creep Component (mm)**	**Seasonal Component (mm)**
January 24th 2008	0.0	0.0	0.0
November 20th 2008	18.7	12.9	5.8
TH07-S (South Slope)			
Date	**Total Movement (mm)**	**Creep Component (mm)**	**Seasonal Component (mm)**
January 24th 2008	14.4	11.0	3.4
November 20th 2008	31.5	23.0	8.5
Difference (mm)	17.2	12.0	5.1

Table 5-9: Summary of Total, Creep and Seasonal Movements Recorded at Boreholes TH07-W, TH07-S and TH07-N between April 10th and August 14th 2008

Borehole		TH07-W	TH07-S	TH07-N
Distance from Toe (m)		196.5	186.6	177.5
Total Displacement (mm)	April 10th 2008	3.8	18.9	0.0
	August 14th 2008	14.4	25.4	21.7
	Net Value	10.6	6.6	21.7
Creep Component (mm)	April 10th 2008	3.3	14.0	0.0
	August 14th 2008	8.7	19.1	5.2
	Net Value	5.4	5.0	5.2
Seasonal Component (mm)	April 10th 2008	0.5	4.8	0.0
	August 14th 2008	5.7	6.4	16.5
	Net Value	5.2	1.5	16.5

Table 5-10: Summary of Predicted Contributions of each Component of Movement at Boreholes TH07-W, TH07-S and TH07-N

Borehole	Creep (mm)	Seasonal Movement (mm)		Total Expected in 2008 (mm)
		Pore Pressure Changes Effect (mm)	Toe Erosion Effect (mm)	
TH07-W	15.6 (63.8%)	2.6 (10.7%)	6.2 (25.5%)	24.4
TH07-S	14.6 (84.8%)	2.6 (15.2%)	~ zero	17.2
TH07-N	15.1 (35.0%)	2.6 (6.1%)	25.4 (58.9%)	43.2

Figure 5-1: A map for Alberta Showing the Location of the Little Smoky Slide

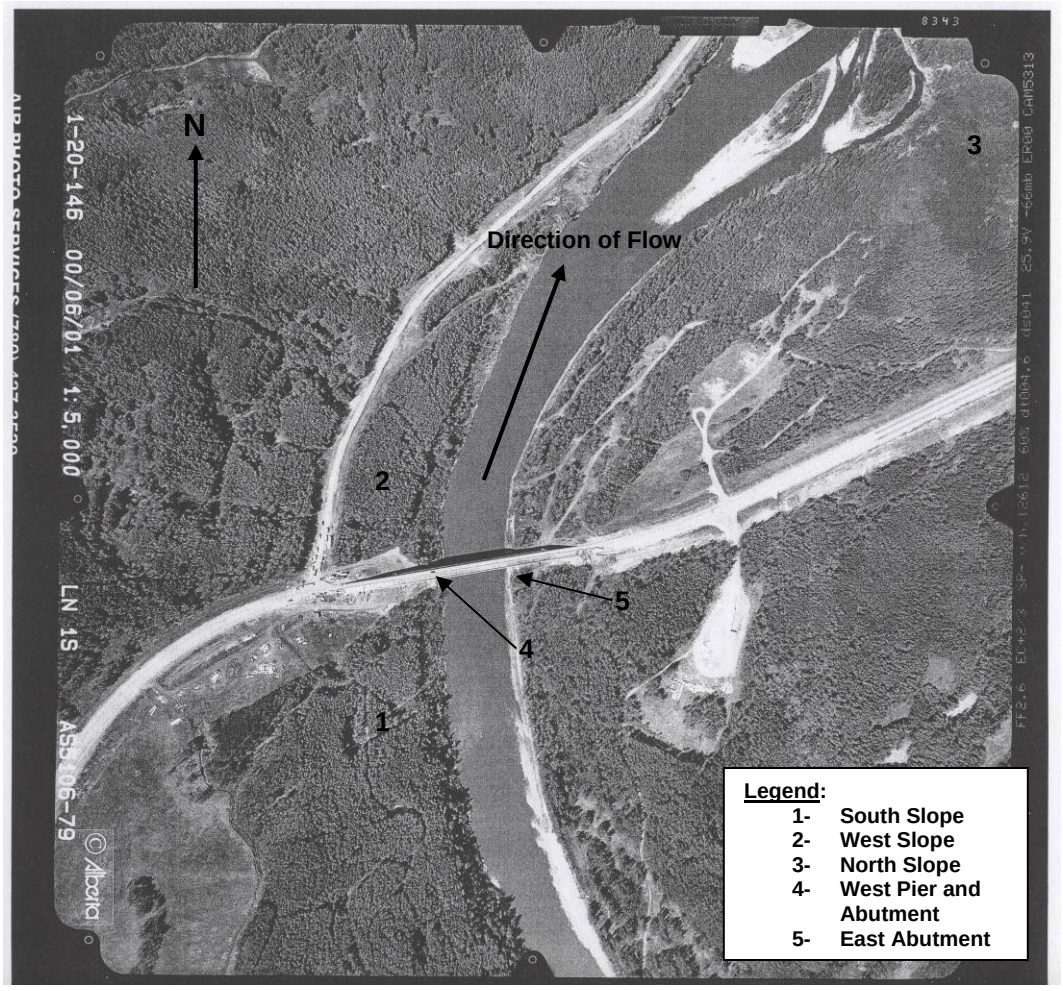

Figure 5-2: Air Photo AS5106-79 of the Little Smoky Slide on June 1st 2000 Showing the Locations of the West, South and North Slopes (Reproduced with Permission from Alberta Sustainable Resources Development, Air Photo Distribution)

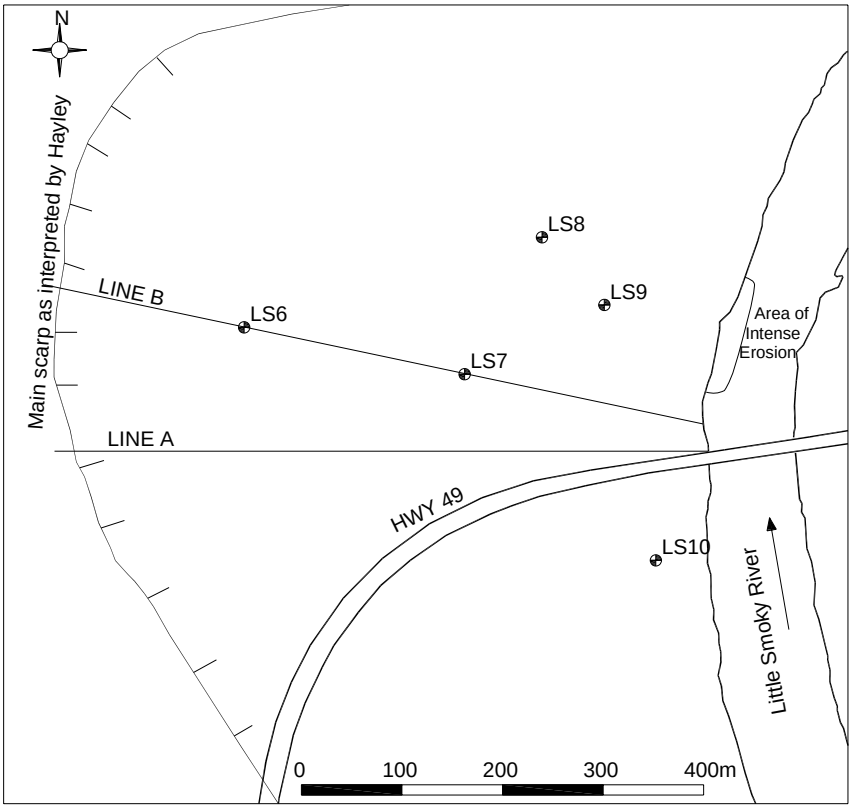

Figure 5-3: A Plan Showing the Instrumentation Used for Monitoring the West Slope in the Late Sixties (Modified after Hayley, 1968)

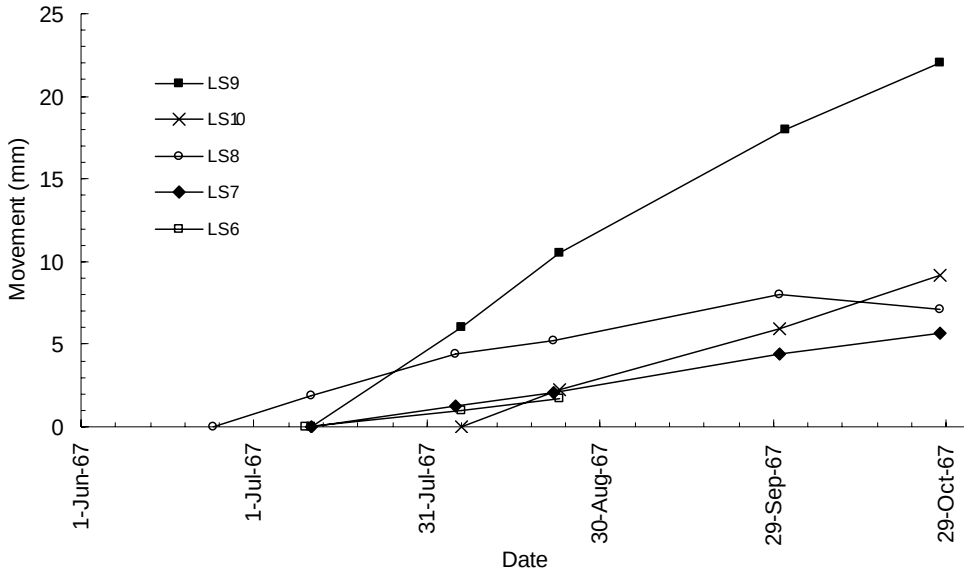

Figure 5-4: Movement versus Time Plots for Inclinometers LS6, 7, 8, 9 and 10 (Modified after Hayley, 1968)

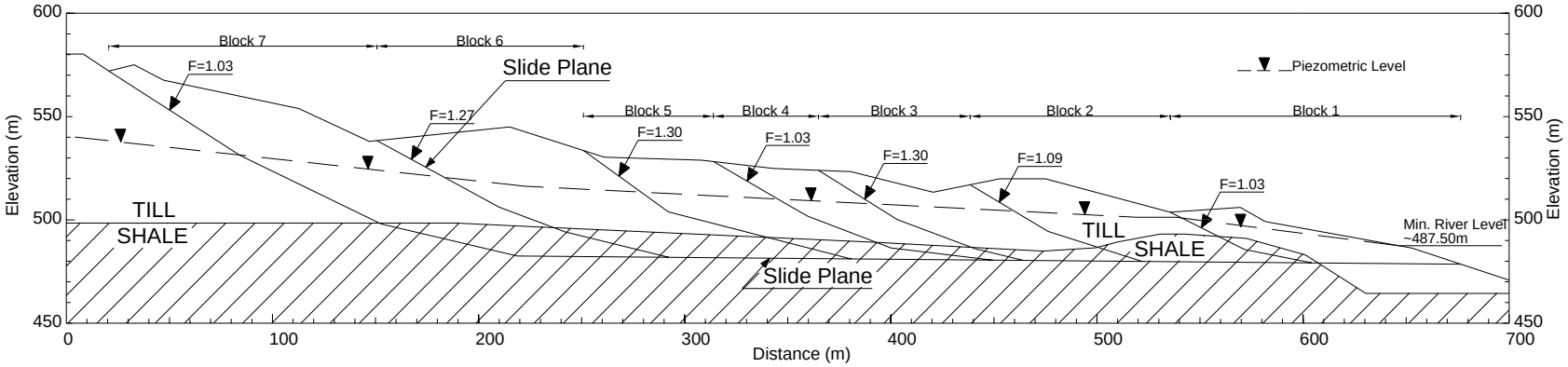

Figure 5-5: Failure Planes of Different Blocks as Used by Thomson and Hayley (1975) (Modified after Thomson and Hayley, 1975)

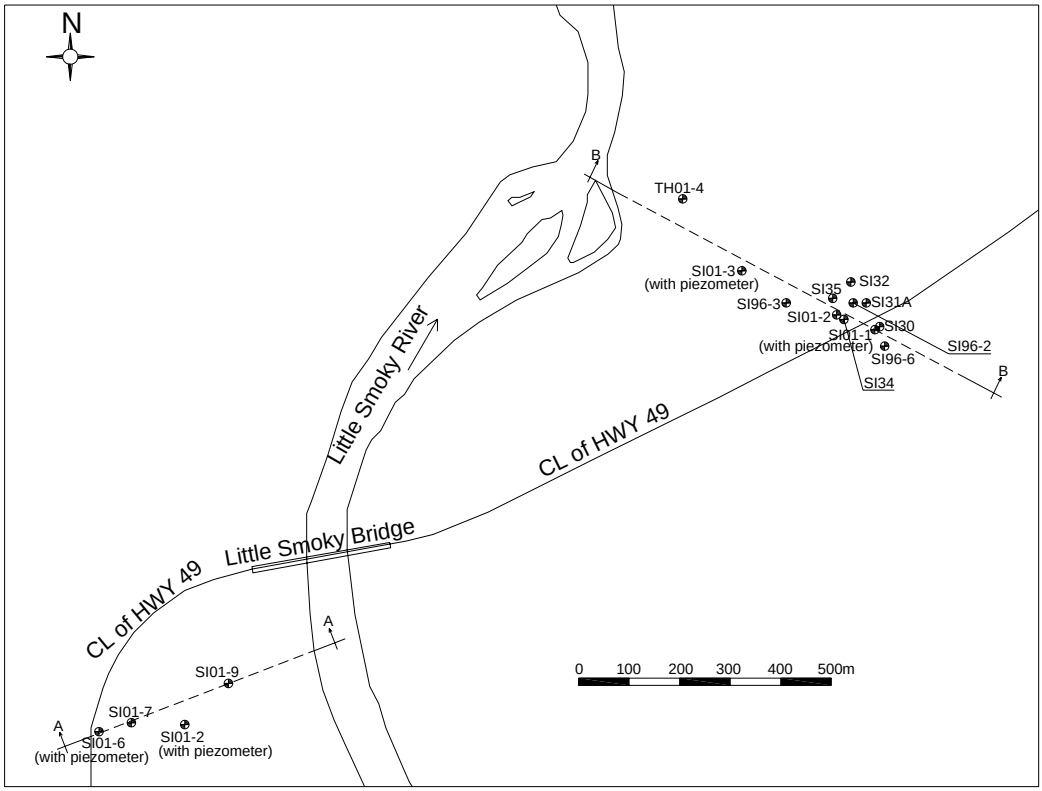

Figure 5-6: A schematic Diagram Showing the Locations of the Instrumentation Boreholes Installed in 2001 (Modified after Proudfoot and Tweedie, 2002)

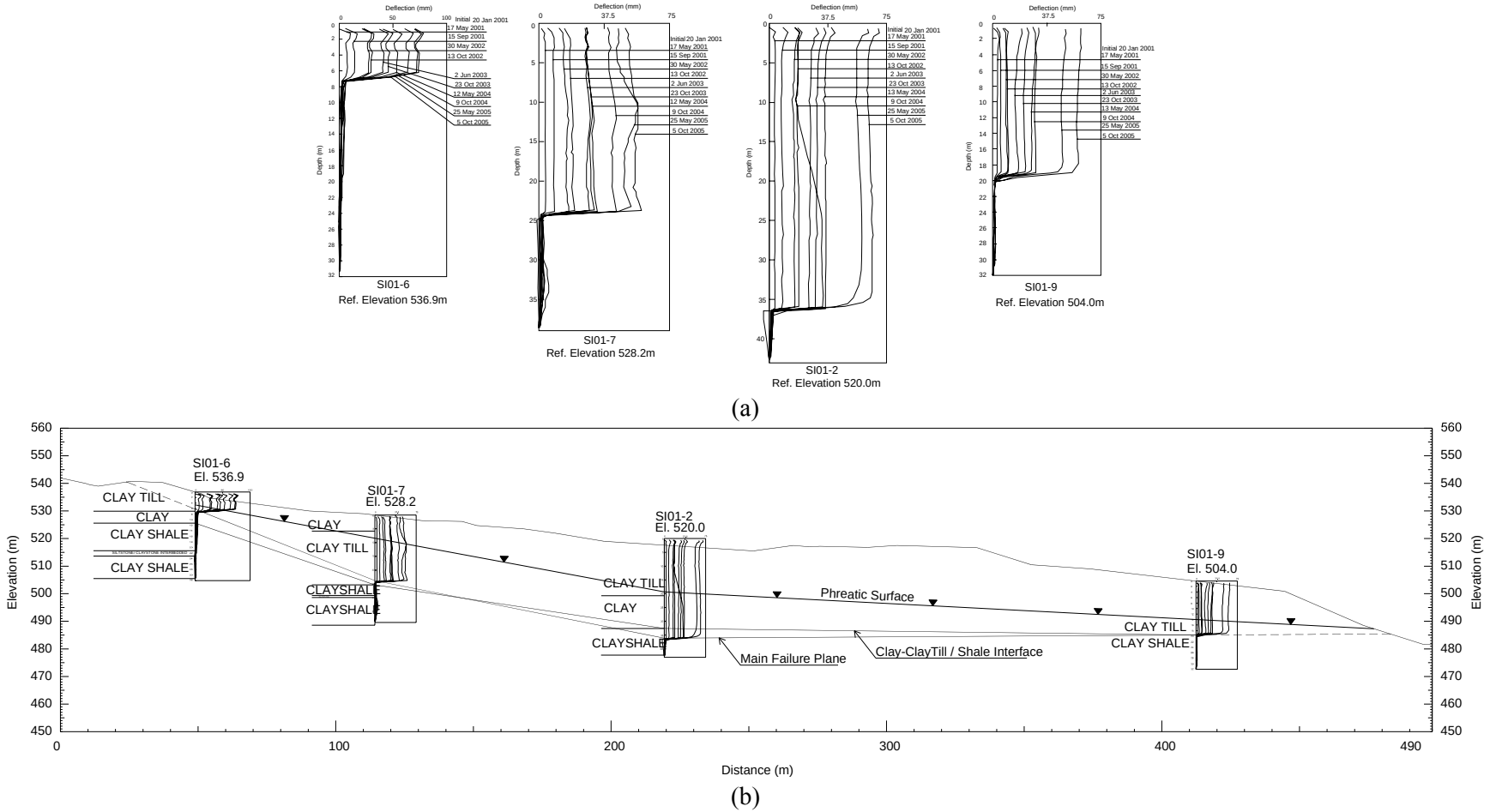

Figure 5-7: (a) Profiles of the Resultant Cumulative Displacements for the Four Inclinometers Installed in 2001 and (b) Cross-section A-A through the South Slope of the Little Smoky Slide as Interpreted by Proudfoot and Tweedie, 2002 (Modified after Proudfoot and Tweedie, 2002)

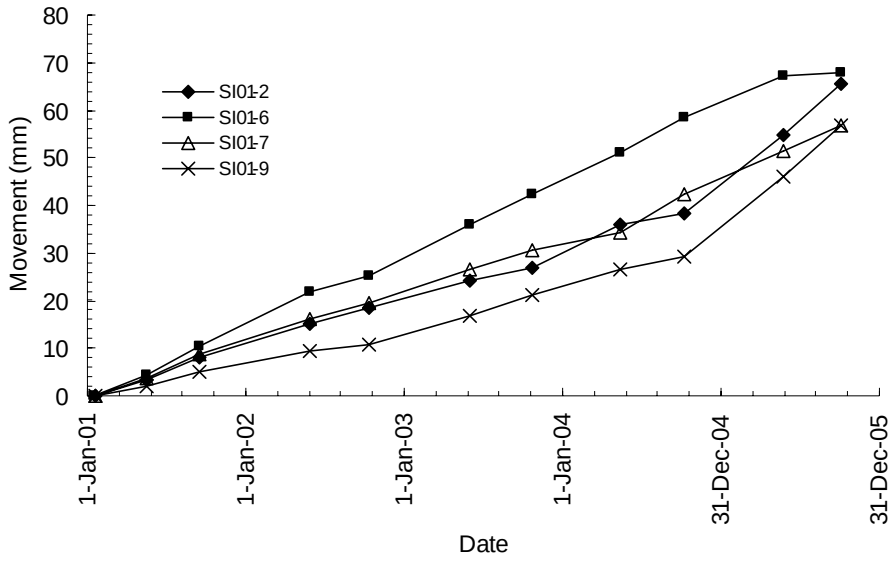

Figure 5-8: Movement versus Time Plots for the Four Inclinometers Installed in 2001 in the South Slope (Data Files Provided by Thurber Engineering Ltd.)

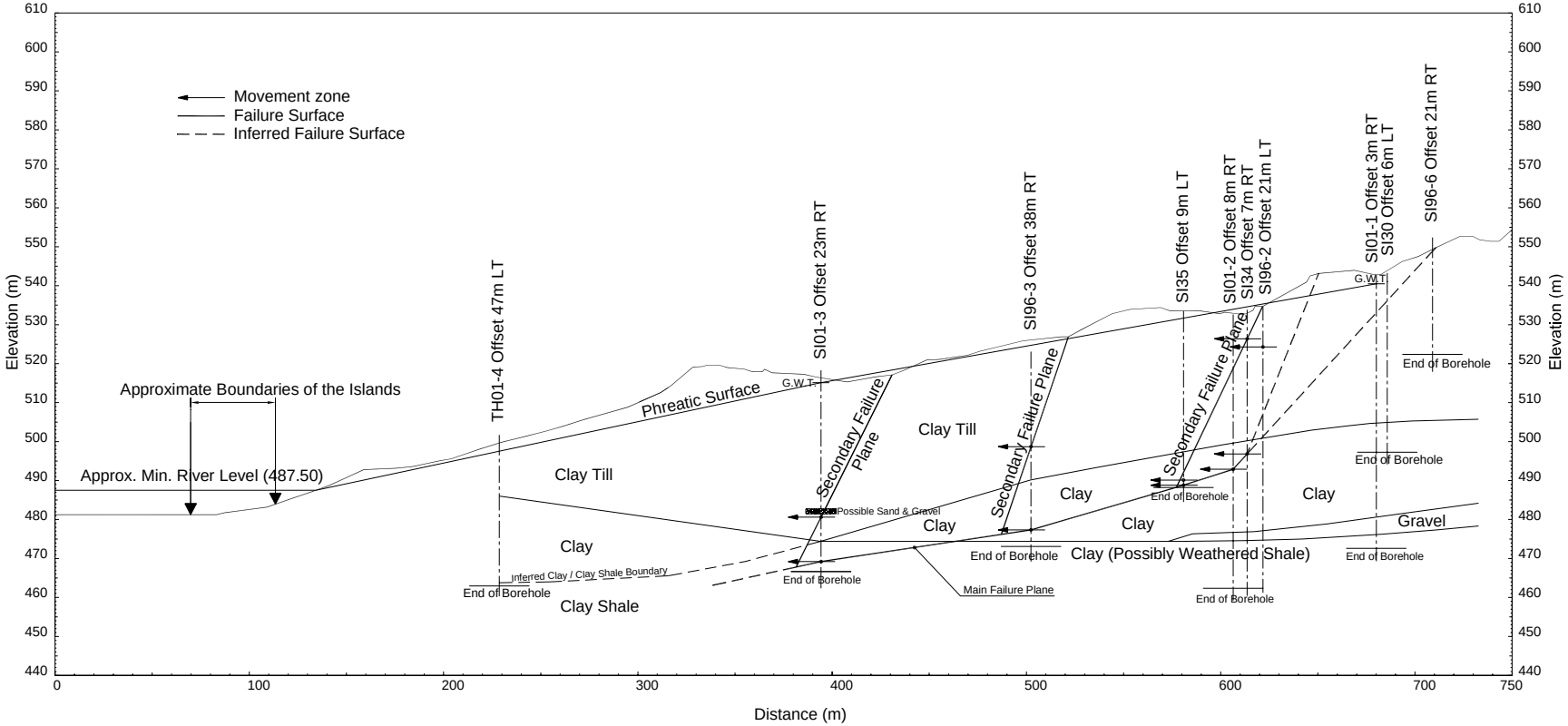

Figure 5-9: Cross-section B-B through the North Slope Showing the Stratigraphy, the Phreatic Surface and the Failure Planes

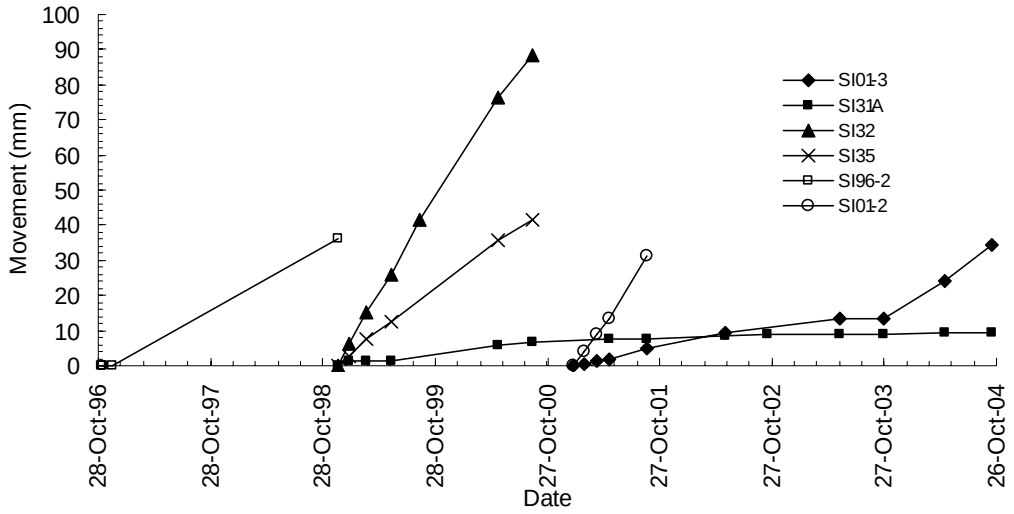

Figure 5-10: Movement versus Time Plot for Some Slope Indicators Installed in the North Slope (Data Files Provided by Thurber Engineering Ltd.)

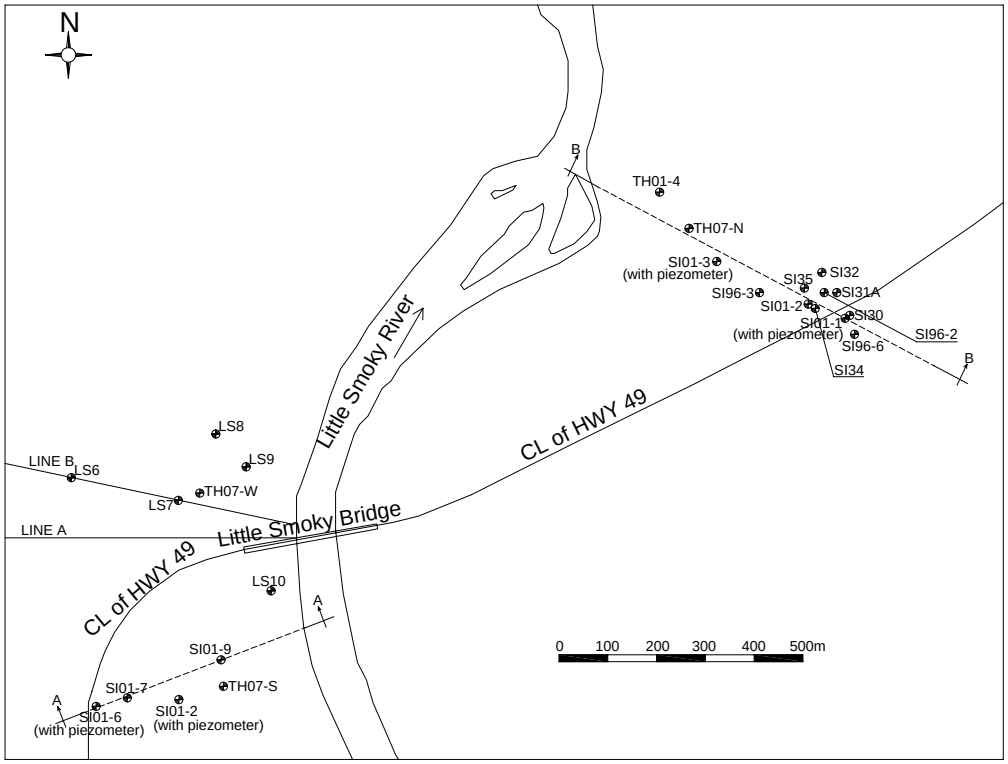

Figure 5-11: A Plan Showing All the Previous and the Most Recent Instrumentation in 2007

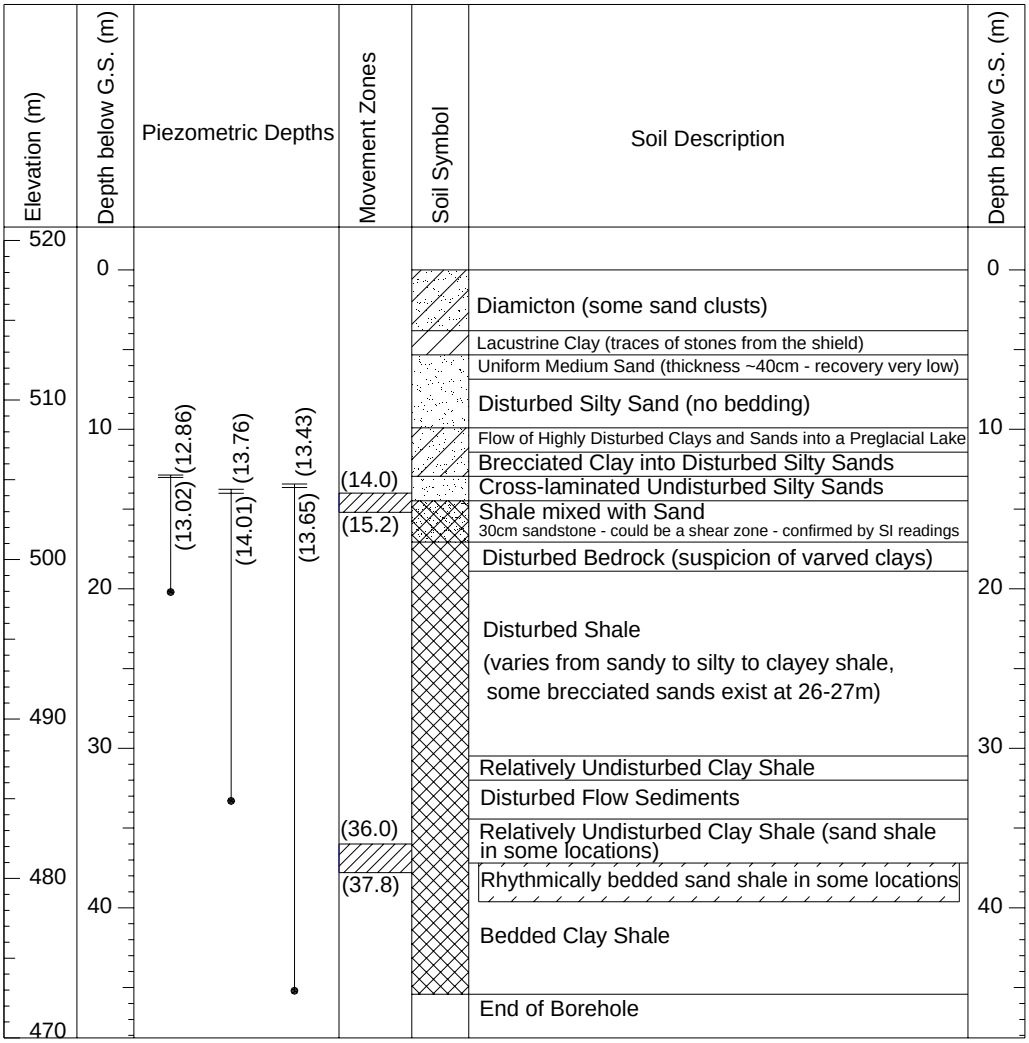

Figure 5-12: Borehole TH07-W Log

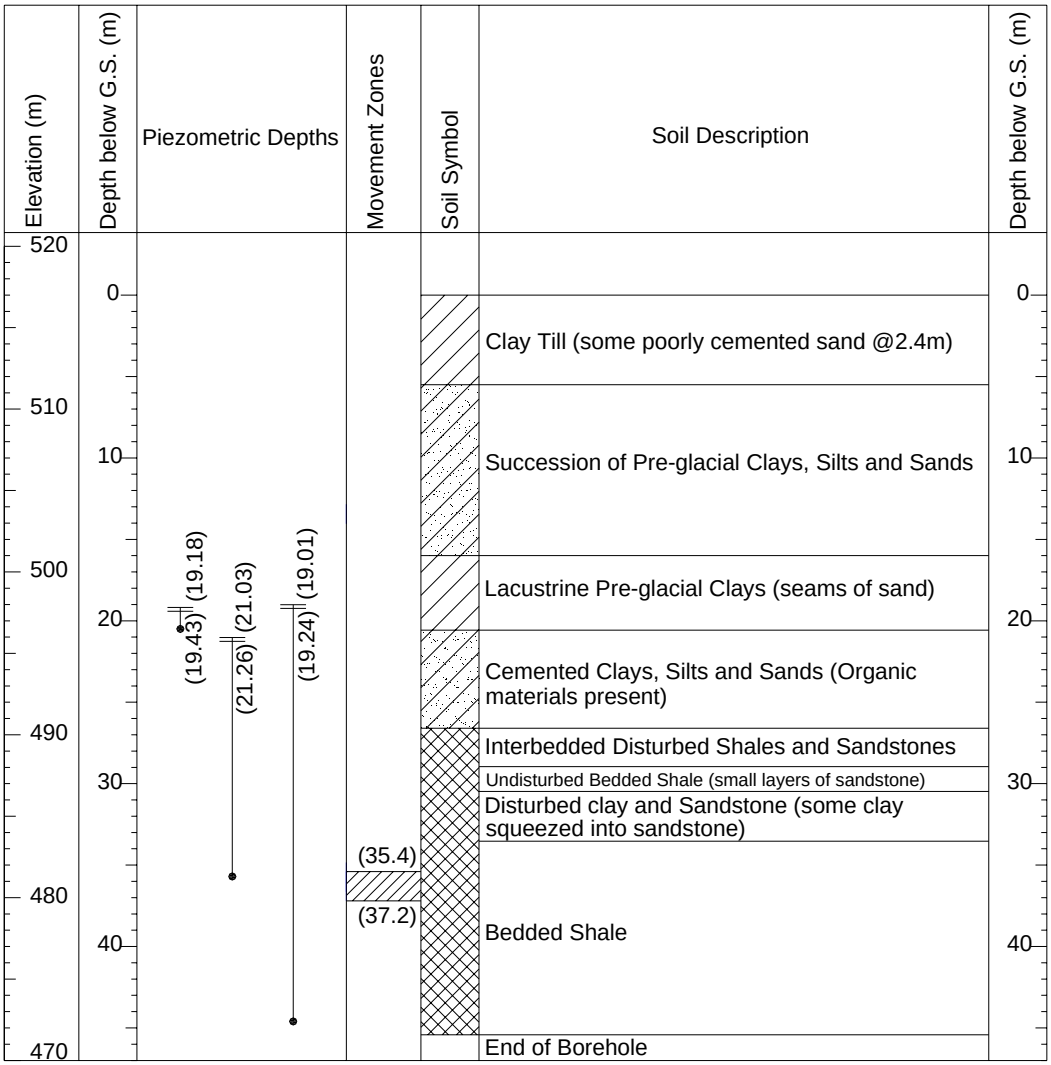

Figure 5-13: Borehole TH07-S Log

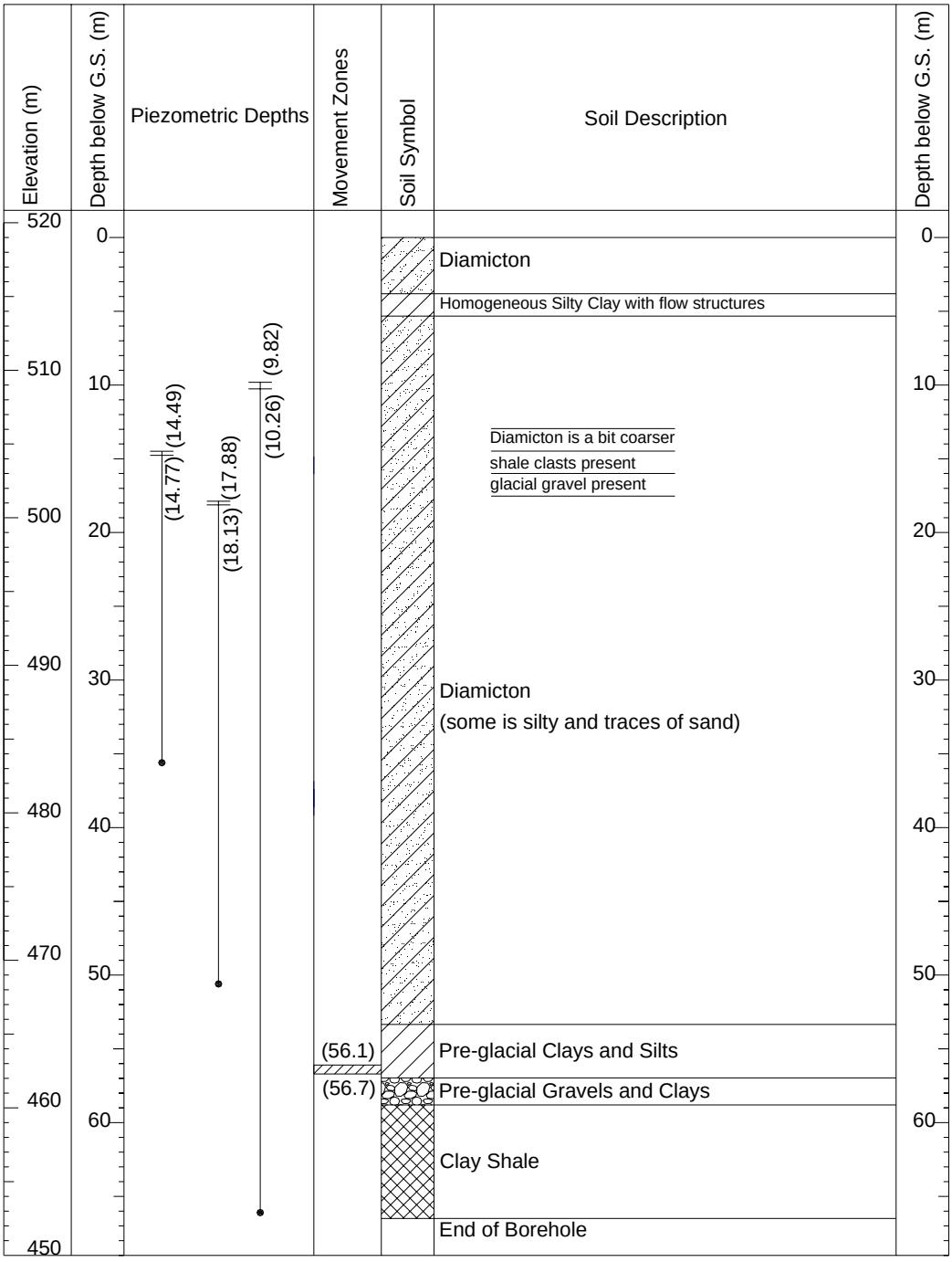

Figure 5-14: Borehole TH07-N Log

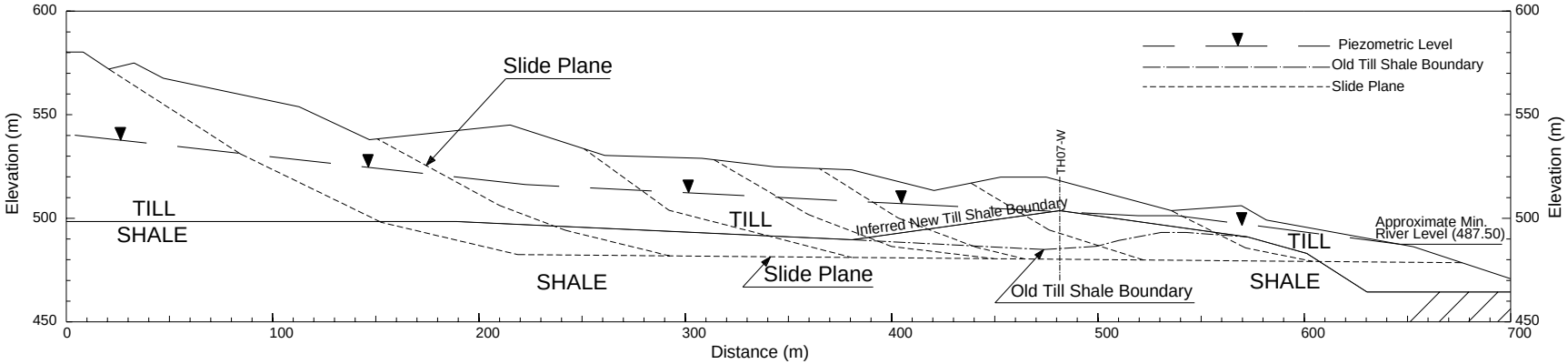

Figure 5-15: Updated Cross-section through Line B of the West Slope

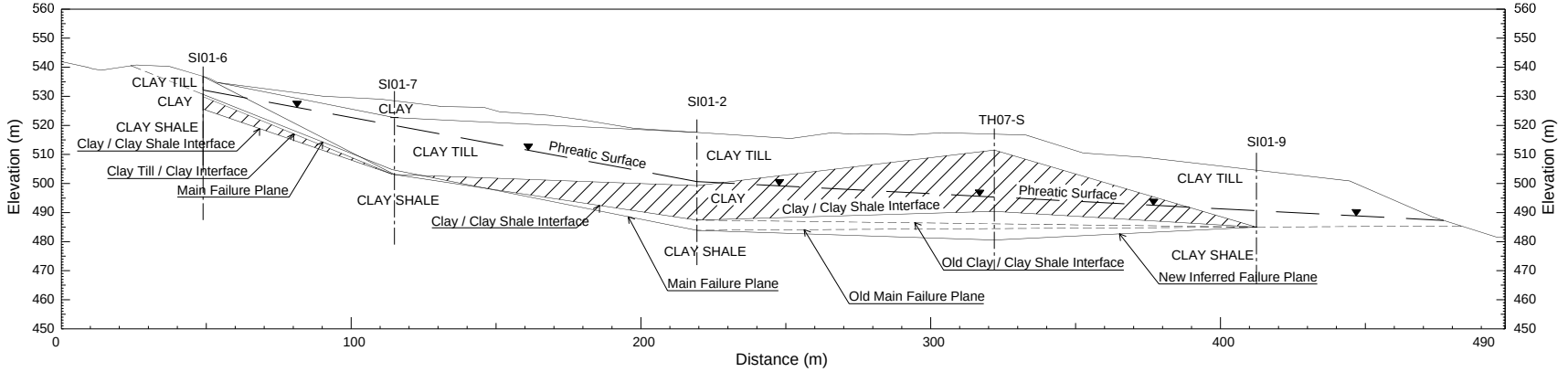

Figure 5-16: Updated Cross-section A-A through the South Slope

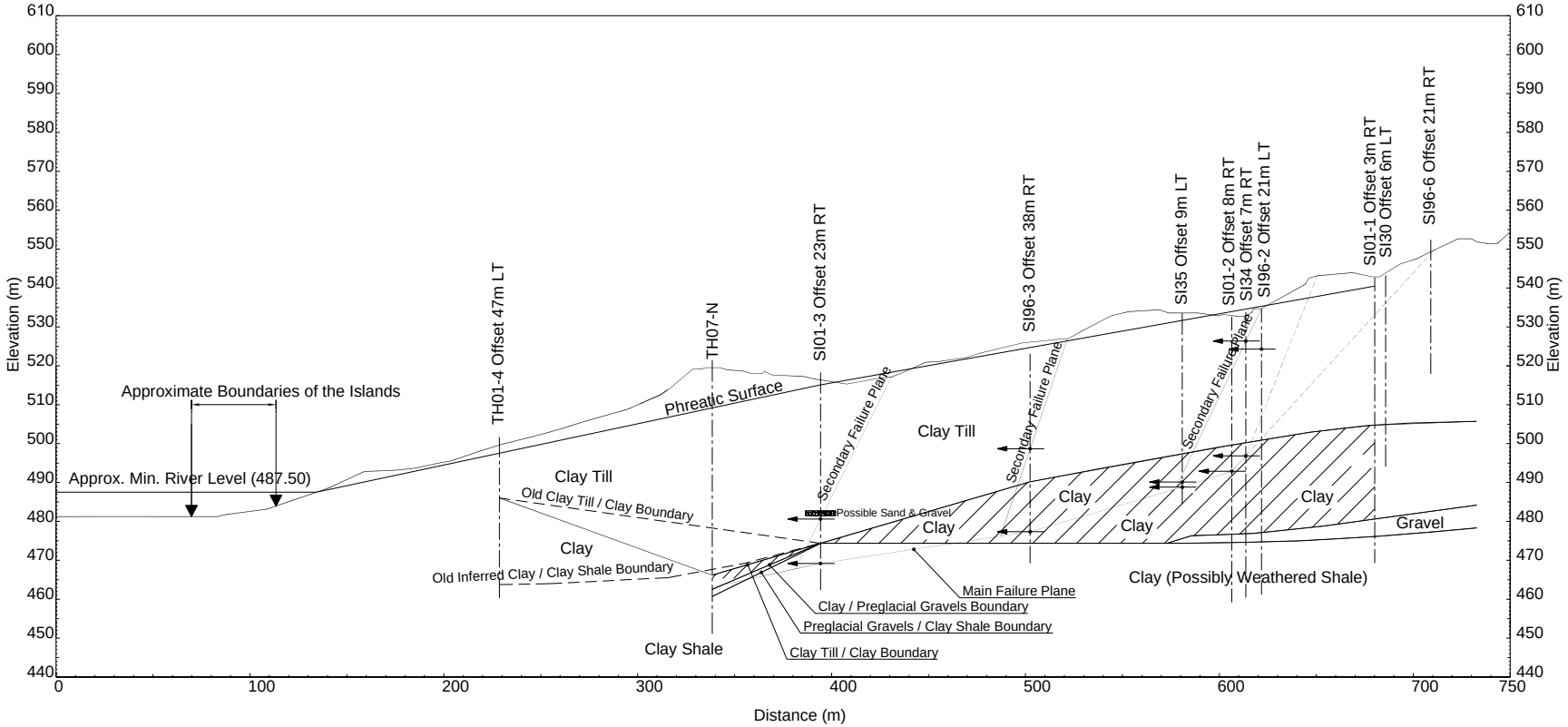

Figure 5-17: Updated Cross-section B-B through the North Slope

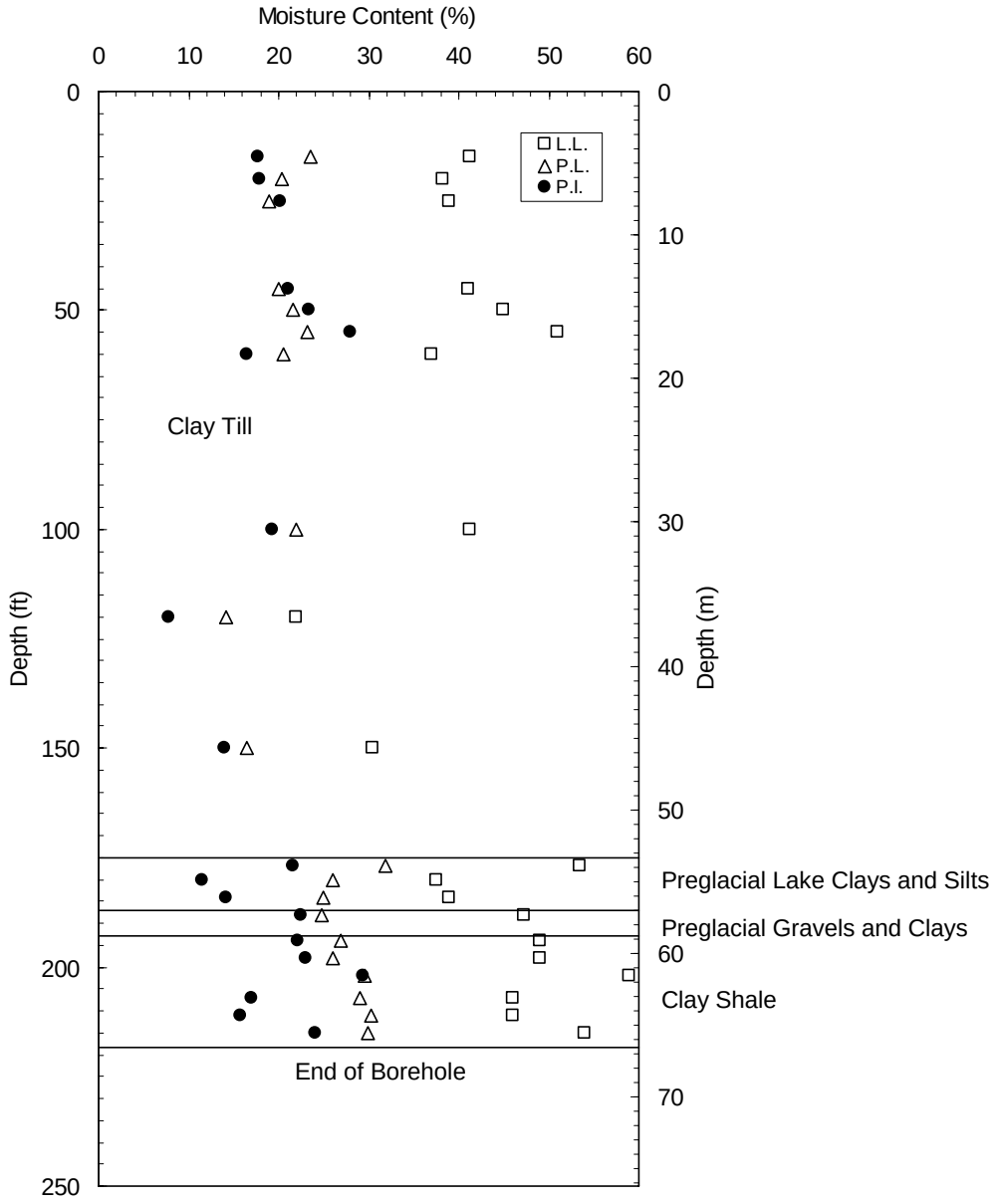

Figure 5-18: Atterberg Limits at Various Depths in Borehole TH07-N

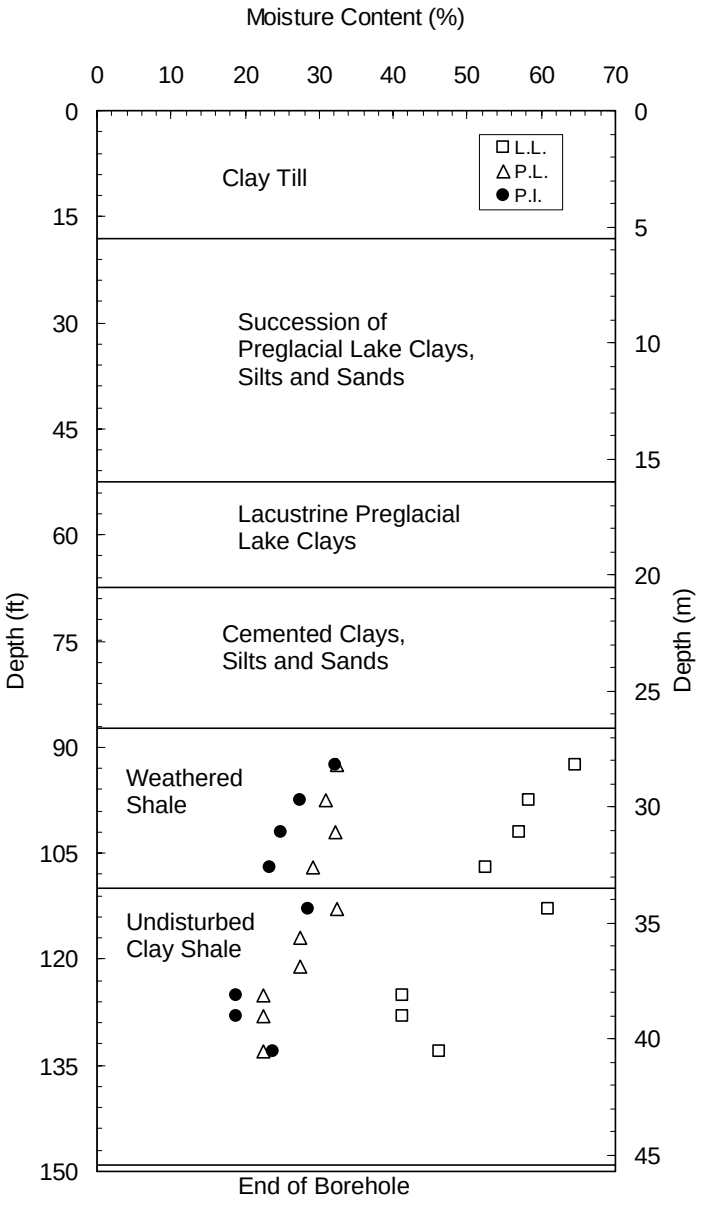

Figure 5-19: Atterberg Limits at Various Depths in Borehole TH07-S

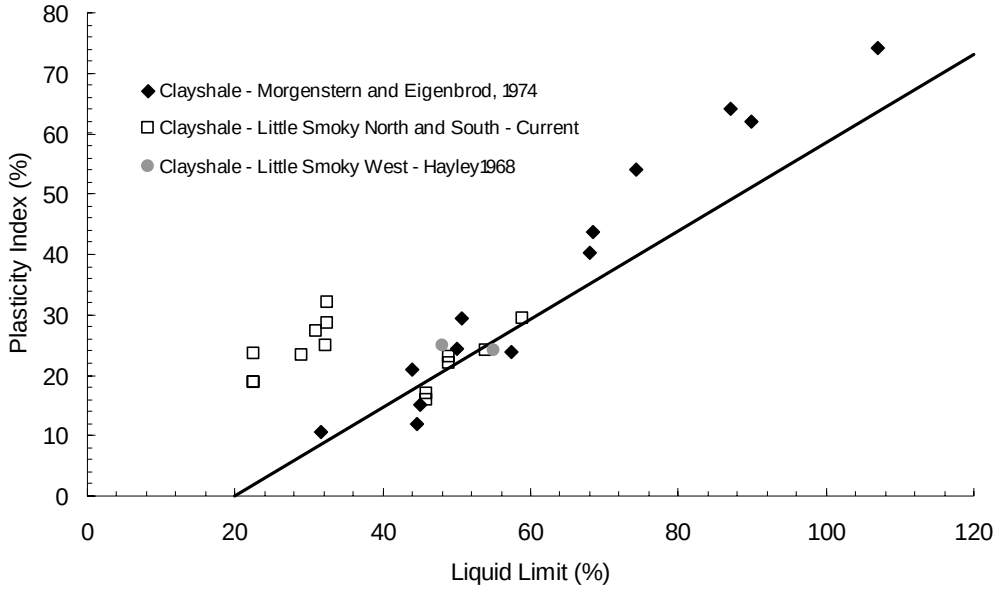

Figure 5-20: Plasticity Chart for Atterberg Limit Values of Clay Shales from Previous and Current Investigations

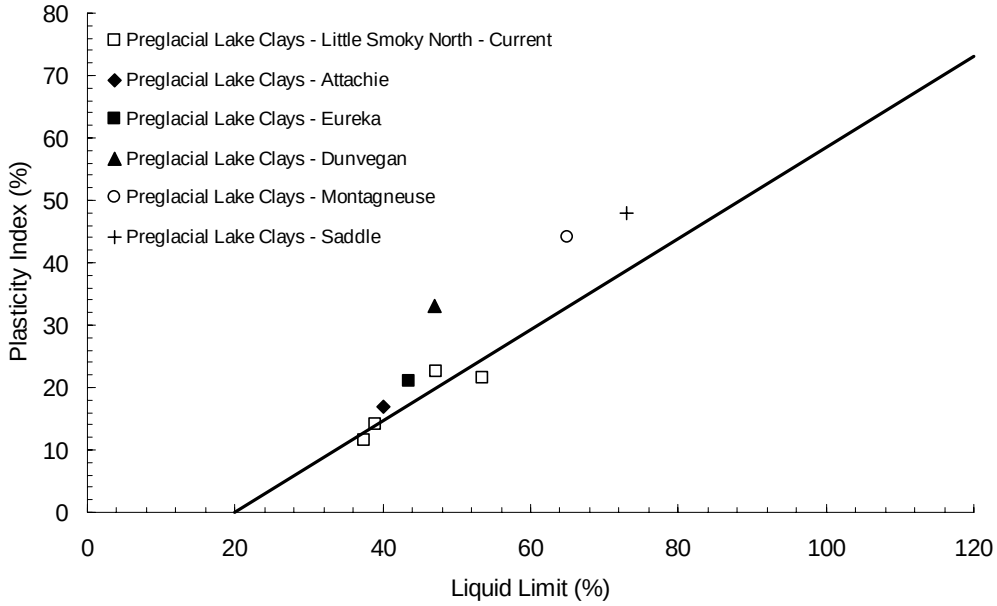

Figure 5-21: Plasticity Chart for Atterberg Limit Values of Preglacial Lake Clays from Previous and Current Investigations

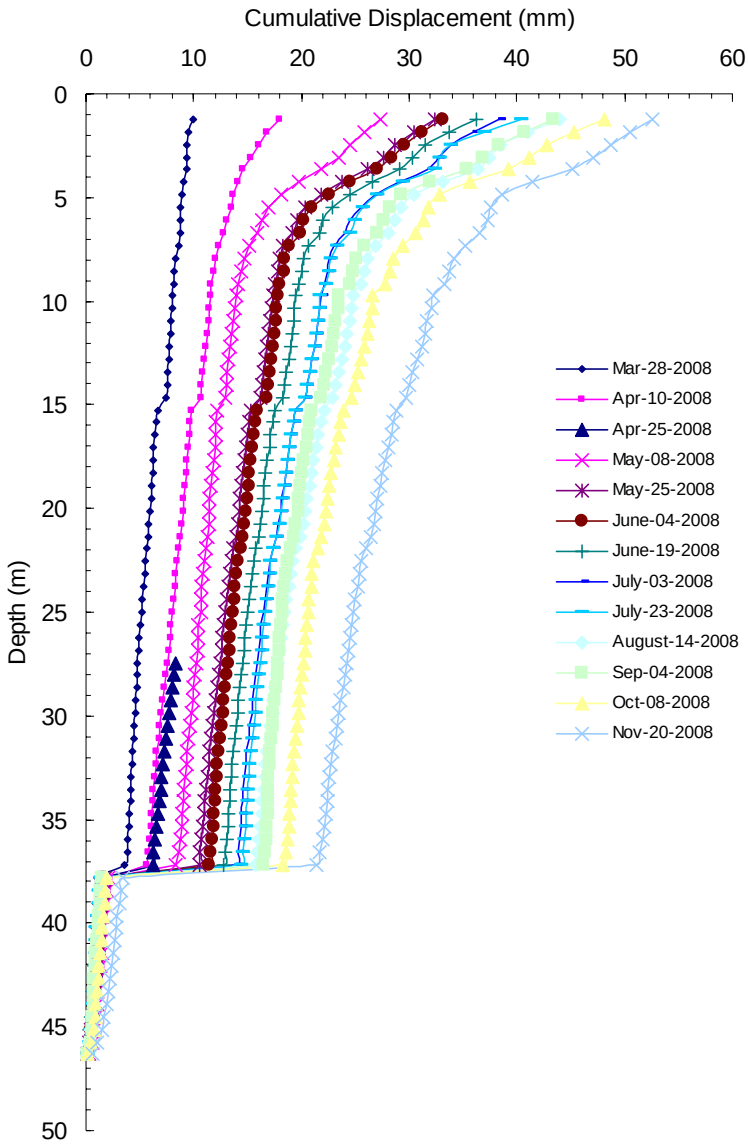

Figure 5-22: Cumulative Displacement Profiles at Borehole TH07-W in the West Slope

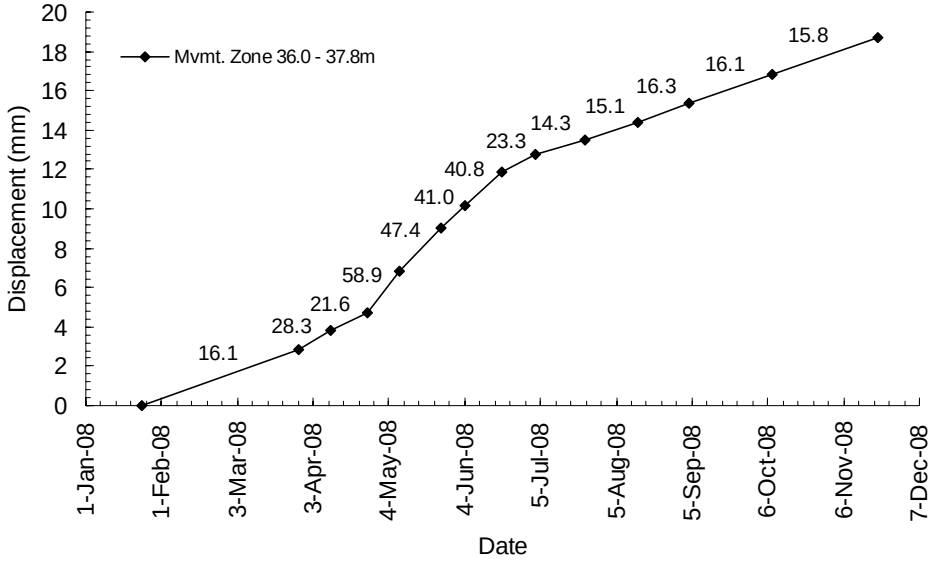

Figure 5-23: Displacement versus Time Plot of the Main Movement Zone at the Location of Borehole TH07-W with Displacement Rates Displayed in Units of mm/yr

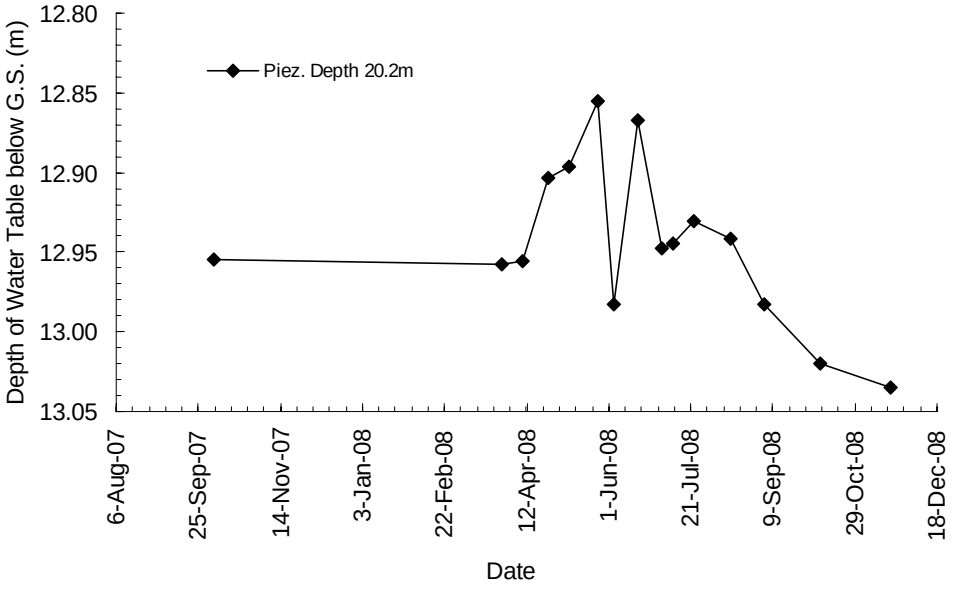

Figure 5-24: Piezometric Depth Variation with Time at Depth 20.2m in Borehole TH07-W

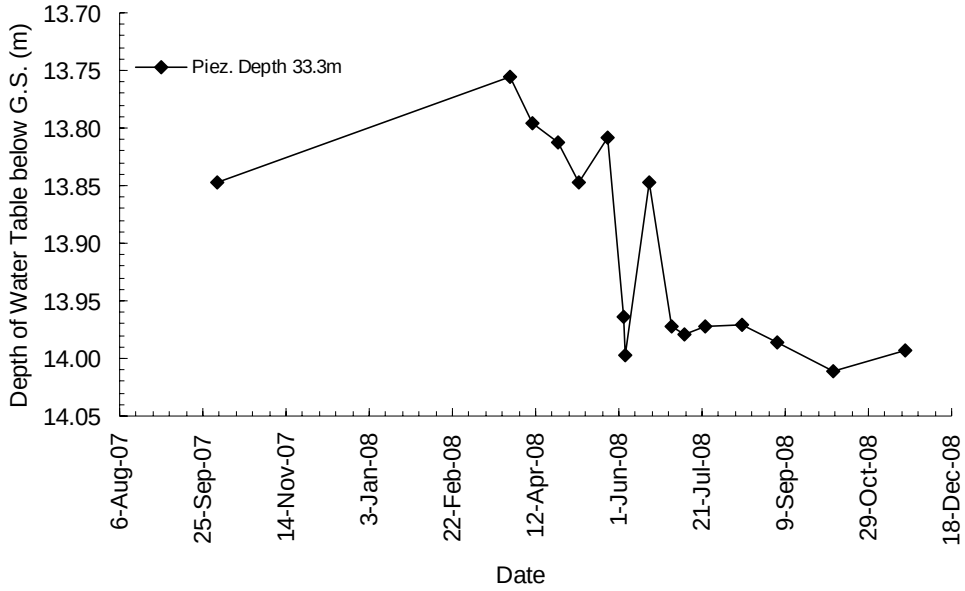

Figure 5-25: Piezometric Depth Variation with Time at Depth 33.3m in Borehole TH07-W

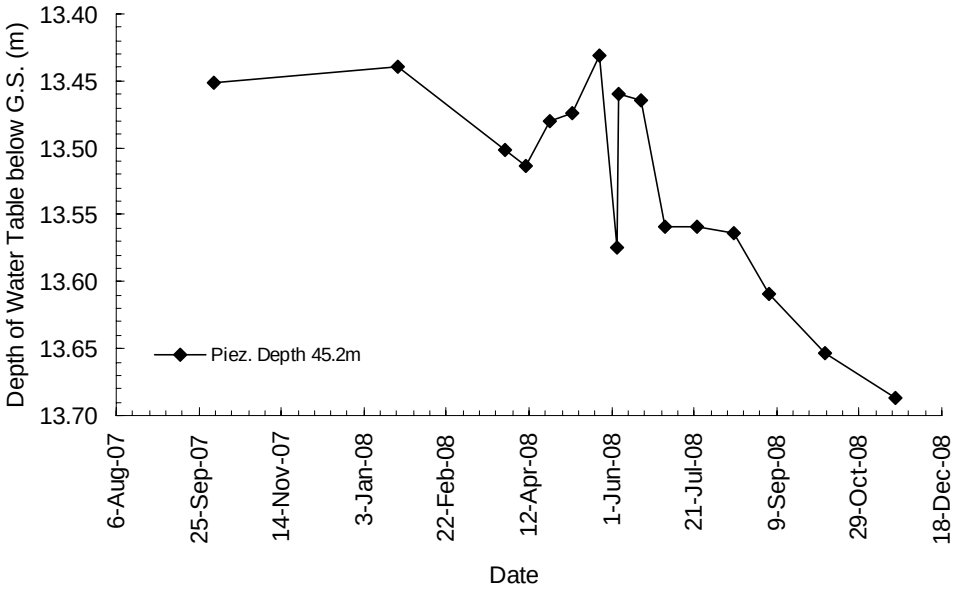

Figure 5-26: Piezometric Depth Variation with Time at Depth 45.2m in Borehole TH07-W

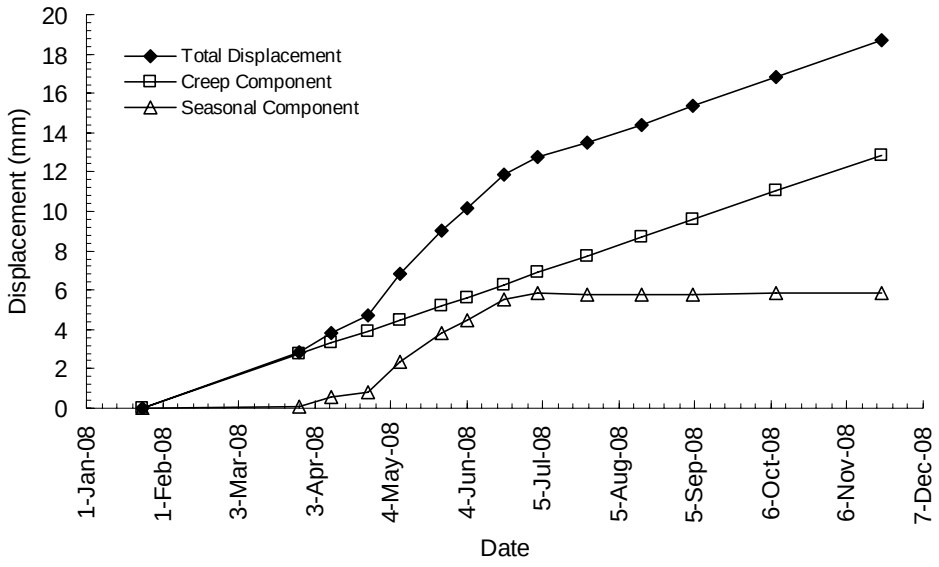

Figure 5-27: The Variation with Time of each of the Creep Component, the Seasonal Component and the Total Displacement at the Location of Borehole TH07-W

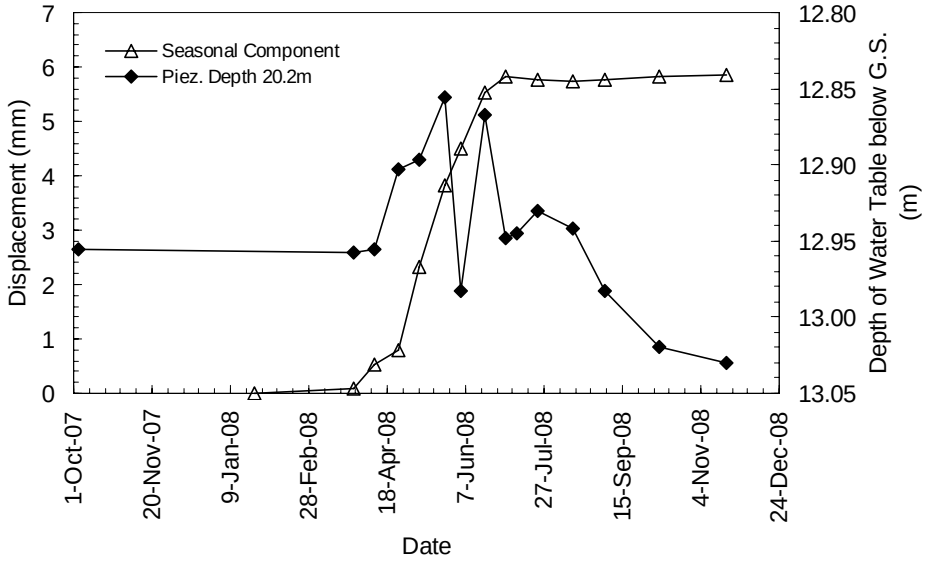

Figure 5-28: Seasonal Displacement and Piezometric Depth Variations with Time for the Piezometer Installed at Depth 20.2m in Borehole TH07-W

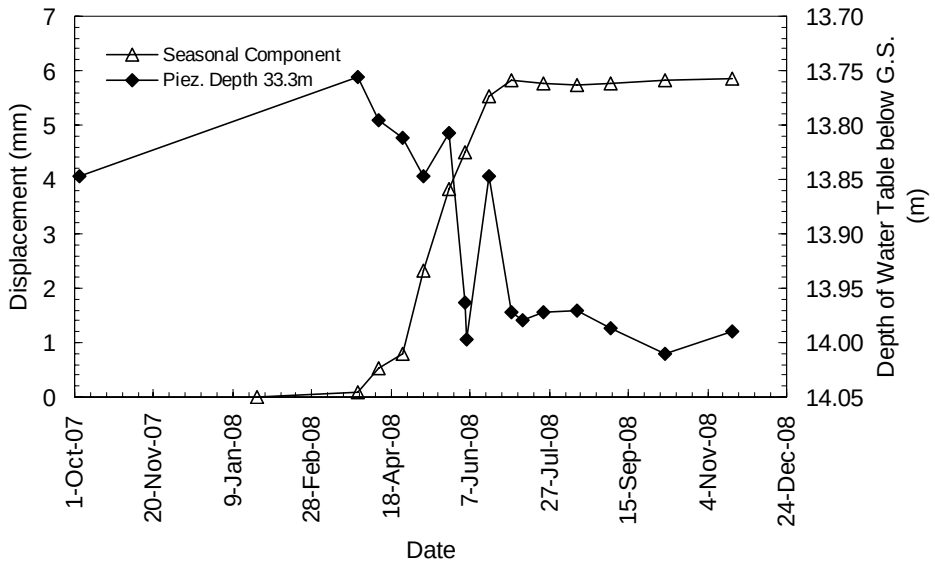

Figure 5-29: Seasonal Displacement and Piezometric Depth Variations with Time for the Piezometer Installed at Depth 33.3m in Borehole TH07-W

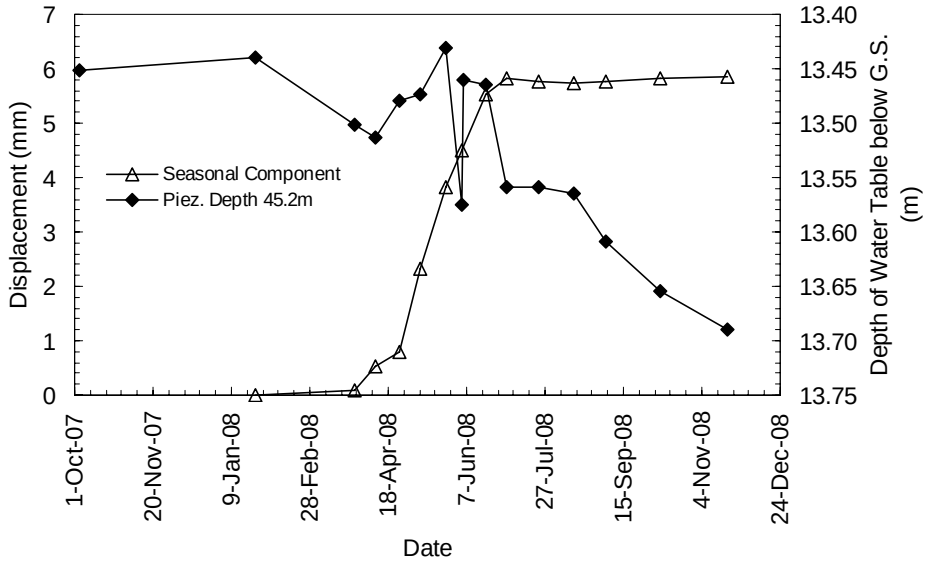

Figure 5-30: Seasonal Displacement and Piezometric Depth Variations with Time for the Piezometer Installed at Depth 45.2m in Borehole TH07-W

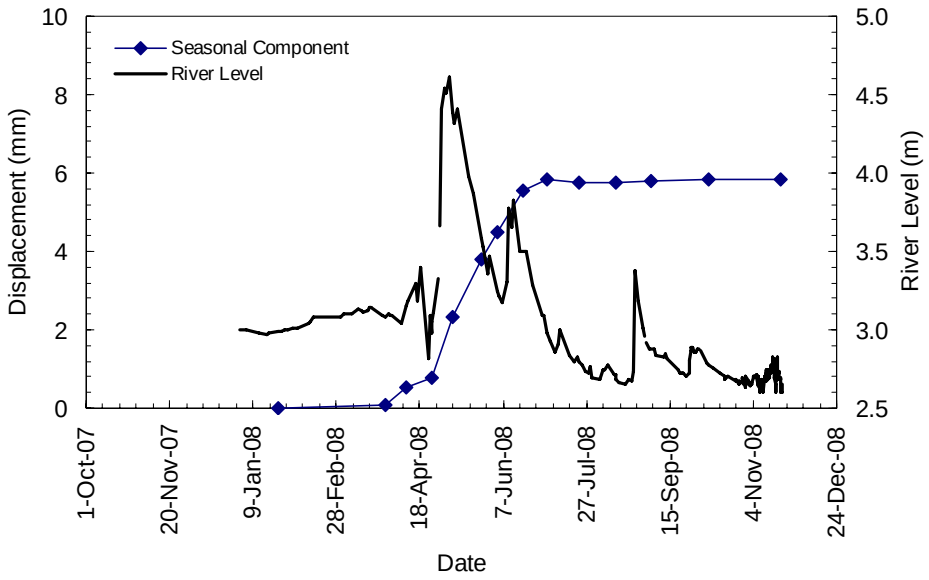

Figure 5-31: Seasonal Component of Displacement at Borehole TH07-W together with River Level Plotted against Time

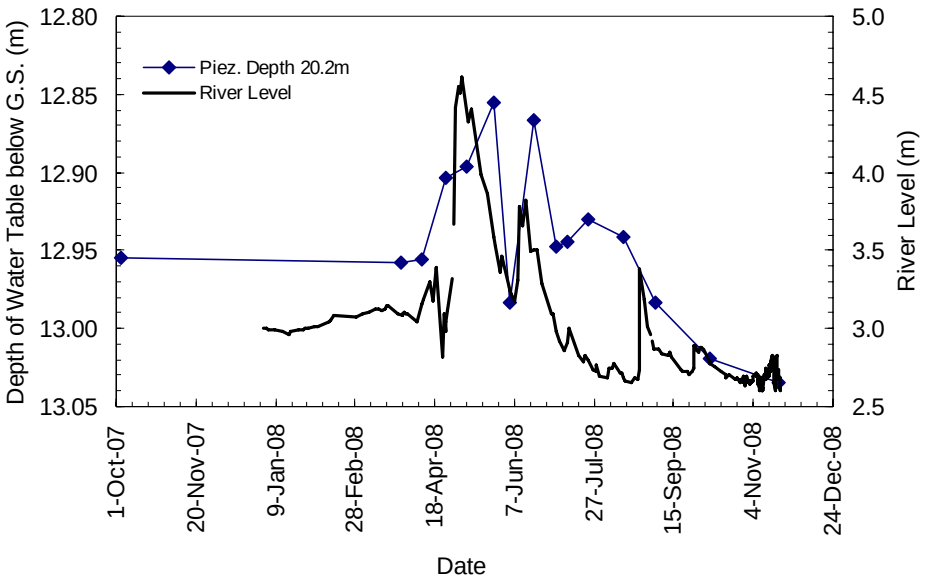

(a)

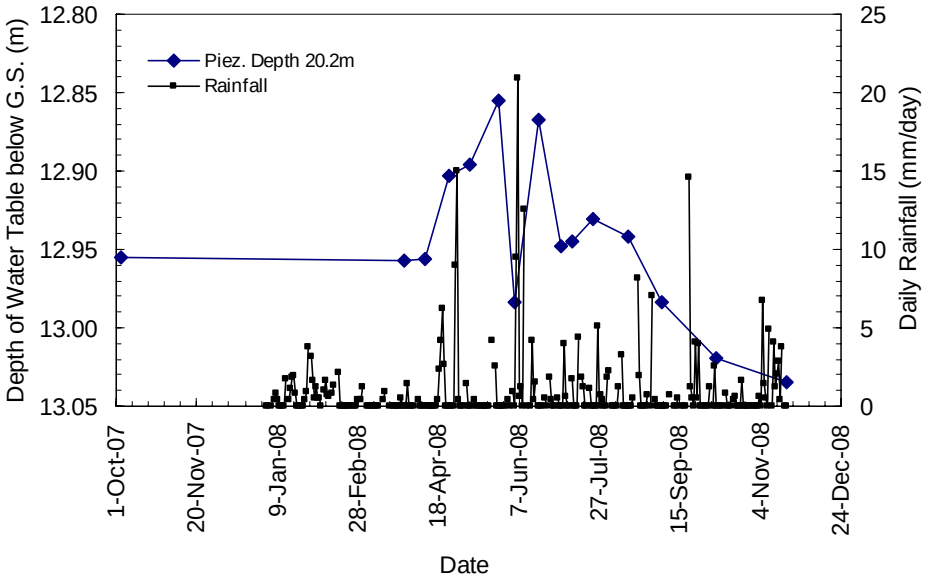

(b)

Figure 5-32: Piezometric Depth Variation with Time at Depth 20.2m in Borehole TH07-W together with (a) River Level Records and (b) Daily Rainfall Records

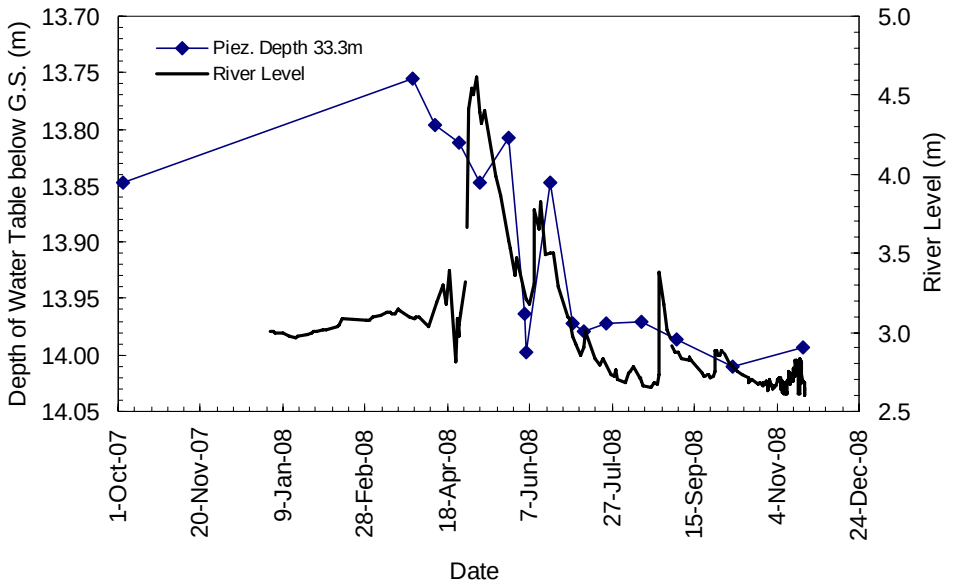

(a)

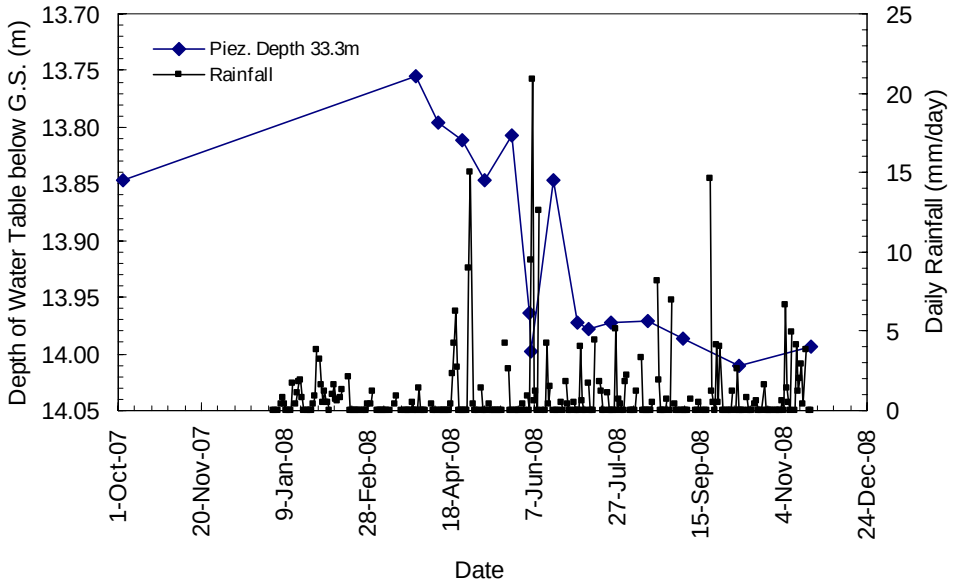

(b)

Figure 5-33: Piezometric Depth Variation with Time at Depth 33.3m in Borehole TH07-W together with (a) River Level Records and (b) Daily Rainfall Records

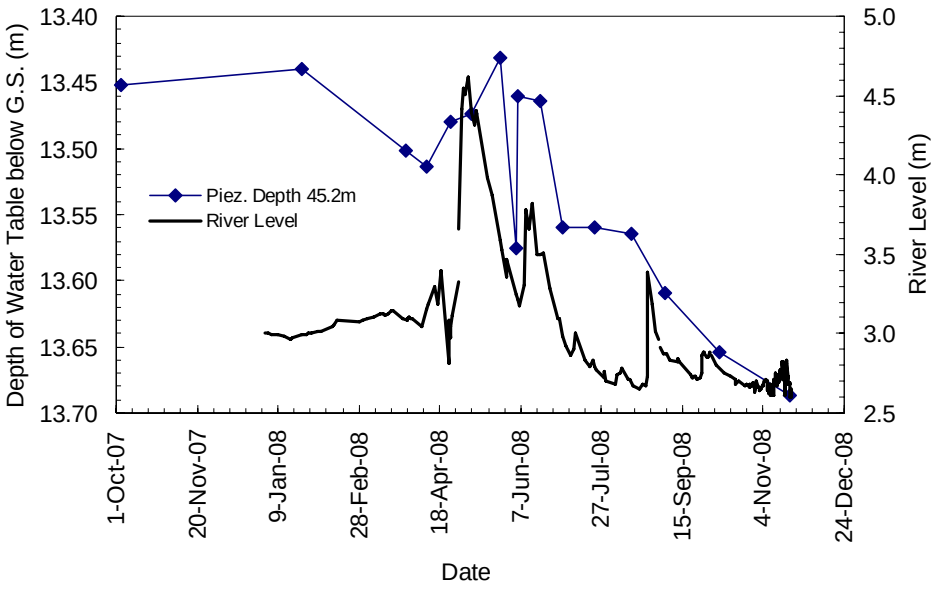

(a)

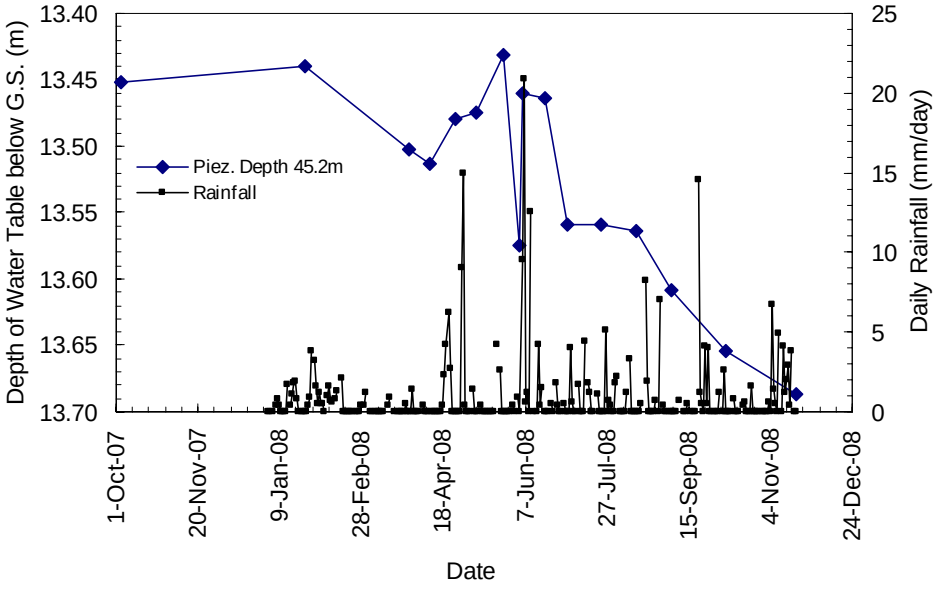

(b)

Figure 5-34: Piezometric Depth Variation with Time at Depth 45.2m in Borehole TH07-W together with (a) River Level Records and (b) Daily Rainfall Records

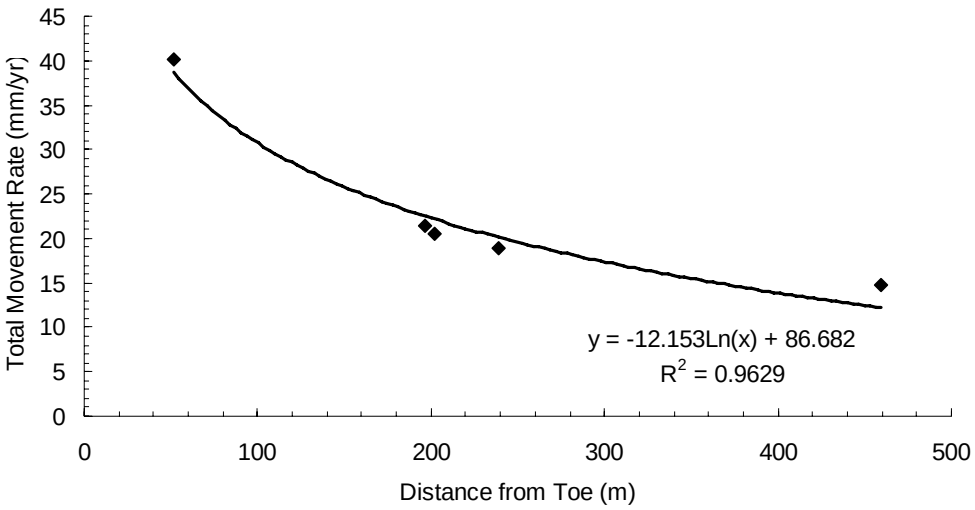

Figure 5-35: The Variation of Total Movement Rate with the Distance from the Toe of the West Slope

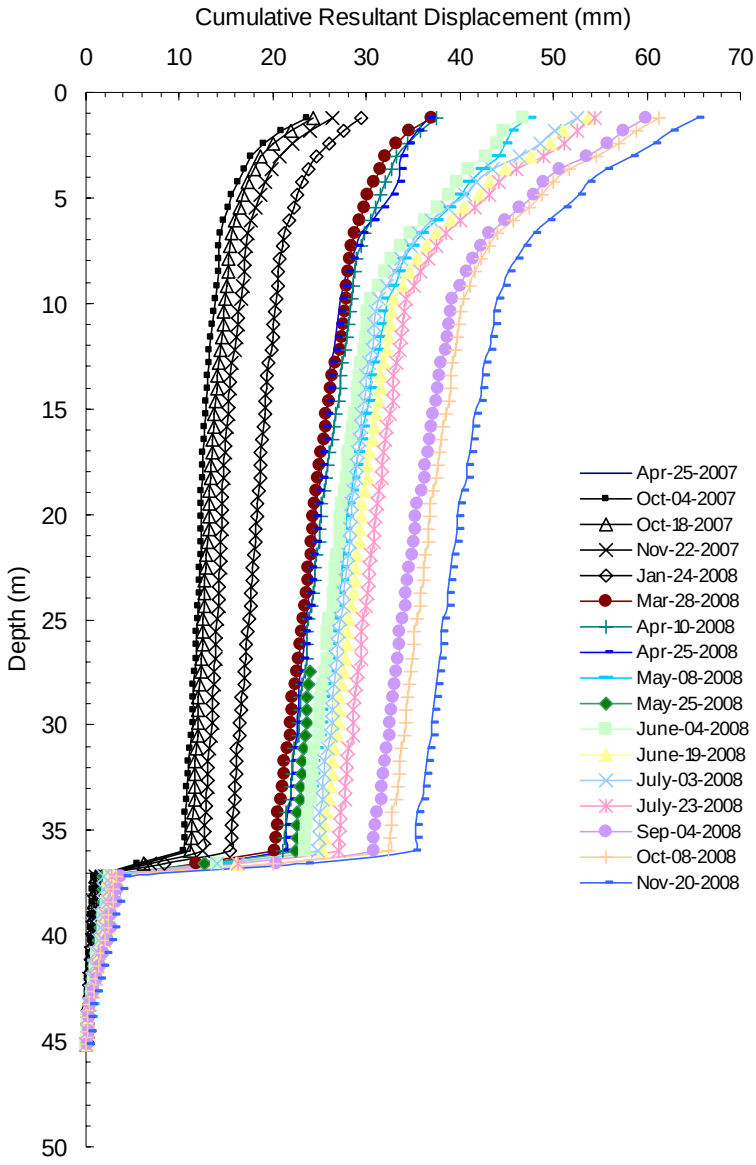

Figure 5-36: Cumulative Displacement Profiles at Borehole TH07-S in the South Slope

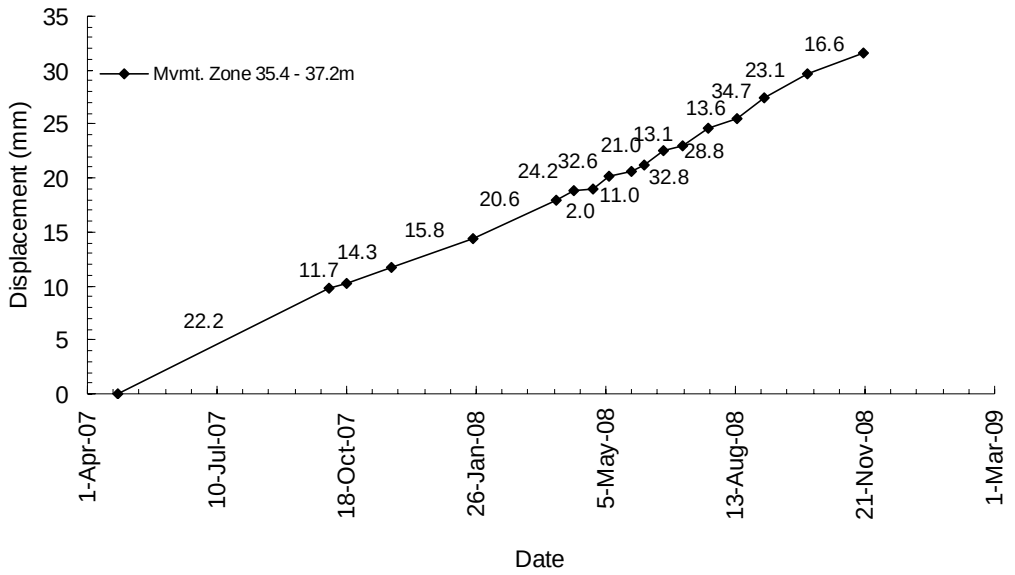

Figure 5-37: Displacement versus Time Plot of the Main Movement Zone at the Location of Borehole TH07-S with Displacement Rates Displayed in Units of mm/yr

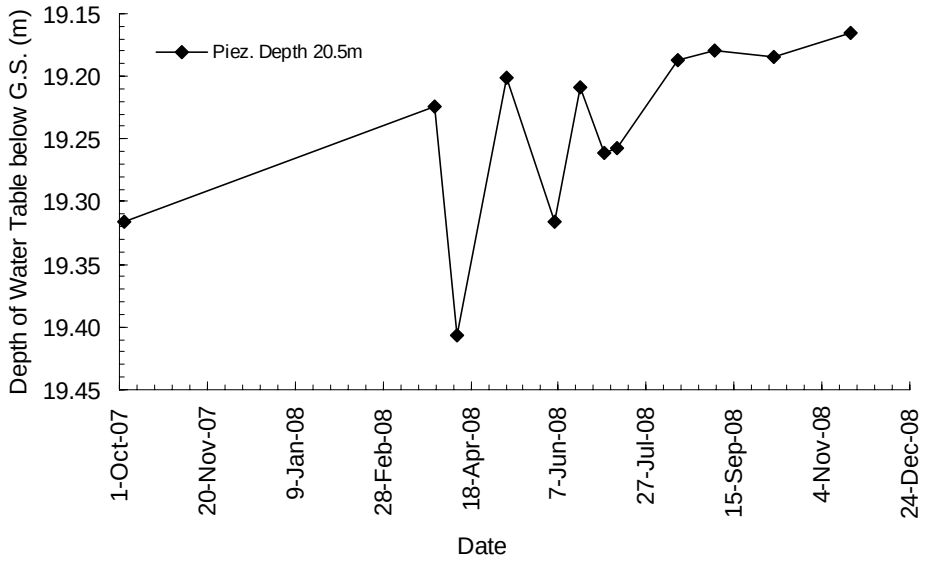

Figure 5-38: Piezometric Depth Variation with Time at Depth 20.5m in Borehole TH07-S

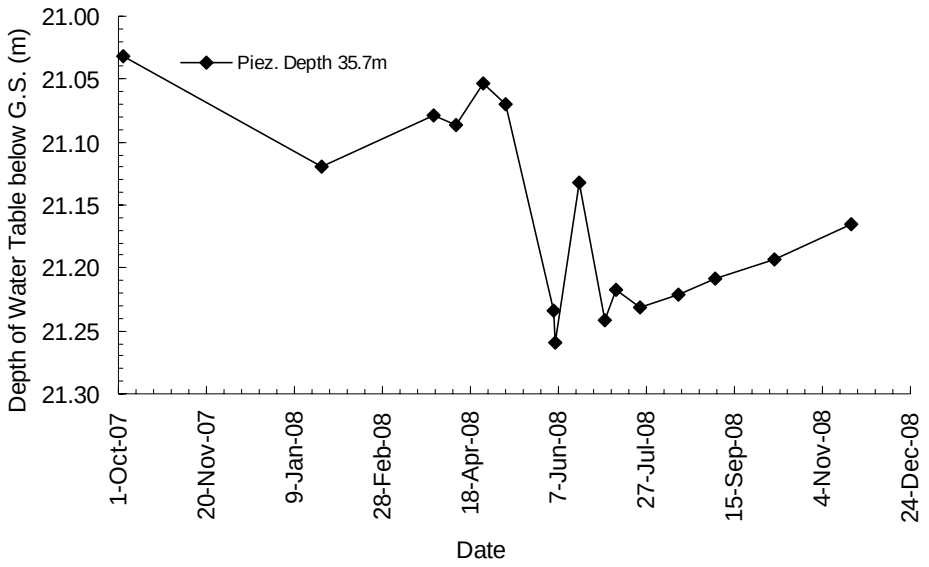

Figure 5-39: Piezometric Depth Variation with Time at Depth 35.7m in Borehole TH07-S

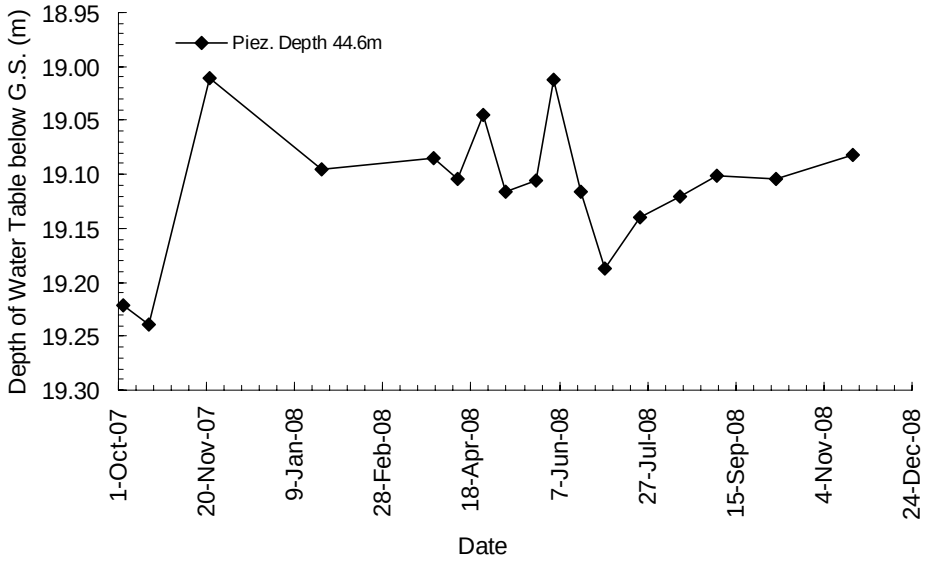

Figure 5-40: Piezometric Depth Variation with Time at Depth 44.6m in Borehole TH07-S

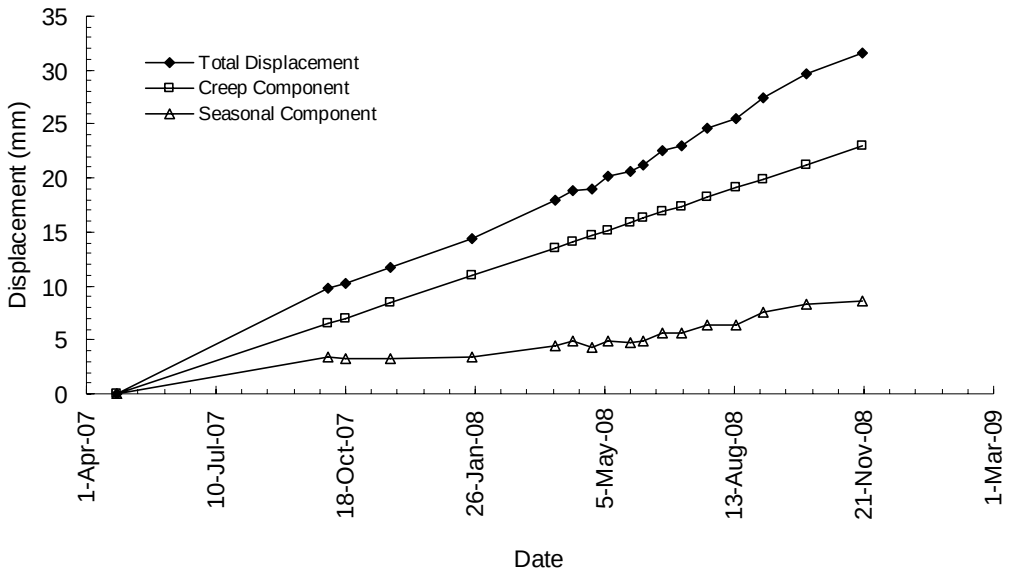

Figure 5-41: The Variation with Time of each of the Creep Component, the Seasonal Component and the Total Displacement at the Location of Borehole TH07-S

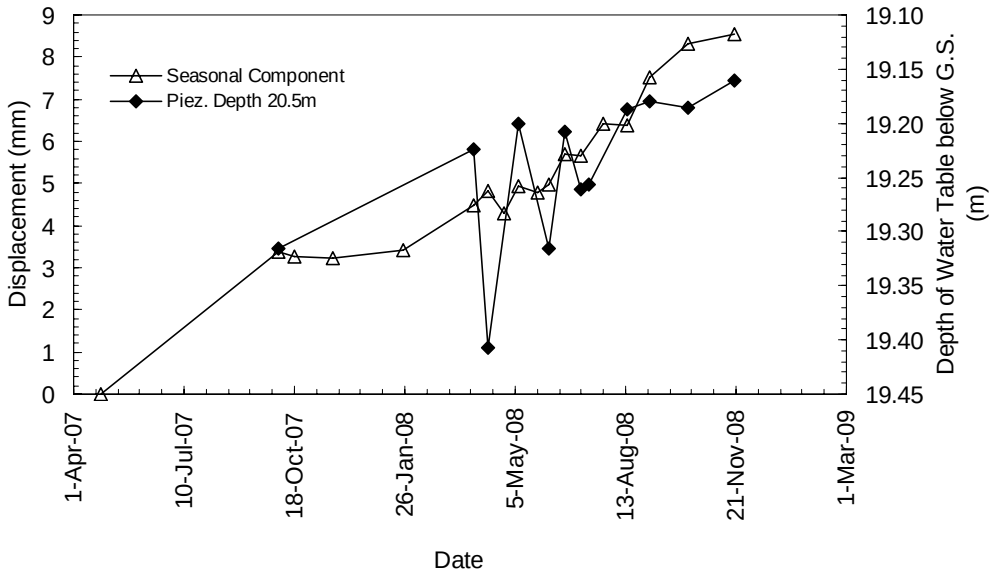

Figure 5-42: Seasonal Displacement and Piezometric Depth Variation with Time for the Piezometer Installed at Depth 20.5m in Borehole TH07-S

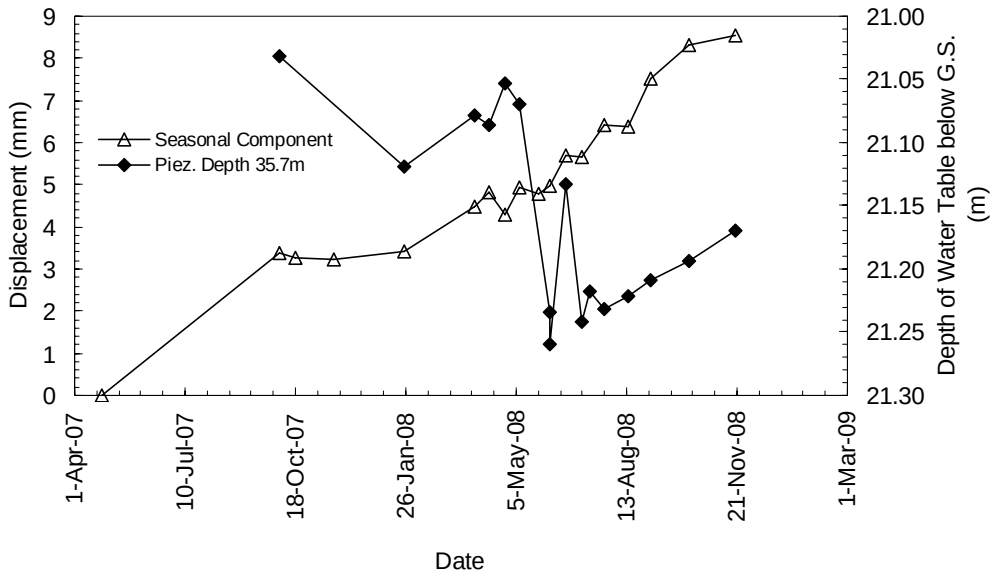

Figure 5-43: Seasonal Displacement and Piezometric Depth Variation with Time for the Piezometer Installed at Depth 35.7m in Borehole TH07-S

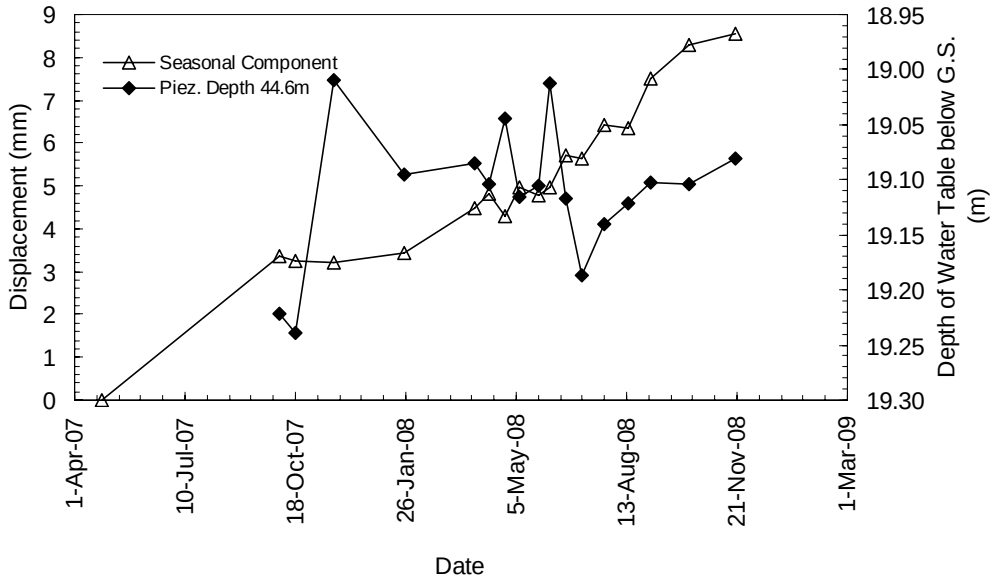

Figure 5-44: Seasonal Displacement and Piezometric Depth Variation with Time for the Piezometer Installed at Depth 44.6m in Borehole TH07-S

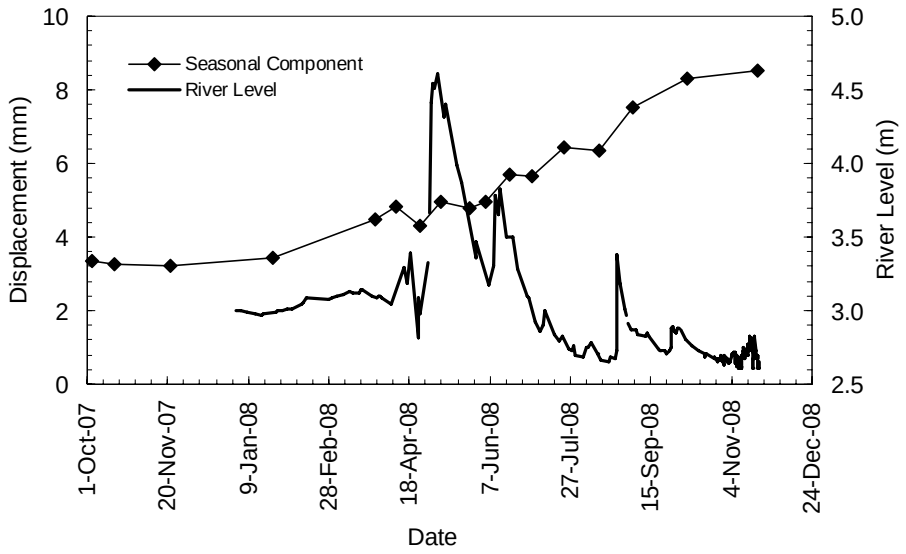

Figure 5-45: Seasonal Component of Movement at Borehole TH07-S together with River Level Plotted against Time

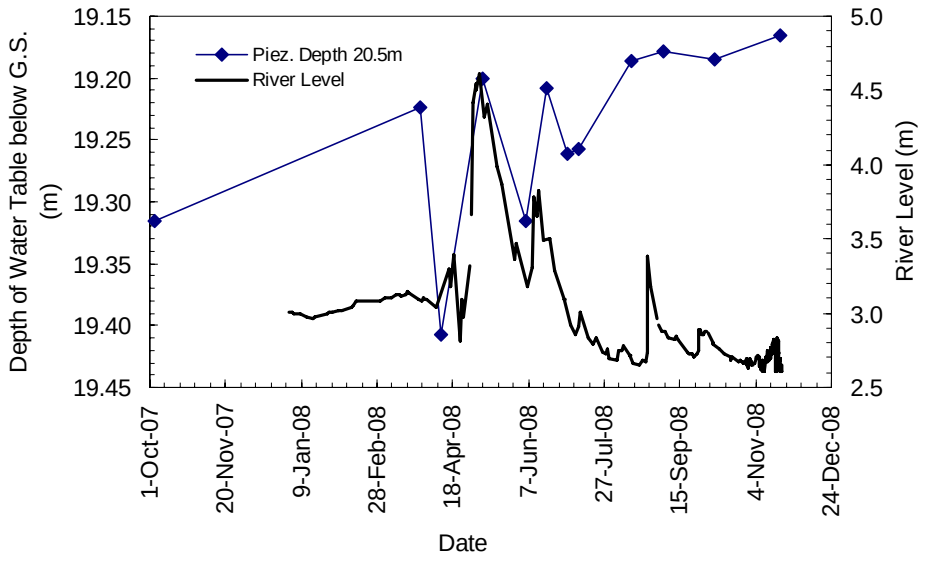

(a)

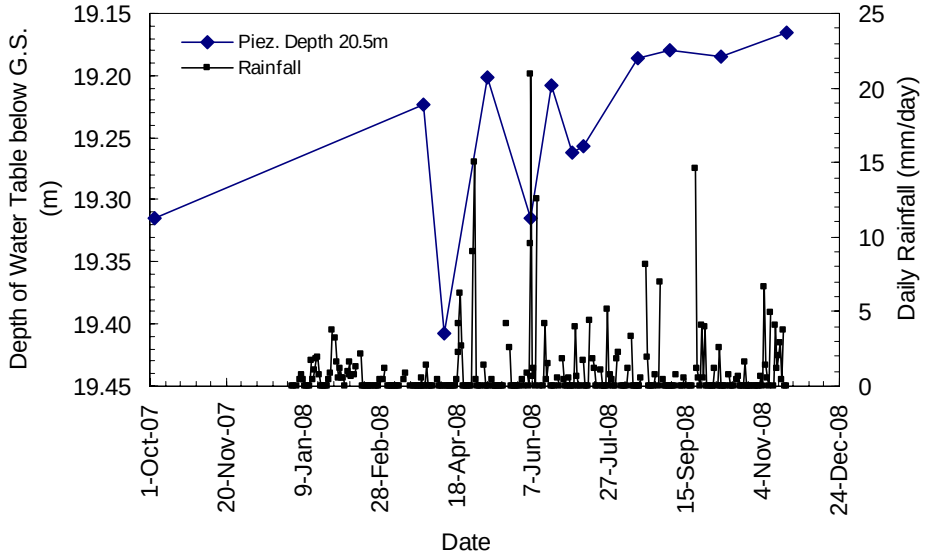

(b)

Figure 5-46: Piezometric Depth Variation with Time at Depth 20.5m in Borehole TH07-S together with (a) River Level Records and (b) Daily Rainfall Records

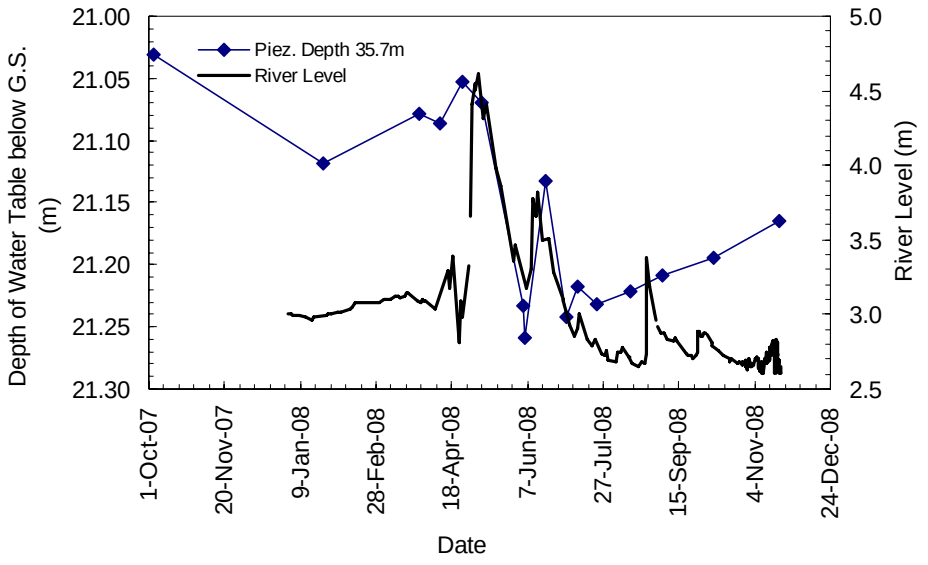

(a)

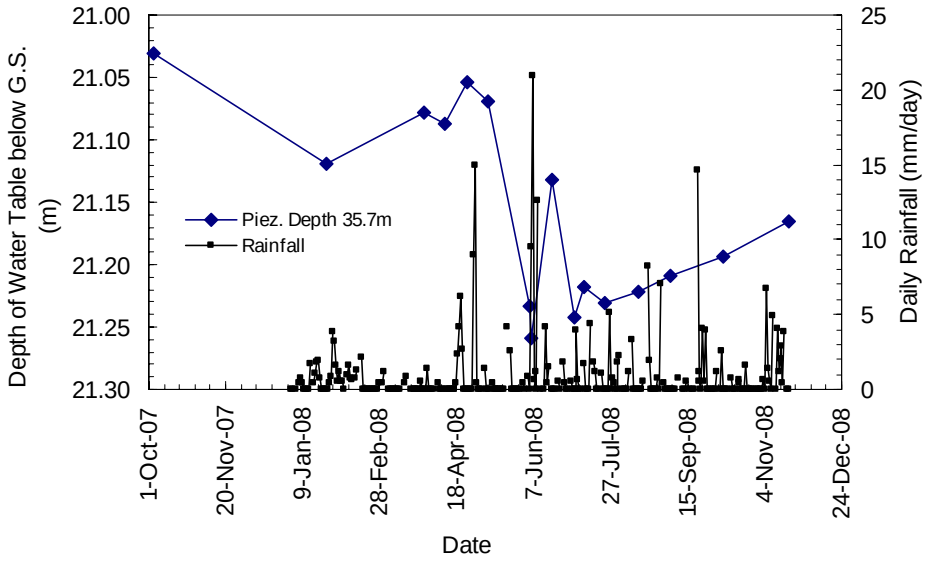

(b)

Figure 5-47: Piezometric Depth Variation with Time at Depth 35.7m in Borehole TH07-S together with (a) River Level Records and (b) Daily Rainfall Records

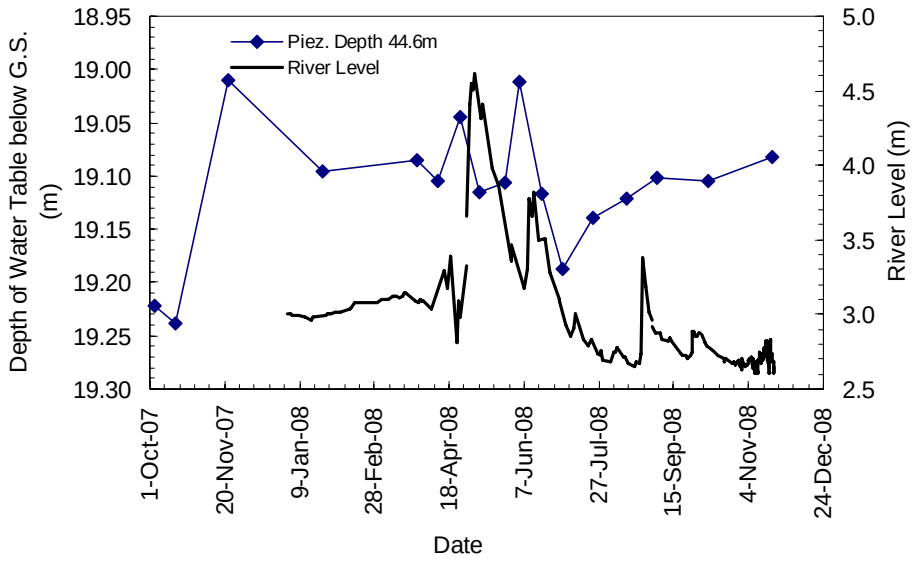

(a)

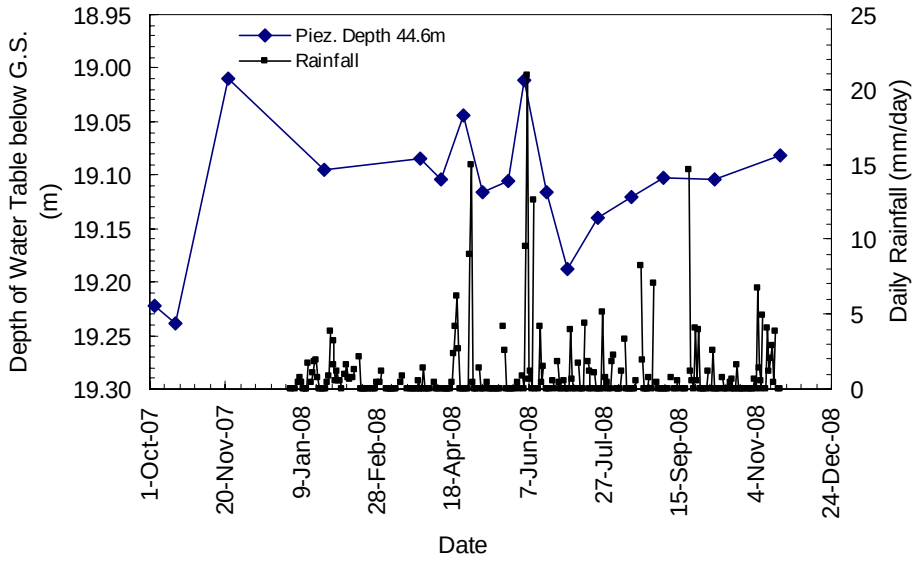

(b)

Figure 5-48: Piezometric Depth Variation with Time at Depth 44.6m in Borehole TH07-S together with (a) River Level Records and (b) Daily Rainfall Records

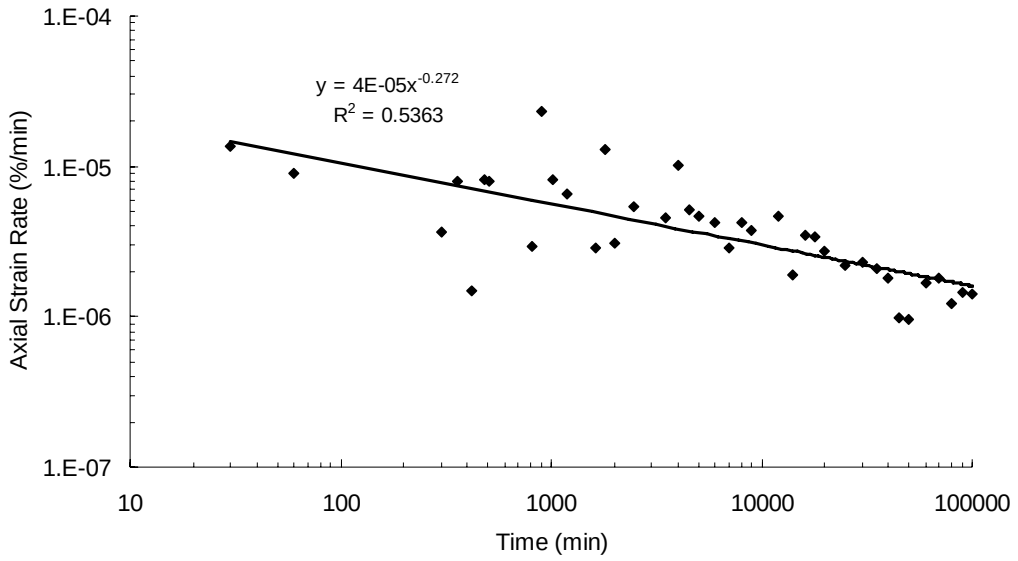

Figure 5-49: The Variation of Axial Strain Rates with Time on a Logarithmic Plot for a Sample Taken from the Main Movement Zone at Borehole TH07-S

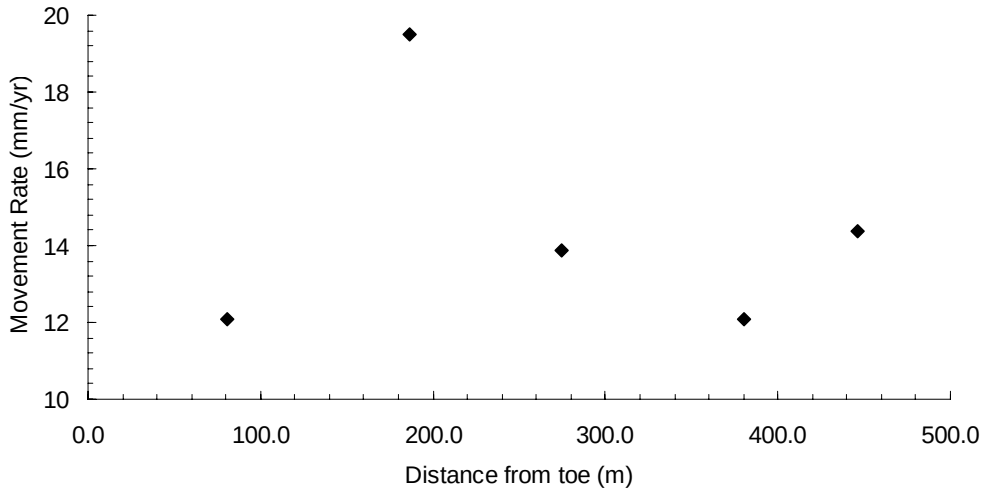

Figure 5-50: The Variation of the Total Movement Rate with the Distance from the Toe of the South Slope

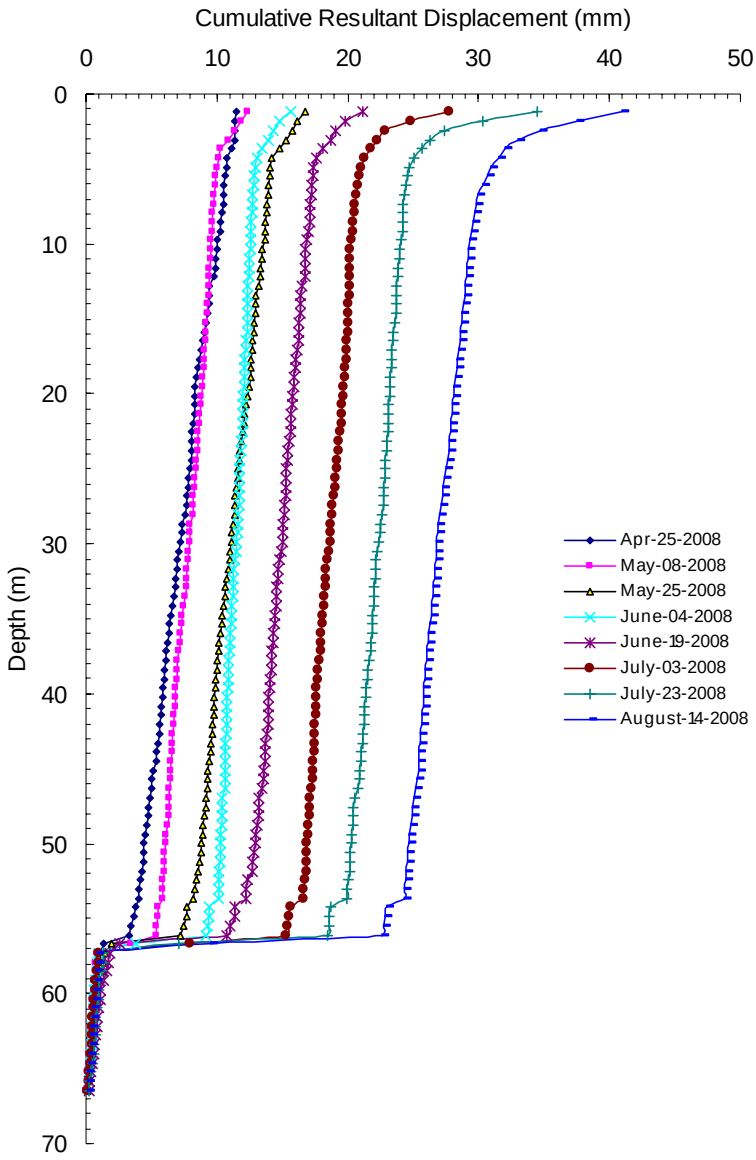

Figure 5-51: Cumulative Displacement Profiles at Borehole TH07-N in the North Slope

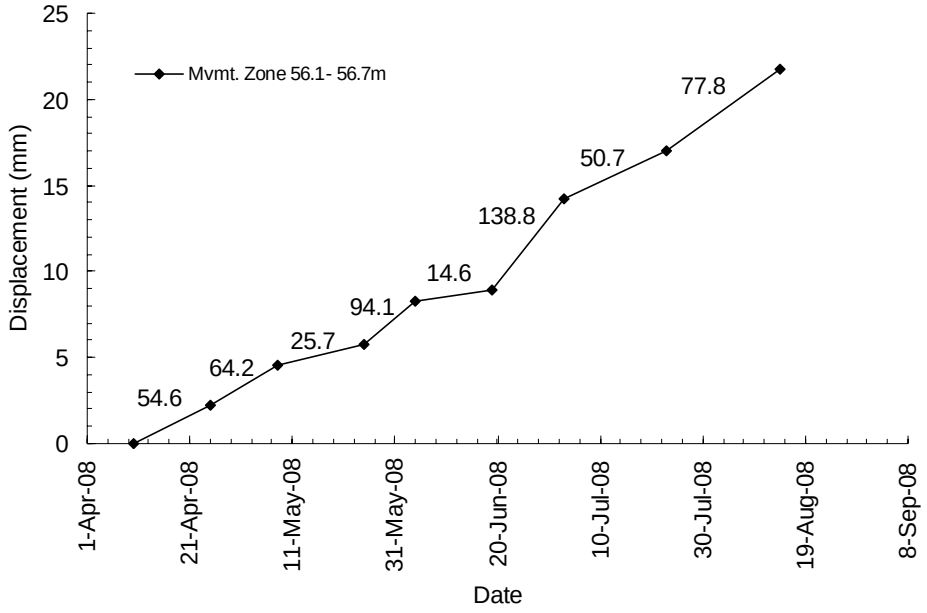

Figure 5-52: Displacement versus Time Plot of the Main Movement Zone at the Location of Borehole TH07-N with Displacement Rates Displayed in Units of mm/yr

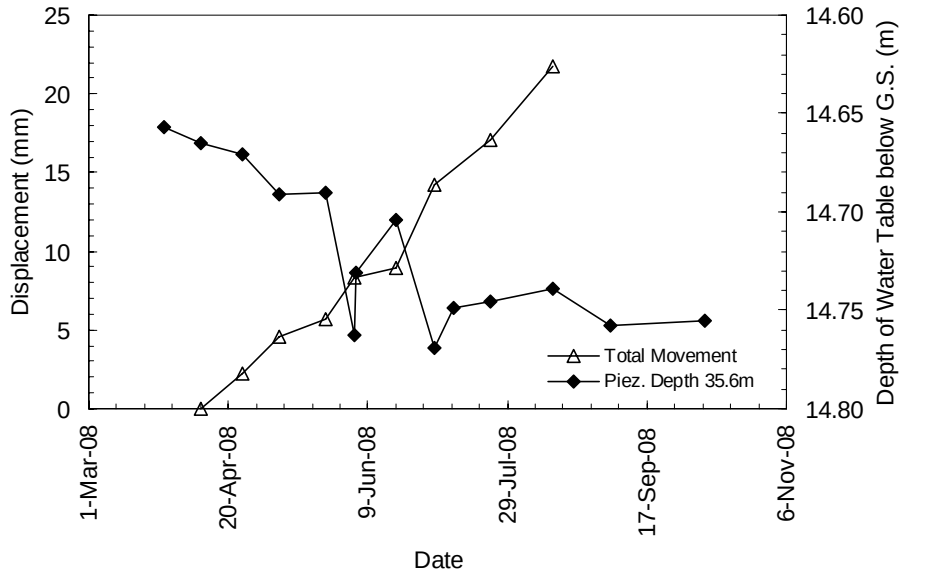

Figure 5-53: Total Movement and Piezometric Depth Variations with Time for the Piezometer Installed at Depth 35.6m in Borehole TH07-N

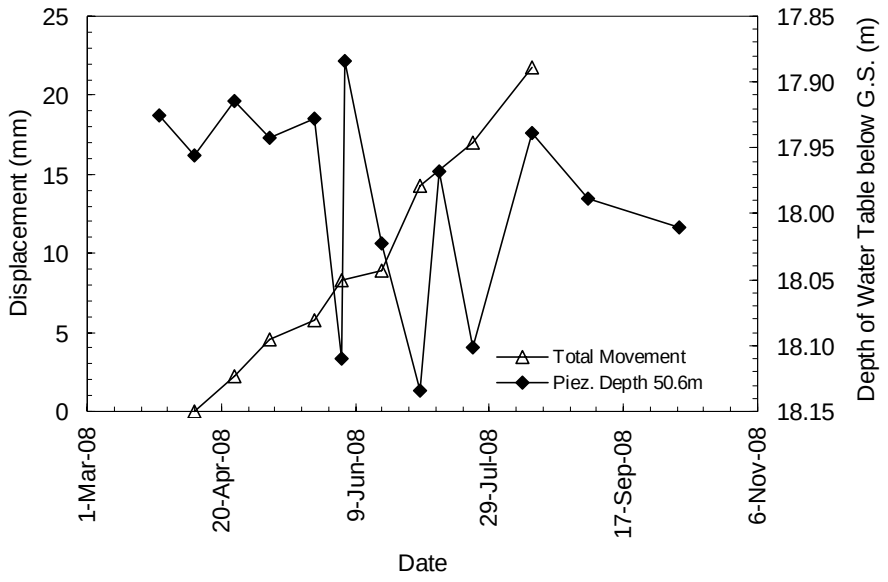

Figure 5-54: Total Movement and Piezometric Depth Variations with Time for the Piezometer Installed at Depth 50.6m in Borehole TH07-N

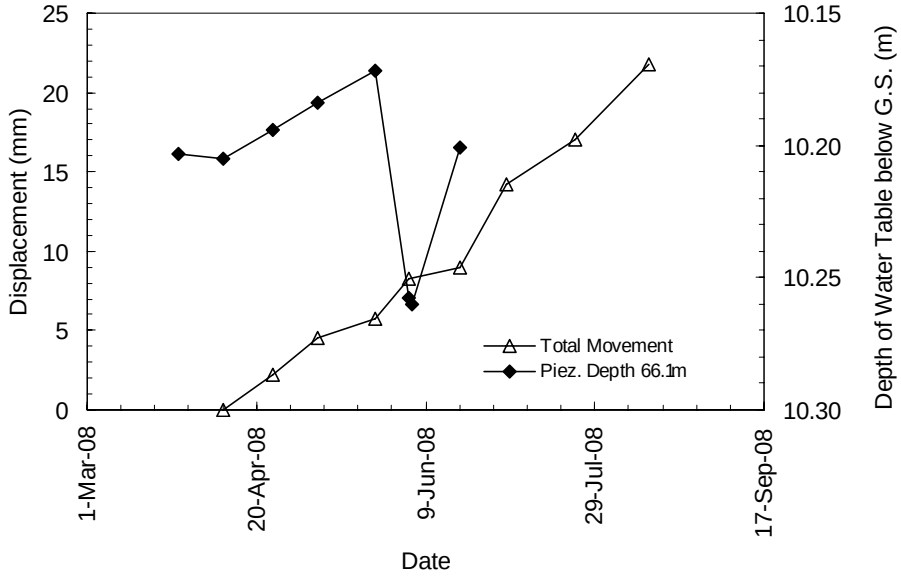

Figure 5-55: Total Movement and Piezometric Depth Variations with Time for the Piezometer Installed at Depth 66.1m in Borehole TH07-N

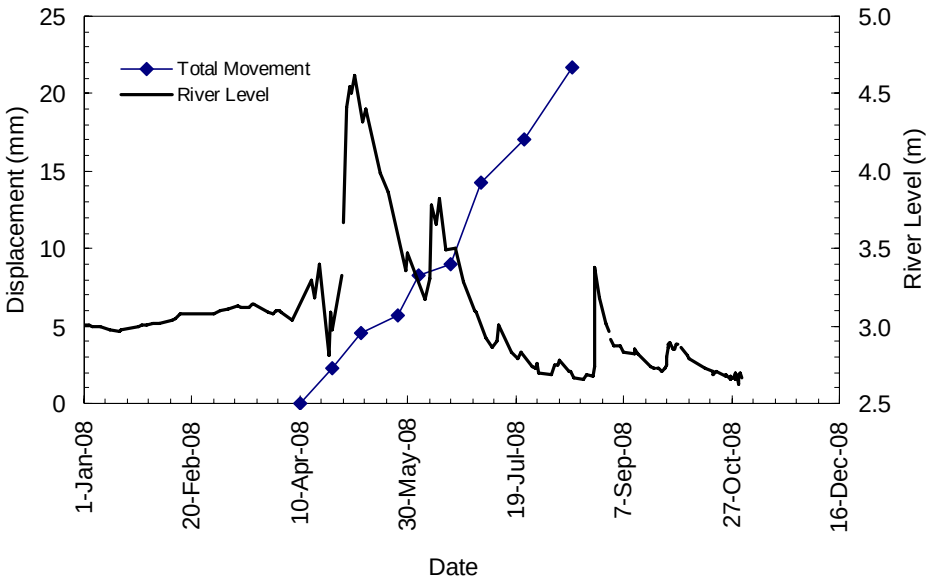

Figure 5-56: Total Movement at Borehole TH07-N together with River Level Plotted against Time

Figure 5-57: A View of the North Slope Bank from the West Slope Bank Showing the Effect of Toe Erosion at the West Slope

Figure 5-58: A Closer View of the North Slope Bank from the West Slope Bank Showing the Tilting of Trees at the Toe of the North Slope – Note the Gravel Island

Figure 5-59: An Exposure of the North Slope Toe

Figure 5-60: Another Exposure of the North Slope Toe showing Some Stratified Sediments

Figure 5-61: Block Samples of Sub-till Clays Obtained from an Exposure of the North Slope Toe. Varves Not Visible

Figure 5-62: A Closer View of the Sub-till Clay Samples Taken from the North Slope Toe

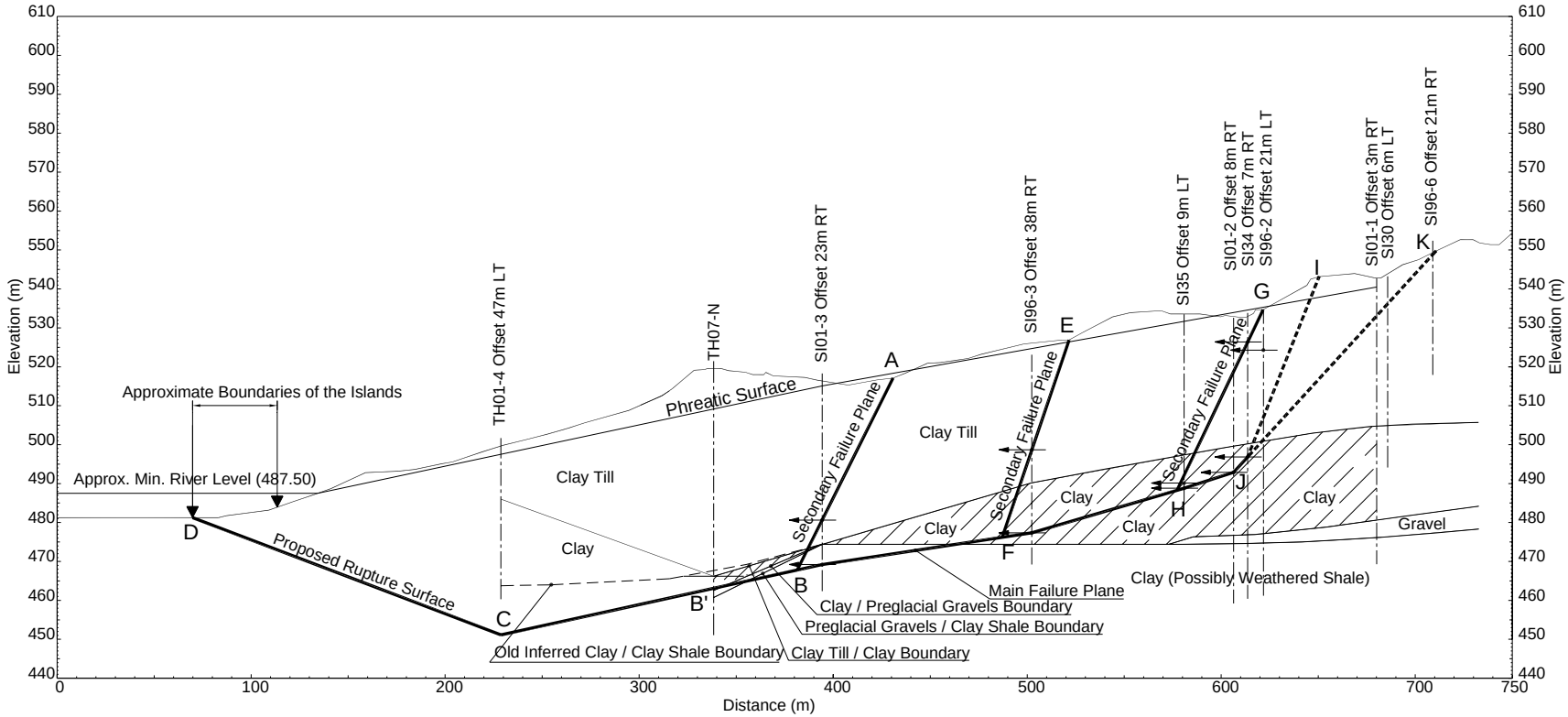

Figure 5-63: Proposed Rupture Surface Location Downslope Borehole TH07-N

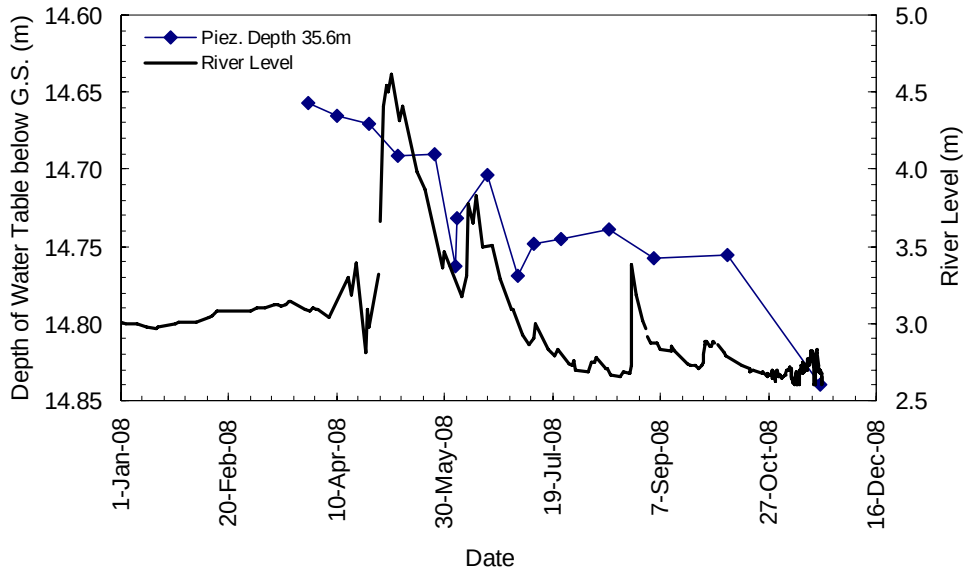

(a)

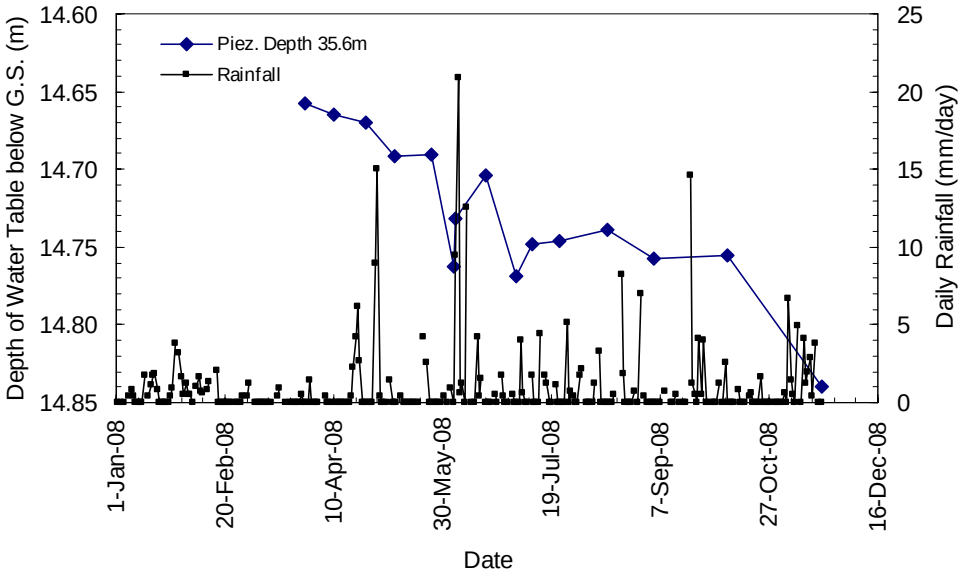

(b)

Figure 5-64: Piezometric Depth Variation with Time at Depth 35.6m in Borehole TH07-N together with (a) River Level Records and (b) Daily Rainfall Records

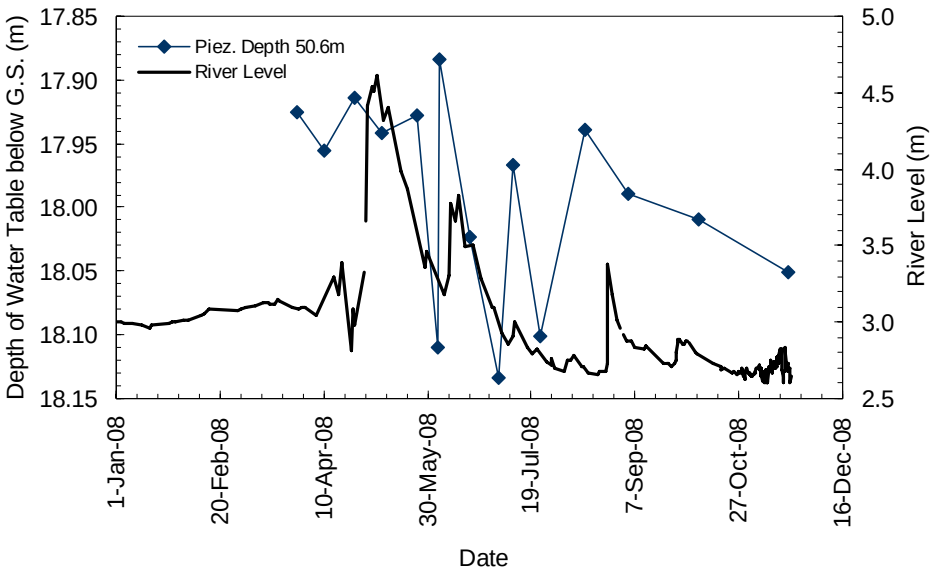

(a)

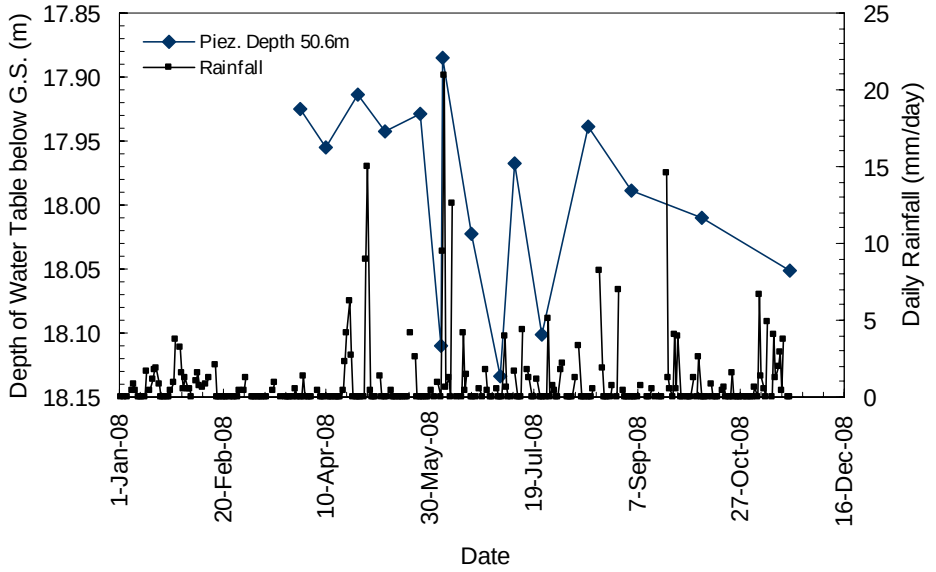

(b)

Figure 5-65: Piezometric Depth Variation with Time at Depth 50.6m in Borehole TH07-N together with (a) River Level Records and (b) Daily Rainfall Records

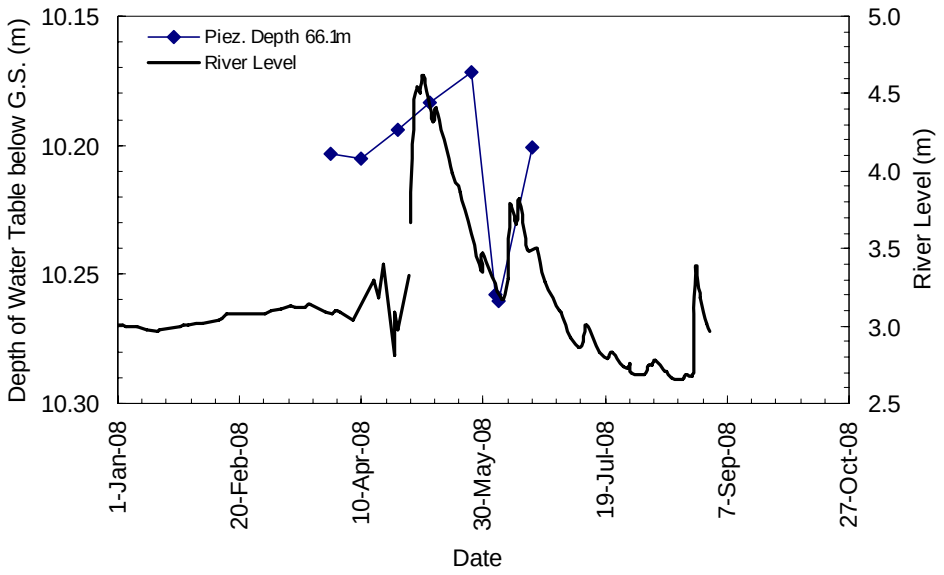

(a)

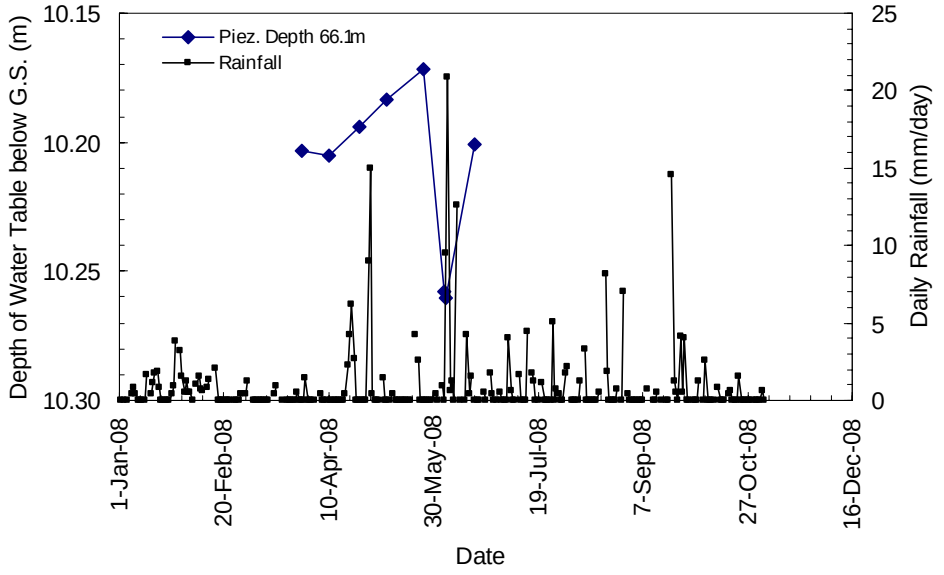

(b)

Figure 5-66: Piezometric Depth Variation with Time at Depth 66.1m in Borehole TH07-N together with (a) River Level Records and (b) Daily Rainfall Records

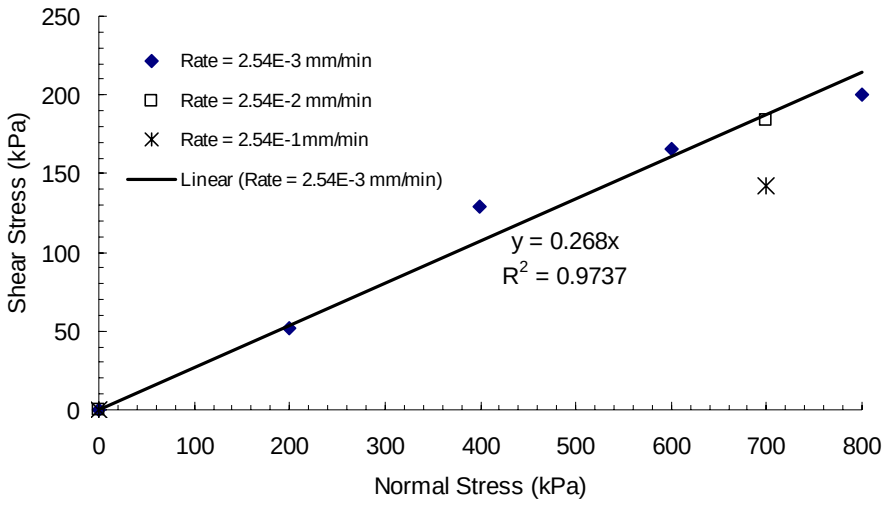

Figure 5-67: Direct Shear Tests Results on Clay Shale Samples from the South Slope

6 Summary, Conclusions and Recommendations for Future Research

6.1 Summary and Conclusions

The study is concerned with investigating the vulnerability and movement behaviour of slow moving slides. The term "slow slides" in the context encompasses extremely slow, very slow and slow slides that move at rates ranging from as low as few millimetres a year up to 13 meters per month. An extensive review of the literature is presented in Chapter 2 where the effects of pore pressure changes on the movement reactivation of shallow and moderately thick slides are presented. The time dependent behaviour of fine geotechnical materials is also reviewed. The review includes creep, rate effects and stress relaxation, but the creep behaviour is reviewed in more detail.

Vulnerability is one of two main components of landslide risk. The other component is the hazard probability. This study gives more insight into the vulnerability of different facilities to slow moving slides. More than fifty cases of extremely slow, very slow and slow slides adversely affecting urban communities, highways, railways, bridges, dams and linear infrastructure are reviewed. The average annual rate of movement and the degree of damage caused by the slide movements to the vulnerable facility are compiled. This extensive review shows, as expected, that the degree of damage becomes more severe with an increase in the slide velocity. This finding allows for the development of new damage scales that help to assess the vulnerability of a facility founded on a landslide-prone area, based on preliminary estimates of the movement rate. The developed scales will be a useful guide to engineers in the design phase of any structure on a landslide-prone area, because the proper mitigation measures can be designed and installed during construction. These measures will help to lower the associated risk.

The study of the movement behaviour involves the determination of all the causal factors that control the movement. This requires an adequate observation and investigation of the trend of the movement variation with time. The geomechanical behaviours of two typical deep-seated and moderately thick slides are investigated in this study.

The Little Chief Slide is a rock slide with movement taking place on soft movement zones composed mainly of micaceous clay gouges that contain slickensides. The movement zones are located at depths ranging from 100 to 300 meters. The slide is located about three kilometres north of the Mica Dam along the course of the former south-flowing Columbia River in British Columbia. The dam was constructed in the late sixties, and, hence, the Kinbasket reservoir was formed. The early investigations did not detect all the deep movement zones, but

revealed that the average rate of movement is 10 – 14 mm/yr based on surface movement monitoring. The most recent investigation started in 2005 with the purpose of developing adequate geomechanical and hydro-geological models. Piezometers and in-place inclinometers were installed in order to obtain continuous pore pressure and movement records. The groundwater flow regime of the Little Chief Slide is simulated by using a two-dimensional continuum seepage model as part of this research. The finite element-based code SEEP/W is utilized in the analysis. The seepage analysis proceeded in four steps; a steady state analysis for the initial conditions before the construction of the dam, a transient analysis for the effect of the reservoir filling on the groundwater pressures and two transient analyses for the effects of the rainfall and reservoir level fluctuations on the pore pressure variations with time.

The analyses results are compared with the actual measurements and show that the model is successful in establishing the initial in-situ conditions and in simulating the reservoir filling effect on the groundwater pressures. The reservoir filling does not have any effect on the water table for locations further than 1000 meters from the reservoir shoreline. Due to the huge dimensions of the slope, the model ceases to model the effect of thin inward dipping shear bands on the groundwater regime. Regarding the effects of the reservoir fluctuations and rainfall, the model can predict only 30 to 65% of the measured ranges in the field. However, the model is capable of correctly simulating the trend of the piezometric elevation variation with time and, hence, of detecting the zones where the pore pressure response is dominated by either the reservoir level fluctuations or rainfall. The results of the numerical analysis show that the reservoir level fluctuations have a dominant effect on the pore pressure response at the locations close to the slope toe. At the locations far upslope, however, the pore pressures are dependent mainly on the infiltration rate.

The in-place inclinometer displacement records at six movement zones are analyzed in order to investigate the movement behaviour, i.e., to investigate whether the movement proceeds at a constant rate irrespective of the pore pressure changes or follows an annual cycle. The movement records analysis took into account the outcome of the numerical seepage analyses, which define the zones of influence of each of the rainfall and reservoir level fluctuations on the pore pressure changes. The movement records analysis results show that the movement sometimes proceeds during periods of zero pore pressure changes, i.e., under constant effective stresses. Hence, this movement is due to creep deformation. Creep contributes to as little as 25% and as much as 100% of the total movement of the Little Chief Slide at different movement zones. The other components of the movement are due to the pore pressure changes that occur in response to the infiltration and/or reservoir level fluctuations, and due to forces acting on the slide like lateral water pressures in the tension cracks and water ponding. The contribution of creep to the total movement is about 25 – 50% at the movement zones further than 1000m upslope from the reservoir shoreline. The contribution increases to 90% at locations near the reservoir shoreline. The

average contribution of creep is 73%. The important conclusion is that the application of any drainage measures may be efficient only at upslope locations where the creep contribution is the lowest and the seasonal effects are the highest. The separation of the total movement vector into individual components is important to estimate the future reduced movement rates after the implementation of the suitable mitigation measures.

The creep behaviour of the soft materials forming the movement zones of the Little Chief Slide is investigated in the laboratory in order to develop a governing equation and to compare the field and laboratory creep behaviours. A triaxial drained creep testing program is carried out on some of the available cores. Creep behaviour is investigated by subjecting the samples to constant effective stresses for periods of time lasting for three weeks in some cases. The results show that the axial strain rates drop with time possibly according to a power law and increase with deviatoric stress level possibly according to an exponential function. Hence, the creep behaviour of the Little Chief Slide movement zones could be represented by the three-parameter Singh-Mitchell equation (Singh and Mitchell, 1968). The field creep strain rate of one of the movement zones is comparable to the minimum laboratory creep strain rate after which the strain accelerates. In addition, the field shear stress level is approximately equal to the laboratory deviatoric stress level that causes strain acceleration. This observation indicates that there is a possibility of a localized movement acceleration of the Little Chief Slide even if the applied mitigation measures can keep the piezometric levels at minimum values. However, this conclusion is based on the investigation of the field and laboratory creep behaviours of one movement zone only. The lack of suitable cores from other movement zones for triaxial testing does not allow for further investigations.

The geomechanical behaviours of the Little Smoky valley north, west and south slides are also investigated in detail. The slides lie at the intersection of Highway 49 with the Little Smoky River in Alberta. The bridge carrying Highway 49 across the north-flowing river was completed in 1957. Slope movements occurred after the bridge construction. The stability of the west valley slope was studied in the late sixties. Slope movements and pore pressures were monitored, and limit equilibrium analyses were carried out. Movement rates up to 100mm/yr were recorded. The study concluded that the movement was retrogressive and was triggered by toe erosion. The south and the north valley slopes movements and pore pressures were monitored between 2001 and 2005. Readings were taken semi-annually, so a general picture of the movement rates of these slopes and their acceleration times was drawn. The average annual movement rates of the south and north valley slopes were 15 – 20 and more than 45 mm/yr, respectively. The locations of the main and secondary movement zones were determined, and the groundwater flow regime was understood. However, no quantification of the effect on the movement of the different causal factors was obtained.

The most recent investigation started in 2007 as part of this research. It involved monitoring the displacements and pore pressures at small time intervals at three boreholes drilled into the west, south and north slopes. The geological cross-sections of the three slopes are updated. A nearly complete annual cycle of readings is acquired. The movement and pore pressure records are plotted against each other and against the river level and daily rainfall records. It was found that the location of the main rupture surface is controlled by one of three stratigraphic settings: (1) the preglacial lake clays as in the north slope, (2) the interface between the overlying till or preglacial lake clays and bedrock as in the south slope, or (3) the upper layer of the clay shale, which is usually weakened by weathering as in the west slope. This conclusion is in accordance with previous investigations of the interior plains slides.

The analysis of the movement and pore pressure records indicates that the movement proceeds during the periods when the pore pressure changes are essentially zero. Hence, this movement is due to creep deformations. Creep contributes to about 15.6mm/yr of the west slope movement and 14.6mm/yr of the south slope movement. The contribution of creep to the total movement of the north slope is assumed to have an average value of 15.1mm/yr because the monitoring period did not include times at which the effective stress is nearly constant.

Seasonal movements also take place and are partially triggered by pore pressure changes due to the rainfall and/or river level fluctuations. This component exists in the three slopes with the same value as long as the distance of the point of interest from the slope toe is equal. This component might be due to a river level drawdown mechanism at the north slope only. Based on the records of the movement, pore pressures and hydrological conditions in 2008, this component contributes to 6 – 15% of the total movement of the Little Smoky Slides.

A fraction of the seasonal movements is triggered by toe erosion. This component exists in the three slopes with varying magnitudes. The toe erosion component is higher in the west slope than in the south slope because the west slope lies downstream from the bridge. The highest contribution of toe erosion is at the north slope due to the existence of a confined flow condition at the toe of the slope. Based on the records of the movement, pore pressures and hydrological conditions in 2008, this component contributes to 26% and 59% of the total movement of the Little Smoky west and north slides, respectively.

Seasonal movements could also be triggered by water ponding on the slope surface and lateral water pressures in the tension cracks. However, the available piezometric and hydrological records allow only for correlating the seasonal movements to pore pressure changes and toe erosion.

The seasonal movements of the west, south and north slopes contribute to 61%, 15% and 65% of the total movement, respectively. The installation of the suitable

mitigation measures would reduce the movement of the Little Smoky valley slopes to a minimum rate of about 15mm/yr.

The quantification of the contribution of the different causal factors to the total movement of the two studied slides has important practical implications. If the total movement records are strongly correlated to the pore pressure records or hydrological data, for example, this does not mean that the movement will be arrested after applying the proper mitigation measures, like drainage measures or toe armours. The movement slows down to a minimum rate that equals the creep deformation rate of the material forming the rupture surface.

Therefore, the outcome of the study provides guidelines for estimating the expected future reduced movement rate of the slide when the implemented mitigation measures bring the pore pressure changes to zero. This reduced value is the creep deformation rate of the materials forming the rupture surface, as mentioned above. The laboratory triaxial creep tests carried out in this study on samples from the Little Chief Slide movement zones and the south Little Smoky Slide showed a good match between the field creep rates and the laboratory minimum strain rates. However, the initial time of the field creep movements is totally different from the initial time of the laboratory creep strains, which is usually set to unity. More investigations are needed before laboratory creep tests can be used to evaluate field creep rates.

6.2 Recommendations for Future Research

The conclusions of the study are of significance for engineers dealing with slow moving slides problems. Recommendations for future research are presented in this section in order to gain more understanding of more aspects of the problem. The proposed recommendations are summarized in the following points:

1. The groundwater flow regime of the Little Chief Slide is numerically simulated by a two-dimensional continuum seepage model. The model is considered partially successful in modeling the flow regime. The drawbacks arise from the assumption of plane flow conditions, the disregard of both the discontinuity of the domain at some locations and the effects of thin inward dipping shear zones, and the uncertainty about the variation of the volumetric water content and hydraulic conductivity functions with suction. A more complicated and advanced numerical model may be able to overcome these issues. Once the model is developed and calibrated, the future trends of pore pressure variation with time in response to hydrological boundary conditions changes can be predicted based on historical records.

2. The deduced movement behaviour of both slides is based on observing the trends of the measured movement and pore pressure data. Numerical

simulation of the movement variation with time will give more confidence in the deduced behaviour and will allow for the determination of the movement based on the pore pressure input and the creep parameters of the materials forming the rupture surface. The constitutive model of the materials forming the rupture surfaces should, however, account for time effects; i.e., the constitutive model should be a stress-strain-time model. Usually, the limited number of measurements taken in the field and the difficulty in simulating the toe erosion effect on movement reactivation are the main challenges facing the development of such models.

3. The laboratory creep behaviour of the soft materials forming the movement zones of the Little Chief Slide may obey the Singh-Mitchell equation (Singh and Mitchell, 1968). The effect of the confining stress on the axial strain rate behaviour is examined in this study by testing three samples only, and no clear trend was found. Testing a larger number of samples may result in developing a modified equation with confining stress-dependent parameters. In addition, some anomalies in the responses of the specimens shortly after the application of the deviatoric stress increments should also be examined in more detail.

4. The quantification of the contribution of different components of the movement of the two studied slides shows a higher contribution of creep to the total movement in deep-seated slides as expected and vice versa in moderately thick slides. The investigation and analysis of more slow moving slides in the same way will help to develop an inventory containing all the attributes of different types of slow slides, so the movement behaviour can be preliminarily evaluated based on estimates or few measurements of the total movement.

5. The extensive review presented in Chapter 3 of this thesis on the vulnerability of different facilities to slow moving slides has aided in the development of new scales showing the degree of damage expected from various movement rates. The inclusion of more cases will help to improve and refine the developed scales. This needs to be considered in future research.

References

Abdel-Hady, M., and Herrin, M. 1966. Characteristics of Soil-Asphalt as a Rate Process. Journal of the Highway Division, ASCE, **92**(HW1): 49 – 69.

Air Photo Distribution Office, Edmonton, Alberta, CANADA. http://www.srd.gov.ab.ca/land/g_airphotos.html

Alberta Infrastructure, 1998. Little Smoky Bridge Rehabilitation – General Layout. File 74440, Sheet 1 of 33, Drawing no. 17553-C.

Angeli, M. G., Gasparetto, P., Menotti, R. M., Pasuto, G., and Silvano, S. 1996. A Visco-plastic Model for Slope Analysis Applied to a Mudslide in Cortina d'Ampezzo, Italy. Quarterly Journal of Engineering Geology, **29**: 233 – 240.

Augustesen, A., Liingaard, M., and Lade, P. V. 2004. Evaluation of Time-Dependent Behavior of Soils. International Journal of Geomechanics, ASCE, **30**(3): 137 – 156.

Ayra, L.M., and Paris, J.F. 1981. A Physico-empirical Model to Predict the Soil Moisture Characteristic from Particle-size Distribution and Bulk Density Data. Soil Science Society of America Journal, **45**:1023-1030.

Bai, J., Lu, S. and Han, J. 2008. Importance of Creep Sliding Mechanism to Prevention and Treatment of Reservoir Landslide. In Chen et al. (eds.). Proceedings, 10th International Symposium on Landslides and Engineered Slopes, Xi'an, China, **2**: 1071 – 1076.

Bala, G. and Proudfoot, D. W. 2007. HWY 49:12 – Little Smoky River (SH3 and SH4) Geotechnical Investigation. Report to Alberta Infrastructure and Transportation. Thurber Engineering Ltd., Edmonton, Alberta. File 15 – 85 – 62.

Barlow, J. P. 2000. Slope Movement Patterns in Young Valley Slopes in Northern Alberta, Canada. Landslides in Research, Theory and Practice. In Bromhead et al. (eds.). Proceedings, 8th International Symposium on Landslides, Cardiff, UK, **1**: 113 – 120.

Barlow, P., McRoberts, E., and Tenove, R. 1991. Stabilization of Urban Landslides in Peace River, Alberta. Proceedings, 43rd Canadian Geotechnical Conference, **1**: 85 – 90.

Barton, M. E. and McCosker, A. M. 2000. Inclinometer and Tiltmeter Monitoring of a High Chalk Cliff. Landslides in Research, Theory and Practice. In Bromhead et al. (eds.). Proceedings, 8th International Symposium on Landslides, Cardiff, UK, **1**: 127 – 132.

Beaumont, D. and Forth, R. A. 1996. The History of Slope Instability of an Embankment in County Durham, England. Landslides. In Senneset (ed.). Proceedings, 7th International Symposium on Landslides, Balkema, Rotterdam, **2**: 629 – 635.

Bell, R., Thiebes, B., Glade, T., Becker, R., Kuhlmann, H., Schauerte, W., Burghaus, S., Krummel, H., Janik, M. and Paulsen, H. 2008. The Technical Concept within the Integrative Landslide Early Warning System (ILEWS). In Chen et al. (eds.). Proceedings, 10th International Symposium on Landslides and Engineered Slopes, Xi'an, China, **2**: 1083 – 1088.

Berre, T. and Bjerrum, L. 1973. Shear Strength of Normally Consolidated Clays. Proceedings of the Eighth International Conference on Soil Mechanics and Foundation Engineering, Moscow, **1**: 39 – 49.

Bhuyan, G. S. 2006. Little Chief Slide – Laboratory Testing. In P. Rapp, 2006. Mica Dam – Little Chief Slide, 2005 Field Investigation Report. Engineering Report no. E434.

Bishop, A. W. and Lovenbury, H. T. 1969. Creep Characteristics of Two Undisturbed Clays. Proceedings, 7th International Conference on Soil Mechanics and Foundation Engineering, Mexico, **1**: 29 – 37.

Bjerrum, L. 1967. Engineering Geology of Normally-Consolidated Marine Clays as Related to Settlements of Buildings. Seventh Rankine Lecture, Geotechnique, **17**(2): 82 – 118.

Blikra, L. H. 2008. The Aknes Rockslide: Monitoring, Threshold Values and Early Warning. In Chen et al. (eds.). Proceedings, 10th International Symposium on Landslides and Engineered Slopes, Xi'an, China, **2**: 1089 – 1094.

Bonnard, Ch., Mayoraz, F. and Noverraz, F. 2000. Monitoring Principles of Civil Works Located in Landslide-Prone Areas. Landslides in Research, Theory and Practice. In Bromhead et al. (eds.). Proceedings, 8th International Symposium on Landslides, Cardiff, UK, **1**: 145 – 150.

Bonnard, Ch., Tacher, L. and Beniston, M. 2008. Prediction of Landslide Movements Caused by Climate Change: Modelling the Behaviour of a Mean Elevation Large Slide in the Alps and Assessing its Uncertainties. In Chen et al. (eds.). Proceedings, 10th International Symposium on Landslides and Engineered Slopes, Xi'an, China, **1**: 217 – 227.

Bressani, L. A., Pinheiro, R. J. B., Bica, A. V. D., Eisenberger, C. N. and Soares, J. M. D. 2008. Movements of a Large Urban Slope in the Town of Santa Cruz do Sul (RGS), Brazil. In Chen et al. (eds.). Proceedings, 10th International Symposium on Landslides and Engineered Slopes, Xi'an, China, **1**: 293 – 298.

Brooker, E. W. and Peck, P. B. 1993. Rational Design Treatment of Slides in Overconsolidated Clays and Clay Shales. Canadian Geotechnical Journal, **30**: 526 – 544.

Buccolini, M. and Sciarra, N. 1996. The Caramanico Landslide (Abruzzo, Italy). Landslides. In Senneset (ed.). Proceedings, 7th International Symposium on Landslides, Balkema, Rotterdam, **2**: 661 – 666.

Bunza, G. 2000. Investigation and Monitoring of Landslides with Torrential Significance in the Bavarian Alps. Landslides in Research, Theory and Practice. In Bromhead et al. (eds.). Proceedings, 8th International Symposium on Landslides, Cardiff, UK, **1**: 195 – 202.

Calcaterra, D., Ramondini, M., Calo, F., Longobardi, V., Parise, M. and Galzerano, C. M. 2008. DInSAR Techniques for Monitoring Slow-Moving Landslides. In Chen et al. (eds.). Proceedings, 10th International Symposium on Landslides and Engineered Slopes, Xi'an, China, **2**: 1095 – 1101.

Campanella, R. G. 1965. Effect of Temperature and Stress on the Time-Deformation Behaviour in Saturated Clay. Ph.D. Thesis, University of California, Berkeley.

Campanella, R. G., and Vaid, Y. P. 1974. Triaxial and Plane Strain Creep Rupture of an Undisturbed Clay. Canadian Geotechnical Journal, **11**(1): 1 - 10.

Carson, A. M. and Fisher, J. 1991. Management of landslides within Shropshire. Slope Stability Engineering, Developments and Applications. Edited by R. J. Chandler. Thomas Telford, London: 95 – 99.

Cascini, L., Calvello, M., Grimaldi, G. M. 2008a. Modelling the Transient Groundwater Regime for the Displacement Analysis of Slow-Moving Active Landslides. In Chen et al. (eds.). Proceedings, 10th International Symposium on Landslides and Engineered Slopes, Xi'an, China, **1**: 607 – 613.

Cascini, L., Ferlisi, S., Peduto, D., Pisciotta, G., Di Nocera, S. and Fornaro, G. 2008b. Multitemporal DInSAR Data and Damages to Facilities as Indicators for the Activity of Slow-Moving Landslides. In Chen et al. (eds.). Proceedings, 10th International Symposium on Landslides and Engineered Slopes, Xi'an, China, **2**: 1103 – 1109.

Catalano, A., Chieppa, V., and Russo, C. 2000. Interaction between Dams and Landslides: Three Case Histories. In E. N. Bromhead, N. Dixon, and M. L. Ibsen (eds.), Landslides in Research, Theory and Practice. Proceedings, 8th International Symposium on Landslides, Cardiff, **1**: 227 – 232.

Ceccucci, M., Maranto, G. and Mastroviti, G. 2008. The Serre La Voute Landslide (North-West Italy): Results from Ten Years of Monitoring. In Chen et al. (eds.). Proceedings, 10th International Symposium on Landslides and Engineered Slopes, Xi'an, China, **2**: 1111 – 1117.

Chan, D. H., and Morgenstern, N. R. 1992. User Manual of Program PISA. University of Alberta, Edmonton, Alberta, Canada.

Chandler, K. R. and Broise, M. 2000. Remediation of the Watawala Landslide, Sri Lanka. Landslides in Research, Theory and Practice. In Bromhead et al. (eds.).

Proceedings, 8th International Symposium on Landslides, Cardiff, UK, **1**: 245 – 250.

Christensen, R. W., and Wu, T. H. 1964. Analysis of Clay Deformation as a Rate Process. Journal of the Soil Mechanics and Foundations Division, ASCE, **90**(SM6): 125 – 157.

Clementino, R. V., Proudfoot, D. W., Law, D. J. and Skirrow, R. 2008. Embankment Slope Stabilization Using Subhorizontal Drains at Highway 39 near Drayton Valley, Alberta. Proceedings, 4th Canadian Conference on Geohazards, Quebec, Canada: 511 – 517.

Clifton, A. W., Yoshida, R. T. and Chursinoff, R. W. 1986. Regina Beach – a Town on a Landslide. Canadian Geotechnical Journal, **23**: 60 – 68.

Comegna, L., Urciuoli, G., and Picarelli, L. 2004. The Role of Pore Prerssure on the Mechanics of Mudslides. In W.A. Lacerda (ed), Proceedings, 9th International Symposium on Landslides, Rio de Janeiro, in press. Balkema, Rotterdam.

Cruden, D. M., Keegan, T. R., and Thomson, S. 1993. The Landslide Dam on the Saddle River near Rycroft, Alberta. Canadian Geotechnical Journal, **30**: 1003 – 1015.

Cruden, D. M. and Varnes, D. J. 1996. Landslide Types and Processes. In Turner and Schuster (eds.). Landslides, Investigation and Mitigation. Special Report 247. Transportation Research Board, National Research Council. National Academy Press, Washington, USA, **3**: 36 – 75.

Cruden, D. M., Lu, Z-Y., and Thomson, S. 1997. The 1939 Montagneuse River Landslide, Alberta. Canadian Geotechnical Journal, **34**: 799 – 810.

D'Elia, B., Lanzo, G. and Rossi-Doria, M. 2000. Slow Movements of Earthflow Accumulations along the Ionic Coast (South-Eastern Italy). Landslides in Research, Theory and Practice. In Bromhead et al. (eds.). Proceedings, 8th International Symposium on Landslides, Cardiff, UK, **1**: 439 – 446.

De Josselin De Jong, G. 1968. Consolidation Models Consisting of an Assembly of Viscous Elements or a Cavity Channel Network. Geotechnique, **18**(2): 195 – 228.

Environment Canada. National Climate Archive.
http://climate.weatheroffice.ec.gc.ca/

Environment Canada. Water Survey of Canada.
www.wsc.ec.gc.ca

Eshraghian, A. 2007. Hazard Analysis of Reactivated Earth Slides in the Thompson River Valley, Ashcroft, British Columbia. Ph.D. Thesis, Department of Civil and Environmental Engineering, University of Alberta, Edmonton, Canada.

Eshraghian, A., Martin, C. D., and Cruden, D. M. 2005. Earth Slide Movements in the Thompson River Valley, Ashcroft, British Columbia. Proceedings, 58th Canadian Geotechnical Conference, Saskatoon, Canada, **1**: 276 – 284.

Eshraghian, A., Martin, C. D., and Morgenstern, N. R. 2007. A Review of Pore Pressure Induced Reactivation of Translational Earth Slides. Proceedings, 60th Canadian Geotechnical Conference, Ottawa, Canada, **3**: 2245 – 2251.

Esser, A. J. 2000. Case of a Slope Failure in Lacustrine Deposits. Landslides in Research, Theory and Practice. In Bromhead et al. (eds.). Proceedings, 8th International Symposium on Landslides, Cardiff, UK, **1**: 531 – 536.

Evans, S. G., Hu, X. Q., and Enegren, E. G. 1996. The 1973 Attachie Slide, Peace River Valley, near Fort St. John, British Columbia, Canada: A Landslide with a High-Velocity Flowslide Componenet in Pleistocene Sediments. Proceedings, 7th International Symposium on Landslides, Trpndheim, Norway. A. A. Balkema, Rotterdam, **2**: 715 – 720.

Finn, W. D. Liam, and Snead, D. 1973. Creep and Creep Rupture of Undisturbed Sensitive Clay. Proceedings of the 8th International Conference on Soil Mechanics and Foundation Engineering, Moscow, **1**(1): 135 – 142.

Fort, D. S., Clark, A. R. and Cliffe, D. G. 2000a. The Investigation and Monitoring of Coastal Landslides at Barton-on-Sea, Hampshire, UK. Landslides in Research, Theory and Practice. In Bromhead et al. (eds.). Proceedings, 8th International Symposium on Landslides, Cardiff, UK, **2**: 567 – 572.

Fort, D. S., Clark, A. R., Savage, D. T. and Davis, G. M. 2000b. Instrumentation and Monitoring of the Coastal at Lyme Regis, Dorset, UK. Landslides in Research, Theory and Practice. In Bromhead et al. (eds.). Proceedings, 8th International Symposium on Landslides, Cardiff, UK, **2**: 573 – 578.

Foss, I. 1969. Secondary Settlements of Buildings in Drammen, Norway. Proceedings, 7th International Conference on Soil Mechanics and Foundation Engineering, Mexico City, Mexico, **2**: 99 – 106.

Fredlund, D. G., Xing, A. and Huang, S. 1994. Predicting the Permeability Function for Unsaturated Soils using the Soil-Water Characteristic Curve. Canadian Geotechnical Journal, **31**: 533 – 546.

Freeze, R. A. 1977. Computer Modeling of Groundwater Conditions on Downie Slide. Repot Submitted to BC Hydro. File no. 2298 – 2805.

Friele, P. and Clague, J. 2006. Quaternary History of Little Chief Slide, near Mica Dam. In P. Rapp, 2006. Mica Dam – Little Chief Slide, 2005 Field Investigation Report. Engineering Report no. E434.

Fuchsberger, M. and Mauerhofer, G. 1996. Slip at a Major Cut for a Motorway in the Austrian Alps – A Case History of its Cause and its Stabilisation. Landslides. In Senneset (ed.). Proceedings, 7th International Symposium on Landslides, Balkema, Rotterdam, **3**: 1687 – 1692.

Fujisawa, K., Higuchi, K., Koda, A. and Harada, T. 2007. Landslide Detection, Monitoring, Prediction, Emergency Measures and Technical Instruction in a Busy City, Atami, Japan. Proceedings, First North American Landslide Conference, Vail, Colorado: 65 – 73.

Gavin, G. J. 1969. Reservoir Slope Investigations – Mica Project. Report Submitted to BC Hydro. File number 100.218. Drawing number 211 – C02 – D652.

Gibo, S., Egashira, M., Ohtsubo, M., and Nakamura, S. 2002. Strength Recovery from Residual State in Reactivated Landslides. Geotechnique, **52**(9): 683 – 686.

Gibson, R. E. and Henkel, D. J. 1954. Influence of Duration of Tests at Constant Rate of Strain on Measured "Drained" Strength. Geotechnique, **4**: 6 – 15.

Gillon, M. D. and Saul, G. J. 1996. Stabilisation of Cairnmuir Landslide. Landslides. In Senneset (ed.). Proceedings, 7th International Symposium on Landslides, Balkema, Rotterdam, **3**: 1693 – 1698.

Hardy, R. M., Brooker, E. W., and Curtis, W. E. 1962. Landslides in Over-Consolidated Clays. Engineering Journal, **45**: 81 – 89.

Hayley, D. W. 1968. Progressive Failure of a Clay Shale Slope in Northern Alberta. M. Sc. Thesis, Department of Civil Engineering, University of Alberta, Edmonton, Canada.

HBT AGRA Limited, Edmonton, Alberta, 1992. Geotechnical Investigation – 99th Street Slope Stabilization – Lots 4-22, Block 3, Plan 6472NY, Peace River, Alberta. Report no. EG-07480.

Ibadango, C. E., Soto, J., Tamay, J., Escudero, P. and Porter, M. 2005. Mass Movements in the Loja Basin – Ecuador, South America. Proceedings, International Conference on Landslide Risk Management, Vancouver, Canada. I010.

Jworchan, I., O'Brien, A. and Rizakalla, E. 2008. Landslide Stabilization for Residential Development. In Chen et al. (eds.). Proceedings, 10th International Symposium on Landslides and Engineered Slopes, Xi'an, China, **2**: 1757 – 1763.

Kalteziotis, N., Zervogiannis, H., Frank, R., Seve, G. and Berche, J. C. 1993. Experimental Study of Landslide Stabilization by Large Diameter Piles. In A. Anagnostopoulos, F. Schlosser, N. Kalteziotis and R. Frank (eds) Geotechnical Engineering of Hard Soils Soft Rocks. Proceedings, International Symposium under the Auspices of the International Society for Soil Mechanics and Foundation Engineering (ISSMFE), The International Association of Engineering

Geology (IAEG) and The International Society for Rock Mechanics (ISRM), Athens, Greece. A. A. Balkema, Rotterdam, **2**: 1115 – 1124.

Kang, S. H., Kim, J. H. and Park, N. S. 2000. A Case Study on the Deformation of a Bridge by the Reactivation of a Pre-Exiting Sliding Plane. Landslides in Research, Theory and Practice. In Bromhead et al. (eds.). Proceedings, 8th International Symposium on Landslides, Cardiff, UK, **2**: 807 – 812.

Kavazanjian, E. and Mitchell, J. K. 1980. Time Dependent Deformation Behavior of Clays. Journal of the Geotechnical Engineering Division, ASCE, **106**(GT6): 611 – 630.

Lacasse, S., Eidsvig, U., Nadim, F., Hoeg, K. and Blikra, L. H. 2008. Event Tree Analysis of Aknes Rock Slide Hazard. Proceedings, 4th Canadian Conference on Geohazards, Quebec, Canada: 551 – 558.

Krahn, J. 2004. Seepage Modeling with SEEP/W – An Engineering Methodology. SEEP/W Manual. First Edition.

Lacerda, W. A. and Houston, W. N. 1973. Stress Relaxation in Soils. Proceedings, 8th International Conference on Soil Mechanics and Foundation Engineering, **1**(34): 221 – 227.

Ladanyi, B. and Benyamina, M. B. 1995. Triaxial Relaxation Testing of a Frozen Sand. Canadian Geotechnical Journal, **32**: 496 – 511.

Lee, E. M. and Clark, A. R. 2000. The Use of Archive Records in Landslide Risk Assessment: Historical Landslide Events on the Scarborough Coast, UK. Landslides in Research, Theory and Practice. In Bromhead et al. (eds.). Proceedings, 8th International Symposium on Landslides, Cardiff, UK, **2**: 905 – 910.

Leroueil, S., Kabbaj, M., Tavenas, F. and Bouchard, R. 1985. Stress-Strain-Strain Rate Relation for the Compressibility of Sensitive Natural Clays. Geotechnique, **35**(2): 159 – 180.

Liingaard, M., Augustesen, A., and Lade, P. V. 2004. Characterization of Models for Time-Dependent Behavior of Soils. International Journal of Geomechanics, ASCE, **30**(3): 157 – 177.

Liverman, D. G. E., Catto, N. R. and Rutter, N. W. 1989. Laurentide Glaciation in West-Central Alberta: A Single (Later Wisconsinan) Event. Canadian Journal of Earth Sciences, **26**: 266 – 274.

Lokin, P., Petricevic, M., Vasic, M. and Sakovic, S. 1996. Landslide along the Danube Bank at Novi Sad, Yugoslavia. Landslides. In Senneset (ed.). Proceedings, 7th International Symposium on Landslides, Balkema, Rotterdam, **2**: 803 – 808.

Lu, Z. Y., Cruden, D. M., and Thomson, S. 1998. Landslides and Preglacial Channels in the Western Peace River Lowlands. Proceedings, 51st Canadian Geotechnical Conference, Edmonton, Canada, **1**: 267 – 274.

Malone, A. W., Hansen, A., Hencher, S. R. and Fletcher, C. J. N. 2008. Post-Failure Movements of a Large Slow Rock Slide in Schist near Pos Selim, Malaysia. In Chen et al. (eds.). Proceedings, 10th International Symposium on Landslides and Engineered Slopes, Xi'an, China, **1**: 457 – 461.

Mansour, M. F., Martin, C. D. and Morgenstern, N. R. 2008. Characterization of Creep Movements at the Little Chief Slide, BC. Proceedings, 61st Canadian Geotechnical Conference, Edmonton, Canada: 461 – 468.

Mantovani, M., Marcato, G., Silvano, S., Zannoni, A., Pasuto, A., and Tagliavini, F. 2004. Slope Instability around the Sauris Reservoir (North-Eastern Italy). In W.A. Lacerda (ed), Proceedings, 9th International Symposium on Landslides, Rio de Janeiro, **1**: 70 – 84.

Mcleod, J. A. 2006. X-ray Diffraction Analysis of Little Chief Slide Material. In P. Rapp, 2006. Mica Dam – Little Chief Slide, 2005 Field Investigation Report. Engineering Report no. E434.

Mihalinec, Z. and Ortolan, Z. 2008. Landslide "Granice" in Zagreb (Croatia). In Chen et al. (eds.). Proceedings, 10th International Symposium on Landslides and Engineered Slopes, Xi'an, China, **2**: 1587 – 1593.

Miller, B. G. N. 2000. Two Landslides and their Dams, Peace River Lowlands, Alberta. M. Sc. Thesis, Department of Earth and Atmospheric Sciences, University of Alberta, Edmonton, AB.

Miller, B. G. N. and Cruden, D. M. 2002. The Eureka River Landslide and Dam, Peace River Lowlands, Alberta. Canadian Geotechnical Journal, **39**: 863 – 878.

Mitchell, J. 1976. Fundamentals of Soil Behavior. John Wiley and Sons, Inc.

Moore, D. P., Watson, A. D., and Martin, C. D. 2006. Deformation Mechanism of a Large Rockslide Inundated by a Reservoir. Workshop on the Mechanics and Velocity of Large Landslides, Technical Report, Italy.

Moore, R. and Brunsden, D. 1996. Physical-Chemical Effects on the Behavior of a Coastal Mudslide. Geotechnique, **46**(2): 259 – 278.

Morgenstern, N. R. 1987. Geological Control of Stability on Large Projects. Proceedings, 8th Pan American Conference on Soil Mechanics and Foundation Engineering, Cartagena, **1**: 293 – 316.

Morgenstern, N. R. and Price, V. E. 1965. The Analysis of the Stability of General Slip Surfaces. Geotechnique, **15**(1): 79 – 93.

Morgenstern, N. R. and Eigenbrod, K. D. 1974. Classification of Argillaceous Soils and Rocks. Journal of the Geotechnical Engineering Division, ASCE, **100**(GT10): 1137 – 1156.

Morsy, M. M. 1994. Effective Stress Modeling of Creep Behavior of Clay. PhD Thesis, Department of Civil and Environmental Engineering, University of Alberta, Edmonton, Canada.

Murayama, S. and Shibata, T. 1961. Rheological Properties of Clays. Proceddings of the 5th International Conference on Soil Mechanics and Foundation Engineering, Paris, France, **1**: 269 – 273.

Nelson, J. D. and Thompson, E. G. 1977. A theory of Creep Failure in Overconsolidated Clay. Journal of the Geotechnical Engineering, Proceedings of the American Society of Civil Engineers, **103**(GT11): 1281 – 1293.

Nichol, D. and Lowman, R. D. W. 2000. Stabilisation and Remediation of a Minor Landslide Affecting the A5 Trunk Road at Llangollen, North Wales. Landslides in Research, Theory and Practice. In Bromhead et al. (eds.). Proceedings, 8th International Symposium on Landslides, Cardiff, UK, **3**: 1099 – 1104.

Odqvist, F. K. G. 1966. Mathematical Theory of Creep and Creep Rupture. Oxford Mathematical Monograph, Clarendon Press, Oxford, pp. 268.

Oppikofer, T., Jaboyedoff, M., Blikra, L. H. and Derron, M. H. 2008. Characterization and Monitoring of the Aknes Rockslide Using Terrestrial Laser Scanning. Proceedings, 4th Canadian Conference on Geohazards, Quebec, Canada: 211 – 218.

Ortigão, J. A. R. and Kanji, M. A. 2004. Landslide Classification and Risk Management. In J. Ortigão and A. Sayao (eds.). Handbook of Slope Stabilisation. Springer.

Picarelli, L., Russo, C. and Urciuoli, G. 1995. Modeling Earth-Flow Movement Based on Experiences. In Danish Geotechnical Society (ed), The Interplay between Geotechnical Engineering and Engineering Geology. Proceedings, 11th Eurpoean Conference on Soil Mechanics and Foundation Engineering, **6**: 157 – 162.

Picarelli, L. and Russo, C. 2004. Remarks on the Mechanics of Slow Active Landslides and the Interaction with Man-Made Works. In W.A. Lacerda (ed), Proceedings, 9th International Symposium on Landslides, Rio de Janeiro, **2**: 1141 – 1176.

Picarelli, L., Urciuoli, G. and Russo, C. 2004. Effect of Groundwater Regime on the Behaviour of Clayey Slopes. Canadian Geotechnical Journal, **41**: 467 – 484.

Prevost, J. H. 1976. Undrained Stress-Strain-Time Behavior of Clays. Journal of Geotechnical Engineering, **102**(12): 1245 – 1259.

Proudfoot, D. W. and Tweedie, R. W. 2002. HWY 49:12 – Little Smoky North (SH3) Geotechnical Investigation. Report to Alberta Transportation. Thurber Engineering Ltd., Edmonton, Alberta. File 15 – 76 – 30.

Provincial Archives of Alberta – Map printed at the Office of the Surveyor General, June 1922.

Rapp, P. 2006. Mica Dam – Little Chief Slide, 2005 Field Investigation Report. Engineering Report E434.

Remondo, J., Bonachea, J. and Cendrero, A. 2004. Probabilistic Landslide Hazard and Risk Mapping on the Basis of Occurrence and Damages in the Recent Past. In W.A. Lacerda (ed), Proceedings, 9th International Symposium on Landslides, Rio de Janeiro, **1**: 125 – 130

Rennie, R. J., 1966. Residual Strength of a Clay-Till applied to Little Smoky River Landslide. Unpublished M. Sc. Thesis, University of Alberta, Edmonton, Canada.

Russo, C., Chan, D., and Picarelli, L. 2004. Role of Viscous Soil Properties on Landslide Movement Triggered by Pore Water Fluctuations. In W.A. Lacerda (ed), Proceedings, 9th International Symposium on Landslides, Rio de Janeiro, in press. Balkema, Rotterdam.

Saito, M. 1965. Forecasting the Time of Occurrence of a Slope Failure. Proceedings, 6th International Conference on Soil Mechanics and Foundation Engineering, Montreal, **2**(6): 537 – 541.

Schuster, R. L. 1996. Socioeconomic Significance of Landslides. In Turner and Schuster (eds.). Landslides Investigation and Mitigation. Special Report, Transportation Research Board, National Research Council. National Academy Press, Washington, USA, **2**: 12 – 35.

Scott, J.S. 1989. Engineering geology and land use planning in the Prairie region of Canada. In Quaternary geology of Canada and Greenland. Edited by R.J. Fulton. Geological Survey of Canada, Geology of Canada, **1**: 713 – 723.

Singh, A. and Mitchell, J. K. 1968. General Stress Strain Time Function for Soils. Journal of the Soil Mechanics and Foundations Division, ASCE, **94**(SM1): 21 – 46.

Skempton, A. W. 1985. Residual Strengths of Clays in Landslides, Folded Strata and the Laboratory. Geotechnique, **35**(1): 3 – 18.

Skirrow, R., Proudfoot, D., Froese, C., and Thomson, S. 2005. Update on the Little Smoky Landslide. Proceedings, 58th Canadian Geotechnical Conference, Saskatoon, Canada, **1**: 471 – 478.

Soe Moe, K. W., Cruden, D. M., Martin, C. D., Lewycky, D., and Lach, P. R. 2007. Study of a Century Old Landslide in Edmonton: The Forest Heights Park Landslide. Proceedings, 60th Canadian Geotechnical Journal, Ottawa, Canada, **1**: 770 – 777.

Spizzichino, D., Falconi, L., Delmonaco, G., Margottini, C. and Puglisi, C. 2004. Integrated Approach for Landslide Risk Assessment of Crago Village (Italy). In W.A. Lacerda (ed), Proceedings, 9th International Symposium on Landslides, Rio de Janeiro, **1**: 237 – 242.

Stephen, M. and Renton-Rose, D. 2000. Stabilisation of a Landslip near Godstone, Surrey. Landslides in Research, Theory and Practice. In Bromhead et al. (eds.). Proceedings, 8th International Symposium on Landslides, Cardiff, UK, **3**: 1407 – 1412.

Suklje, L. 1957. The Analysis of the Consolidation Process by the Isotaches Method. Proceedings, 4th International Conference on Soil Mechanics and Foundation Engineering, London, England, **1**: 200 – 206.

Sun, H. W., Ho, K. K. S., Campbell, S. D. G. and Koor, N. P. 2000. The 2 July 1997 Lai Ping Road Landslide, Hong Kong – Assessment of Landslide Mechanism. Landslides in Research, Theory and Practice. In Bromhead et al. (eds.). Proceedings, 8th International Symposium on Landslides, Cardiff, UK, **3**: 1425 – 1430.

Tavenas, F, and Leroueil, S. 1977. Effects of Stresses and Time on Yielding of Clays. Proceedings of the 9th International Conference on Soil Mechanics and Foundation Engineering, Tokyo, Japan, **1**: 319 – 326.

Tavenas, F., Leroueil, P. L., and Roy, M. 1978. Creep Behavior of an Undisturbed Lightly Overconsolidated Clay. Canadian Geotechnical Journal, **15**: 402 – 423.

Terzaghi, C. 1931. The Static Rigidity of Plastic Clays. Journal of Rheology, **2**(3): 253 – 262.

Thomson, S. and Hayley, D. W. 1975. The Little Smoky Landslide. Canadian Geotechnical Journal, **12**: 379 – 392.

Topal, T. and Akin, M. 2008. Investigation of a Landslide along a Natural Gas Pipeline (Karacabey-Turkey). In Chen et al. (eds.). Proceedings, 10th International Symposium on Landslides and Engineered Slopes, Xi'an, China, **2**: 1647 – 1652.

U.S.C.E. 1960. Stability of Earth and Rockfill Dams. Manual EM 1110 – 2 – 1902.

Vaid, Y. P., Robertson, P. K. and Campanella, R. G. 1979. Strain Rate Behavior of Saint-Jean-Vianney Clay. Canadian Geotechnical Journal, **16**: 34 – 42.

Varnes, D. J. 1984. Landslides Hazard Zonation: A Review of Principles and Practice. UNESCO, Paris, pp. 10.

Vulliet, L. and Hutter, K. 1988. Viscous-type Sliding Laws for Landslides. Canadian Geotechnical Journal, **25**: 467 – 477.

Walker, L. K. 1969. Secondary Compression in the Shear of Clay. Journal of Soil Mechanics and Foundations Division, ASCE, **95**(SM1): 167 – 188.

Wang, F. W., Wang, G., Zhang, Y. M., Huo, Z. T., Peng, X. M., Araiba, K., and Takeuchi, A. 2008. Displacement Monitoring on Shuping Landslide in the Three Gorges Dam Reservoir Area, China from August 2004 to July 2007. In Chen et

al. (eds.). Proceedings, 10th International Symposium on Landslides and Engineered Slopes, Xi'an, China, **2**: 1321 – 1327.

Wasowski, J., Casarano, D., Bovenga, F., Refice, A., Nutricato, R. and Nitti, D. O. 2008. Landslide-Prone Towns in Daunia (Italy): PS Interferometry-Based Investigation. In Chen et al. (eds.). Proceedings, 10th International Symposium on Landslides and Engineered Slopes, Xi'an, China, **1**: 513 – 518.

Watts, B. D. 1981. Lateral Creep Deformations in the Foundation of a High Dam. M. Sc. Thesis, Civil Engineering Department, University of Alberta, Edmonton, Canada.

Wedage, A. M. 1995. Influence of Rate Effects on the Residual Strength of Moving Slopes. PhD Thesis, Department of Civil and Environmental Engineering, University of Alberta, Edmonton, Canada.

Wu, M. J., Li, Z. C., Yuan, P. J. and Jiang, Y. H. 2008. Twenty Years of Safety Monitoring for the Landslide of Hancheng PowerStation. In Chen et al. (eds.). Proceedings, 10th International Symposium on Landslides and Engineered Slopes, Xi'an, China, **2**: 1335 – 1341.

Wu, T. H., El Refai. A. N., and Hsu, J. R. 1978. Creep Deformation of Clays. ASCE Journal of the Geotechnical Engineering Division, **104**(GT1): 61 – 76.

Yener, A. B., Durmaz, S. and Demir, B. M. 2008. The Importance of Geological and Geotechnical Investigations of Landslides Occurred at Dam Reservoirs: Case Studies from the Havuzlu and Demirkent Landslides (Artvin Dam, Turkey). In Chen et al. (eds.). Proceedings, 10th International Symposium on Landslides and Engineered Slopes, Xi'an, China, **1**: 531 – 534.

Zhou, Y. 2000. Research and Treatment of Shazhou Landslide, Sichuan. Landslides in Research, Theory and Practice. In Bromhead et al. (eds.). Proceedings, 8th International Symposium on Landslides, Cardiff, UK, **3**: 1647 – 1652.

APPENDIX "A"

Case Histories on the Vulnerability to Slow Moving Slides

A-1 Vulnerability of Urban and Suburban Communities

Cascini et al. (2008b) utilized both an available landslide inventory map based on geological and geomorphologic information and a dataset on landslide induced damage to properties to evaluate the reliability of a Differential Synthetic Aperture Radar Interferometry (DInSAR) in measuring slow moving landslides displacement rates. The landslides inventory maps included information about the location, classification and state of activity based on geological and geomorphologic criteria. The study area covers about 489 km^2 in the upper part of the territory of the National Basin Authority of Liri – Garigliano and Volturno Rivers (NBA – LGV) in Italy. Generally, Quaternary deposits overlie upper Miocene bedrock. Rainfall is primarily responsible for movement reactivation. The data set on damage to facilities showed that around 30% of the surveyed buildings and 24% of the investigated roads showed evidences of damages that affect their serviceability. The comparison of the damage to facilities map, the landslides inventory and the DInSAR results showed that the areas vulnerable to landslides coincided with the locations and velocities of active landslides. For example, an area vulnerable to landslides coincided with an extremely slow active rotational slide moving at 5mm/yr. No more values of velocities were reported.

Wasowski et al. (2008) applied Persistent Scatterers Interferometry (PSI) to monitor the continued ground displacements in two towns in the Daunia Apennines in southern Italy; namely Casalnuovo Monterotaro and Pietramontecorvino. The persistent scatterers were man-made structures within the two towns. The stratigraphy at the Daunia region consists of clay-rich deformed flysch formations which are more prone to landsliding than other formations in the area that contain higher proportions of sandstone and limestone. Peaks in rainfall as well as construction activity are considered the main triggers of landsliding. The maximum recorded displacement rate was ~8mm/yr. Although the measured movements were associated with observed cracks in some buildings and retaining walls in the towns under investigation, it was not clear in all the investigated areas whether the movements and associated cracks have resulted from subsidence of the town buildings, from actual horizontal ground displacements or from deterioration of the man-made structures. Local geomorphologic and/or geotechnical investigation is essential for deciding.

Ortigão and Kanji (2004) described the extremely slow movements of the Puriscal landslide. The landslide adversely affects the town of Santiago de Puriscal in Costa Rica. The velocity is estimated to be few millimetres per year, i.e., <10mm/yr.The stratigraphy at the site consists of residual silty clays overlying cohesive saprolitic soils underlain by weathered igneous rock. Movement is triggered by rainfall and seismic activity. The extremely slow movements caused cracks to appear in some buildings and on the ground in many places in the town.

The Triesen village is located at the toe of the Triesenberg landslide in eastern Switzerland and the Triesenberg village lies at mid-slope (Bonnard et al., 2008). The infrastructure of the two villages experienced damage due to the slow movement of the slide. The average annual rate ranges from some mm/yr to a cm/yr. The velocity may, however, jump to a few dozens of centimetres per year during peak periods. Since the movements are slow, development of some areas of the slope has not been affected. The soil type is clayey shales. The displacement is measured using surface surveying of topographic points

Jworchan et al. (2008) studied the stabilization of a slope proposed for residential development. The site is in the West Pennant Hills, Sydney, Australia. Geotechnical investigations indicated that the stratigraphy at the site consists of colluvium underlain by residual soils that overlie bedrock. Slip surfaces are within the colluvium/residual soils or at the interface between the residual soils and bedrock. The results of the inclinometers monitoring showed that the upper 4m of the slope moved 5mm in about 5 months (April to September, 2006; ~12 mm/yr). Movement acceleration was found to occur in a timely manner with high rainfalls and rising ground water levels. An embankment within the site had experienced tension cracks at the crest. According to the "Landslides Risk Management Concepts and Guidelines" outlined by the Australian Geomechanics Society, Jworchan et al. (2008) considered the likelihood of slope movements at this location to be "almost certain". Hence a probability factor of $\sim 10^{-1}$ was assigned to this area. The consequences were considered major and hence the risk level is very high. Some trees were bent in another location of the site. The probability was considered $\sim 10^{-3}$, the consequences were considered medium and hence the risk was considered moderate. It was concluded that subsurface drainage may be more successful in lowering the ground water pressures and hence the risk level will be reduced to low. Other mitigation options include retaining structures and excavation and replacement.

Barton and McCosker (2000) measured the horizontal displacement of a coastal cliff that is about 15 – 30m away from a coastal road in Afton Down, UK. The cliff is mainly composed of well jointed rock without any shear surfaces. The displacement rates measured by inclinometers did not exceed 12mm/yr. This maximum rate was associated with notably stormy winters in 1987/88. There was a threat to the nearby road however.

HBT AGRA Limited (1992) carried out a geotechnical investigation in the town of Peace River that involved the 99th street slope stabilization. The installed slope indicators showed that the movement rate varies from zero to 14mm/yr. The reported instabilities included removal of a portion of one of the streets. This would probably correspond to the maximum movement rate because the report mentioned that other instabilities occurred but with insignificant impact on roadways or residential properties. Reported instabilities included structural distress to some houses, ground cracking and damage to a small retaining wall.

Calcaterra et al. (2008) have carried out detailed field surveys in order to evaluate the degree of landslide damage to buildings of the village of Moio della Civitella in Salerno province in Italy. They used a scale divided from 1 to 7. Class "1" corresponds to negligible damage and class "7" indicates a total collapse of the building. Class "2" refers to light damage: walls having cracks of few centimetres. Class "3" refers to a moderate damage: open cracks in the walls, wall disjunction and badly working casings. Class "5" refers to very serious damage: collapse of partition and outer walls together with seriously damaged floor and lintels. Out of about 93 examined buildings, 17.2% were classified as class 1, 23.7% were classified as class 2, 46.2% were classified as class 3, 5.4% as class 4 (serious), 2.2% as class 5 (very serious), 4.3% as class 6 (partial collapse) and 1.1% as class 7 (total collapse).

In addition, a Permanent Scatterer Synthetic Aperture Interferometry (PS-InSAR) technique is used to measure the slow landslide movements. As mentioned above, the PS are generally man made objects such as statues, lamps, building roofs, sewage covers, etc… The results of the PS-InSAR monitoring were confirmed by inclinometer readings. An average rate of 16.2 mm/yr (extremely slow rate) was detected for the village during the period from 1992 to 2001. Rainfall triggers the movement. Since about 87% of the village buildings lie within the first three classes, then this movement rate would cause damages up to open cracks in walls, wall disjunction and badly working casings.

The Caramanico landslide took place in the Abruzzo region in Italy in October 1989 after several days of intense rainfall (Buccolini and Sciarra, 1996). The slide damaged some dwelling houses and caused disruption of a 700m reach of a highway where the slide scarp passed through it. The slide area has been investigated using inclinometers, surface monuments and piezometers. Pore pressures showed good correlation with rainfall records. Movement rates at the ground surface ranged between 19 and 26 mm/yr. The stratigraphy consists of rigid limestone breccias overlying plastic marly clays that host the rupture surface. The plastic marly clay layer is characterized by the presence of numerous shear zones.

Ortigão and Kanji (2004) described the El Turi landslide located on the outskirts of the town of Cuenca, Ecuador. The slide moves at 30mm/yr, measured by surface surveying. The rupture surface is located at the interface between soil and bedrock. Movement is triggered by high pore pressures, mostly due to rainfall. The very slow movements caused about 10^0 tilt in the walls of a farmhouse.

Blikra (2008) described the monitoring system of the Aknes rockslide in Norway. The slide volume is 30 – 40 million m^3. The average slide velocity is 30 – 100 mm/yr. However, the slide may speed up locally to more than 365 mm/yr during peak seasonal changes. The main threat posed by the rockslides is the possibility of large tsunamis generation when the rockslides plunge into the fjords. The monitoring instruments included extensometers, single lasers, GPS, total station,

geophones, inclinometers and piezometers. A warning system was designed based on historical data from the Aknes slide and from other historical slides as well. The normal situation in the warning system is the green level where the movement rates are in the order of 36 – 180 mm/yr (very slow rates). During large seasonal fluctuations, the warning level becomes blue, corresponding to movement rates of 180 – 730 mm/yr (very slow rates). When the velocity of the slide continues to develop under the effect of the seasonal changes, the warning level becomes yellow, corresponding to movement rates of 730 – 1800 mm/yr (in the upper range of very slow rates). The orange level indicates acceleration preceding a major event. That level includes movement rates of 1800 – 3600 mm/yr (slow rates range). The red level means an event in progress with velocities in excess of 3.6 m/yr. Since the average movement rate lies in the green range, it is considered that only minor damages may be expected from this slide.

Long range Terrestrial Laser Scanning (TLS) of the Aknes Rockslide in Norway revealed that the slide is moving at a rate of 60 – 70mm/yr (Oppikofer et al., 2008). The movement may accelerate however to 200mm/yr in the most unstable parts of the slope. The rates are then consistent with the values measured by Blikra (2008). The Aknes Rockslide lies on the western flank of Sunnylvsfjord, a branch of the Storfjord. The slide volume has been estimated recently to be about 35 million m^3. The main threat posed by the Aknes Rockslide is the possibility of occurrence of a tsunami in the fjord. Previous tsunamis caused by similar slides were up to 60m high and led to the death of 40 people. Displacement acceleration of rockslides that leads to tsunamis is often preceded by warning signs such as increased displacement rate and local sliding (Lacasse et al. 2008). Lacasse et al. (2008) identified the triggers of the rockslides in the European Alps in general. Rainfall and earthquakes are the most likely triggers followed by mining operations and snow melt.

Bressani et al. (2008) studied the instability of an urban slope in the city of Santa Cruz do Sul, RGS, Brazil. The movements occur at the interface of an overlying colluvium and siltstones of the Santa Maria formation. The formation is composed of clayey siltstones with smectite type clays. The average rate of displacement is 34.4 mm/yr. However, rates up to 80mm/yr were recorded using inclinometers in some of the damaged houses. The reported damages were sometimes in the form of cracked pavements and sometimes considered severe. Movement is triggered by rainfall. The area affected by movements was around 8 hectares. The affected structures were made of reinforced concrete supported by concrete or steel piles.

Fort et al. (2000b) investigated the instability of the coastal landslides at the town of Lyme Regis in Dorset, UK. The observed damage included cracks in roads and footpaths in addition to damage to seawall structures. The maximum recorded movement rates were about 91mm/yr. Inclinometers as well as surface survey markers were used to measure the displacement. Coastal erosion and rainfall are the main triggers of movement.

The village of Tiefenbach near Oberstdorf, Germany has been threatened by the debris flow of the torrent Flkenbach due to the presence of a landslide upslope (Bunza, 2000). The slide is an enlarging rotational slide. Following floods, the developed torrents at the toe cause erosive forces that trigger the slide. Elevated pore pressures due to intense rainfall and snow melt play an important role as well. The slide materials range between gravel and silt. Horizontal displacements have been measured using extensometers. The average rate over a 2 years measuring period was 92 mm/yr. Pore pressures changes were found to follow the rainfall cycle.

Clifton et al. (1986) studied the vulnerability of Regina beach in Saskatchewan, Canada to some retrogressive landslides. The rupture surface lies at a depth of 31.5 meters in bentonitic clay shales of Bearpaw formation. In retrogressive slides, structures located completely on a block will be less susceptible to damage. However, structures located on head scarps will experience more damage. Historical movement rates at Regina beach range from 10 mm/year to more than 200mm in less than a week. Modern dwellings break down when a certain amount of differential movement (vertical or horizontal) occurs. The authors found that this amount equals approximately 200mm. In one case, a foundation break-down occurred when a total movement of 250mm occurred in 30 years (~8mm/year). In another case, the dwelling had been stable for 10 years before a total movement of 200mm occurred in one week. In a third case, failure took place after 4 years with an average annual rate of 50 mm. Inclinometers showed that the movement rates ranged from 1 to 9mm/month (12 to 108mm/yr). The highest rate was the closest to the shoreline. Hence river erosion seems to be the likely trigger of movement. In the area of the highest rates, evidence of cracking was abundant. Rupture of service utilities was continuous and ground cracking was visible. Where smaller rates were encountered, little evidence of landslide movement was present on the streets. A six years old concrete sidewalk showed no evidence of cracking attributable to slope movement. The researchers reported that the movement rate required to break a municipal water line is in the order of 100 mm/year.

Wang et al. (2008) monitored the displacements of the Shuping landslide that terminates at the reservoir of the Three Gorges Dam in China. During the impoundment of the reservoir, a rapid landslide other than the Shuping landslide took place and led to the death of 24 people; 11 of them were killed on the deformed slope and 13 were killed by the Tsunami caused by the movement. Regarding the Shuping landslide, an impoundment of 40 meters was achieved in 15 days in June 2003. Cracks in roads and houses were observed as soon as the first impoundment was completed. Measurement of cracks' widths during 2007 indicated that a width of 10cm was attained in 3 months. GPS stations were installed in the summer of 2007. By the end of the year the toe moved about 90mms (15mm/month or 180mm/year). The deformation at the toe was higher than those near the scarp. Cracks deformation rate reached however 1100 mm/yr

(very slow). Some extensometers were installed in 2004 and monitored for 2 years. The measured maximum rate was ~170mm/yr which confirms the GPS measurements. A new set of 11 extensometers were installed in 2006 and has been monitored for a year. The movement rate was around 240mm/yr. The researchers found that the movement is reactivated by both rainfall and the reservoir level changes. The effect of the drop in the reservoir level is more pronounced than the effect of water impoundment. Many landslide in the area occurred in a layer that contains colluvial deposits of sandy mudstone and muddy sandstone.

Mihalinec and Ortolan (2008) described the landslide improvement activities for a landslide in Zagreb, Croatia. The slide is a shallow translational one. Urban communities of some ten housing units are located at the lower part of the slide. Comparison of topographic maps in 1962 and 1995 indicated that the slide moved 5 – 10m during this period (152 - 303mm/yr). The houses that are located at the lower part of the slope suffered damages due to the movement (no description was provided for the type of damages). Some of the houses were moving with the slide. The slide becomes more active during rainy seasons. The slide plane materials are clay. Drainage trenches were used to reduce the pore pressure within the slope and hence improving stability. The movement had slowed down after the installation of the trenches.

The extremely to very slow movements of a slope next to a residential complex in Ohio, USA had caused serious damages to some houses founded on the crest of the slope (Esser, 2000). The rupture surfaces are hosted in layers of plastic lacustrine clays. Movements were recorded using inclinometers. The maximum recorded rate was 306mm/yr. Extremely slow movements as low as 16mm/yr were also recorded. The moving was likely to be caused by construction activities. The damage caused by the moving ground included:

- Cracks began to appear
- The back of one of the houses moved downslope
- The walls buckled
- Doors and windows began to bend
- The rear wall of a garage has failed by moving downslope. It moved suddenly for 25 cm.
- The back of the house continued moving downslope even after rebuilding the wall.

Fort et al. (2000a) investigated the instability of the undercliff of the 1.5km long Barton-on-Sea shore in Hampshire, UK. Major slope failures had been recorded in 1974 and in 1987/88 below the Cliff House Hotel in the area. Instabilities continued in the nineties. The materials involved in the slide are stiff, fissured overconsolidated Barton Clay. Both toe erosion and pore pressure changes contribute to movement. The toe has however been armoured and hence the current movement are primarily dependent on seasonal fluctuations which indicates the role of rainfall in the slope movement. The maximum recorded

movement rate was 3.3m in about 46months; i.e. 861 mm/yr. Movement was monitored using surface monuments.

A landslide occurred in Shazhou town, Guangyuan city, northern Sichuan in China on December 30, 1998 (Zhou, 2000). The slope has showed signs of distress in the form of cracks on November 6th. Hence the slope was extensively monitored. The slope moved 20 – 24 mms between November 6th and December 5th. On December 29th, the displacement reached 300mm. This indicates that the average movement rate was ~2000 mm/yr and reached more than 4000 mm/yr in the three weeks preceding the failure. The movement was observed to accelerate since December 25th. A warning was given to the local inhabitants to evacuate their houses. Due to this successful early monitoring, no loss of lives resulted from the slide. However, the sliding mass reached the back walls of some buildings which threatened the buildings' safety. Part of the rupture surface moved along a soil rock interface and the rest moved on a soil pebble layer interface. The slope has been stabilized by anchoring the moving mass into the stable ground.

Spizzichino et al. (2004) analyzed the air photos of the years 1955, 1972 and 1997 of the Crago village in Italy. Direct field surveys have been carried out as well in order to study the geomorphologic evolution of the Crago slopes. Their temporal analysis showed that the main scarp of one of the slopes had retrogressed by about 50m between 1955 and 1972. This caused severe damages to buildings in the vicinity of the slope area. In other slopes, failures had seriously affected a road and a reinforced wall founded on piles. Movement is reactivated by rainfall and human activity. The rupture surface lies in a clayey layer. Some reactivated slides were followed by earth flows that moved an average of 100m between 1972 and 1997 (4m/yr).

Ibadango et al. (2005) investigated the mass movements in the Loja Basin in Ecuador, South America. Most of the elongated valley is inhabited and includes the city of Loja. The construction activities have led to an increase in the activity of the landslides. Some regions have been moving extremely slowly at 16mm/yr or less. However, slow rates of 1.6 to 13m/yr have been also recorded in some large to medium size landslides. Buildings, roads, water supply pipelines, waste water collection facilities and electrical and telecommunication towers are all adversely affected by the movements. Some residents described that parts of their houses were separated by about 1 meter in 2 months. Movement was recorded by Differential GPS. The rupture surface is hosted by sedimentary rocks.

Fujisawa et al. (2007) investigated the condition of a national highway that lies at the toe of a slope and showed signs of distress during the late summer and early fall of 2003 after a high precipitation in August. On the 15th and 16th of August, the rainfall was 103 and 233mm respectively. The occurrence of slope failures was evidenced by the upheaval of a part of the highway. In addition, the back of a nearby car repair factory collapsed on the 22nd of August. Some water service

pipes buried alongside the road were ruptured as well. Later in November, another water service pipe was ruptured. Hence a monitoring program was initiated that involved installing extensometers. The slide velocity increased from 5mm/day (1.8m/yr) to 24.8mm/day (9.1m/yr) from the 21st of November to the 6th of December, 2003. These rates while high but are still in the range of slow slides. In addition to the extensometers, inclinometers were installed. The results showed the slide plane to be at a depth of 24m. Both water drainage and earth filling works at the toe were considered as emergency measures. By the end of 2003 and the beginning of 2004, the velocity dropped down to 3 – 5 mm/day and the landslide was restrained by anchors as a permanent measure.

Mantovani et al. (2004) investigated the slope instabilities around the Sauris reservoir in north eastern Italy. The "La Maina" landslide has moved 1400mm in 10 days (51.1m/yr) in October 2002 following a high intensity rainfall. This event caused a partial collapse of a house located along the border of the Sauris Lake at the foot of the landslide. The slide took place in quaternary terrain. A monitoring program started in 2003 after recognizing that the landslide is adversely affecting some houses located on the slope surface, a provincial road at the toe and Sauris Lake. Due to the absence of any significant rainfall events in 2003, the average recorded movements between March and December 2003 were around 7mm (~9.3 mm/yr).

Carson et al. (1991) studied the adverse effects of ground movements in the county of Shropshire, England. Rivers in the area are actively downcutting through the bed. Natural processes have lowered the bed approximately a meter between 1933 and 1978 (average 22.2 mm/year). Mining works caused subsidence as well that led to the development of fractures. The fractures have accelerated the weathering of the top layer. Ground movements have affected the highway network. Due to the limited maintenance budget of the lightly trafficked roads, the approach was to "live with them". One of the roads has experienced a slip in 1951 and it was proposed to install drains to relieve excess pore pressures. However, that option was not adopted and armoring the toe was found to reduce the rate of movement (Note: No values of the movement rate were reported).

Barlow et al. (1991) have studied the slide hazards in the town of Peace River. Distress in a slope located uphill of one of the streets was first noticed as ground cracking in the spring of 1987. Cracking propagated over a period of two years. Slide debris spilled over the street causing maintenance and traffic problems. No values of movement rate were however reported.

Remondo et al. (2004) determined the vulnerability of different structures to landslides in a municipality in the lower Deva valley in Spain. The calculation of the vulnerability was a part of a quantitative landslide risk mapping considering both hazard and vulnerability. The vulnerability was calculated by comparing the value of damages to a certain structure to its actual present value. There were different types of linear infrastructures in the study area; motorways, national

roads, regional roads, local roads and railway tracks. These linear elements had a total length of 670km and covering a 3.6km^2 surface area. Table A - 1 shows the calculated values of vulnerability of different elements. Although the researchers did not mention typical movement rates of the studied landslides, they are likely to be slow moving since no severe damage to any of the studied structures was reported. About 75% of the studied cases were shallow landslides and flows.

Table A - 1: Vulnerability of Different Structures to Landslides in a Municipality in the Lower Deva Valley in Spain (From Remondo et al., 2004)

Name	Cost (€/m)	Losses (€/m)	Vulnerability (unitless)
Railway	110	75	0.68
Local	100	50	0.50
Regional Road (B)	700	111	0.16
Regional Road (A)	1200	111	0.09
National Road	1500	360	0.24
Motorway	6000	990	0.16

Bell et al. (2008) described the instrumentation involved in the Integrative Landslide Early Warning System (ILEWS). One of the study areas (Lichtenstein-Unterhausen) in southern Germany is a settlement area that is subject to extremely slow movements. The movements exert considerable stresses however on at least one house that suffers cracking. Sliding is initiated in spring and summer after snow melt and heavy rainfall. The warning system will utilize the results of the continuous data monitoring, especially rainfall and soil moisture, to calculate the factors of safety. When the safety factor drops below a certain threshold value, preliminary warning messages will be generated. The stratigraphy consists mainly of limestones overlying marls and clays.

Ortigão and Kanji (2004) discussed the stabilization works of the Laranjeiras Slide that affected the city of Rio De Janeiro in Brazil. The slide was triggered by a severe rainstorm where the maximum daily rainfall reached 250mm/day. The slide took place at the interface between residual soils and jointed gneisses. However, no values of movement rates were mentioned.

A-2 Vulnerability of Highways and Railways

The widening of a former railway embankment in the County of Durham, UK in order to construct a new dual lane carriage way had caused stability problems (Beaumont and Forth, 1996). Movements started during construction in the late 1960's and have continued. Many drainage measures have been applied to the site without being successful in arresting the movement. The drains were not deep enough to reach the layers that experience high pore pressures. An extensive program started in 1992 that involved installing inclinometers in addition to boreholes; as well as laboratory testing. The maximum recorded movement was about 4.5mm in approximately 4 months. Hence the annual movement rate is 13.8 mm/yr. This extremely slow movement caused cracks in the road pavement. The cracks were of such width and extent that the road needed re-pavement every 3 –

4 years. The embankment rests on a 40 meters thick glacial deposit that consists of a succession of sands, gravels and clays underlain by lower boulder clay. The cause of the initial movement was found to be mining subsidence due to mining activities in the vicinity of the site. The mining works have previously required the implementation of remedial measures for the former railway embankment as well. If the mining subsidence stopped, minor drainage measures will be sufficient to arrest the movement.

Kalteziotis et al. (1993) studied the slope stability problems at the 36th km of the national road from Athens to Sounion, near Aktea. Instabilities have been observed for more than 30 years. Soon after the road widening, cracks have appeared in the road pavement. Hence the site was monitored with many inclinometers and open standpipe piezometers. The ground beneath the original road was moving at a rate of about 13 – 19 mm/year. The downhill ground was moving at a faster rate (not indicated).

The Caramanico landslide that has been described in the previous section caused disruption to a 700m reach of a highway where the slide scarp passed through it (Buccolini and Sciarra, 1996). Movement rates at the ground surface ranged between 19 and 26 mm/yr. More details about the slide are mentioned in the previous section.

Clementino et al. (2008) investigated the required remedial options for a section of a highway that crosses a landslide. The highway lies east of the town of Drayton valley in Alberta, Canada. While the highway embankment slope is bounded at its toe by a 12m wide creek, erosion at the toe was not considered a likely trigger of movement. The movement was believed to be triggered by high pore pressures resulted from the formation of an upslope pond due to the blockage of a culvert after the slide occurred. It was required to construct an added climbing lane and hence concerns were raised regarding the adverse effect of the added fill on the stability of the slope. Geotechnical investigations revealed that the slide plane is hosted by a pre-sheared bentonitic clay shale/sandstone layer at a depth of 20 – 26m and the movement rate is 35mm/yr as indicated by the installed inclinometers. This rate caused cracks in the highway that needed patching once or twice every year. In order to slow down the slide, it was decided to drain the surface pond in addition to installing sub-horizontal drains. Stability analyses before and after the installation of the drainage measures showed that the safety factor would be improved by about 30%. The recorded pore pressures have dropped noticeably after the drainage measures installation. In addition, the movement rate was found to drop to zero as a result of the successful drainage options adopted.

Cascini et al. (2008a) modeled numerically the pore pressures and displacements of the Porta Cassia earth slide in Italy. The slide has been suddenly reactivated in 1900 mostly in response to a rainfall with a high return period. That reactivation caused lots of damage and has interrupted a major road and the Rome-Florence

railway. The monitored displacements between 1996 and 2000 using slope indicators showed an average rate of 44mm/yr. While the movement rate accompanying the 1900 reactivation was indeed higher than the recent rate, it is still thought to lie in the "slow" slides range. The slide plane is hosted in a softened clay stratum.

The Little Smoky Bridge was constructed in 1957 and soon after the completion of the bridge; movements of the Little Smoky valley slopes were noticed and are still persisting. To maintain the serviceability of the bridge, the piers were periodically extended to accommodate the movements, as it was impractical to stop them. The maximum recorded rate of movement was 100m/yr. Movement is recorded using both inclinometers and surface monuments. The rupture surface is hosted by Upper Cretaceous Clay Shales. The movement was found by Hayley (1968) to be mostly triggered by toe erosion. Recent monitoring of movement of the south slope indicated a velocity range of 15 – 20mm/yr. The rate increases to 45mm/yr and higher at the north slope. The movement of the valley slopes has led to the formation of cracks in the highway pavement (Hayley, 1968; Thomson and Hayley, 1975 and Skirrow et al., 2005). Based on the information provided by Alberta Infrastructure and Transportation, asphalt patching is performed once a year for both valley slopes in addition to some milling in the spring to the highway proximate to the north side.

Ceccucci et al. (2008) monitored the Serre La Voute landslide in North West Italy. The latest movement reactivation took place in 1957. It led to the collapse of a significant part of the slope involving a long stretch of a national road. In 1993 a slide has obstructed the Dora Riparia river bed. The slide planes' depths ranged between 35m and 80m. The slide materials are composed of Quaternary deposits in addition to dislocated bedrock. The slide has been under extensive monitoring from 1998 to 2007. The highest movement rate recorded was around 65mm/yr following an exceptional rainfall period where 250mm of rain has been recorded in 3 days. Movement was recorded using inclinometers. However, this peak velocity (65mm/yr) did not cause any severe effect on the road.

D'Elia et al. (2000) found strong correlations between the extremely to very slow movements of earthflow accumulations along the Ionic coast, Italy and the accumulated rainfall. Rainfall causes rises in the groundwater levels that trigger movements. Movement rates as slow as 0.5 mm/yr and up to 132 mm/yr were successfully correlated to the accumulated rainfall. The main sliding plane is at the overlying soil-bedrock contact. Inclinometers were used to record displacements. The overlying soil consists mainly of intensely fissured clay shale and limestones. The earthflow accumulations threaten a main road and a railway. However the extent of damage to these facilities was not mentioned.

Landslides continued to occur for around 20 years at a roadside cutslope above Lai Ping Road, Sha Tin, China (Sun et al., 2000). The amount of movement that occurred during this period has been estimated using evidence from topographic

maps, aerial photographs, geological mapping and dendrochronology of trees. The total horizontal movements were estimated to be 9 meters during that period. Hence the average rate of movement would be 450 mm/yr. One of the slides took place in July 1997 after a severe rainstorm. This single incident involved the dispatch of about 4000 m^3 of earth along a 135m long reach of the slope. The slide debris blocked the Lai Ping Road. It is expected that the ground moved with a higher rate than 450mm/yr during that slide. The stratigraphy at the site consists of up to 23m thick volcanic saprolite overlying a competent rock.

Lee and Clark (2000) have studied all the available historical information about a number of coastal cliff instabilities on the Scarborough coast, UK. One of the documented cases was the large rotational slide at Clarence Gardens. A road at the cliff foot as well as a seawall was constructed and the gardens were laid out in the late nineteenth century. Serious ground movements occurred in 1914 following the winter season that adversely affected the gardens and caused heave at the toe. This heave seriously affected the road. The seawall was then supported in 1916/17 by a number of buttresses. After 4 years, the seawall moved 2.1-2.4m (~560mm/yr). Surface movement monitoring during 1921/22 confirmed the movement rate. The installation of deep vertical drains was found to slow down the movements. The stratigraphy at the Scarborough coastline is composed of sedimentary rocks of Jurassic age overlain by glacial till. The coastline in general is subject to marine erosion at the toe which triggers landsliding along a 5km length of the coast.

The ground excavation to construct a new motorway in the Austrian Alps caused instability issues to the side slopes (Fuchsberger and Mauerhofer, 1996). Soon after excavation started, a number of superficial shallow fissures developed. When excavation approached the dredge line, further large fissures and small scarps in the upper part of the cut had developed. The slide took place in an intensely sheared shaley graphite phyllite layer of low strength. It was believed that the slide was a dormant fossil slide that has been reactivated by construction activities. The cut slope was first remedied by diverting the motorway, placing a substantial counterweight of fill material at the toe and then by constructing a bored pile wall with sufficient depth below the sliding surface. The maximum recorded movements from the installed inclinometers before implementing the mitigation measures indicated a rate of 105mm in about 65 days; i.e. 590 mm/yr. The rate dropped to approximately zero after the installation of the remedial measures. It can be inferred from this study that such a slide would have caused a major traffic disruption for the motorway if no remedial measures were taken.

A minor rotational landslide had occurred on the seventh of December, 1994 and caused traffic obstruction along a 5km reach of the A5 Trunk Road between London and Dublin (Nichol and Lowman, 2000). The slide took place at the southeastern skirts of the town of Llangollen. After a long dry summer in that year, high rainfall during November and December triggered the slide. The downslope movements ranged between 50 and 500mm. Assuming that the period

of the high rainfall lasted for one month, the rate of movement would range between 600 – 6000 mm/yr. In addition to the traffic obstruction, the boundary between the road and the rear garden of a residential property located upslope has been breached. The stratigraphy at the site consists of a thin drift cover a glacial till underlain by a sequence of mudstones and siltstones. The slide takes place at the interface between the upper glacial till and the underlying mudstones and siltstones.

The Watawala landslide had caused severe disruption to an important railway corridor from Colombo to Bodalla in Sri Lanka since 1980 (Chandler and Broise, 2000). The slide took place in a colluvium filled valley. The colluvium materials are mainly sandy silts but clayey silts are also present. The slide has moved about 89m in 16years between 1976 and 1992; i.e. an average annual rate of 5.6m/yr. The slide is mainly driven by rainfall. Peaks in rainfall may cause the movements to accelerate up to 8m/month; i.e. 96m/yr which is still in the slow velocity range. Groundwater levels were found to respond to rainfall variations. Hence it was decided to design and implement some drainage measures that helped to lower the groundwater table and slow down the slide. Temporal analysis of the available air photos is the likely method of estimating the displacement.

Malone et al. (2008) monitored the movements of a slow compound rock slide from failure in 2003 until the end of 2006. The total movement during this period was 21m (~7m/yr). Total station and photogrammetric surveys were used to measure the movement. The movement started with a high rate then the velocity decreased year after year. Peaks in movement rate coincided with peaks in rainfall. The movements were associated with hillside excavation for a new highway in Malaysia. The gross movements that occurred in 2003 caused disruption to the highway construction.

Fujisawa et al. (2007) investigated the condition of a national highway that lies at the toe of a slope and showed signs of distress during the late summer and early fall of 2003 after a high precipitation in August. The case was described in detail in the previous section and will not be repeated here. The occurrence of slope failures was evidenced by the upheaval of a part of the highway. The maximum recorded slide velocity was 24.8mm/day (9.1m/yr).

Several landslips occurred to the M25 London Orbital Motorway near Godstone, Surrey during the 1980's following periods of high rainfall (Stephen and Renton-Rose, 2000). The slips caused damages to the boundary fence but no disruption occurred to the motorway. The stratigraphy consists of soft clay deposits overlying stiff fissured clay. Although three inclinometers were installed to measure the movements, the movement rate values were not mentioned.

A-3 Vulnerability of Bridges

Seven cases are summarized in this section about the adverse effects of slow movements on bridges' serviceability. Lokin et al. (1996) investigated the instability problem of the SLOBODA bridge landslide along the Danube River bank at Novi Sad, Yugoslavia. The rupture surface is located in a layer of weathered marly clays. The installed inclinometers indicated that the average annual movement rate is 10mm/yr at most. The erosion at the slope toe is responsible for movement reactivation. The slide is considered to seriously threaten the bridge although no actual damages were reported. The future mitigation plan (at the time of the study) involved drainage measures accompanied by movement monitoring. If the movements did not stop, the second stage remedial works should involve driving reinforced concrete boxes around the bridge piers.

Carson et al. (1991) studied the adverse effects of ground movements on the county of Shropshire, England. Rivers in the area are actively downcutting through the bed. An ancient bridge was affected by an annual movement of approximately 3mm. A U-shaped reinforced concrete portal strut was constructed beneath the river bed in order to resist the abutment movements. Another bridge in the county has been remedied by extending the bridge piers to accommodate movements. Between 1954 and 1967, a bearing extension of 300mm has been taken up and additional allowance of 450mm was added. This corresponds to an average movement rate of 300mm/13yr or 23mm/yr. From 1967 to 1991, the movement was 180 mm (~7.5mm/yr). In another location within the county, the construction of an embankment 20 meters high has reactivated an ancient slide along deep bentonitic layers. Barettes of diaphragm walls were constructed as an aggressive way of remediation.

Bonnard et al. (2000) described the details of the monitoring program of the Polmengo Bridge, crossing the Ticino River near Faido, Switzerland. The east abutment of the masonry arch bridge rests on a very large slide. The slide is generally moving at a rate of 10 – 30mm/yr and up to 60mm/yr in some parts of the slide. Numerous cracks were formed in the abutment following a very high flood. Movement reactivation occurs in response to high rainfall. Movement was recorded using inclinometers and surface monuments.

The Peace River suspension bridge was constructed across the Peace River in BC. In the period between 1955 and 1957, the movement rate ranged between 90 and 120mm/yr as estimate by the officer in charge of the highway. The final catastrophic movements preceding failure took place in 4 days. The rupture surface lies in a clay shale layer. The slide caused one of the bridge anchors to move towards the river and hence the bridge collapsed. The slide movement was preceded by a break in a 500mm diameter water pipeline crossing the slide area. It is assumed that the rapid movement was a result of combination of many factors like toe erosion, precipitation, horizontal forces from the bridge anchor

and progressive reduction of shear strength on the failure surface (Brooker and Peck, 1993).

The Little Smoky Bridge is another example. The case was mentioned in detail in the previous section of Highways. The maximum annual movement rate is 100mm/yr. The bridge deck rests on rollers. The bridge piers are continuously extended to accommodate the movements (Hayley, 1968 and Thomson and Hayley, 1975).

Brooker and Peck (1993) reviewed many slides in overconsolidated clays and clay shales. The Bismarck Bridge construction across the Missouri River, USA was completed in October 1882. By the beginning of 1883, the pier and abutment started moving. Moving continued between 1883 and 1888 with an average rate of 40mm/year. In the early of 1889, two concrete dowels were cast in pits down to firm materials in an attempt to key the slide mass to the underlying material. In 1898, the pier was underpinned. An additional 150mm of movement had occurred between 1898 and 1902; i.e. the same average movement rate was maintained. In 1918 a cofferdam was constructed around the pier. The cofferdam needed reconstruction in 1940 and it was found to approach the pier again in 1950. The adopted way of stabilization was to excavate volumes of soil from the sliding mass. The safety factor has increased by up to 70% for an optimum choice of the amount of the excavated mass. The slide velocity dropped to 10mm/yr in 1963. The average rate of movement between 1944 and 1957 was 100mm/yr. The pier was extended periodically to accommodate the movements.

The Sugock Bridge, located in Andong, Korea, suffered severe deformations due to the reactivation of an ancient slide in the slope over which it rests (Kang et al., 2000). The bridge is located around the Iymha dam reservoir. The bridge was constructed in December 1989 before the formation of the dam reservoir and it became deformed soon after construction. The slide area is an alternating competent sandstones and incompetent shales. The initial failure was thought of being the result of softening along the sandstone shale interface due to the seepage of water through the joints formed by the weathering of surficial layers. Reactivations are caused by the construction of the bridge in addition to the dam reservoir level fluctuations. Lateral deformations of the bridge piers have been measured between February 1992 and November 1995. The maximum recorded lateral movement rate during this period was 70 – 90 cm. Hence the maximum rate of movement is 240 mm/yr.

A-4 Vulnerability of Dams

About seven cases have been collected; six of which are rich in movement data and the extent of damage occurring to either the dam itself or the hydropower station structures. The Little Chief Slide lies about 3 km upstream of Mica Dam in British Columbia. The slide is currently extremely slowly moving at 10 – 14 mm/yr as indicated by both inclinometers and surface monuments. Movement

takes place on thin clay gouges. While the slide is not currently adversely affecting the dam or its structures, it is being heavily instrumented in order to investigate the current behaviour and the possibility of future acceleration of movement (Rapp, 2006; Moore et al., 2006 and Mansour et al., 2008). Previous studies indicated that reservoir level fluctuations and rainfall account for movement reactivation. The Little Chief Slide is studied in detail in this thesis.

Wu et al. (2008) monitored the vertical and horizontal displacements of a landslide that occurred in the Hengshan Mountain after the construction of the Hancheng power station in 1979. The slide caused uplifting of a large area of the station as well as serious damage to the station structures. The movement was triggered by underground coal mining in the area. Sliding takes place on coal beds within sandstones, sandy mudstones and mudstones. Fifteen inclinometers have been installed in the site and the results showed that the movement persisted at a rate of 57mm/yr for the period from 1991 to 1994. The movement has slowed down since then and until 2005 to 6.4mm/yr. The overall movement rate was 17mm/yr. The drop in the displacement rate is attributed to stopping the mining operations in 1994 and the installation of a gravity drainage curtain.

Catalano et al. (2000) presented some cases that illustrated the vulnerability of landslides to dams. The stratigraphy at the Trinita Dam consists of a highly permeable formation resting on a clayey formation. The upper layer of the clay formation is weathered. Clay is approximately at its plastic limit and the friction angle averages 15 degrees unless when sand percentage is high so it may reach 32 degrees. Earth flows, 8m thick, of the superficial weathered clay layer occur over the underlying intact one. Spillway was founded on piles due to the existence of the landslide. Between 1953 and 1964; the measured maximum displacement was 1.4m (~127 mm/yr). A new reactivation took place in 1965 causing damage to the electric cabin and the guardian's house. The guardian's house experienced more damages in 1981. It was reconstructed on piles. Detailed geotechnical investigation was carried out in 1990. The average displacement rate was 10mm/year using inclinometers. Neither the dam experienced any visible deformation due to these movements nor did the spillway and bottom outlets. However, the displacement of the guardian's house backyard wall indicated the presence of progressive uphill movements. The movements caused as well lifting of the concrete pavement and damage to the house bricks. Reactivated movements occurred following the dam construction, so it is assumed that the reservoir impoundment is responsible for movement reactivation.

The Casanuova Dam was built between 1981 and 1993. The first monitored filling occurred in 1991. The maximum recorded velocity was 1 – 2 mm/day; five times larger than the rates measured previously (most probably in 1984). In 1984, fissures and cracks were observed in response to the slow landslides movements. It can be then observed that in 1984 the displacement rate ranged from 0.2 to 0.4 mm/day; i.e. ~110 mm/year when the fissures and cracks were observed. Movement is recorded using topographic monuments. The slide thickness is

approximately 70m. Movement occurs along a softened clay layer having a peak friction angle of 16 degrees and a residual value of 8 degrees. Reactivations are due to pore pressure rise in response to reservoir filling. Displacement rates responded in a timely manner to reservoir fluctuations (Catalano et al., 2000).

Movement rates up to 15 mm/month (180 mm/yr) of the Cairnmuir rock slide are expected to seriously affect the Clyde Dam in the South Island of New Zealand (Gillon and Saul, 1996). The planar rock slide is moving on a discrete, slickensided sandy silt clay gouge 100 – 300 mm thick. Its volume (20 million m^3) is sufficient to block the Lake Dunstan reservoir. The failure surface daylights about 60m above the lake level on the steep toe slopes. A rapid failure of the slide could form a wave height greater than the free board of the dam. The main trigger of movement is rainfall. Movement was estimated by investigating geological features in addition to aerial survey data. Remedial measures included drainage control in addition to surface infiltration protection. There has been a marked reduction in movement after installing the remedial measures.

Bai et al. (2008) investigated some landslides on the upstream side of the Lijiaxia hydropower station. The possible slide generated waves in the reservoir may endanger the serviceability of the hydropower station. The slide was reactivated following the reservoir impoundment. They performed an in-situ landslide acceleration test by injecting water into the slope and monitoring pore pressures and displacements. The average rate attained during the 135 days period was 730 mm/yr and the maximum rate attained in the last 15 days was 2400 mm/yr. Such rates caused some localized disintegrated loose slide mass on the surface of the slope bank to fail. The materials involved in the slide are fine grained material with a clay percent sometimes over 90%.

Yener et al. (2008) constructed a landslide susceptibility map for a huge area upstream of a proposed dam in Turkey. The landslides were analyzed by investigating aerial photos, topographic and geological maps, in addition to field measurements and observations. Laboratory experiments were carried out as well on samples taken from the study area. The results showed that 88.9% of the existing landslides have high to very high susceptibilities to reactivation. The generated waves in the reservoir by the expected reactivation would overtop the dam crest and cause damages to the dam power buildings. As the reactivation is expected to lie in the category of slow moving slides, this case was added to our review. The slide materials of two of the large slides in the area are clayey gravel and green to gray clay, silt and gravel.

A-5 Vulnerability of Linear Infrastructure

The very slow down-slope movement at a rate of 100mm/yr caused bending of the oil well casings in the Swan Hills Oil Field to the extent that oil production was lost. Inclinometers were used to record the movement. The movements occur mostly in late September and October following an annual peak precipitation in

July and August. The rupture surface lies in a clay shale layer. The well casings were protected by constructing a protective caisson to the full depth of the active ground (Brooker and Peck, 1993).

The collapse of one of the anchors of the Peace River suspension bridge was accompanied by a break in a 500mm diameter water pipeline crossing the slide area. The movement rate ranged between 90 and 120mm/yr. This case is previously mentioned and will not be detailed again (Brooker and Peck, 1993).

Barlow (2000) compiled the data of 17 investigated slopes in north eastern Alberta north to the city of Fort McMurray. The area primarily relies on oil industry in addition to logging. The persisting very slow movement rates of theses slopes pose a real challenge to resource development. The adversely affected facilities include pipelines and roads. The stratigraphy in the studied area is generally composed of glacial deposits overlying Cretaceous sedimentary clay shale overlying oil sands. Usually the clay shale is the layer that contains the rupture surface of the slide. Stream incision is responsible for the sliding activity. Five out of the seventeen studied cases can be classified as extremely slow moving slides (29.4%). The rest did not exceed the upper limit of very slow moving slides. The maximum recorded rate was 188mm/yr. The studied slopes move an average of 54mm/yr. The movement rate was sometimes inferred from the relative position of buried pipelines in the layer of colluvium. In addition, cracks have been observed on the roads located on the surface of the slopes. However, no signs of distress were visible on the surface for slopes moving slower than 50mm/yr. Drainage measures were used in 10 out of the 17 cases. The movement rate was reduced by 94% on average.

Fujisawa et al. (2007) investigated the condition of a national highway that lies at the toe of a slope and showed signs of distress during the late summer and early fall of 2003 after a high precipitation in August. The slide posed a serious threat to a highway and a car repair factory; in addition to water service pipes. This case has been mentioned twice in two previous sections. Hence it will be kept very brief here. Some water service pipes buried alongside the road were ruptured. In November 2003, another water service pipe was ruptured. The maximum recorded slide velocity was 9.1m/yr before remedial measures were installed.

Topal and Akin (2008) performed detailed geological and geotechnical investigations for a landslide that caused the break down of a pipeline between Turkey and Greece. The investigation was performed because a new pipeline is planned to be located next to the broken one. Soft-firm clayey layers slide over claystone. The slide type is rotational at the crest and translational downslope. Toe erosion by the action of a flowing stream seems to be responsible for the landslide movements. The inclinometer results indicated that the slide is moving “very slowly”. The values of movement rates were not however reported.

APPENDIX “B”

Borehole Logs, Hydraulic Conductivity Data and In-Place Inclinometer Data of the Little Chief Slide

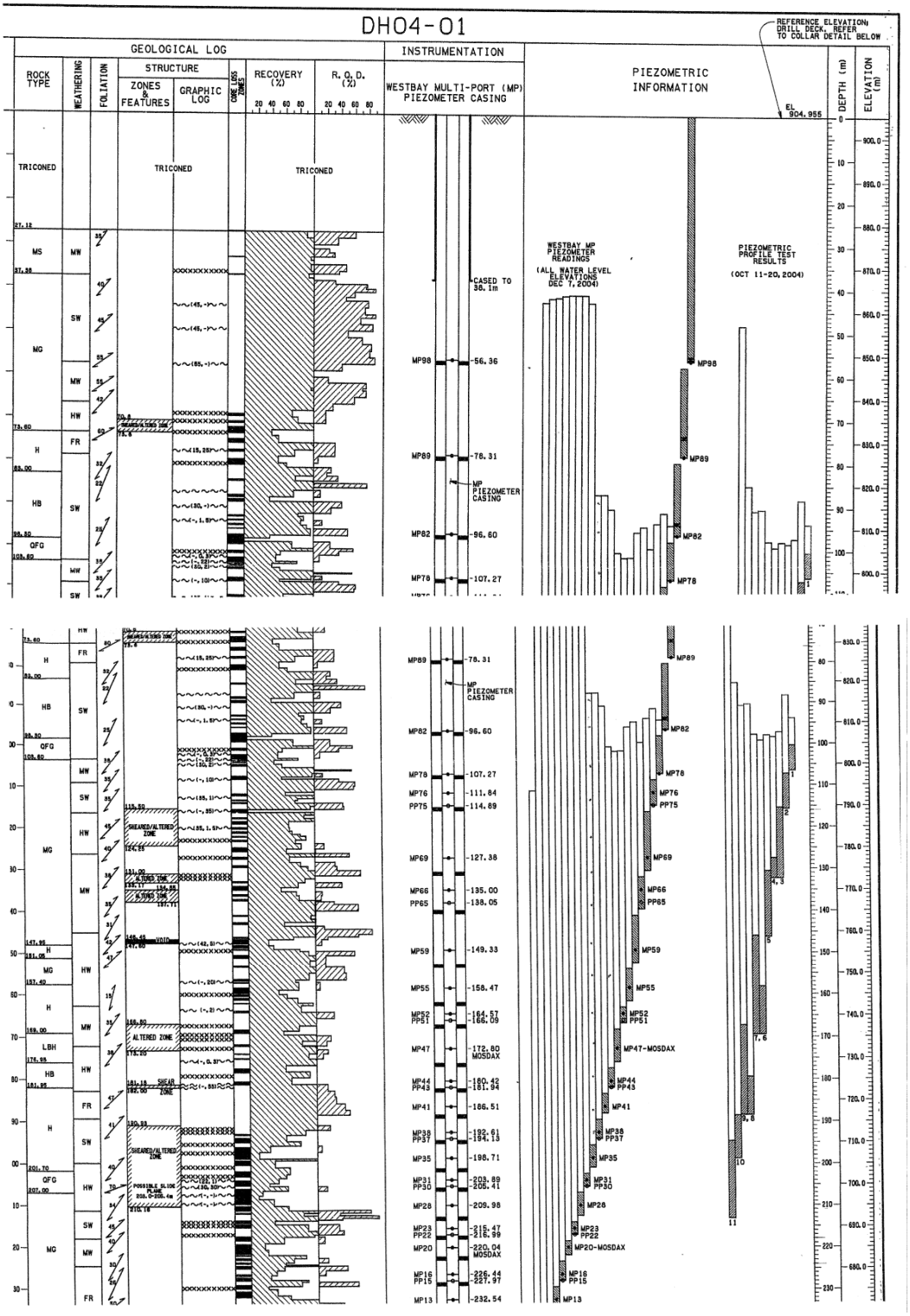
DH04-01
GEOLOGICAL LOG
INSTRUMENTATION
PIEZOMETRIC INFORMATION
ROCK TYPE
WEATHERING
FOLIATION
STRUCTURE
ZONES & FEATURES
GRAPHIC LOG
CORE LOSS ZONES
RECOVERY (%)
R.Q.D. (%)
WESTBAY MULTI-PORT (MP) PIEZOMETER CASING
REFERENCE ELEVATION: DRILL DECK, REFER TO COLLAR DETAIL BELOW
EL 904.955
DEPTH (m)
ELEVATION (m)
TRICONED
MS
MG
HB
QFG
H
LBH
SW
MW
HW
FR
CASED TO 38.1m
MP98 -56.36
MP89 -78.31
MP PIEZOMETER CASING
MP82 -96.60
MP78 -107.27
WESTBAY MP PIEZOMETER READINGS
(ALL WATER LEVEL ELEVATIONS DEC 7, 2004)
PIEZOMETRIC PROFILE TEST RESULTS
(OCT 11-20, 2004)
SHEARED/ALTERED ZONE
ALTERED ZONE
SHEAR ZONE
POSSIBLE SLIDE PLANE
MP76 -111.84
PP75 -114.89
MP69 -127.38
MP66 -135.00
PP65 -138.05
MP59 -149.33
MP55 -158.47
MP52 -164.57
PP51 -166.09
MP47 -172.80
MOSDAX
MP44 -180.42
PP43 -181.94
MP41 -186.51
MP38 -192.61
PP37 -194.13
MP35 -198.71
MP31 -203.89
PP30 -205.41
MP28 -209.98
MP23 -215.47
PP22 -216.99
MP20 -220.04
MOSDAX
MP16 -226.44
PP15 -227.97
MP13 -232.54
MP47-MOSDAX
MP20-MOSDAX

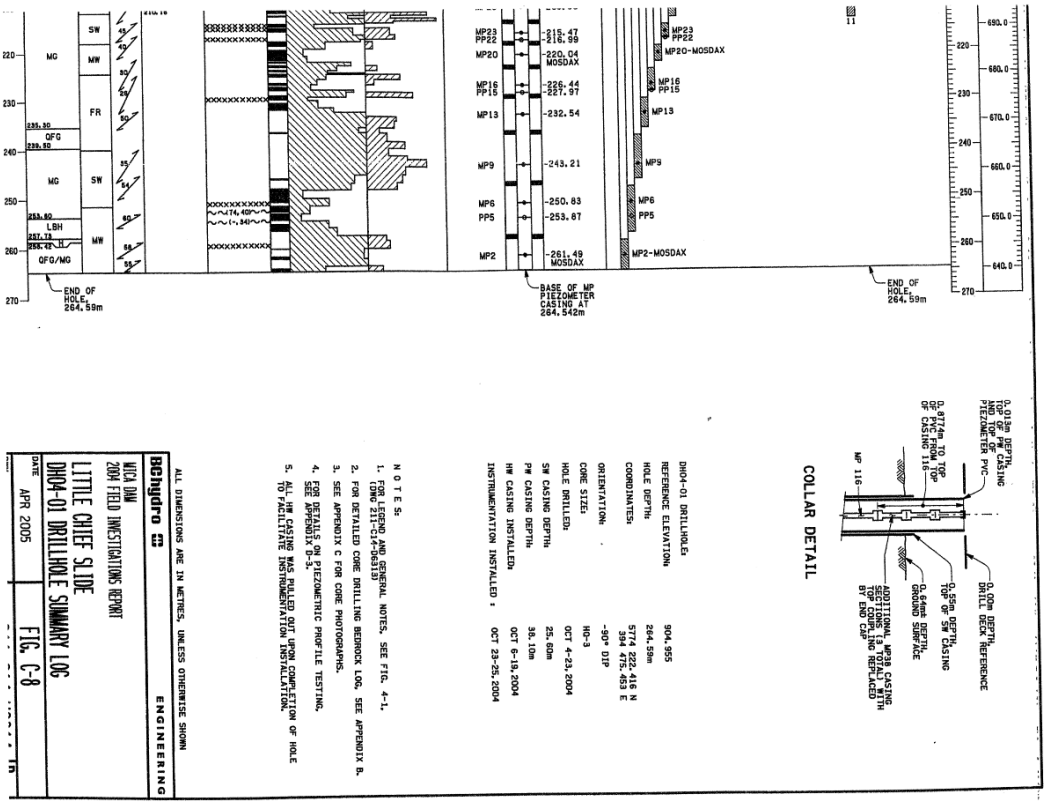

Figure B - 1: Detailed Core Log for Borehole DH04-01 (Source: 2005 BC Hydro Field Investigation Report, Rapp 2006. Reproduced with Permission from BC Hydro)

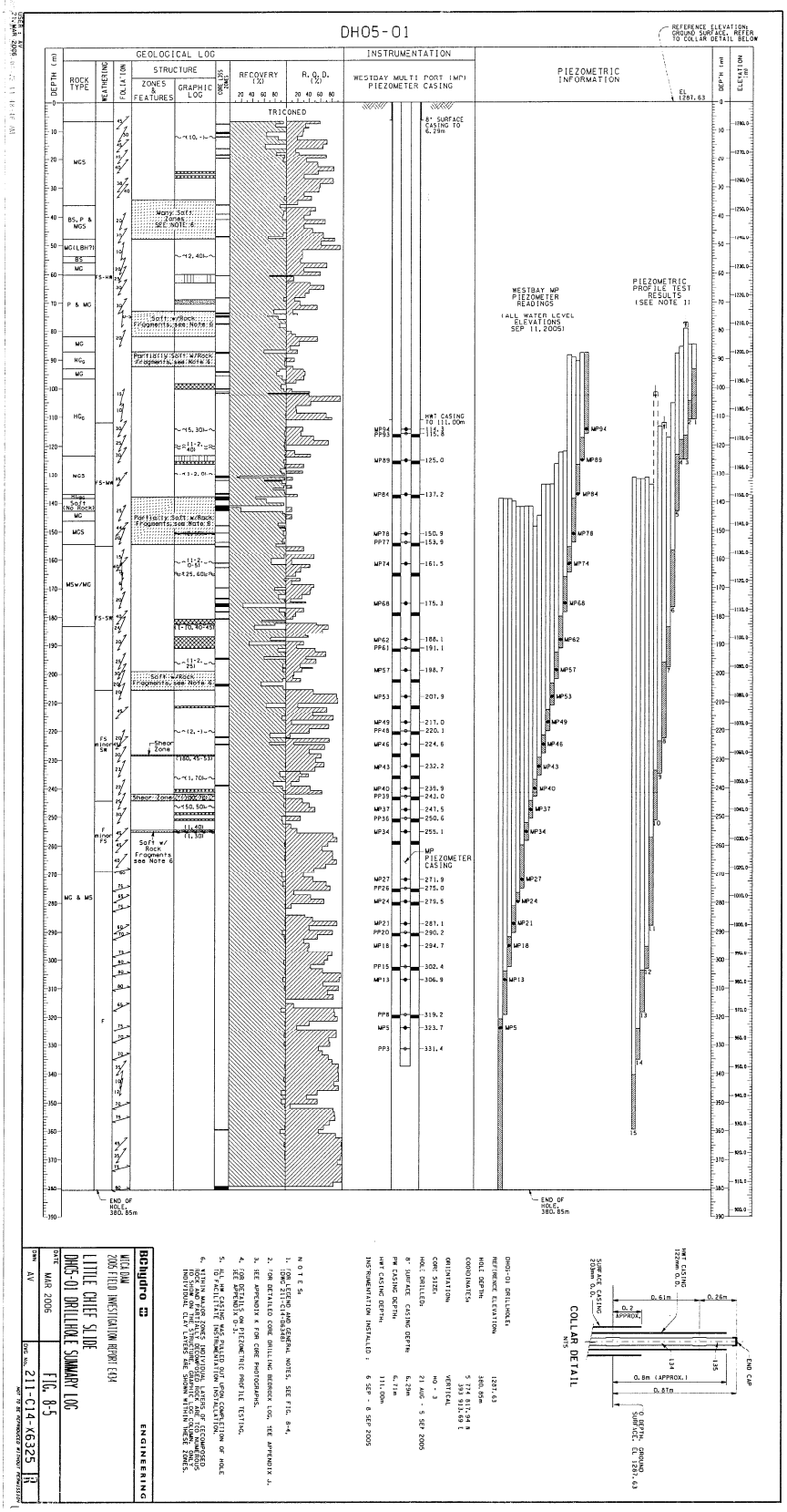

Figure B - 2: Detailed Core Log for Borehole DH05-01 (Source: 2005 BC Hydro Field Investigation Report, Rapp 2006. Reproduced with Permission from BC Hydro)

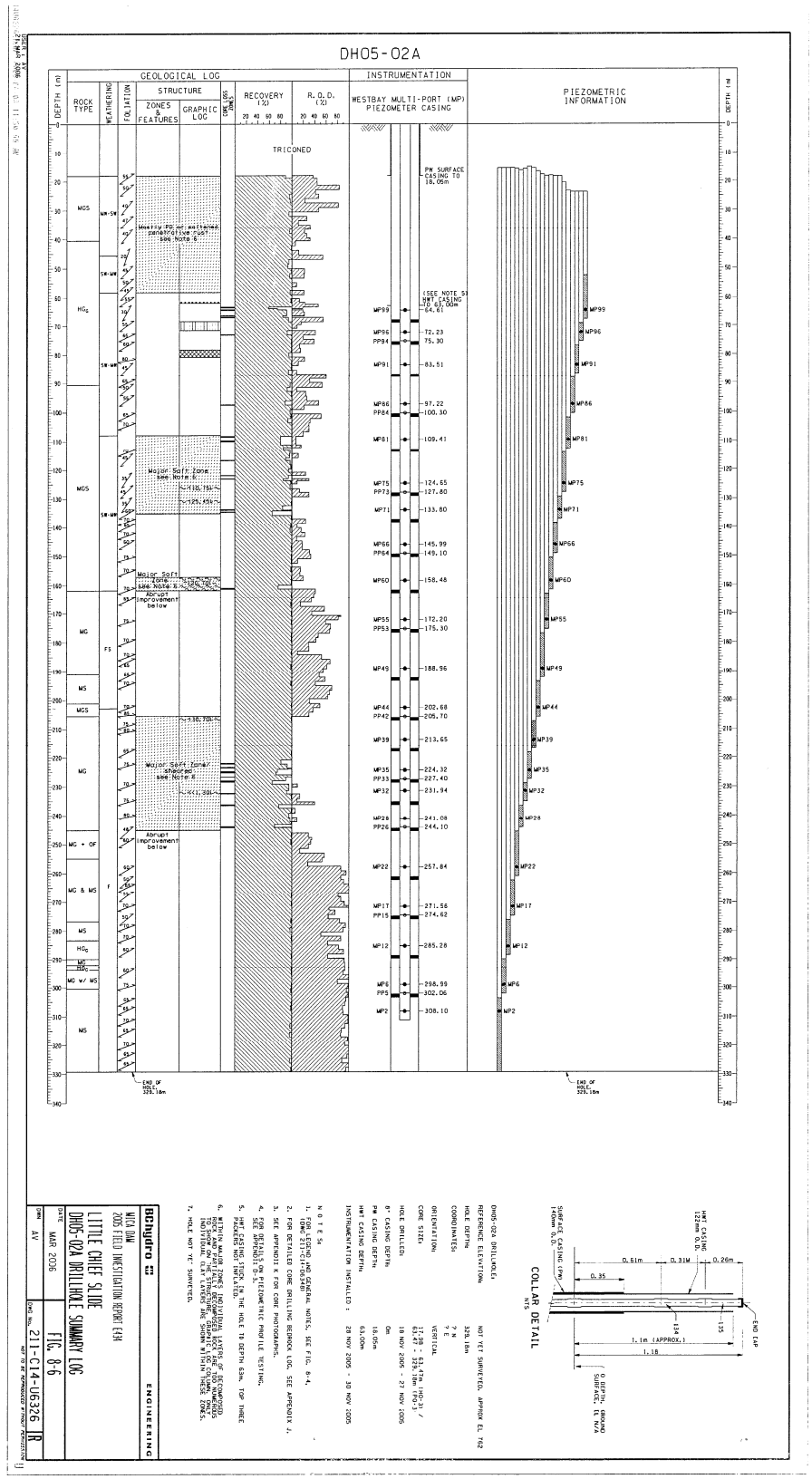

Figure B - 3: Detailed Core Log for Borehole DH05-02A (Source: 2005 BC Hydro Field Investigation Report, Rapp 2006. Reproduced with Permission from BC Hydro)

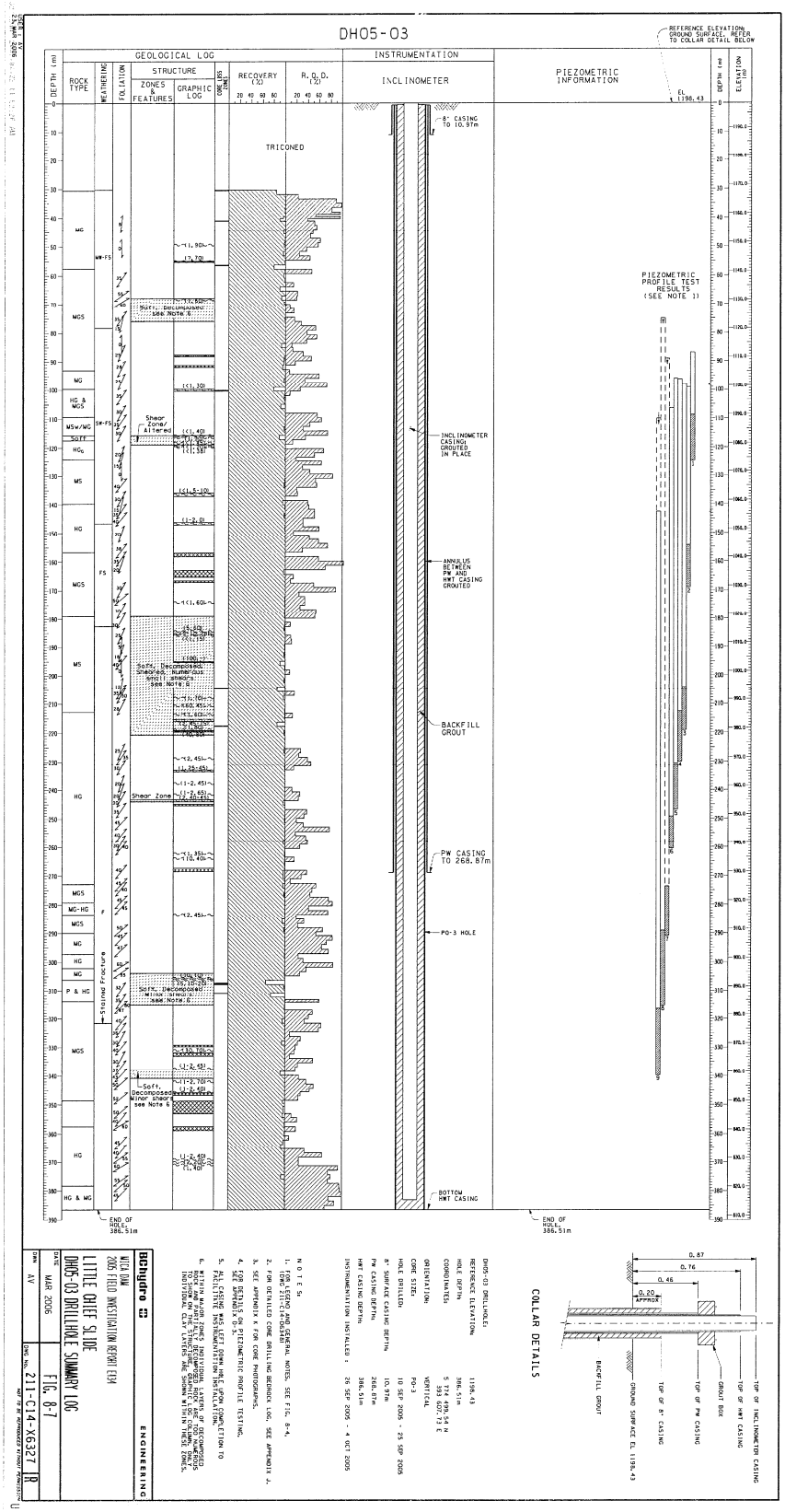

Figure B - 4: Detailed Core Log for Borehole DH05-03 (Source: 2005 BC Hydro Field Investigation Report, Rapp 2006. Reproduced with Permission from BC Hydro)

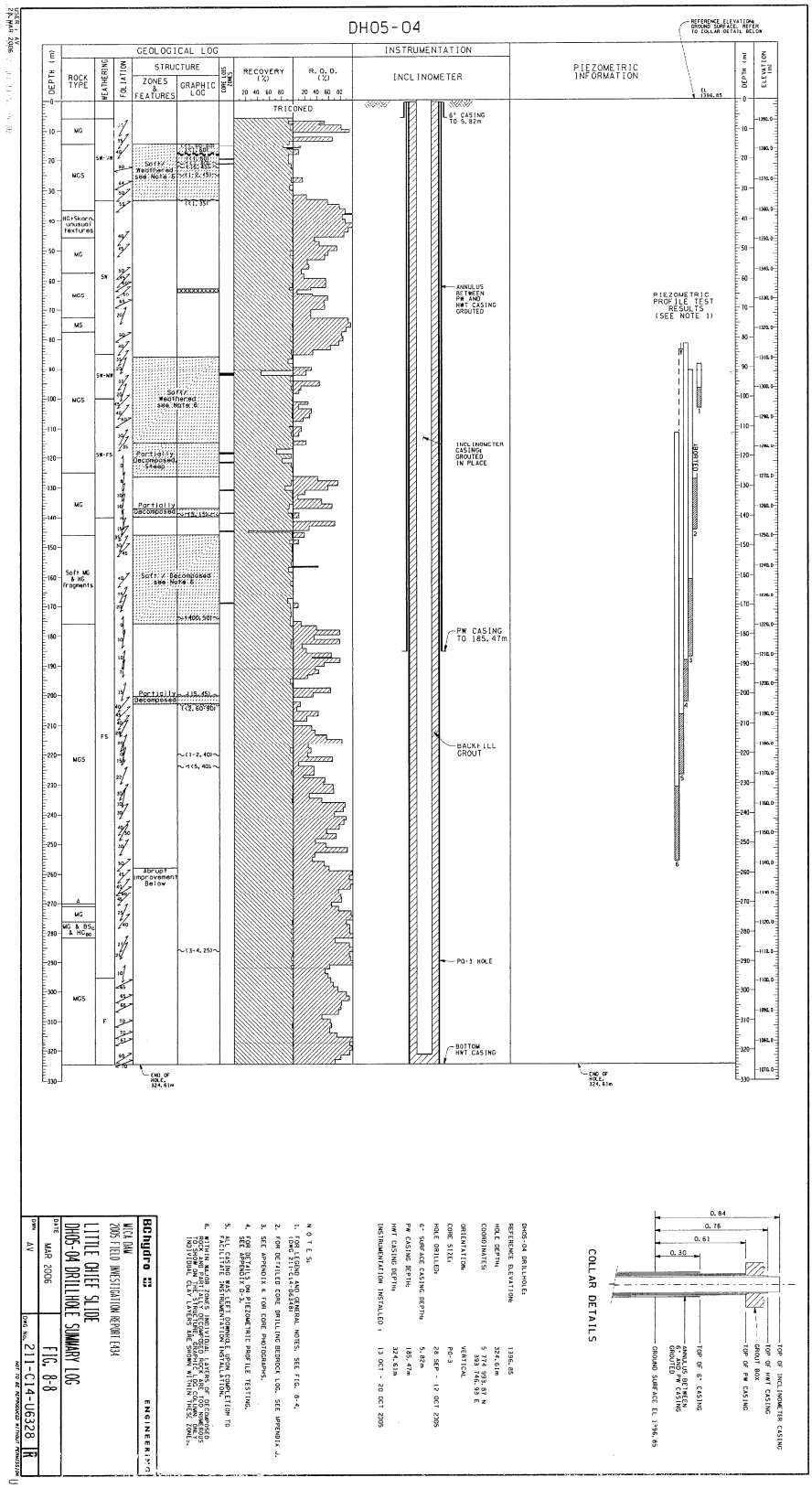

Figure B - 5: Detailed Core Log for Borehole DH05-04 (Source: 2005 BC Hydro Field Investigation Report, Rapp 2006. Reproduced with Permission from BC Hydro)

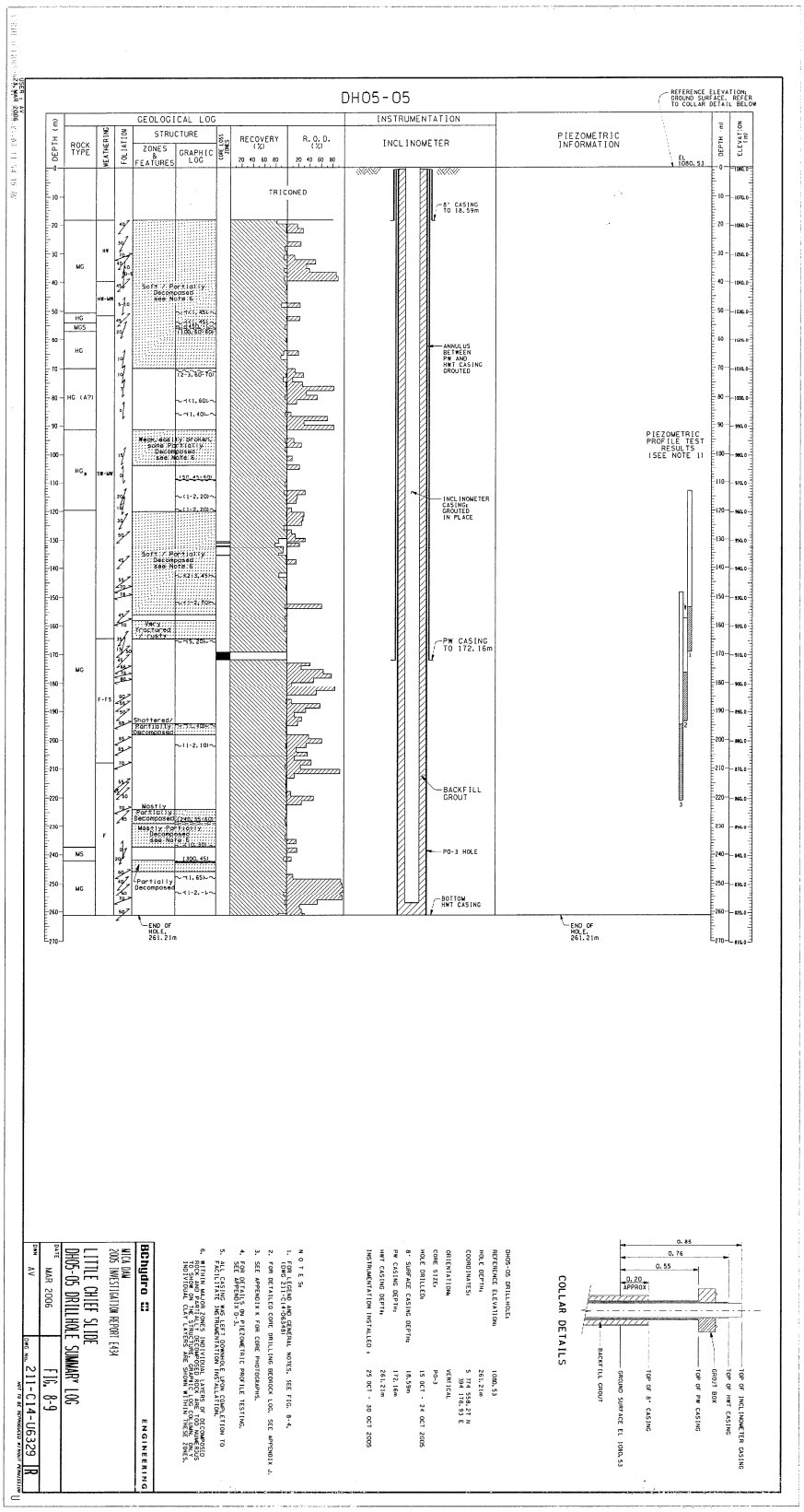

Figure B - 6: Detailed Core Log for Borehole DH05-05 (Source: 2005 BC Hydro Field Investigation Report, Rapp 2006. Reproduced with Permission from BC Hydro)

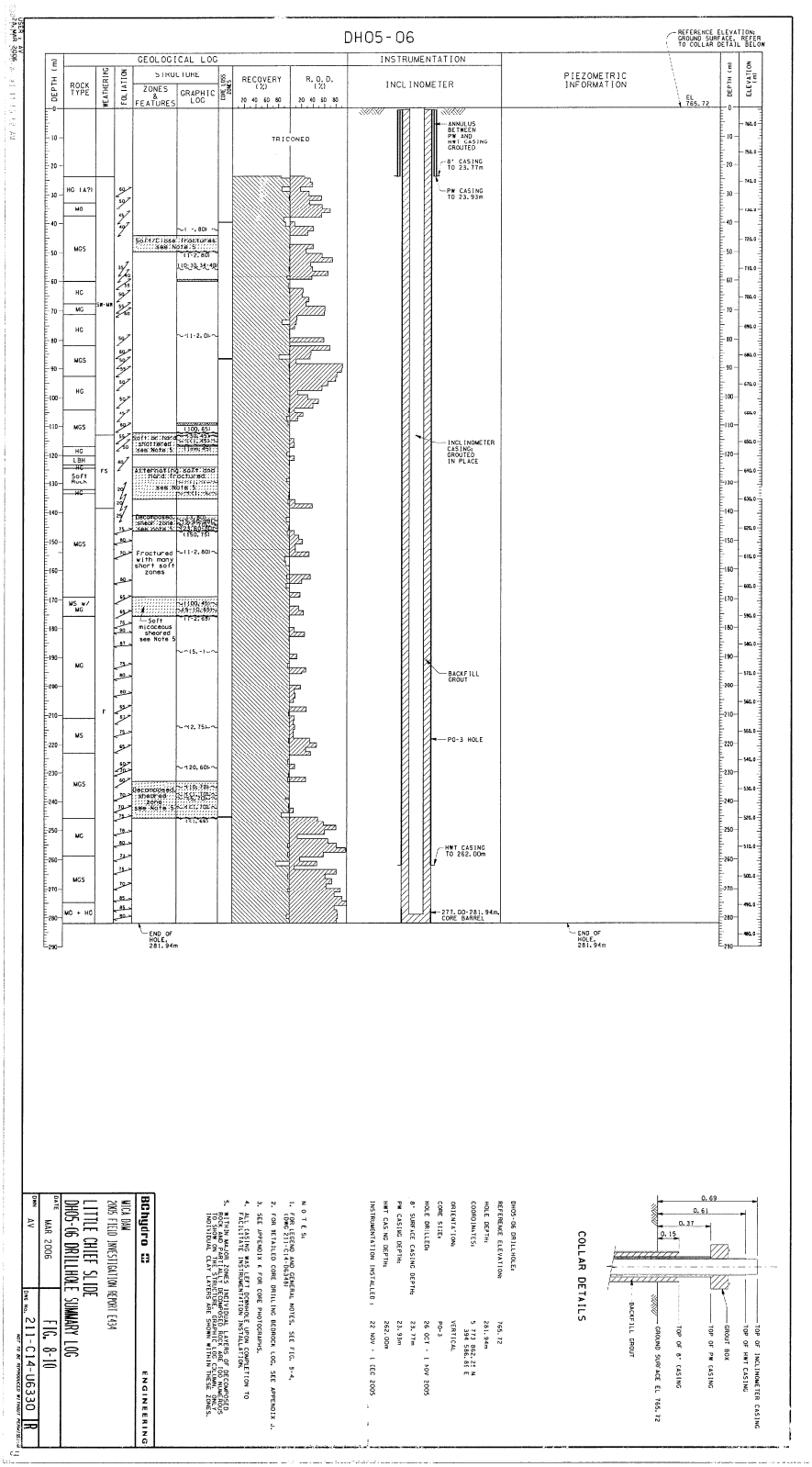

Figure B - 7: Detailed Core Log for Borehole DH05-06 (Source: 2005 BC Hydro Field Investigation Report, Rapp 2006. Reproduced with Permission from BC Hydro)

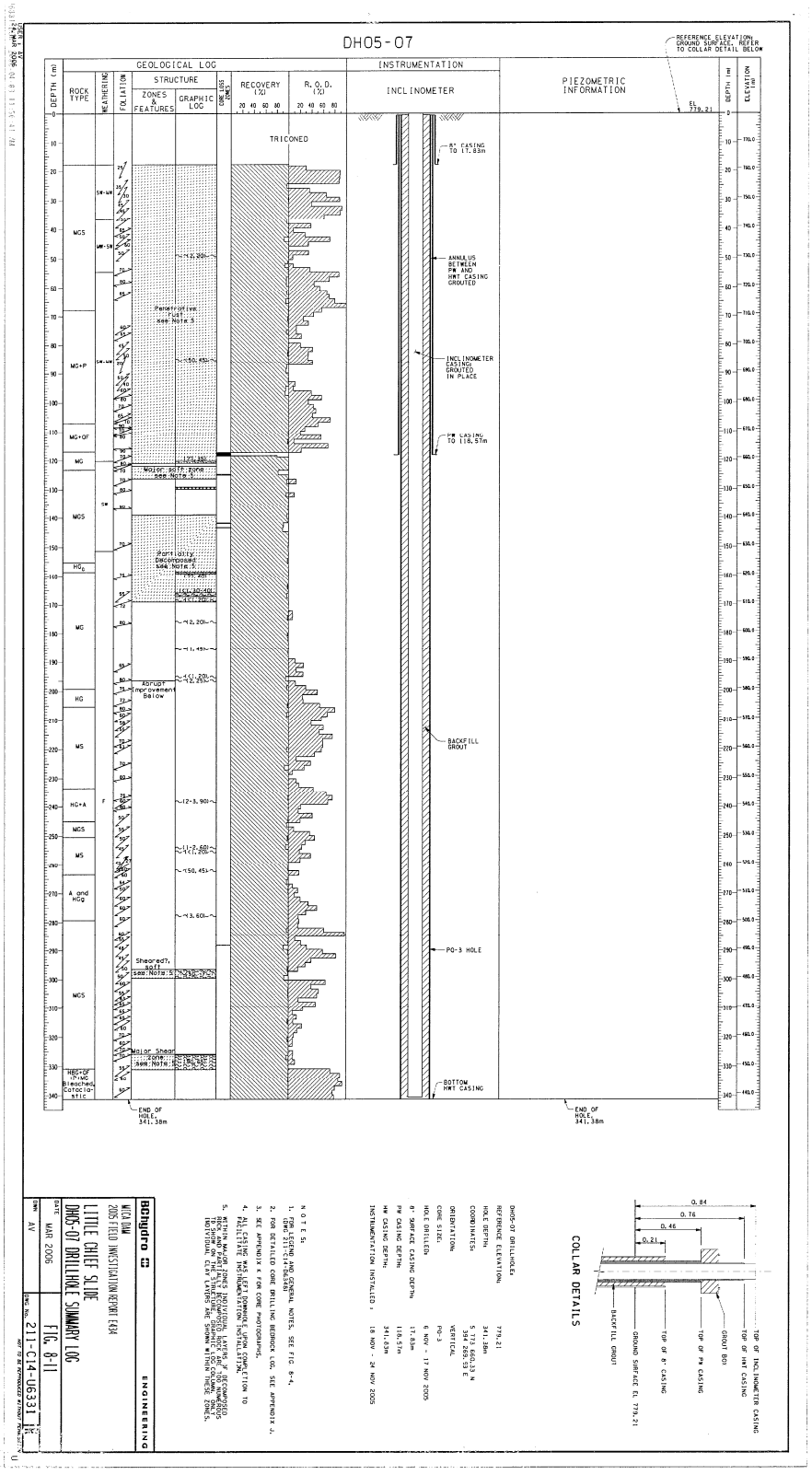

Figure B - 8: Detailed Core Log for Borehole DH05-07 (Source: 2005 BC Hydro Field Investigation Report, Rapp 2006. Reproduced with Permission from BC Hydro)

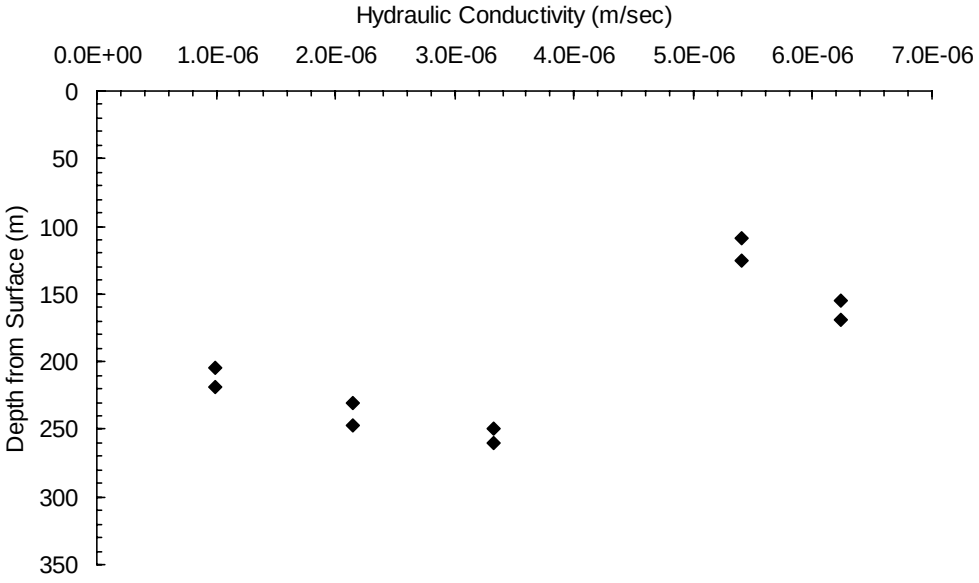
Hydraulic Conductivity (m/sec)
0.0E+00
1.0E-06
2.0E-06
3.0E-06
4.0E-06
5.0E-06
6.0E-06
7.0E-06
Depth from Surface (m)
0
50
100
150
200
250
300
350

(a)

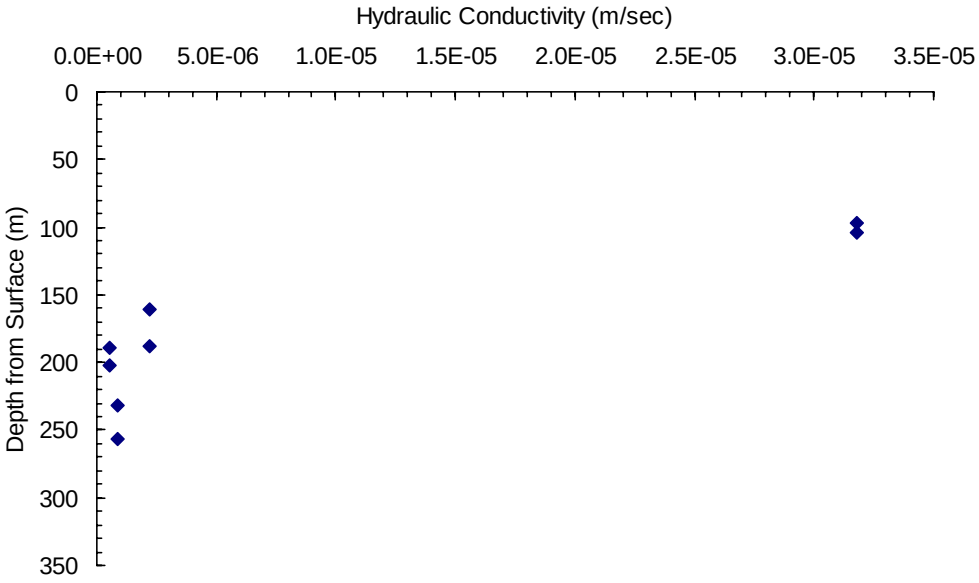
Hydraulic Conductivity (m/sec)
0.0E+00
5.0E-06
1.0E-05
1.5E-05
2.0E-05
2.5E-05
3.0E-05
3.5E-05
Depth from Surface (m)
0
50
100
150
200
250
300
350

(b)

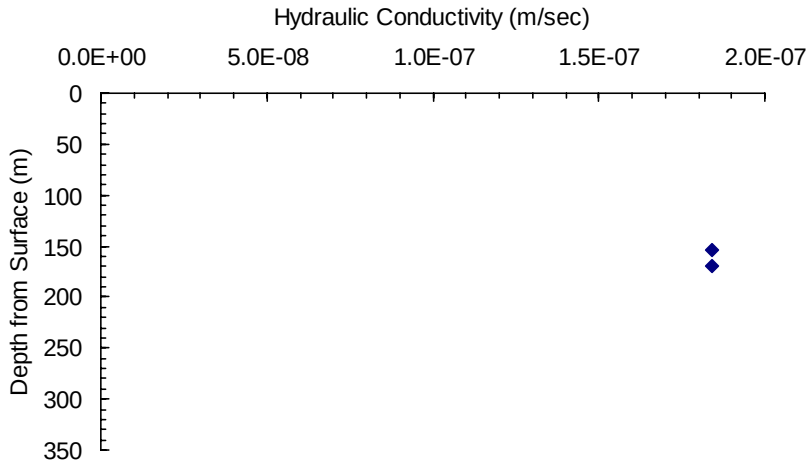

(c)

Figure B - 9: Hydraulic Conductivity data from boreholes: (a) DH05-03, (b) DH05-04 and (c) DH05-05 (Little Chief Slide)

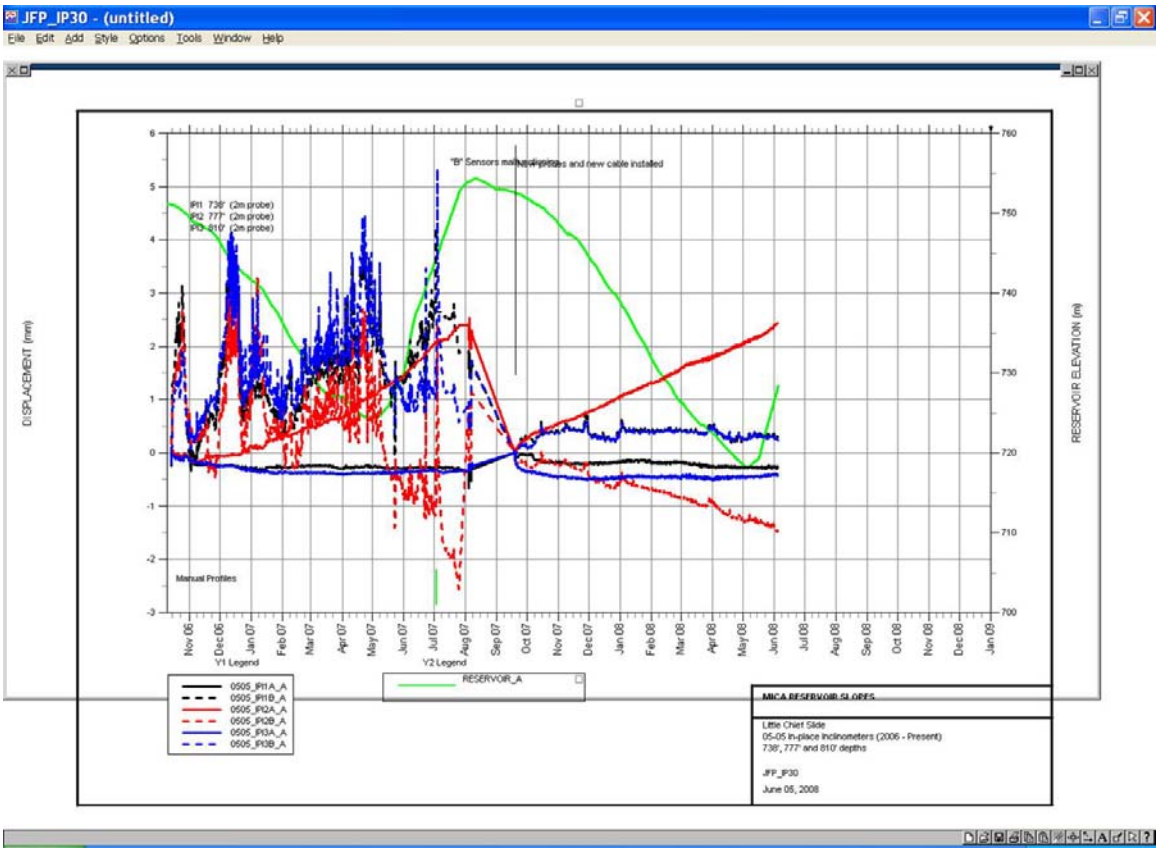

Figure B - 10: Scanned Image of the Displacement versus Time Plots Recorded at Different Depths in Borehole DH05-05 (Data Provided by BC Hydro)

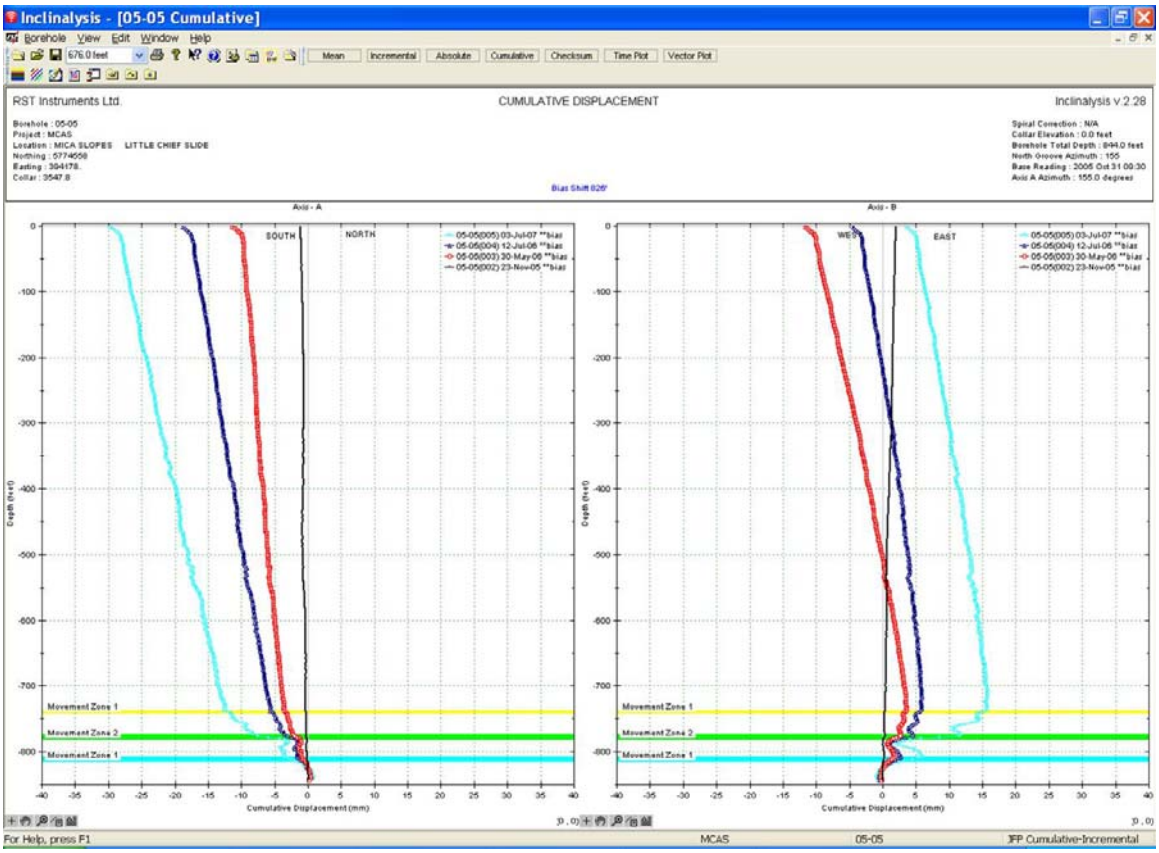

Figure B - 11: Scanned Image for the Results of the Manual Inclinometer Recordings in Borehole DH05-05